D 2019

U.PORTO
FEUP FACULDADE DE ENGENHARIA
UNIVERSIDADE DO PORTO

DURABILITY OF THERMAL RENDERING AND PLASTERING SYSTEMS

JOANA FERNANDES MAIA
DOCTORAL THESIS PRESENTED TO
FACULTY OF ENGINEERING OF UNIVERSITY OF PORTO IN
CIVIL ENGINEERING

U.PORTO

FEUP FACULDADE DE ENGENHARIA UNIVERSIDADE DO PORTO

DURABILITY OF THERMAL RENDERING AND PLASTERING SYSTEMS

JOANA FERNANDES MAIA

Master in Building Construction of Faculty of Engineering of University of Porto

Doctoral Thesis submitted to obtain the Doctor Degree in Civil Engineering

---

Supervisor: Professor Nuno Manuel Monteiro Ramos

Co-Supervisor: Doctor Maria do Rosário Veiga

APRIL 2019

COMPETE 2020 | PORTUGAL 2020 | UNIÃO EUROPEIA Fundo Europeu de Desenvolvimento Regional | FCT Fundação para a Ciência e a Tecnologia | PD-F FCT PhD PROGRAMMES

DOCTORAL PROGRAM IN CIVIL ENGINEERING

Phone. +351-22-508 1901

Fax +351-22-508 1446

✉ prodec@fe.up.pt

Edited by

FACULDADE DE ENGENHARIA DA UNIVERSIDADE DO PORTO

Rua Dr. Roberto Frias

4200-465 PORTO

Portugal

Phone. +351-22-508 1400

Fax +351-22-508 1440

✉ feup@fe.up.pt

http://www.fe.up.pt

To my family

Para a minha família

Your efforts will pay off.

ACKNOWLEDGEMENTS

A long-term work, such as a Doctoral Thesis, is the result of several joint efforts and not only an individual process. It requires different knowledge, which is applied during all the process in the distinct phases. The most insignificant contribute may be the key to complete the puzzle that is the Doctoral Thesis.

I wish to thank Professor Nuno Ramos, my thesis supervisor, for all the support and friendship during all these years. For believing in my capacities, in my skills and encouraging me to achieve more and more knowledge. To Doctor Maria do Rosário Veiga, my co-supervisor, for the untiring commitment. Allways available, assertive and meticulous. For all the support in the visits to LNEC, which were crucial to the development of the experimental works. Thank you, Professor Nuno and Engineer Rosário for the readiness, guidance, suggestions and affection. I am lucky for having you both in my professional path.

My special thanks to Saint-Gobain Weber, especially to Luís Silva and Hélder Gonçalves, to Sival – Gessos Especiais, especially to Ângela Sousa, to Secil Argamassas, especially to Dina Frade and to Fradical, especially to Engineer Cartaxo, for the execution of all the specimens and technical support.

To FCT-Fundação para a Ciência e a Tecnologia, the funding of the Doctoral Grant PD/BD/52659/2014, through the Doctoral Programme EcoCoRe. I also would like to thank to EcoCoRe Professors and Collegues the wise advices and the good moments during the Summer Schools.

This work was financially supported by UID/ECI/04708/2019- CONSTRUCT - Instituto de I&D em Estruturas e Construções funded by national funds through the FCT/MCTES (PIDDAC).

This work was financially supported by Project PTDC/ECI-CON/28766/2017 and POCI-01-0145-FEDER-028766 funded by FEDER funds through COMPETE2020 - Programa Operacional Competitividade e Internacionalização (POCI) and by national funds (PIDDAC) through FCT/MCTES.

To all the Professors and Colleagues of LFC-CONSTRUCT for being always there in this long journey, especially to Sara, for the support with climatic data, and to my long-standing friend Pedro. To Professor Luísa Sousa from Mechanical Engineer Department of FEUP, the support in the thermo-mechanical simulation with ABAQUS software.

To all the laboratory technicians and colleagues of the Building Coatings and Thermal Insulation Unit of LNEC, especially to Acácio Monteiro and Dora Santos for the support in the experimental campaign, to Luís Matias in the obtention of thermograms, to Catarina Farinha and Cláudio Cruz in the use of the optical microscope, to Ana Marques for showing me the best material ever to bonding the Karsten tubes, to Sofia Malanho and Bento Sabala for the scientific and technical advices.

To Music and to God! I have no doubt that it was crucial to have balance, peace and joy!

To the most important part of my life: Friends and Family! To my special friends Claudia, Sara, Filipe, Ana and Hugo, for being like family! To Alexandra and Bruno, for receiving me at their home in the several working visits to LNEC. To my godson Bernardo, to my godfather Rogério, to my aunts and uncles, to my cousins, especially to the kindest girl, my cousin Vera. To the joy of my life, my nieces Margarida and Maria, to my dear brother Nuno, to my love Bruno, to the most wonderful and exceptional people in the world, my mother Fernanda and my father Horácio. Obrigada por me ensinarem os verdadeiros valores da vida!

All of you have a special place in my heart! Thank you very much for being my guiding light!

ABSTRACT

The increase of thermal demands in buildings and the changes in the European thermal regulations implied the decrease of the thermal transmission of building envelopes. As such, researchers and manufacturers started searching for new solutions, such as thermal renders and plasters. However, a gap in the durability assessment of thermal rendering and plastering systems was observed, since the existing standardization for the durability assessment of hardened mortars does not allow a consistent evaluation, considering thermal mortars, especially in multilayer systems.

Therefore, the main goal of this Doctoral Thesis consisted of the development and implementation of durability assessment methodologies applicable to thermal rendering and plastering systems. The methodology used to achieve this main objective was based on the analysis of the characteristics and specificities of thermal rendering and plastering systems, the related existing standards and methodologies for the durability assessment and, throughout numerical simulation and laboratory tests, presenting specific methodologies for the durability assessment of this type of systems.

The determination of the physical, hygrothermal and mechanical properties allowed deepening the knowledge of thermal renders/plasters and systems, contributing to develop more reliable simulations. The determination of the most relevant properties allowed observing important findings, such as the high contribution of the capillary network in increasing the moisture content and therefore the increase of the thermal conductivity. The thermal renders/plaster presented low water vapour resistance comparing to EPS (expanded polystyrene), allowing higher water vapour exchanges, which contributes to greater compatibility with ancient materials, than low vapour permeability materials. Regarding the adhesive strength, these systems presented low adhesive strength, but in the order of magnitude of ETICS (External Thermal Insulation Composite Systems).

The numerical simulation allowed evaluating the most significant degradation mechanisms and the related failure modes of thermal rendering and plastering systems. The hygrothermal simulation highlighted the great impact of the finishing coatings in the water content of the inner layers. The thermo-mechanical simulation showed a reduction of the thermal induced stresses in thermal systems with low differences of rigidity between the thermal and finishing renders. Thermal rendering systems present lower condensation potential than the studied ETICS, for the same insulation thickness. A behavioural dependence of thermal rendering systems on climate conditions and material properties was observed.

The lack of durability assessment procedures directly applicable to thermal rendering and plastering systems motivated the development of a new durability assessment methodology, filling the existing gap. The methodology takes into account the intrinsic properties of the materials that constitute the system, the type of application (exterior or interior), the climatic conditions and consequent degradation mechanisms to which the system will be subjected. The knowledge of these parameters allows defining the accelerated ageing cycles that reproduce the real degradation mechanisms. The combination of the analysis of existing procedures with the hygrothermal simulation allowed the development of accelerated ageing hygrothermal cycles, applied to thermal rendering systems, taking into account the European climatic context, throughout a theoretical algorithm.

KEYWORDS: Thermal rendering and plastering systems, Durability, Accelerated ageing, Material properties, Experimental tests, Hygrothermal performance, Thermo-mechanical performance, Numerical simulation.

RESUMO

O aumento das exigências térmicas nos edifícios e as alterações às regulamentações térmicas europeias tiveram implicação na redução da transmissão térmica da envolvente dos edifícios. Como tal, investigadores e fabricantes procuraram desenvolver novas soluções, como rebocos térmicos. No entanto, observou-se uma lacuna no que diz respeito à avaliação da durabilidade de sistemas de reboco térmico, visto que os procedimentos normalizados existentes para a avaliação da durabilidade de argamassas endurecidas não permite uma avaliação consistente de argamassas térmicas, especialmente se inseridas em sistemas multicamada.

Portanto, o principal objetivo desta Tese de Doutoramento consistiu no desenvolvimento e implementação de metodologias de avaliação da durabilidade aplicáveis a sistemas de reboco térmico. A metodologia utilizada para atingir este objetivo principal baseou-se na análise das características e especificidades dos sistemas de reboco térmico, nas normas e metodologias existentes para a avaliação da durabilidade e no desenvolvimento de metodologias específicas para a durabilidade deste tipo de sistemas, através de simulação numérica e ensaios laboratoriais.

A determinação das propriedades físicas, higrotérmicas e mecânicas permitiu aprofundar o conhecimento sobre rebocos térmicos e sistemas, contribuindo o mesmo para o desenvolvimento de simulações numéricas mais confiáveis. A determinação das propriedades mais relevantes permitiu observar uma grande contribuição da rede capilar no aumento do teor de humidade e, consequentemente, no aumento da condutibilidade térmica. Os rebocos térmicos apresentaram baixa resistência ao vapor de água em comparação com EPS, permitindo maiores trocas de vapor de água e contribuindo para uma maior compatibilidade com materiais antigos, do que materiais com baixa permeabilidade ao vapor. Quanto à aderência, os rebocos térmicos apresentaram baixa resistência, porém da ordem de grandeza de ETICS correntes.

A simulação numérica permitiu avaliar os mecanismos de degradação mais significativos e os modos de rotura relacionados com sistemas de reboco térmico. A simulação higrotérmica evidenciou o grande impacto das camadas de acabamento no teor de água das camadas internas. A simulação termomecânica permitiu observar uma redução das tensões induzidas por ação térmica em sistemas com menores diferenças de rigidez entre as camadas de reboco térmico e de acabamento. Os sistemas de reboco térmico apresentaram menor potencial de condensação do que o ETICS analisado, para a mesma espessura de isolamento. Observou-se uma relação de dependência dos sistemas de reboco térmico com as diferentes condições climáticas e as propriedades dos materiais.

A inexistência de procedimentos de avaliação da durabilidade diretamente aplicáveis a sistemas de reboco térmico motivou o desenvolvimento de uma nova metodologia de avaliação da durabilidade, colmatando a lacuna existente. A metodologia tem em consideração as propriedades intrínsecas dos materiais que constituem o sistema, o tipo de aplicação (exterior ou interior), as condições climáticas e consequentes mecanismos de degradação a que estará sujeito. O conhecimento destes parâmetros permite definir os ciclos de envelhecimento acelerado que reproduzam os mecanismos de degradação reais. A combinação da análise de procedimentos existentes com a simulação higrotérmica permitiu o desenvolvimento de ciclos higrotérmicos de envelhecimento acelerado, aplicados a sistemas de reboco térmico, tendo em conta o contexto climático europeu, através de um algoritmo teórico.

PALAVRAS-CHAVE: Sistemas de reboco térmico, Durabilidade, Envelhecimento acelerado, Propriedades dos materiais, Ensaios laboratoriais, Desempenho higrotérmico, Desempenho termo-mecânico, Simulação numérica.

CONTENTS

INDEX OF FIGURES

INDEX OF TABLES

NOMENCLATURE

ROMAN-LETTER NOTATIONS

Symbol	Unit	Meaning
A	m^2	Section area
A_F	–	Acceleration factor
A_w	$kg/m^2.s^{0.5}$	Water absorption coefficient
A_{1h}	kg/m^2	Water absorption coefficient after 1h
A_{24h}	kg/m^2	Water absorption coefficient after 24h
b	%/M.-%	Moisture-induced thermal conductivity supplement
b'	–	Approximation factor (moisture storage function)
B	–	Constant of the product failure mechanism and test conditions
c	J/kg.ºC	Specific heat
C	–	General constant
C_{lab}	–	Laboratory test conditions
C_{nat}	–	Natural conditions
CP	–	Condensation potential
d_{flex}	mm	Specimen depth
d	m^2/s	Thermal diffusivity
D_φ	kg/(m·s)	Liquid conduction coefficient of the building material
D_w	m^2/s	Liquid transport coefficient
D_{ws}	m^2/s	Moisture diffusivity for suction
D_{ww}	m^2/s	Moisture diffusivity for redistribution
e	$J/ m^2.s^{0.5}.ºC$	Thermal effusivity
E	Pa	Young modulus
E_d	Pa	Dynamic elastic modulus
E_A	eV	Activation energy of the failure mode
F	N	Maximum applied load
F_L	Hz	Longitudinal fundamental resonance frequency
g	$kg/(m^2·s)$	Density of water vapour flow rate
g_w	$kg/(m^2·s)$	Liquid transport flux density
G	kg/s	Water vapour flow rate through specimen

Symbol	Unit	Meaning
I	W/m^2	Net radiation at the component surface
I_e	[W/m^2]	Long-wave emission radiation of the surface
I_l	[W/m^2]	Long-wave counterradiation
I_s	[W/m^2]	Short-wave solar radiation
h	–	Humidity constant
h_v	J/kg	Evaporation enthalpy of water
H	J/m^3	Total enthalpy
k	–	Matrix of constants which depends on the Young's modulus, Poisson's ratio and shear modulus
k_B	eV/K	Bolzmann's constant (8.617x10^{-5})
K	–	Temperature cycle exponent
l	m	Length of the specime
l_{flex}	mm	Distance between the axes of the support rollers
m	–	Linear slope
m_0	kg	Dry mass
m_h	kg	Immersed mass
$m_{w(\varphi)}$	kg	Mass in equilibrium with the ambience φ
m_{ti}	kg	Mass at the beginning of the test
m_{tf}	kg	Mass at the end of the test
m_{ref}	kg	Mass after 3 minutes immersion
m_{1h}	kg	Mass after 1 hour immersion
m_{24h}	kg	Mass after 24 hours immersion
N_f	–	Number of cycles to fail
p_{sat}	[Pa]	Water vapour saturation pressure
P_0	%	Open porosity
$P_v(air)$	Pa	Water vapour partial pressure in the air close to the surface
$P_{sat}(surface)$	Pa	Water vapour saturation pressure on the surface
q	–	Heat source
Q	W/m^2	Heat flow density through the component
Q'	W	Heat transfer
R^2	–	Coefficient of determination
R_{flex}	MPa	Flexural strength

Symbol	Unit	Meaning
R_{comp}	MPa	Compressive strength
R_{se}	m².ºC/W	Exterior surface resistance
s_d	m	Water vapour diffusion-equivalent air layer thickness
t	s	Time
t_f	s	Total time
T –	ºC	Temperature
T_{se}	ºC	Exterior surface temperature
T_{si}	ºC	Interior surface temperature
U	W/m².ºC	Thermal transmission
v	m/s	Velocity
V_t	ml or ml/m²	Absorbed volume
x, y and z plane	–	Plane directions
w	kg/m³	Water content
w_f	kg/m³	Saturated water content
w_φ	kg/m³	Water content in equilibrium with φ
w_{max}	kg/m³	Maximum water content
W_p	kg/(m²·s·Pa)	Water vapour permeance
∅	mm	Dent diameter

GREEK-LETTER NOTATIONS

Symbol	Unit	Meaning
a	–	Short-wave radiation absorptivity of the surface
a'	x10^{-6}/ºC	Thermal expansion coefficient
δ_p	kg/(m·s·Pa)	Water vapour permeability
ε	–	Long-wave emissivity and absorptivity of the surface
ε_S	–	Strain
λ	W/(m.ºC)	Thermal conductivity, in dry conditions
$\lambda_{10,dry}$	W/(m.ºC)	Thermal conductivity at 10 ºC, in dry conditions
$\lambda_{20,dry}$	W/(m.ºC)	Thermal conductivity at 20 ºC, in dry conditions
λ_w	W/(m.ºC)	Thermal conductivity of the moist material
μ	–	Water vapour resistance factor

Symbol	Unit	Meaning
ρ	kg/m^3	Dry bulk density
ρ_r	kg/m^3	Real density
ρ_{rh}	kg/m^3	Water density
σ	Pa	Stress
υ	–	Poisson's ratio
φ	–	Relative humidity

MATHEMATICAL OPERATORS

Symbol	Meaning
d	Operator for total differential
∂	Operator for partial differential
∇	Nabla operator
Δ	Variation operator

ACRONYMS

Symbol	Meaning
3D	Three Dimensional
av.	Average
AA	After Ageing
BA	Before Ageing
ABCB	Australian Building Codes Board
AIJ	Architectural Institute of Japan
APFAC	Portuguese Association of Manufacturers of Mortars and ETICS
ASTM	American Society for Testing And Materials
ASHRAE	American Society of Heating, Refrigerating and Air-Conditioning Engineers
BS	British Standard
BREEAM	Building Research Establishment Environmental Assessment Method
C	Finishing Render/Plaster
Ce	Cement
CF	Carbon Fibre
CIB	International Council for Building
CSA	Standards Council of Canada

Symbol	Meaning
CSTB	*Centre Scientifique et Technique du Bâtiment*
ČSN	Czech State Norm
EN	European Norm
EU	European Union
EAE	European Association for External Thermal Insulation Composite Systems
EMO	European Mortar Industry Organisation
EPS	Expanded Polystyrene
EPBD	Energy Performance of Buildings Directive
EPSC	Crushed Expanded Polystyrene Package Granules
ETAG	European Technical Approval Guideline
ETICS	External Thermal Insulation Composite Systems
FE Pa	Test Procedures for Walls
FEM	Finite Elements Method
FEUP	Faculty of Engineering of University Of Porto
GF	Glass Fibre
GM	Gypsum Matrix
GHP	Guarded Hot Plate
GRP	Glass Reinforced Plastic Waste
HC	Heat-Cold
HF	Heat-Freezing
HP	Helium Pycnometry
HR	Heat-Rain
HW	Hot Wire
HumF	Humidification-Freezing
FT	Freeze-Thawing
IR	Infra-Red
IBP	Fraunhofer Institute for Building Physics
ISO	International Organization for Standardization
IUCN	International Union for Conservation Of Nature
IUPAC	International Union of Pure and Applied Chemistry
LFC	Laboratory of Building Physics

Symbol	Meaning
LEED	Leadership in Energy and Environmental Design
LNEC	National Laboratory for Civil Engineering
LiderA	Leed For The Environment
LEPABE	Laboratory for Process Engineering, Environment, Biotechnology and Energy
M	Mica
MIP	Mercury Intrusion Porosimetry
N	Nancy
NEOPOR	Grey Coloured Expanded Polystyrene
O	Oslo
OSB	Oriented Strand Board
P	Porto
P1%	1st Percentile
P99%	99th Percentile
Pe	Perlite
PP	Polypropylene
PAW	Polyamide Powder Waste
PCG	Cork Granules from Pruning and Forest Cleaning
PCM	Phase Change Materials
PFW	Polyurethane Foam Waste
PSA	Paper Sludge Ash
PVA	Polyvinyl Alcohol
PRODEC	Doctoral Programme in Civil Engineering
S	Thermal Rendering/Plastering System
S1-M	Thermal Rendering System 1 with Mineral Coating
S1-O	Thermal Rendering System 1 with Organic Coating
SBTool	Sustainable Building Tool
TR	Thermal Render/Plaster
UV	Ultra-Violet
V	Vermiculite
WUFI	*Wärme und Feuchte Instationär*
WBCSD	World Business Council For Sustainable Development

MOLECULAR FORMULAS

Symbol	Meaning
CaO	Calcium oxide
$CaClO_2$	Calcium hypoclorite
CO_2	Carbon dioxide
$NaCl$	Sodium chloride
SO_2	Sulphur dioxide
$CaSO_4$	Calcium sulfate
$Ca(OH)_2$	Calcium dihydroxide
$CaCO_3$	Calcium carbonate
KNO_3	Potassium nitrate
H_2O	Water
MgO	Magnesium oxid

1. INTRODUCTION

1.1. MOTIVATION

The realization that even well designed and built structures are subjected to the occurrence of unexpected deterioration, demands a higher focus on durability measures. As such, the methodologies for evaluating durability during the product development stage play a very important role. The durability of materials and the increase of their service life contribute to sustainability by lowering the production of waste and the emission of pollutant gases into the atmosphere.

The construction industry presents a high consumption of materials and energy (Pérez-Lombard, Ortiz and Pout 2008), with a significant impact on the emission of CO_2. According to The World Bank (2014) data, the manufacturing and the construction industries are presented as one of the main responsible in CO_2 emissions, as can be seen in Fig. 1.

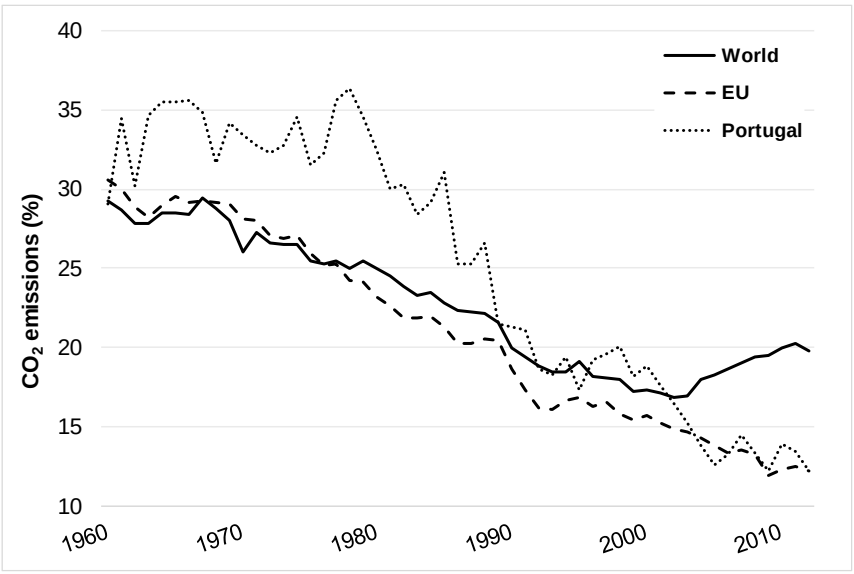

Fig. 1 – CO_2 emissions from the manufacturing and the construction industries (% total fuel combustion) (The World Bank 2014).

The data show that from 1975 onwards, CO_2 emissions in the European Union were lower than the rest of the world, with a constant decline. Portugal presents much higher and inconsistent values, at the beginning of the second half of the 20th century. However, from the '90s onwards, a significant decrease is observed and, in 2002, the emissions became lower than the rest of the world, where from 2003 to 2012 a progressive increase is registered.

As such, the construction industry, from the point of view of the durability and sustainability of products and solutions, will be one of the paths to achieve the outlined objectives. The building construction, taking into account the durability of the materials and the increase in their service life, contributes directly to the lowering of waste production, emission of polluting gases into the atmosphere and, consequently, to achieve sustainability. A sustainable building can only be considered as such when the several dimensions of sustainable development - environmental, economic and social - are envisaged during the design phase (Pinheiro 2006).

The increase of thermal demands in buildings and the changes in the European thermal regulations introduced by the revised Energy Performance of Buildings Directive (EPBD) (ECEEE 2018) imply higher thermal resistance of building envelopes. That demand is not only imposed by the limitation of the overall energy consumption of each building but also by the limitation of specific U-values. Therefore, the need to reduce the thermal conductivity of envelope materials is of major importance. In the Portuguese case, the current thermal regulation (Government of Portugal 2013) defined reference U-values for walls ranging from 0.3 to 0.4 W/(m^2.ºC), depending on the climatic region.

The demand for a better performance of walls has lead the industry to search for new solutions, evaluating the potential benefits (Dylewski and Adamczyk 2011). In the case of masonry walls, a traditional solution in south Europe countries, the optimization of masonry units geometry (Sousa et al. 2011; del Coz Díaz et al. 2007) and adoption of low conductivity materials in both masonry units (Ünal, Uygunoğlu and Yildiz 2007; Sariisik and Sariisik 2012) and renderings (Brás, Leal and Faria 2013; Ferrándiz-Mas et al. 2014) are some of the paths being pursued. Consequently, wall systems with thermal characteristics may have a potential contribution also on sustainability, which results from their contribution to the buildings energy efficiency. Also, the incorporation of recycled materials or natural and renewable raw materials leads to the achievement of a more sustainable environment. This type of materials, usually applied in a multilayer system, and also the External Thermal Insulation Composite Systems (ETICS), can combine the different layers in order to make interesting solutions in the building rehabilitation sector. As shown in Fig. 2, the construction of new buildings has slowed in the past decade. On the contrary, the rehabilitation is increasingly becoming more important in the sector. Consequently, continuous growth over the next decade is expected.

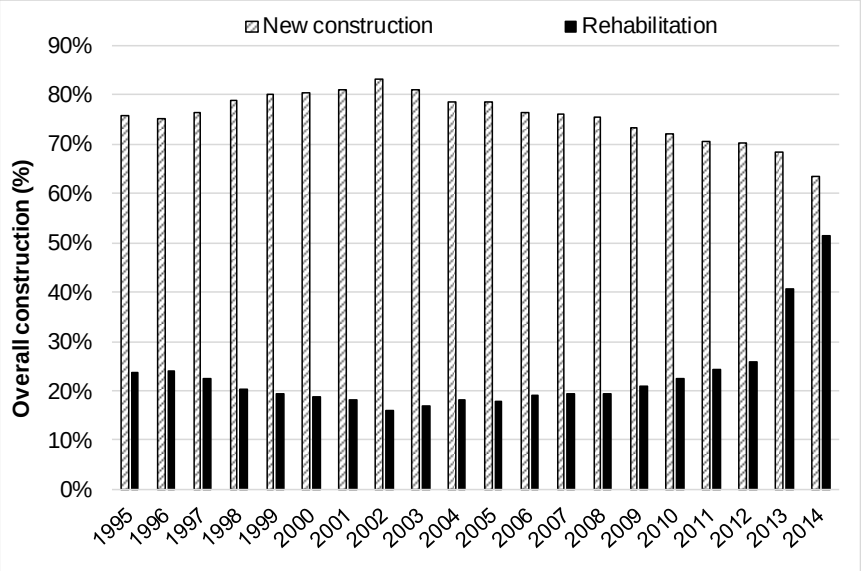

Fig. 2 – Evolution of the construction sector in Portugal, in the last decades – New construction vs. Rehabilitation (INE 2015).

Fig. 3 presents the use of dry mortars and ETICS, in Portugal, between 2008 and 2014 (APFAC 2015b).

Concerning the use of industrial dry mortars, there has been a decrease in their use in recent years. However, in 2014 there was a reversal in this trend, which may be largely related to the improvement of the economy and the increasingly significant use of technical mortars, in particular with thermal characteristics.

In terms of the application of ETICS, there is an increasing trend in their use. The period of peak economic crisis in the construction sector is observed by the stagnation in 2010-2011 and the decrease in 2012. 2013 was a turning point in this decreasing trend, related to the slight recovery of the economy and to a higher investment in the construction sector, particularly in rehabilitation.

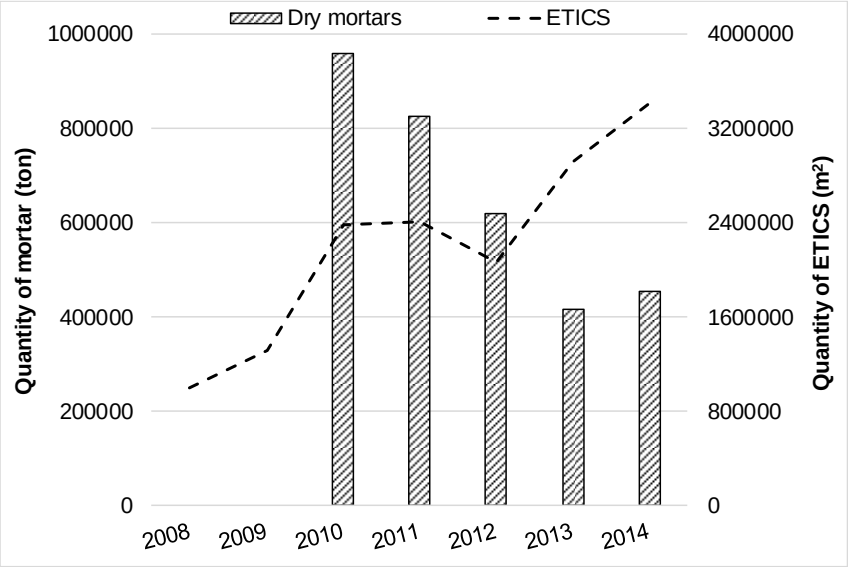

Fig. 3 – Evolution of the use of industrial dry mortars and ETICS, in Portugal (APFAC 2015b).

Fig. 4 shows a trend in the use of renders, in Portugal, highlighting the use of coloured renders.

Regarding the use of renders, their application has been declining over the last few years. However, due to a bigger focus on aesthetic issues, the growth of coloured renders between 2013 and 2014 is evident.

However, despite the growing interest in solutions with enhanced properties, the lack of knowledge in their application experience and performance can result in harmful consequences on buildings and also on users. Consequently, the durability assessment is a crucial aspect that needs further investigation.

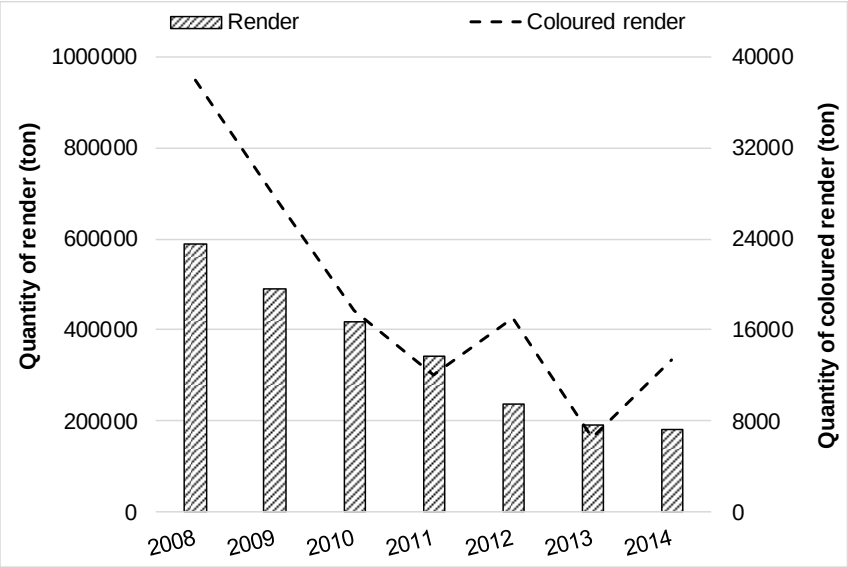

Fig. 4 – Evolution of the use of renders, in Portugal (APFAC 2015b).

1.2. OBJECTIVES

The production and application of durable thermal rendering and plastering systems lead to large gains in society, both for:

- The industry, which may present a wider range of products with proven durability and properties that evidence it;
- And the society in general, from a perspective of improving the performance of buildings, in terms of external envelope, hygrothermal conditions, energy efficiency and sustainability.

The need to guarantee that thermal rendering and plastering systems possess an adequate service life motivates the proposal of a specific research question: how should the durability of thermal rendering and plastering systems be evaluated? Therefore, the main goal of this Doctoral Thesis consists of the development and implementation of durability assessment methodologies applicable to thermal rendering and plastering systems. Regarding the thermal rendering systems, the methodology is based on the development of accelerated ageing cycles, which are implemented in industrial thermal rendering systems, and optimized by numerical simulation.

In order to reach the main objective of the Doctoral Thesis, several sub-goals were defined:

- Determine the most relevant properties – physical, hygrothermal and mechanical – of exemplary thermal rendering and plastering systems;
- Define and analyse the main degradation mechanisms in thermal rendering and plastering systems;
- Propose and demonstrate durability assessment methodologies through the implementation on exemplary thermal rendering and plastering systems.

1.3. METHODOLOGY

The methodology used to achieve this aim will be based on the analysis of the characteristics and specificities of thermal rendering and plastering systems, the related existing methodologies for the durability assessment and, throughout numerical simulation and laboratory tests, present a specific methodology for the durability assessment of this type of systems. As such, several tasks are defined:

- Review of the state of the art of:
  - Thermal renders/plasters: identify the existing standards, the most important characteristics, the existing durability assessment procedures and relevant studies from different authors;
  - Thermal wall systems: analyse other materials and systems (e.g. ETICS);
  - Degradation mechanisms: identify the main causes of degradation of thermal rendering and plastering systems;
  - Durability assessment: analyse existing durability methodologies and the related accelerated ageing cycles and experimental tests.
- Involvement of the Portuguese industry to guarantee the materials supply and technical support, enhancing the practical application of the Thesis results;
- Laboratorial test campaign for the determination of the physical, hygrothermal and mechanical properties of the different materials that compose the thermal rendering and plastering systems. Beyond the wide knowledge of the materials and the systems characteristics, these properties are necessary to a more accurate numerical simulation, since they are used as an input;
- Selection and application of numerical models for the evaluation of the hygrothermal and thermo-mechanical impact of relevant degradation mechanisms in the durability of thermal rendering and plastering systems;
- Design of adapted ageing procedures and relevant durability tests that will integrate the durability assessment methodologies;
- Laboratorial test campaign for the implementation of the durability assessment methodologies;
- Development of hygrothermal cycles, by hygrothermal simulation, adapted to the European climate context.

The methodology to achieve the main goal – development of a durability assessment methodology applied to thermal rendering systems – will be based on the evaluation of the existing methodologies for the durability assessment of similar materials. The numerical simulation (hygrothermal and thermo-mechanical) and the laboratory tests will be the key aspects of the development of the specific methodology. Fig. 5 shows the methodological plan that will be carried out in the present thesis.

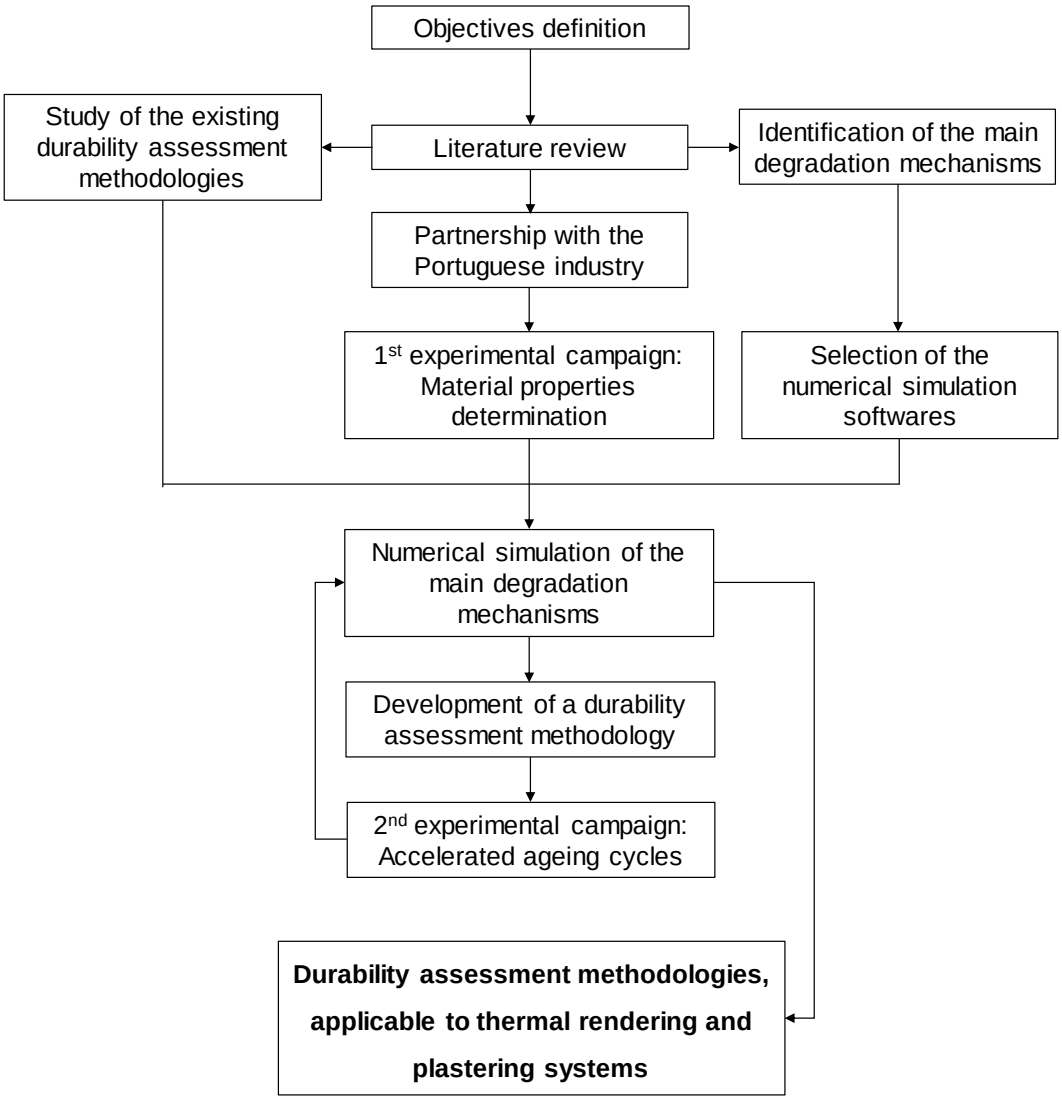

Fig. 5 – Thesis methodology.

1.4. THESIS OUTLINE

The thesis text comprises the following 6 chapters:

- Chapter 1 – presents a short introduction to the topic, definition of goals and methodology for the proposed work;
- Chapter 2 – describes the state of the art of the most important subjects studied in this thesis, focused on the defined objectives. This chapter summarises the main definitions and the standards applied to thermal renders and plasters, sustainability, eco-construction and durability assessment. The development of thermal mortars and durability assessment procedures carried out by several authors are also analysed;
- Chapter 3 – describes the experimental characterization and performance of the studied thermal rendering and plastering systems;
- Chapter 4 – refers to the numerical simulation of the main degradation mechanisms in thermal rendering and plastering systems. The analysis of the hygrothermal impact is performed using the WUFI Pro software, whereas the ABAQUS software is used to the thermo-mechanical impact assessment;

- Chapter 5 – presents the durability assessment of thermal rendering and plastering systems, based on existing durability procedures and on a new durability assessment methodology applicable to thermal rendering and plastering systems, throughout the experimental results combined with the numerical simulation. The results of the implementation of this new durability assessment methodology are shown;
- Chapter 6 – summarizes the main conclusions of each chapter and envisages the future developments.

2. STATE OF THE ART

2.1. FRAMEWORK

The present work started with a literature review in order to collect information on the state of the art in key areas for this doctoral thesis. The following sub-chapters present the state of the art in the areas presented in Fig. 6.

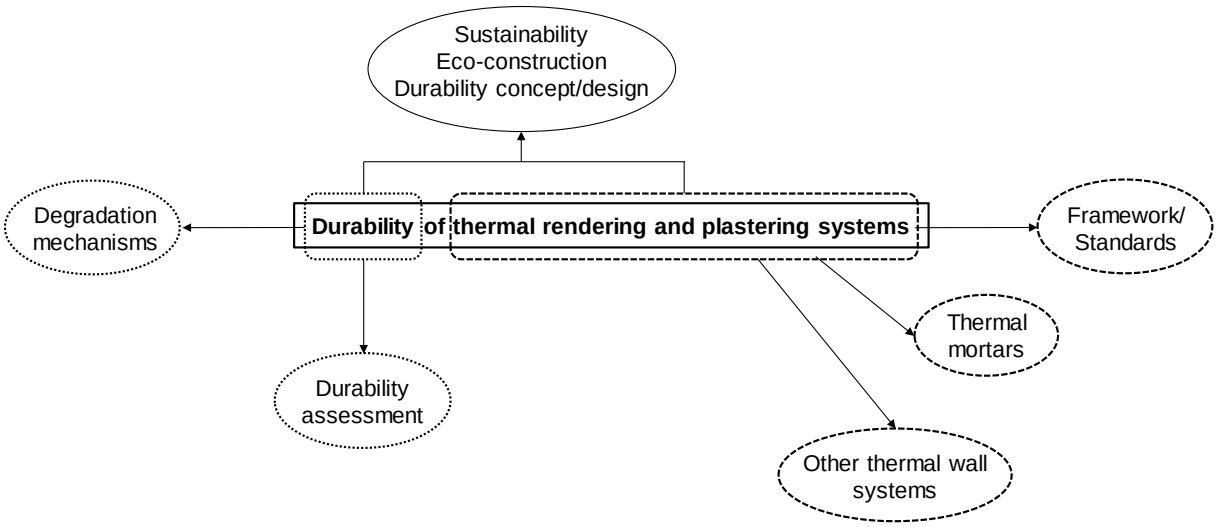

Fig. 6 – Interconnection of the different areas presented in the state of the art.

2.2. THERMAL WALL SYSTEMS

2.2.1. INTRODUCTION

Different kinds of systems can be included in the general designation of Thermal Wall Systems, such as thermal rendering and plastering systems, ETICS or other systems with enhanced thermal properties composed of different layers. Wall systems are usually applied in different layers, which properties are enhanced to achieve particular characteristics. Currently, thermal renderings and plasterings and ETICS are systems with thermal enhanced properties that lead to the reduction of the thermal transmission of the façades (where they are usually applied). However, their application history is recent, being mortars the main coating of the façades.

Mortars consist of a mixture of a binder with an aggregate. Mortars are one of the oldest building materials, which the main function was to join the masonry elements (e.g. stone and brick). Besides this

function, they were also widely used as render/plaster (protection of building elements, aesthetic purposes and substrate for frescoes), floors, ceilings, mosaics and tiles. Mortars may have different characteristics in terms of binder combination, type and size of aggregate and the binder/aggregate ratio, in order to guarantee specific construction requirements (Borges, Santos Silva and Veiga 2014).

Historically, mortars have been used for thousands of years for the construction of walls, fences and coatings, with a preference for the use of lime and gypsum binders, with additions of rye flour, rice gluten, lard, milk curd, malt and other glutinous materials (Salavessa et al. 2013).

Regarding the use of coatings in construction, their origins are not precisely known. Alvarez, Sequeira and Costa (2005) verified the use of mortars since the X a.C. century, in Galilee, with the presence of lime and gypsum in buildings. In the VIII a.C century, hydraulic mortars were found in cisterns, in Jerusalem. At the same time, XVII a.C, in Çatal Hüyüc in Turkey, the use of gypsum as a plaster was seen. The Greek and Roman peoples used calcined limestone. However, because lime did not harden under water, the Romans included crushed lime and volcanic ash, a natural pozzolan, or crushed baked clay tiles, which conferred hydraulic properties. Activated silica and alumina present in the ashes and tiles combined with lime resulted in the well-known pozzolanic cement (Barbero Barrera 2011).

During the Middle Ages and the Renaissance, although the use of hydraulic binders had slowed down, they continued to be used in pavements and foundations. However, the selection of the materials was not as careful as previously done (Borges, Santos Silva and Veiga 2014). At the end of the Middle Ages, there was a partial recovery of mortar application techniques, promoted by the development of large Gothic cathedrals, with the application of lime mortars as a binder and also as a mosaic adhesive (Barbero Barrera 2011).

According to D'Orazio and Stazi (2006), in the XVII and XVIII centuries, mortars were characterized by their complexity, since they are constituted by different layers. These layers were composed of different materials, which had different microstructures, responsible for the moisture transfer control.

In the 19th century, Leitão (1896) described the use of two different layers, both with gypsum and lime in their constitution. However, these layers presented different characteristics, since one was applied as a base coat and the other as a finishing coating, in the interior. In 1856, Desachy patented a fibrous mortar that had in its constitution calcium sulfate, burnt or boiled gypsum with jute fibre (Millar and Bankart 2009), also for application as an inner coating. Only in 1830, Louis Vicat demonstrated the existing relation between the hydraulic characteristics of mortars and the presence of clay in limestone. The Industrial Revolution period proved to be a time of great developments of methods and techniques for the production of new products, like cement, which would become one of the most used hydraulic binders (Silva 2013).

The factory production of mortars occurred in the 20th century, around the 1930s, in Germany and also in the United Kingdom, where the dry mix of binders and aggregates was performed to be delivered on site. In Portugal, the production of industrial mortars only occurred in the 1980s (Duarte 2015).

Concerning thermal renders, they emerged and were widely applied in Europe in the 1980s. According to data from the *Centre Scientifique et Technique du Bâtiment* (CSTB) in France, at that time there were certified solutions with Avis Technique (CSTB 2016). In Spain, according to the Institute of Construction Sciences Eduardo Torroja, in 1988, renders with lightweight aggregates with Technical Competence Document, classified as thermal correction systems arised (IETcc 2016).

Thermal insulation mortars are coating products with improved thermal performance and low density (below 600 kg/m^3), obtained by introducing lightweight aggregates (Veiga 2010). They are usually applied as a multilayer system, which can have different constitutions. Fig. 7-a) presents an example of

a multilayer system. Normally, thermal rendering systems have at least two different layers: thermal render and finishing coating. The thermal render layer is applied with a relatively high thickness (at least 4 cm), which varies according to the required thermal performance. Beyond the regularization function of the base coat, the finishing layers provide greater resistance (hygric and mechanical) to the final system. Usually, to achieve higher mechanical resistance a glass fibre mesh is included. Thermal renders are usually applied by mechanical spraying, as shown in Fig. 7-b).

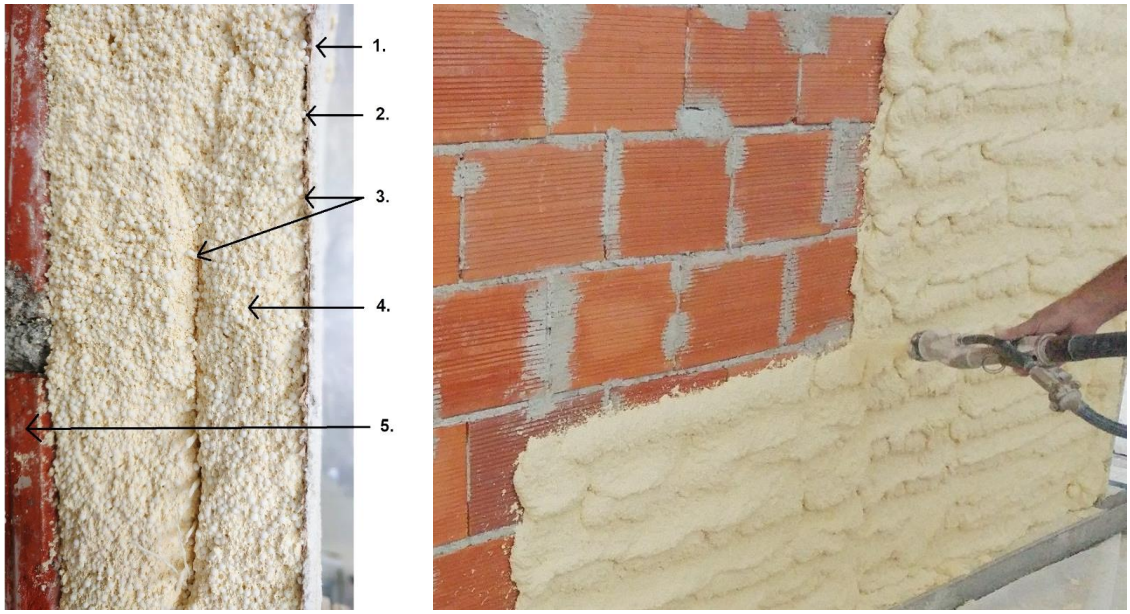

a) b)

Fig. 7 – a) Example of a thermal render system: 1. Finishing coat; 2. Base coat/finishing render; 3. Glass fibre mesh; 4. Thermal render; 5. Substrate; b) Application of thermal render by mechanical spraying.

Thermal renders are addressed in the standard EN 998-1:2010 (CEN 2010), with the designation of *Thermal Insulating Mortar* and are divided into two categories: T1 (thermal conductivity $\leq$ 0.10W/m.ºC) and T2 (thermal conductivity $\leq$ 0.20W/m.ºC). Table 1 presents the requirements applied to thermal insulating mortars according to the referred standard.

The EN 998-1 standard refers to the standard EN 1015-21 for durability test methods in mortars (CEN 2002a). However, this standard is only applicable to rendering and plastering mortars, not taking into account the different material layers (system as a whole).

Considering gypsum-based plasters, the standard EN 13279-1:2008 (CEN 2008) classifies thermal plasters as C4 – thermal insulation plaster – included in the group of gypsum plasters for special purposes. Initial setting time is the only defined requirement (> 20 min) and the manufacturers are advised to verify the thermal insulation properties by means of suitable methods (described in the referred standard).

Table 1 – Requirements applied to thermal insulating mortars according to EN 998-1 (CEN 2010).

Material properties	Test procedure	Requirement
Dry bulk density (kg/m^3)	EN 1015-10	Declared value
Compressive strength (category)	EN 1015-11	CS I: 0.40 to 2.50 N/mm^2 (28 days) CS II: 1.50 to 5.00 N/mm^2 (28 days)
Adhesive strength (N/mm^2 and fracture pattern)	EN 1015-12	≥ Declared value and fracture pattern
Adhesive strength, after ageing cycles (N/mm^2 and fracture pattern)	EN 1015-21	-
Capillary water absorption	EN 1015-18	W1: C ≤ 0.40 kg/m^2.min$^{0.5}$
Water penetration depth, after capillary water absorption test (mm)	EN 1015-18	-
Water permeability, after ageing cycles	EN 1015-21	-
Water vapour diffusion factor (for exterior application)	EN 1015-19	≤ 15
Thermal conductivity (average values)	EN 1745:2002	T1 ≤ 0.10; T2 ≤ 0.20 (W/m.ºC)
Reaction to fire (class)	EN 13501-1	>1% de organic materials – according to EN 13501-1 and declared class < 1% - class A1 (no test required)
Durability	-	Freeze-thaw behaviour

In addition to the thermal rendering systems, there are other multilayer systems, such as the External Thermal Insulation Composite Systems (ETICS). ETICS is one of the types of thermal insulation solutions applicable in exterior walls. This type of system can be applied to masonry walls (e.g. made of bricks, concrete blocks or autoclaved cellular concrete blocks) or in concrete walls (in situ or prefabricated concretes) (LNEC 2010b). Fig. 8-a) presents an example of an ETICS fixed by an adhesive mortar (usually is the same as the base coat). In Fig. 8-b), another ETICS fixation mechanism is shown. The mechanical fasteners allow a direct contact with the substrate.

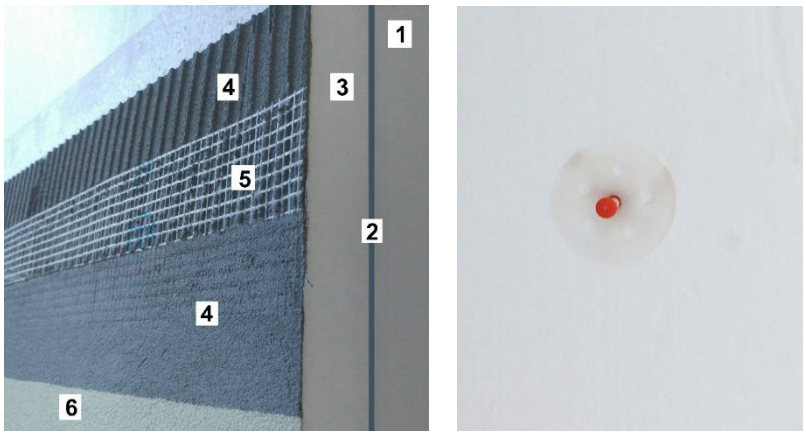

a) b)

Fig. 8 – Example of an ETICS: a) 1: Substrate; 2: Adhesive mortar; 3: Thermal insulation; 4: Base coat; 5: Glass fibre mesh; 6: Finishing coating; b) Fixation through mechanical fasteners.

Historically, in the 1940s, after World War II, in Sweden, a thermal insulation system applied to exterior façades, consisting of mineral wool and a cement and lime-based mortar, emerged. According to some authors, the development of an ETICS with expanded polystyrene and similar to the currently existent systems will appear later by the responsibility of Edwin Horbach. In the United States of America, also in the '60s, a system similar to the ETICS was introduced but adapted to the constructive reality of the country (Freitas and Miranda 2014).

ETICS is a widely used solution throughout Europe since the 1960s, both in new construction and rehabilitation. In the mid-1980s, this system was applied in Portugal, but the associated pathologies led to its disuse for some time. It was not until the early 1990s that the introduction of ETICS in our country was widespread. Fig. 9 shows the evolution of ETICS in Portugal.

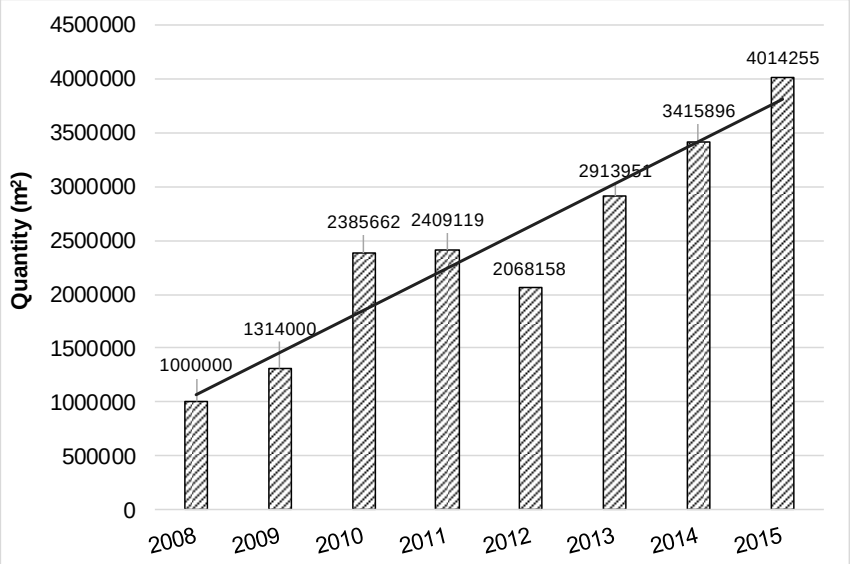

Fig. 9 – Evolution of ETICS in Portugal (APFAC 2015b).

It is possible to observe a great increase in the use of ETICS in 2010, as it is a solution of technical and economic interest, directly related to thermal requirements. A growing trend can be observed, with a significant increase after 2012.

The European Guide ETAG 004 - Guideline for European Technical Approval of External Thermal Insulation Composite System with rendering (EOTA 2013) provides a comprehensive guide for the testing and evaluation of ETICS performance. A significant number of these systems already exist on the national market with European Technical Approval (LNEC 2016b) or with National Approval Document (LNEC 2016a).

2.2.2. BINDERS AND LIGHTWEIGHT AGGREGATES

In order to better understand the measured properties of the different materials, some relevant concepts related to binders and lightweight aggregates that constitute the thermal render systems are presented.

According to EN 197-1 “cement is a hydraulic binder, i.e. a finely ground inorganic material that, when mixed with water, forms a paste that sets and hardens due to hydration reactions and processes and, after hardening, keeps its mechanical strength and stability under water” (CEN 2000a). Being a hydraulic

binder means that it both sets in air and in water, being durable in the two different environments. As such, cement is the most used hydraulic binder by the mortar industry, due to its properties and also its economic cost-effectiveness. Cement results from the cooking of a mixture of limestone, marl and clay, which is subjected to temperatures between 1400 and 1500 °C, resulting in a mass called clinker. The final processing consists on the fine grinding of the clinker, the additions to control the setting time and other additives (limestone "fillers", fly ashes, steel slags, etc.), which will origin several types of cement (Gomes, Pinto and Pinto 2013b).

One of the oldest inorganic binders results from the cooking of limestone, mainly composed of $CaCO_3$, abundant in nature. The calcination of pure limestone gives rise to calcium oxide, which constitutes lime, while the calcination of marly limestone originates hydraulic limes depending on the content of clay and natural cement (Coutinho 2002). Lime was the most used binder in the constructions until the 19th century, being later replaced by hydraulic lime and then by Portland cement. To obtain lime, the limestone is subjected to temperatures between 850 and 1100 °C, resulting in calcination or decarbonation of the raw material and the formation of quick lime (calcium oxide and magnesium oxide). The chemical reaction of the transformation of calcium carbonate into calcium oxide, which occurs at about 894 ° C, corresponds to the dissociation of calcium carbonate into calcium oxide and carbon dioxide (Coutinho 1988). Hydraulic lime is a hydraulic binder that results from the calcination of limestone, with a content of clay between 5 and 20%. The presence of clay in the limestone allows the production of silicates and calcium aluminates, which give the hydraulic characteristics to lime and, therefore, the ability to harden both in dry and moisture conditions. For the production of hydraulic lime, the calcium carbonate and clay must be brought to temperatures around 1200ºC to 1300ºC, necessary for the calcination. Hydraulic lime presents higher mechanical strength than lime but lower than cement (Gomes, Pinto and Pinto 2013a).

Gypsum is produced from the gypsite mineral, which exists in several places and has numerous applications, due to its ease of dehydration and rehydration. This mineral is a calcium sulfate bihydrate ($CaSO_4$ $2H_2O$). Gypsite is a low-strength mineral that dehydrates partially under the action of heat (125-180 °C), losing three-quarters of the water of crystallization, resulting in a hemihydrated compound known commercially as gypsum ($CaSO_4$ $1/2H_2O$ – calcium sulphate hemihydrated). The mixture of gypsum with water gives rise to a paste, which has a short setting time as a result of its hydration (CETEM 2005).

One of the most used non-natural lightweight aggregates is EPS (expanded polystyrene), which consists of a polymer – polystyrene – which after expanded presents a cellular structure, containing closed air voids. During the manufacturing process, it is possible to define some properties as the density, usually between 10 and 30 kg/m^3, which influences most of the properties. Although being a lightweight material, it presents good mechanical resistance. EPS has good thermal properties, is economically viable and almost impermeable to water (ACEPE 2014) (Futureng 2016).

A lightweight aggregate widely used in Portugal is cork, presenting a cellular structure, with non-linear elastic behaviour and good compressibility, without rupture, which results in an efficient mechanism of energy dissipation. In addition to good mechanical properties, cork presents good characteristics as thermal and acoustic insulation and low water permeability (Brás, Leal and Faria 2013). The air voids created by the cork cells present an important role in their properties (Pereira 1979). The cells consist of a thin internal wall (lignin-rich middle lamella), a thick secondary wall constituted by alternated suberin and wax lamella and a thin tertiary of polysaccharides. Suberin gives compressibility and elasticity characteristics to cork, while, polysaccharides provide structural rigidity to the cork cell. The wax acts as a water repellent, contributing to the improvement of hygric properties (Silva et al. 2005).

2.2.3. THERMAL RENDERS AND PLASTERS

Previous work of different authors, on the laboratory characterization of hardened thermal insulating mortars, focused not only on standard properties but also on additional ones. In the study described in (Brás, Leal and Faria 2013), an EPS and cork cement mortars comparison was based on the results of flexural and compressive strength, open porosity and pore size distribution, capillary water absorption and thermal conductivity. The study of mortars containing EPS and paper sludge ash (PSA) (Ferrándiz-Mas et al. 2014) explored the reduction of thermal conductivity and compressive strength, compared to control mortars. Also in (Dylewski and Adamczyk 2014), the authors checked whether it is beneficial to use of EPS render on the external walls of the building instead of cement render.

The study of mortar containing waste cork conducted in (Panesar and Shindman 2012) identified a thermal conductivity reduction influenced by the percentage of cork and not by the cork size and cork gradation. The concern with hygric properties in addition to the thermal behaviour of plasters can be found in other contributions (Mazhoud et al. 2016; Stahl et al. 2012), stressing the importance of a holistic view for the correct evaluation of product performance.

Thermal renders and plasters continue to awaken the interest of the researchers (Borges, Flores-Colen and de Brito 2018; Soares et al. 2018; Westgate, Paine and Ball 2018; Nosrati and Berardi 2018) and the manufacturers (Saint-Gobain Weber 2016; Sival - Gessos Especiais 2017; Secil Argamassas 2017; Fassa Bortolo 2017).

Therefore, the following subchapter presents a summary of some research works developed by several authors, about thermal renders, which have in their constitution cement, cement and lime or gypsum binders.

2.2.3.1.Cement and lime based mortars with thermal characteristics

Several authors studied the development of mortars with thermal enhanced properties, using traditional binders like cement and lime. Expanded polystyrene (EPS) and cork are of the most common used lightweight aggregates.

Šeputyte-Jucike et al. (2014) studied the use of crushed expanded polystyrene package granules (EPSC), a lightweight porous aggregate, in the composition of thermo-insulating mortars. Its effectiveness is compared to that of spherical granules of expanded polystyrene – white coloured (EPS) and grey coloured (NEOPOR). The investigation focused on relevant properties, such as density, compressive strength, thermal conductivity and water vapour permeability. The EPSC content added to the thermo-insulating mortar higher than 1.25 lt/kg of dry mix of mortar, ensures the CSI class strength (compressive strength of 0.4 MPa for the mortar containing only 10% of Portland cement). It was established that EPSC in the above mentioned quantity improves the material properties in comparison with a mortar without lightweight aggregates (current lime-cement mortar) in the following way:

- Thermal conductivity coefficient – from 0.25 to 0.13 W/m.ºC;
- Water vapour resistance – from 11.2 to 6.2;
- Density – from 1350 to 620 kg/m^3.

In their paper, Dylewski and Adamczyk (2014) checked whether it is beneficial to use thermal insulation bims granules (resulting from freezing basalt lava mixed with volcanic gases (water vapour and carbon dioxide) and ash) or EPS as lightweight addition in renders to apply on external walls of buildings instead of a cement mortar in particular (see Table 2).

Table 2 – Properties of cement, bims granules and EPS mortars studied by Dylewski and Adamczyk (2014).

Properties/Mortar	Cement	Bims granules	EPS
Density (kg/m^3)	1600	334	200
Thermal conductivity (W/m.ºC)	0.930	0.068	0.070
Adhesion (N/mm^2)	0.50	0.46	0.08
Vapour resistance factor (after 120 days)	10	4.8	10

Bims granules mortar presents better mechanical properties compared to EPS addition, and similar to the cement mortar. Besides, it has a far smaller density and is characterized by very good adhesion. Presents also good thermal insulation properties comparable with typical thermal insulation materials.

Brites, Frade and Santos (2014) intended to present an evolution to the current thermal mortars available in the Portuguese market, by using different types of binders and different lightweight aggregates. Table 3 presents some comparative results of the developed mortars, evaluating the thermal performance, but also the mechanical resistance.

Table 3 – Properties of thermal mortars studied by Brites, Frade and Santos (2014)

Mortars/ Properties	Dry bulk density (kg/m^3)	Thermal conductivity (W/m.ºC)	Young modulus (MPa)	Flexural strength (MPa)	Compressive strength (MPa)	Capillary water absorption (kg/(m^2 min$^{0.5}$)
White cement, hydrated lime and EPS (Formulation A)	294	0.0774	216	0.3	0.5	0.16
White cement, hydrated lime and EPS (Formulation B)	227	0.0559	159	0.5	0.3	0.20
Hydrated and hydraulic lime and EPS	285	0.0627	164	0.2	0.3	0.07
White cement, hydrated lime and expanded silica	406	-	561	0.5	0.9	-
White cement, hydrated lime and expanded glass	544	0.1286	2173	2.0	5.0	-

It was verified that mortars with EPS addition present good thermal properties, classified as T1, and also a low capillary absorption, classified as W2, by the EN 998-1 (CEN 2010). Mortars with expanded silica and expanded glass present better results in terms of mechanical strength, but thermal conductivity and bulk density higher than the mortars with EPS addition. All mortars present, in general, satisfactory results to be classified as thermal mortars. The 2nd and 3rd formulations present a compressive strength

below the minimum requirements (0.4 MPa), but the other properties are generally better than the remaining formulations.

The work presented by Vale et al. (2014) performs an analysis of the mechanical and physical properties of four industrial thermal mortars, compared to two other mortars produced in a traditional way. These mortars incorporate lightweight aggregates with enhanced thermal properties. Table 4 presents some of the properties obtained for the studied thermal plasters.

Table 4 – Properties of industrial and traditional thermal mortars measured by Vale et al. (2014).

Mortar/ Properties	Dry bulk density (kg/m^3)	Thermal conductivity (W/m.ºC)	Capillary water absorption ($kg/(m^2 min^{0.5})$)	Tensile strength (MPa)	Compressive strength (MPa)	Young modulus (MPa)
Cement (reference)[2]	1885	1.34	0.74	3.43	16.14	15140
Lime/Cement + 100%EPS[1]	237	0.06	0.92	0.21	0.36	70
Lime/Cement + 70-80%cork[1]	432	0.10	0.31	0.77	1.25	620
Cement + 70-80%cork[1]	863	0.23	0.13	1.89	4.44	2110
Natural hydraulic lime + cork[1]	642	0.14	0.67	1.13	2.10	1160
Cement + 80%cork[2]	855	0.27	0.64	1.15	2.08	1420
Cement + 85%EPS[2]	683	0.28	0.23	0.88	2.30	2020

[1]Industrial mortar; [2]Traditionally-produced mortar.

It was found that a high percentage of lightweight aggregates addition (above 70%), significantly affects the mechanical performance. Although this decrease, these mortars are classified as CSI or CSII, owing to the incorporation of additives that improve those characteristics.

The study developed by Sousa, Frade and Santos (2014) refers to innovative solutions, applied to industrial mortars, using cork, as lightweight aggregate, and natural hydraulic lime as a binder. Thus, the authors sought to optimize the thermal, acoustic and hygrothermal characteristics with the use of these two materials. Table 5 presents the measured properties for the characterization of the thermal mortars. The developed mortar shows interesting results in terms of thermal conductivity and density (low values), with relatively good mechanical strength and cohesion fracture in the mortar itself.

Table 5 – Properties of a thermal lime based-mortar with cork addition studied by Sousa, Frade and Santos (2014).

Material properties	Mortar
Dry bulk density (kg/m^3)	600
Thermal conductivity (W/m.ºC)	0.1
Open porosity (%)	46.6
Capillary water absorption (kg/(m^2 min$^{0.5}$)	0.27
Adhesion (MPa)	0.1
Flexural strength (MPa)	0.4
Compressive strength (MPa)	0.78
Dynamic modulus (MPa)	< 600

Since cork presents numerous advantages as a lightweight addition, its incorporation in mortars stirred the interest of several authors.

Panesar and Shindman (2012) examined the impact of cork used as sand or aggregate replacement on the mechanical, transport, microstructural and thermal properties of mortars and concrete, which were prepared to take into account the percentage of cork, cork size, and the cork mixture. The addition of 10% of 0.5-1 mm cork granules used as a sand replacement led to a cube strength of 24.3 MPa for cement-cork composites. For cork granules bigger than 5 mm, a reduction in the cube strength and an increase in the total porosity are observed. The high cube strength could be due to a lower capillary pore volume. In terms of the thermal behaviour, the concrete-cork composites show a reduction of the thermal conductivity, as the concrete density decreases. The concrete-cork composites, containing 20% cork, present a greater thermal resistance (in 46%) comparing to the concrete without cork. The thermal conductivity varies with the percentage of cork, which is attributed to the direct relation between cork density and the concrete-cork composite density. The dimension of the cork granules led to different mechanical and transport properties since finer granules allow to a better performance. However, the durability performance could be compromised due to the higher water permeability.

Cherki et al. (2014b) contributed to a better understanding of the thermal behaviour of the composite material based on granular cork embedded in white cement. The experimental study of the developed material presents its thermal properties and then compare them with a control material (without cork). Table 6 presents the experimental results analysing the white cement without cork addition and three different specimens with granular cork size variation.

Table 6 – Density and thermal conductivity of white cement mortar with different cork additions measured by Cherki et al. (2014b).

Granular cork size	Density (kg/m^3)	Thermal conductivity (W/m.ºC)
White cement (0%cork)	1571.0	0.860
5mm-6.3mm	876.5	0.308
6.3mm-8mm	861.5	0.306
8mm-12.5mm	821.5	0.300

The results allow concluding that the developed material is two times lighter and its thermal conductivity is three times lower than the white cement without cork.

Below, other relevant studies on the development of new mortars with the incorporation of lightweight aggregates or with significant properties are presented. Despite the decrease of thermal performance, these mortars highlight the effect of these additions on other important properties.

Degirmenci and Yilmaz (2009) investigated the use of diatomite as a partial replacement for cement in the production of cement mortar. Diatomite was used at 5%, 10% and 15% replacement by weight for cement while sand and water quantities were kept constant. Compressive and flexural strength, freeze-thaw resistance, sulfate resistance, water absorption and dry unit weight of the mortars were determined. The mechanical strength of the mortar decreased with increasing diatomite content. Diatomite replacement generally increased the compressive strength of the mortar except for 5% diatomite content after 25 freeze-thaw cycles. 10% and 15% diatomite replacement presented better durability to freeze-thaw ageing cycles. This result may be attributed to the filler effect of the diatomite. The water absorption decreased with the increase of diatomite content except for the mortar containing 15% diatomite, which is related to the porous nature of diatomite. According to the test results, it was suggested that diatomite can be used up to 5% as replacement of Portland cement in the production of cement based-mortars. In recent years, studies regarding the incorporation of diatomite in both cement and lime mortars were also stated (Xu et al. 2014; Ahmadi et al. 2018). In Portugal, the interest in using Portuguese diatomites as a mineral addition of mortars has been highly explored (Tavares et al. 2016; Costa et al. 2018).

In Ferrándiz-Mas and García-Alcocel (2013), the objective was to develop lightweight cement mortars with good thermal-insulation properties by incorporating recycled expanded polystyrene (EPS) and paper sludge ash (PSA), both of which are problematic waste materials. Two different types of EPS were used: ground and powdered. The differences between the two types of EPS are mainly related to the particle size. Mortars containing PSA and EPS had lower thermal conductivity than control mortars (cement mortars). For example, the thermal conductivity of mortars containing 30% PSA was reduced by 70% (with ground EPS) and 68% (with powdered EPS) compared to cement mortars. Bulk densities of mortars also reduced with PSA and EPS. In the case of mortars containing 30% PSA, densities were reduced by 45% (with ground EPS) and 42% % (with powdered EPS). Ground EPS reduce thermal conductivity, bulk density and compressive strength more than an equivalent amount of powdered EPS. Mortars containing up to 20% PSA, and either powdered or ground EPS are suitable for type CSIII rendering and plastering applications in Europe. For type CSII applications, mortars containing up to 30% PSA (with powdered EPS) and up to 20% PSA (with ground EPS) are appropriate. For type CSI applications, mortars containing between 30% and 60% PSA (for ground EPS) and between 40% and 50% PSA (powdered and ground) are suitable. EPS and cork additions were chosen by Brás, Leal and Faria (2013) for the production of lightweight cement based-renders since their properties are well known. The objective of this article was to demonstrate the advantage of the use of cork addition when compared to EPS addition. Several properties in the fresh and hardened state, such as rheological, mechanical, microstructure and thermal behaviour, were studied. Six contents of cork and EPS were used (10%, 20%, 40%, 50%, 70% and 80%) and then compared with control mortars. Since the mechanical strength decreases with higher cork or EPS additions, the appropriate type and size of the cork granules should be taken into account. Analysing the microstructure of the mortars, it was verified that the mechanical properties of the cement-cork mixtures are not controlled only by the low density of the cork, but also by the interaction of the cork granules with the cement hydration process. The mortars with EPS addition show that an increase in the percentage of EPS did not contribute to the reduction of thermal conductivity directly compared to the addition of cork. This allowed a reduction in the thermal

conductivity of a cement-based mortar in 75%, while with the EPS decreased by about 60%. Regarding the transient state performance, the mortars with cork addition showed a lower thermal variation when compared to the EPS mortar. This means that the thermal delay caused by the cork is greater than that caused by EPS.

Besides the enhancement of incorporating lightweight aggregates, several authors seek the use of materials that contribute to better mechanical properties and sustainable mortars.

Çavdar (2012) analysed four different types of fibres to incorporate in cement mortars with the aim to investigate their mechanical behaviour under high temperature. Polypropylene (PP), carbon (CF), glass (GF) and polyvinyl alcohol (PVA) fibres were added to cement mortars in five different ratios (0.0%, 0.5%, 1.0%, 1.5% and 2.0% by volume) and the mortars subjected to 21ºC (normal conditions), 100ºC (dry oven), 450ºC and 650ºC. The temperature increase leads to the weakening of the cement matrix, resulting in the occurrence of cracks at 450ºC and 650ºC. The higher the temperature the lower the flexural strength of the non-fibrous mortars (decreasing about 76% at 450ºC and about 87% at 650ºC). However, all the fibrous mortars decrease on average about 60% at 450ºC and about 88% at 650ºC, which means that these fibres are active especially up to 450ºC. Considering the different temperature conditions, the highest increase in flexural strength and the lowest decrease in compressive strength is obtained with 0.5-1.5% CF addition. The optimum fibre addition ratio, of the samples containing PP and GF, is 0.5%, by volume, and between 0.5% and 1.5% by volume, containing PVA.

The use of industrial and construction wastes could be another way to achieve certain required properties and at the same time reducing the ecological footprint. Braga, de Brito and Veiga (2012) studied the performance of cement-based mortars with the incorporation of very fine aggregates from concrete recycling. The experimental program consisted of two distinct phases. In the first one, different mortar compositions were tested, with different sand replacement ratios for fine aggregates of recycled concrete (5%, 10% and 15%), to choose the one with better results. In the second phase, several tests were performed. Table 7 presents the measured properties, for hardened mortars, in the first phase of the experimental tests.

Table 7 – Obtained results from the first phase of the experimental campaign, for hardened mortars (Braga, de Brito and Veiga 2012).

% Addition	Bulk density (kg/m^3)	Flexural strength (MPa)	Compressive strength (MPa)	Water absorption ($kg/(m^2 \, min^{0.5})$)
0 (control)	1725.8	1.36	3.91	1.270
5	1754.6	1.67	5.40	0.905
10	1799.6	2.12	7.67	0.764
15	1814.5	2.71	8.64	0.708

It was verified that the higher the amount of recycled concrete the greater the density and the flexural and compressive strength. Another finding was that the water absorption decrease with the increase of the percentage of recycled aggregate incorporated in the mortar. As such, the sample that presented the best results was the one with the incorporation of 15% of fine particles of recycled concrete. In the second phase, evaluating the mortar with 15% of aggregate addition, an improvement of 36% of the adhesion and of 25% in the retention of water, compared with the control material, was verified. However, with respect to water vapour permeability, Young modulus and dimensional variation, the addition of concrete aggregate has a negative effect, decreasing 18%, 49% and 49%, respectively. The

authors concluded that taking into account the requirements for a coating mortar and the environmental conditions, the incorporation of recycled concrete fine aggregate could lead to improvements in its performance, contributing as well to the construction waste reduction, by reusing concrete.

Oliveira, de Brito and Veiga (2013) carried out a feasibility study of the incorporation of thin aggregates of recycled glass in cement mortars, by partial replacement of sand. The experimental program included three distinct phases. In the first one, tests to determine the most relevant properties of the materials were carried out. In the second phase, three different ratios of sand substitution by glass powder (10%, 15% and 20%) were analysed. In the last phase, more specific tests to evaluate the performance of the optimum percentage of glass powder addition were carried out. Table 8 presents the properties measured in the second phase of the experimental tests for hardened mortars at 90 days.

Table 8 – Results from the second phase of the experimental campaign, for hardened mortars (Oliveira, de Brito and Veiga 2013).

% Addition	Bulk density (kg/m^3)	Young modulus (GPa)	Flexural strength (MPa)	Compressive strength (MPa)	Water absorption ($kg/(m^2\,min^{0.5})$)
0 (control)	1770	6.30	1.44	3.33	1.57
10	1790	8.74	2.13	5.02	0.97
15	1810	10.10	2.26	6.96	0.91
20	1830	12.50	2.71	7.67	0.76

It was verified that the greater the percentage of glass powder addition, the better the properties of the mortar, being 20% the one that led to more satisfactory results and, consequently, chosen for the third test phase. This improvement may be due to the fact that the fine particles of glass fill the voids of the mortar and also to the pozzolanic reactions promoted by these particles. In the last phase, there was a 25% improvement in water retention, compared to the control mortar. For tests carried out after accelerated ageing (according to EN 1015-21), there was also a slight improvement in water permeability (43.0-23.5 mm for mortar with 20% glass powder) and adhesion (0.67 MPa-0.79 MPa for mortar with 20% glass powder). However, cracking increased by about 15% after 100 days. The authors concluded that the incorporation of glass powder as an aggregate of cementitious mortars leads to improvements in their performance compared to standard mortars and contributes to industrial waste reduction.

Tittarelli (2013) developed new possible mortars containing 2.5% and 5% of sand volume replaced by glass reinforced plastic waste (GRP) and 0%, 0.25%, 0.5% and 1% of a hydrophobic addition by cement weight. It was verified that low dosages of GRP dust addition do not significantly affect compressive strength especially in the presence of the hydrophobic admixture. However, flexural strength generally increased. It also did not significantly reduce permeability, but the thermal insulation properties were improved, for low dosages of GRP. Increasing the GRP dosage a significant increase of the vapour diffusion resistance coefficient can be seen. This addition significantly reduces the capillary water absorption of mortars, allowing halving the dosage of the hydrophobic admixture to obtain similar results.

Since lime is a binder with several years of history and a wide application, lime-based mortars also have a great impact on the construction industry. In that way, several authors developed new materials in order to get improved performances, using the mineral metakaolin as an addition to lime-based mortars.

In their work, Velosa and Veiga (2008) intended to develop a lime-based mortar, compatible with historical mortars and respective substrates. As such, the addition of metakaolin from two different manufacturers (F1 and F2) as a way of increasing the speed of application and hardening was tested. Table 9 presents the results from the experimental campaign.

Table 9 – Measured properties at 90 days (Velosa and Veiga 2008).

Sample	Young modulus (MPa)	Flexural strength (MPa)	Compressive strength (MPa)	Water absorption ($kg/(m^2 \, min^{0.5})$)
Lime:Sand 1:3	2350	0.26	0.85	2.20
Lime:Metakaolin F1:Sand 1:1:4	2600	0.38	1.20	1.35
Lime:Metakaolin F2:Sand 1:1:4	2100	0.24	0.70	1.55
Lime:Metakaolin F2:Sand 1:0.5:2.5	3000	0.40	1.30	1.60

It was possible to conclude that metakaolin is a pozzolanic addition suitable for lime mortars, improving the mechanical and water absorption characteristics. Another advantage highlighted by the authors is the low environmental impact, compared with cement-based mortars. It was also verified that a higher addition of metakaolin does not necessarily lead to better results, as it can be seen in the two metakaolin F2 samples. The sample with a lower amount of metakaolin and sand produced a more satisfactory effect on the analysed properties.

Faria, Silva and Flores-Colen (2012) performed a laboratory evaluation of natural hydraulic lime mortars with the addition of artificial pozzolans, as metakaolin, by partial replacement of lime, in order to evaluate the influence of this addition on the characteristics of lime mortars. Laboratory tests were carried out in lime mortar samples with three different types of pozzolans, under different cure conditions. The authors concluded that the curing conditions have a great influence on the characteristics obtained in the mortars, so they should be as rigorous as possible in order to guarantee the best properties. They have also found that the curing conditions may have a greater influence on the properties of the mortars than the addition of pozzolans. However, metakaolin can be beneficial for the environment and to obtain enhanced properties.

Vejmelková et al. (2012) studied several lime–metakaolin mortars, measuring a wide range of material properties. Previous studies have shown that the optimum amount of metakaolin by mass of lime was 20%. In Table 10 the measured properties of a lime-based mortar (with high purity 98.0% of CaO + MgO) with metakaolin addition are presented. The results are compared to a lime-based mortar without metakaolin addition.

Table 10 –Experimental results of a lime plaster without metakaolin and the optimum lime-metakaolin mixture Vejmelková et al. (2012).

% Addition	Density (kg/m^3)	Thermal conductivity (W/m.ºC)	μ (5/25-30% φ)	Water absorption (kg/(m^2 min$^{0.5}$)	Compressive strength (28 days) (MPa)	Bending strength (28 days) (MPa)
0 (Control)	1745	0.650	12.2	0.192	0.67	0.2
20	1767	0.731	16.3	0.151	6.73	1.9

The measured mechanical properties present a remarkable improvement compared with the control mortar. This could contribute to an increase in the durability of this type of mortars in comparison with traditional lime-based mortars. The metakaolin incorporation reduces the liquid water absorption by approximately 20% compared to the control lime mortar. Mortars using lime with high impurity proved to have the worst behaviour, especially in freeze/thaw and mechanical resistance.

2.2.3.2.Gypsum-based plasters with thermal characteristics

Another binder that has a wide range of application, in interior surfaces, is the gypsum. Several authors studied the development of new plasters with enhanced properties by incorporating lightweight materials such as cork, vermiculite and foam wastes.

Considering the incorporation of cork, Hernández-Olivares et al. (1999) describe an experimental analysis of the compatibility between cork granules and gypsum plaster, to obtain a new composite material mainly for building applications. In this concern, four types of cork granules were used, depending on their geographical origin and harvest season. The specimens were produced mixing, by mass, 80% hemihydrated gypsum with 20% cork granules of each type. Two different values of water-gypsum ratios (w/g) 0.8 and 0.6 were used to analyze their influence on the mechanical properties of the final product. Workability of w/g = 0.8 was better than that of w/g = 0.6, which is an important factor to take into account. On the other side, the bending and compression tests showed similar results for both w/g ratios (flexural strength about 2.5 MPa and compressive strength about 3.8 MPa), for all types of cork except those manufactured using winter cork granules from pruning and forest cleaning (PCG) (flexural strength 3.52 MPa and compressive strength 6.58 MPa). This cork type contains a great amount of small vegetable fibres that contribute to increasing the mechanical strength. Nevertheless, this better mechanical behaviour of PCG cork-gypsum composites, has the counterpart of higher density, because of the higher content on soil waste in the cork. To improve the mechanical behaviour of these composites, 2% by mass of short glass fibres were mixed with gypsum-cork (only PCG granules). This small addition of short glass fibres produces quite remarkable increases on both flexural and compressive strength (flexural strength 7.19 MPa and compressive strength 7.94 MPa). Such a remarkable increase in mechanical strength may be mainly attributed to the glass fibre strength, and not to the bonding between the hardened gypsum and glass fibres, which is poor. On the other hand, it is difficult to avoid clustering phenomena between the glass fibres, which is detrimental to the final mechanical properties of the gypsum-cork-glass fibres composites. Concerning the evaluation of thermal conductivity, specimens were manufactured by mixing winter cork granules, hemihydrated gypsum and water at w/g=0.8 ratio in such proportions to obtain three different density and, consequently, different thermal conductivity, as can be seen in Table 11.

Table 11 – Density and thermal conductivity of gypsum-cork plasters developed by Hernández-Olivares et al. (1999).

Density (kg/m^3)	Thermal conductivity (W/m.ºC)
578	0.126
600	0.187
864	0.200

A correlation between the density and thermal conductivity can be observed. Moreover, these measured values allow classifying the materials as thermal insulation plasters T2, according to EN 998-1 (CEN 2010).

Cherki et al. (2014a) determined the thermal properties of a cork-gypsum composite with different size categories of granular cork, to verify if the grain size has an effect on thermal properties. This study shows that increasing the granular cork size reduces the density and, consequently, the thermal conductivity. In addition, comparing this gypsum-cork plaster with a standard gypsum plaster (without cork) it is observed that the density is reduced by half and the thermal conductivity by one-third (see Table 12).

Table 12 – Density and thermal conductivity of gypsum-cork plasters, with different cork granules size, developed by Cherki et al. (2014a).

Granular cork size	Density (kg/m^3)	Thermal conductivity (W/m.ºC)
Gypsum plaster (without cork)	801.76	0.299
2.5mm-5mm	472.14	0.124
5mm-6.3mm	452.13	0.113
6.3mm-8mm	447.34	0.110
8mm-12.5mm	447.32	0.101

Another study carried out by (Maia et al. 2015) consists of experimental characterization of a thermal plaster with granulated cork incorporation. Some hygrothermal tests and subsequently ageing tests under severe conditions were carried out. With the inclusion of cork granules, the material density declined significantly, compared with a traditional gypsum plaster (approximately 1100 kg/m^3 to 600 kg/m^3), which results in a reduction of almost 50% of the thermal conductivity (0.25 to 0.11 W/m.ºC). This material presents also higher hygroscopicity than a traditional gypsum plaster, by the adsorption curves analysis. Concerning the mechanical resistance, a cohesive fracture pattern is observed, with 0.1 MPa and 0.2 MPa for concrete and masonry substrates, respectively. The heat/cold cycles, performing an accelerated ageing test, have not produced a significant reduction in pull-off resistance. However, the accelerated ageing test with heating/freezing cycles resulted in a considerable reduction on pull-off resistance in masonry substrate specimens.

Vermiculite is a mineral that could have a low density and improved thermal properties under the exfoliated form. The exfoliation process converts the dense flakes of vermiculite into lightweight porous granules containing innumerable minute air layers. Melo et al. (2012) presented a solution for improving

the energy efficiency in buildings using local building materials (northeast of Brazil), such as gypsum and vermiculite, to develop a gypsum based mortar with vermiculite incorporation. Some thermal properties were measured and the obtained values were recorded (see Table 13).

Table 13 – Thermal properties obtained for a gypsum-vermiculite plaster by Melo et al. (2012).

Thermal properties	Gypsum/Vermiculite
Bulk density (kg/m^3)	877
Specific Heat (kJ/kg/ºC)	1.443
Thermal Capacity (kJ/m^3/ºC)	1265.5
Thermal Diffusivity (x10^{-6}/m^2/s)	0.21
Thermal Conductivity (W/m.ºC)	0.30

The plasters presented good thermal properties, with low thermal conductivity, taking into account the obtained density. In addition, it presents a great advantage in terms of sustainability, since the transport cost is reduced by using local materials.

Another study carried out by de Oliveira et al. (2012) evaluated the mechanical and physical properties of gypsum-based composites with exfoliated vermiculite addition, from the Araripe region, in Pernambuco, in the northeast of Brazil. To determine the influence of additions rate and water/gypsum ratio on mechanical-physical properties, specimens were made using different vermiculite percentages and water/gypsum ratios. Vermiculite percentages over 25% were not used due to inadequate workability. It was verified that the adhesion between vermiculite and gypsum matrix was quite good, which reflects on a better flexural strength. The percentage of vermiculite that brings better properties proved to be 20%. The water/gypsum ratio has more influence on density and compressive strength compared with vermiculite addition.

Martias et al. (2013) also studied a gypsum-based material with minerals additions. One of the aims of this work was to measure the effective thermal conductivity as a function of the additives proportions introduced in the gypsum matrix, such as exfoliated vermiculite and muscovite (mica). Vermiculite presents low thermal conductivity (0.06 W/m.K), due to the high porosity and low density (0.1 kg/m^3). However, it has a detrimental effect on the mechanical properties. So, to overcome this disadvantage, mica was used because of its good tensile strength. Three plasters were produced: a control gypsum-based plaster, a vermiculite-gypsum plaster and a mica-gypsum plaster. Thermal conductivity was measured by the heat flow method, with results presented in Table 14.

Table 14 – Thermal conductivity of gypsum-based plasters vs. % of mineral addition determined by Martias et al. (2013).

Plaster	100%GM	95%GM + 5%V	75%GM + 25%V	95%GM + 5%M	90%GM + 10%M
Thermal conductivity (W/m.ºC)	0.58	0.46	0.27	0.66	0.67

Note: GM – Gypsum Matrix, V – Vermiculite and M – Mica.

Results show that the thermal conductivity decreases when vermiculite is added in the matrix while it remains constant with mica addition. Furthermore, this study also concluded that increasing the

percentage of vermiculite from 5% to 25% also increases the porosity by 45% whereas mica does not change the composite porosity, which remains around 40%.

In a subsequent study, Martias, Joliff and Favotto (2014) developed a gypsum-based composite for fire protection with 1 w% of glass fibres, 5 w% of vermiculite and 5 w% of mica. The composite showed a good performance to fire, presenting the required properties after 2 hours firebreak and keeping its integrity after the fire test.

Abidi et al. (2015) studied the effect of incorporating vermiculite (under exfoliated form), perlite and cement, in a gypsum matrix. As referred below, vermiculite contains a large amount of air (porosity around 90%) and perlite also presents a similar structure. Table 15 shows the thermal conductivity and porosity obtained in the different mixtures.

Table 15 – Thermal conductivity and porosity vs. % of mineral addition measured by Abidi et al. (2015).

Composite Mixture	Without addition	5%V	25%V	5%Pe	25%Pe	5%Ce	25%Ce
Thermal conductivity (W/m.ºC)	0.50	0.45	0.23	0.35	0.16	0.53	0.52
Porosity (%)	47	51	74	57	76	42	42

Note: V – Vermiculite, Pe – Perlite and Ce – Cement.

Regarding the thermal conductivity, perlite seems to be a better addition than vermiculite to enhance the thermal behaviour of plasters. Otherwise, as expected, cement has no significant effect on thermal properties.

Beyond the use of raw materials, the incorporation of wastes, as performed with other binders, is a trend in the development of mortars. Gutiérrez-González et al. (2012b) studied the properties and thermal behaviour of a gypsum-based plaster with polyurethane foam waste (PFW). Two types of polyurethane foam waste were used: one that is identified by its grey colour, a by-product from the car industry, and other that is white, which results from the manufacturing of polyurethane for thermal insulation in the construction industry. Table 16 presents some experimental results considering only the white PFW because better results were generally obtained for all properties.

Table 16 – Density, thermal conductivity and porosity vs. volume ratio (White PFW/Plaster) determined by Gutiérrez-González et al. (2012b).

Volume Ratio (PFW/Plaster)	0/1	0.5/1	1/1	2/1	3/1	4/1
Density (kg/m^3)	1477	1258	1114	879	674	535
Thermal conductivity (W/m.ºC)	0.3057	0.3160	0.2701	0.1861	0.1285	0.1039
Loss of adhesion (%)	0	2.2	19.6	56.5	65.2	73.9

Decreasing the density, with the addition of PFW, thermal conductivity also decreases, which falls by up to 66% relative to the reference material, without polyurethane foam waste. Although the decrease of the adhesion falls as the percentage of the incorporated waste increases, the type of failure is cohesive, which means that a balance between the loss of adherence and the addition of polyurethane waste must be considered.

In a further experimental study, Gutiérrez-González et al. (2012a) presented the results of the incorporation of polyamide powder waste (PAW) to produce lightweight plasters with improved thermal properties. Table 17 presents the experimental results of the PAW-gypsum based plaster.

Table 17 – Density, thermal conductivity and porosity vs. volume ratio (PAW/Plaster) determined by Gutiérrez-González et al. (2012a).

Volume Ratio (PAW/Plaster)	0/1	0.5/1	1/1	2/1	3/1	4/1
Density (kg/m^3)	1477	1190	1074	909	829	751
Thermal conductivity (W/m.ºC)	0.3057	0.2624	0.2419	0.1902	0.1418	0.1397
Porosity (%)	37.4	35.6	35.0	35.3	33.4	29.2

As it can be seen, the higher the polyamide content the lower the thermal conductivity and the density, improving the thermal resistance of the material. In terms of mechanical properties, the flexural and compressive strength decrease in proportion to the quantity of polyamide present in the mixture. According to the authors, this could be because of the high water absorption of the porous powder compounds that reduces the water in the mix, resulting in a reduction in mechanical strength.

2.2.4. OTHER THERMAL WALL SYSTEMS

One of the most usual thermal wall systems is ETICS (External Thermal Insulation Composite System), widely applied in building construction. The principles of thermal rendering systems application in façades are similar to those of ETICS application and several performance issues can be compared for the two systems.

Being well-known systems, with well-identified properties, characteristics and performance, and having a specific technical evaluation guide (EOTA 2013), ETICS constitute an interesting solution to use as a reference to fill the knowledge gap of thermal rendering systems.

EAE (European Association for External Thermal Insulation Composite Systems) has published a report in May 2015, where building sustainability is identified as a major concern, requiring an assessment in every stage of the life cycle. In addition, it points out the importance of optimizing construction taking into account the three pillars of sustainability - environmental, economic and social (addressed in sub-chapter 2.3.1. In order to obtain sustainable buildings, it is, therefore, necessary to use sustainable products and systems and also to evaluate them based on their life cycle (EAE 2015).

In that way, more sustainable materials, from local areas, arise in the market. However, a large part of these materials is not covered by ETAG 004, which may affect their use. Malanho and Veiga (2014) studied the definition of adapted methods and test techniques to evaluate the performance of ETICS with components not covered by the guide, namely mortars with lightweight additions. Through an

experimental campaign, it was possible to detect several anomalies in the analysed ETICS and, thus, to suggest complementary evaluations to that defined in ETAG 004.

In their work, Hens and Carmeliet (2001) evaluated the application of ETICS on a masonry wall, paying particular attention to the thermal and hygric response of the walls and to the durability of the applied system. After calculation procedures, laboratory and "in situ" tests, it was possible to improve the prediction of the performance of the walls and to provide data for their optimization. As such, it was possible to verify that these systems are highly efficient, presenting low air permeability, and high thermal performance (effects of the reduced thermal bridges). In addition, in order to ensure a proper application of ETICS, the authors suggested a list of requirements that should be verified.

Nilica and Harmuth (2005) evaluated the mechanical strength of ETICS, contributing with real data of mechanical failure for numerical simulation since it is one of the main concerns regarding its durability.

In addition, Daniotti et al. (2012) studied the durability of ETICS under the CIB W080 "Service Life Methodologies", taking into account the failure modes in existing buildings, depending on the type of thermal insulation applied and climate agents. A special focus was put on the Southwest Europe climates and a comprehensive set of hygrothermal simulations was performed. Therefore, it was possible to distinguish the main failure modes of ETICS (cracking, detachment, wrinkling, growth of biological agents) and to identify the agents, actions and degradation effects. One of the main conclusions was that most of the failure modes occurred when one or more agents acted together with water. Through hygrothermal simulations, with Southwest European climates, it was found that using mineral wool as thermal insulation, fast temperature variations were observed. After adding driving rain, despite the decrease of temperature variations, the effects on ETICS were more severe.

Following the previous study, Daniotti et al. (2013) carried out a set of hygrothermal simulations, in order to increase the knowledge about the failure modes on ETICS, for two different thermal insulation, EPS and mineral wool, comparing northern and southern European climates. It was found that there was no significant difference in the surface temperature variation, comparing ETICS with EPS or mineral wool. Considering the location, a greater occurrence of thermal shocks was verified in a northern European city, presenting twice the occurrences of a Mediterranean city. This was possibly due to the direct solar radiation on the wall, so it should be analysed taking into account real climate data, to validate the simulation data. One of the main findings of this study was the need to evaluate the frequency and intensity of thermal shocks as they clearly affect ETICS durability.

In addition to the thermal renders and ETICS, there are also other products which can enhance the thermal performance of walls. Currently, other kinds of products with these characteristics are commercially available, such as rock wool or polyurethane and cellulosic fibres (applied by mechanical spraying, like the thermal renders), cork-based emulsions and aerogels, among others.

Regarding the insulation applied by mechanical spraying, these emerged from the growing of the thermal demand and from the need to insulate areas of difficult access. The manufacturer of sprayed rock wool – Polirigido (2015) – refers to the possibility of application of a coating of sprayed insulation in the renovation of façades or interior walls. It presents advantages such as its high mechanical resistance and adhesion to any substrate and an application thickness of up to 30 mm without reinforcement. One of the advantages reported by the manufacturer of cellulosic fibres – ISORENEL (2015) –, compared to the use of mineral wool, is their hygric behaviour, absorbing up to 15% of moisture without changing their properties. The cork-based emulsion consists of a mixture of selected cork granules, with aqueous resins, mineral fillers and additives, used as a coating of interior surfaces and façades, promoting additional thermal insulation and anti-cracks, according to the technical data sheet (Corkwall 2014).

Some authors focused their studies on developing different types of insulations. Matias et al. (2014) presented experimental results regarding the characterization of a cork-based emulsion. One of the advantages mentioned by the authors, besides the technical advantages, was the use of waste from the cork industry. It acquires importance from the environmental point of view, as pointed in 2.2.2. Several accelerated ageing tests were carried out, complemented by the pull-off test, in order to evaluate the durability of the material. After analysing the mechanical strength, the emulsion demonstrated satisfactory performance. The mechanical behaviour is mainly conditioned by the substrate and not by the coating since for weak substrates the cracks occurred in the latter and not in the coating. In addition, no adhesive ruptures were observed.

The incorporation of PCM's (Phase Change Materials) in construction materials was found as an efficient way to enhance the heat storage capacity of building components, such as wallboards, cement mortar and concrete (Memon 2014). PCM's also improved the thermal transmission (reducing the thermal conductivity) non compromising the latent heat capacity (Amaral et al. 2017) and behaving as a thermal regulator, which is an added value in the reduction of indoor overheating rate (Figueiredo et al. 2017). The aerogels have also gained expression in the market and in research studies developed by the scientific community. According to Ou, Trifu and Caggiano (2013), a product was developed in order to present good mechanical characteristics and low thermal conductivity. Using silica and granules of modified silica aerogel in a mixture of binders or foams it was possible to obtain a product that could be applied by mechanical spraying and adapted to different areas. It presented good mechanical strength, low density and high compressive strength (60% higher compared to products without the addition of aerogels). Buratti et al. (2014) studied an aerogel-based mortar, with the aim of improving the thermal and acoustic characteristics. After experimental tests, it was verified that this material had good hygrothermal properties since it presents low thermal conductivity and allows moisture exchanges with the environment. Its application as a rehabilitation material for degraded walls was emphasized in order to increase its thermal insulation capacities. Owing to the high porosity of the aerogel, the mechanical strength slightly decreases. Concerning the industrial production, it was advisable to use 80% of silica aerogel, thus obtaining a thermal conductivity of 0.005 W/m.ºC.

The NANORENDER project aimed to investigate the use of silica-based aerogels in renders in order to formulate improved-performance renders from a thermal, acoustic and environmental point of view, for application in building walls. Soares et al. (2014) analysed the water resistance of cement-based mortars incorporating silica aerogel, which resulted in significant benefits in terms of the drying process, due to their porous structure, comparing to other lightweight additions (expanded clay and granulated cork). Júlio et al. (2016a) tested a total replacement of silica sand by lightweight aggregates with a binder: aggregate volume ratio of 1:4. Cement-fly ash based mortar with 60 vol% subcritical silica-based aerogel, 20 vol% granular expanded cork, 15 vol% expanded clay and 5 vol% perlite resulted in a density of 652 kg/m^3, a thermal conductivity of 0.084 W/m.ºC, with acceptable mechanical strength and good deformation capacity. Júlio et al. (2016b) studied the addition of silica-based aerogels into cement mixtures. The low thermal conductivity (≈ 0.085 W/m.ºC) and density (≈ 410 kg/m^3) were achieved by total replacement of silica sand with a designed hybrid aerogel. The hygric properties of lightweight mortars, such as the increase the capillary absorption, are of greater importance.

Recently, thermal insulating mortars, with EPS and silica-based aerogel, were also investigated by Gomes et al. (2018). The incorporation of silica aerogel (in a percentage by mass of 100% of the industrial mortar) decreased the thermal conductivity of the mortar comparing to an EPS based mortar. However, both thermal insulating mortars with EPS and silica-aerogel showed an exponential increase with the moisture content. Soares et al. (2018) evaluated the properties of aerogel-based renders according to the EN 998-1 requirements. Despite the T1 classification, the obtained thermal conductivity

is higher than the observed with EPS addition in Gomes et al. (2018). In addition, regarding the capillary absorption, none of the analysed renders complies the EN 998-1 requirements (Gomes et al. 2018; Soares et al. 2018).

2.3. SUSTAINABILITY, ECO-CONSTRUCTION AND DURABILITY

2.3.1. SUSTAINABILITY AND ECO-CONSTRUCTION

A great concern to promote an efficient allocation of scarce natural resources is observed nowadays. This is of great importance for achieving a more sustainable society together with a viable economic approach. Perman et al. (2003) highlight three key subjects in terms of natural resources and environmental economics: efficiency, optimization and sustainability. A substantial part of the environmental economics is concerned with how inefficiencies in the distribution and use of natural resources can be avoided

Several authors have studied and presented, in the last decades, definitions and reflections about the concept of sustainability. Coomer (1979) stated that a "sustainable society is the one that lives within the self-perpetuating limits of its environment. Society ... is not a society of "no growth" [...]. It is instead a society that recognizes the limits of growth ... it looks for alternative forms of growth. ". In 1980, the International Union for Conservation of Nature (IUCN 1980) presented a definition of sustainable development as the maintenance of essential ecological processes and life support systems, the preservation of genetic diversity and the sustainable use of species and ecosystems. In turn, Allen (1980) defined it as the development that likely meets human needs and improves the quality of human life. In 1987, the Brundtland Commission report entitled "Our common future" (Brundtland 1987) defined a set of strategies which outlined the general terms for Agenda 21. There a definition of sustainable development was presented. This report consolidates the idea that development is inevitable and the two largest existing resources – land and population – will meet the current needs without compromising those of the future generations. Emphasizing the idea that “if you take care of nature, nature will take care of humanity. For the conservation, it must be recognized that if you want to save part of the system it is necessary to save the system itself ". According to Perman et al. (2003), the policy of sustainable development is to establish a link between economy, society and environment, to live in a world where the saving of renewable resources can be achieved. This concept raises the idea of meeting the current needs without harming future resources. However, a great difficulty in linking the three fundamental pillars of sustainability is observed, since one of the pillars is usually in opposition to the others. A diagram illustrating the relationship between the three pillars of sustainability and how they interact with each other is presented in Fig. 10.

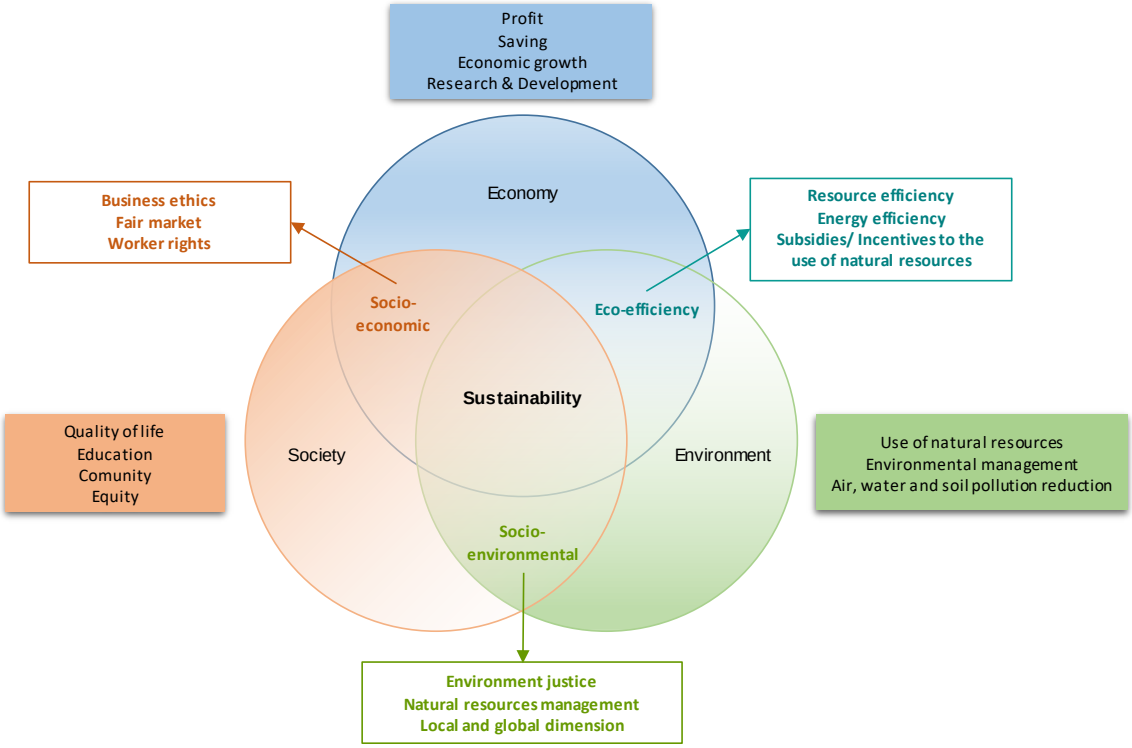

Fig. 10 – Three pillars of sustainability (Perman et al. 2003).

According to Pinheiro (2006), sustainable construction represents a new way of equating design, construction, in-service, maintenance and demolition. From a traditional perspective, the concerns are focused only on product quality, time spent and associated costs. As it can be seen in Fig. 11, sustainable construction goes far beyond traditional concepts and takes into account environmental concerns related to resource consumption, pollutant emissions, health and biodiversity, which constitutes a new challenge in contributing to the quality of life, economic development and social equity. Therefore, (Bourdeau 1998) developed the competitiveness factors present in the traditional construction triangle, demonstrating the line of thought to achieve sustainable construction in several aspects.

The increasing concern and the existence of increasingly strict environmental regulations raise the question of energy and environmental performance as one of the most important points in the construction of buildings and their relationship with the surrounding areas (Bourdeau 1999). As such, it is more and more urgent to consider the associated impacts with the built environment and the design of buildings, in order to implement policies that allow to minimize these impacts or eliminate them if possible. Different approaches and methodologies to evaluate the environmental performance of buildings and support the implementation of practical measures have been developed and progressively adopted. Several countries have been developing and implementing systems for assessing the environmental performance of buildings and adapting them to their reality, pointing out LEED (Leadership in Energy and Environmental Design), BREEAM (Building Research Establishment Environmental Assessment Method), LiderA (Leed for the Environment) and SBTool (Sustainable Building Tool). The analysis of the referred systems allowed proposing a methodology that takes into account the specificities of Portuguese construction, assisting the stakeholders in the design of residential buildings. The location, indoors environment, materials, energy, water use, construction aspects and economics were intended as key aspects in the assessment process (Pedro Júlio, Paiva and Dominguez 2013).

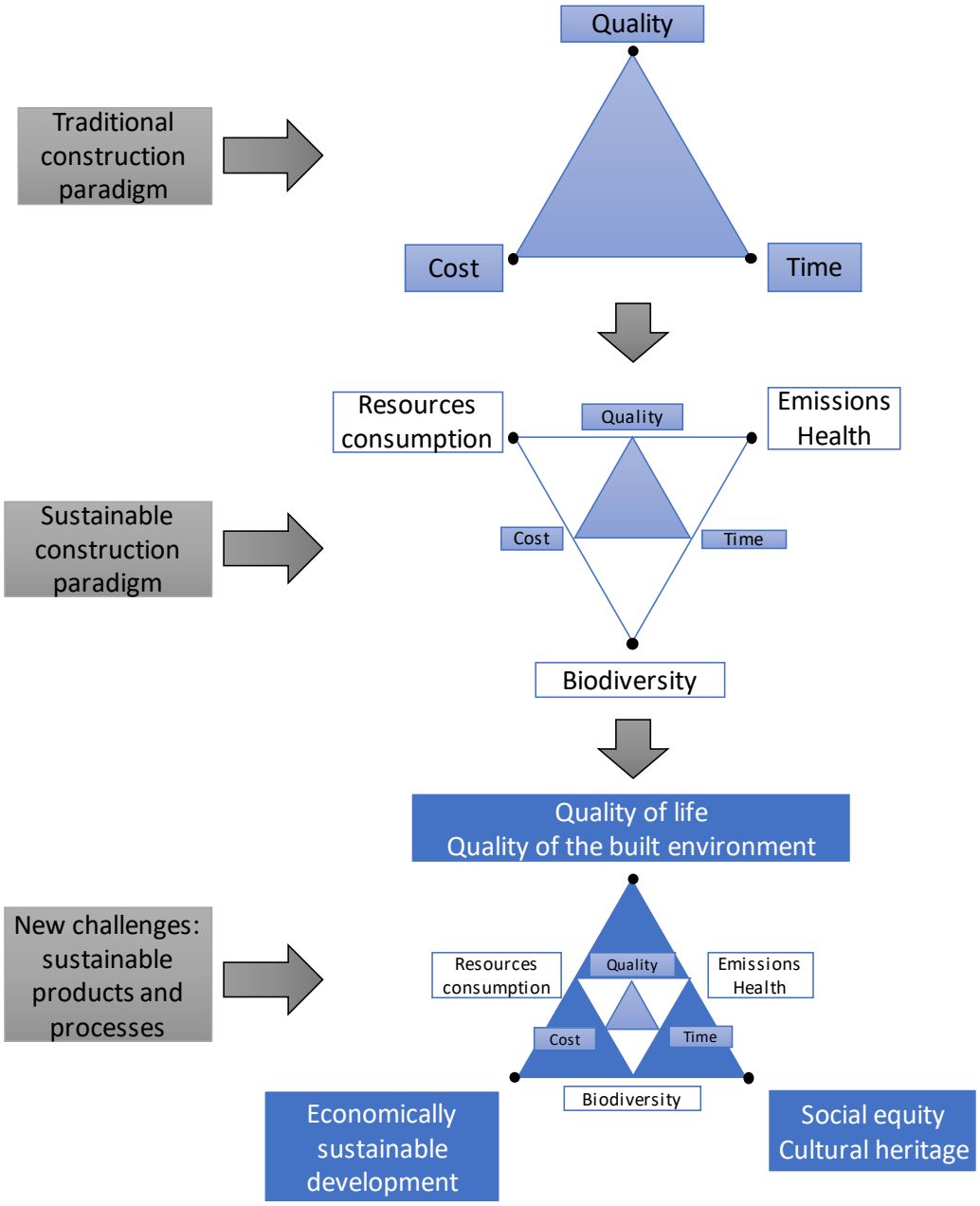

Fig. 11 – Evolution of the main concerns in the construction sector (Bourdeau 1998).

.

Concerning the thermal mortars, the existent and developed products aim to respect these principles. However, a need to deepen and move towards ensuring the compliance with them, especially regarding the durability, is verified.

As defined in the World Business Council for Sustainable Development (WBCSD) in Rio de Janeiro, the concept of eco-design is defined as the development of a product or service, minimizing its impact on the environment (UNEP 2004). According to the WBCSD, eco-efficiency is obtained through the distribution of goods and services, at competitive prices, that provide quality of life for the population, while progressively reducing environmental impacts and the intensity of resources demand, at levels supported by the planet (WBCSD 2000). However, the concept of eco-design should not only relate to the environmental ecology issue (as supported by sustainability spheres), but also to the quality of life

of the users of such products or services, reducing wastes, pollution and the ecological footprint. This concept comprises many concepts, from eco-design to eco-building. The European Commission defines an eco-building as a concept that is expected to be the culmination of several developments in order to support regulatory measures for energy efficiency and optimization of renewable energy use. According to Erhorn et al. (2007), eco-buildings have the capacity to reduce energy consumption and enhance the use of renewable energies, bio-climatically designed, taking into account sun exposure, architectural requirements, increase of the thermal insulation and tightness of the building, throughout new products, constructive solutions and viable technologies. In France, the Actu-Environment (2008) presented a set of basic principles applicable to eco-construction:

- Design according to the local climatic conditions;
- Choose suitable materials;
- Insulate, without completely tight the building;
- Perform adequate ventilation;
- Heat, if necessary;
- Cool down, without mechanical equipment;
- Provide the building with high efficient equipment.

The application of thermal renders in eco-constructive solutions influences several aspects of the sustainability of buildings as the fulfilment of several basic principles stated above is verified. For the European Mortar Industry Organization (EMO), one of its seven objectives is to "raise awareness for sustainability", emphasizing the ecology of mineral mortars and the need to promote the advantages of using this type of products, their durability and lack of hazardous substances in comparison with other materials on the market (EMO 2013). As such, the continuous interest in the development of sustainable solutions with thermal enhanced properties, incorporating different types of wastes (industrial or plant origin), allows the development of new solutions with less harmfull impact to environment than traditional construction materials (Lertsutthiwong et al. 2008; Paiva et al. 2012; Matias, Faria and Torres 2014; Torres and Matias 2016; Skoczylas and Rucińska 2018).

According to Joseph (2016), dry mortars present a contribute to the sustainability of buildings, highlighting these main areas: durability, quality and efficiency. In the perspective of durability, it is intended to obtain products that reduce maintenance costs, since they have been designed taking into account the climatic conditions and the use for which they are intended. With regard to quality, it is important to ensure that it is controlled at the production stage, guaranteeing consistent and high-quality products. As for efficiency, it is related to the application of mortars, which can be by mechanical spraying, increasing productivity and reducing application errors. In the same work, the author also presents practical examples in which these industrially produced dry mortars (also based on cement) have less carbon dioxide incorporated compared to cement mortar produced at the site of application (cement/sand ratio of 1:4/5).

On the other hand, a great use of cement in large amounts in the constitution of mortars is observed, since the cement improves their mechanical resistance. In addition, the embodied carbon of repair actions of mortars, like ordinary Portland cement, are expected to reduce the environmental impact of rendering repair actions in comparison to less hydraulic mortars, since less maintenance intervention is required (Brás and Faria 2017). However, the production of Portland cement generates approximately one tonne of carbon dioxide per ton of cement produced. By reducing the amount of cement by partially replacing it with other materials such as fly ash or slag, it is possible to improve resource efficiency by reducing emissions of polluting gases (Chong 2015).

Lime-based mortars have an advantage, comparing with cement-based mortars, as the bricks laid with lime mortar can be removed without breaking and reused, reducing future waste. Masonry and ash waste in lime mortars can also be used, for the purpose of increasing their durability and reducing cure times (BRE 2008). Another important point, highlighted by producers of lime-based mortars, is the use of lime to the detriment of other binders, as lime only hardens through absorption of CO_2 in the atmosphere. In addition, as the calcination of limestone to produce lime is performed at about 900°C (below the temperature required for cement production, above 1400°C), the consumed energy is also lower (Fradical 2016).

The Portuguese Association of Manufacturers of Mortars and ETICS (APFAC) has been developing studies and reinforcing the importance of the use of industrially produced mortars. Stresses the fact that there is no "constructive consistency" in using increasingly developed products and systems, developing more demanding standards, reducing energy consumption, respecting the environment and searching for sustainability if mortars continue their production on site, without the rigorous control that is currently required (APFAC 2015a).

In order to obtain sustainable thermal mortars, the change of their composition through the incorporation of alternative materials, which partially replace other constituents, is one of the strands. To improve the thermal behaviour of buildings, different products incorporating lightweight aggregates with low density and thermal conductivity have appeared on the market. In addition to the concern with obtaining products with improved thermal characteristics, the reduction of industrial waste by reusing them in the production of mortars is sought. This concern is visible at a European level, particularly in projects funded by the European Union, such as "Eco Alternative Mortar Thermic", with Eco-Innovation as a key issue (EC 2012). The European Directive 2008/98/ EC, which limits the waste production, states that EU countries must guarantee a minimum recycling rate of 70% for construction and demolition waste by 2020. A large part of this waste comes from the demolition of concrete and masonry structures, which has a great potential for recycling and reuse, namely for the production of aggregates for mortars.

2.3.2. DURABILITY AND SERVICE LIFE PREDICTION

According to the Australian Building Codes Board (ABCB 2006), the factors that affect the durability of buildings are the in-service conditions, such as environmental agents and specific conditions, material properties, design and corresponding detail, workmanship and maintenance.

Materials can react differently to the degradation agents that they are subjected to, being the choice of materials with properties that meet the durability requirements of great importance. The knowledge of these parameters is obtained through existing data, which may not include all the relevant agents. In the case of new products, this knowledge does not exist. Consequently, the durability evaluation should be an important aspect in their development, detailing as much as possible their performance. The application should also be highly detailed and performed by specialized workforce for this purpose, in order to guarantee the expected durability.

There are some technical documents, such as regulations, standards, guides, etc., that allow the durability assessment of constructive solutions, such as:

- ISO 15686: Buildings and constructed assets – Service life planning (ISO 2011);
- BS 7543:2003: Guide to the durability of buildings and building elements, products and components (BSI 2003);
- CSA S478-95: Guideline on durability in buildings (CSA 2007);

- Practical guide for service life planning of buildings: Architectural Institute of Japan (AIJ) (Gakkai 1993).

Durability and service life prediction do not have a standard definition, existing several definitions, more or less complete. Following are some definitions described in the above standards. According to the first edition of the ISO 15686-1:2000 (ISO 2000c), durability consists of " capability of a building or its parts to perform its required function over a specified period of time under the influence of the agents anticipated in service" and that " Durability is not an inherent property of a material or component, although the term is sometimes erroneously used as such". However, the second edition cancels and replaces the first edition, which has been technically revised to condense ISO 15686-1 into a more generic process of service life planning and to better reflect the other parts of ISO 15686. (ISO 2011). In this new version, the durability concept was omitted. The British standard BS 7543 defines durability as the ability of a building, or its constituent parts, to perform the function for which they were designed, over a period of time and under the influence of degradation agents, being the durability limit achieved when the performance is compromised, leading to the end of its service life (BSI 2003). According to the Canadian standard CSA S478-95, durability is the ability of a building or any of its components to perform the required functions in its service environment, over a period of time, without unforeseen costs for maintenance or repair (CSA 2007). In the document developed by AIJ (Architectural Institute of Japan), durability is presented as fundamental in every stage of the life cycle of buildings, from design to demolition (Gakkai 1993).

It was verified that in the different presented documents, the definition of the period of time associated with durability is not specified, but is referred in the service life concept. Service life and its prediction and durability are highly dependent on external agents, on the intrinsic material properties or on the ability to withstand to these agents. Thus, considering a specific set of conditions, some materials present a longer service life than others (Athena Institute 2006).

As regards the definition of the service life, ISO 15686 as the “period of time, after installation, during which a facility or its component parts meet or exceed the performance requirements”, which represent the minimum acceptable level of a critical property (ISO 2011). The CSA S478-95 standard describes it as the actual period of time during which the building or any of its components meets its objectives, without unforeseen costs or interruptions to maintenance and repairs (CSA 2007).

In the CIB W080 report "WG3 Test Methods for Service Life Prediction" the service life prediction is considered one of the most important parts of the planning of a building and its components (Bruno Daniotti and Cecconi 2010). Several studies have been carried out taking into account the methodology defined in ISO 15686-2 (ISO 2012).

The service life prediction methodology, developed by the Institute of Architecture of Japan, called the Factor Method, provided the basis for ISO 15686 procedures. According to ISO 15686-1 (ISO 2011), the durability design (through the “Service Life Planning") is defined as the “design process of preparing the brief and the design for the building and its parts to achieve the design life”. In addition, “service life planning can, for example, reduce the costs of building ownership and facilitate maintenance and refurbishment”. In the construction phase, procedures to ensure the quality of execution should also be followed. Already in the in-use phase, maintenance and repair plans should exist, avoiding early degradation. As such, several authors applied the ISO 15686 methodology to case studies.

Kus and Kalmar (2002) studied the use of mortars and surface treatments as an improvement of water resistance of façades. The degradation agents present in the environment, in particular, the humidity, cause degradation of the façades and, as such, compromise their performance and durability. In their work, the authors studied the long-term effects on autoclaved aerated concrete walls, measuring in-situ

climatic parameters and performing several laboratory tests, to compare them with the natural ageing results. The first results, obtained after two years of environmental exposure, indicate that mortars made of inorganic materials improved their initial performance, in terms of humidity, while organic rendering showed the same performance in time. However, taking into account the objective of a long-term evaluation, the results obtained should be carefully analysed, as they may not accurately represent the reality.

(Gaspar and De Brito 2008) presented studies using the factor method, highlighting the lack of guidelines to relate actual deterioration with the quantification of the durability parameters to be used in the factor method. The work described a methodology to quantify the reference service life and its modification in the durability factors in façades with cement-based mortars. The proposed methodology depends on the analysis of the regression of all presented degradation levels. If, on the one hand, the obtained values are related to a specific material and element of the building, on the other hand, the proposed methodology can be applied to other materials and elements in different buildings. One of the conclusions is the recommendation not to use predefined durability factors without reference to the studied building conditions.

Flores-Colen et al. (2010) contributed to the CIB W080 "Service Life Methodologies", within the scope of work developed in the doctoral thesis of the first author (Flores-Colen 2009). The methodology defined in the ISO 15686 to evaluate the performance of renders in façades, through accelerated ageing tests, was used. After laboratory tests, a correlation between the actual and the accelerated ageing period in the laboratory was obtained. As such, a model of durability prediction was defined. The authors suggest the application of the factor method proposed in ISO 15686 to evaluate the influence of specific real conditions. They also recommend the accomplishment of natural ageing tests, in addition to the accelerated ageing tests, and data collection of existing buildings regarding the development and future application of a prediction model to different systems and materials.

Silva, de Brito and Gaspar (2011) developed service life prediction models, based on ISO 15686, applied to façade cladding in natural stone, applying relative weights taking into account the extent and type of visible damages. The obtained results allowed to demonstrate that these weights lead to an improvement in the relationship between the regression curves and the results obtained in situ, achieving a better adjustment to the real situations of the inspected coatings. Therefore, the end of service life can change according to the adopted criteria. It has been found that some coating characteristics contribute to an increase of the service life, which is of great importance in the definition of preventive maintenance plans, contributing to the improvement of the performance and, consequently, to lower repair costs. Further developments were performed by (Silva, de Brito and Gaspar 2012) and (Silva 2015).

The need for energy saving and the rational use of energy resources in building construction and management was evidenced by Alaimo et al. (2012). The research work focuses on the evaluation of the durability of cement-based photocatalytic coatings, containing different types of pigments, used as façade finishing.

Madrigal, Serrano Lanzarote and Fran Bretones (2015) used the ISO 15686 methodology for estimating the service life of exterior walls and ceilings. However, as this methodology was defined for a general application, its practical application to concrete cases is difficult. Owing the scarce amount of reliable information on materials durability, the construction of a service life database of the considered building elements, as well as their constituent materials, based on their usual degradation mechanisms, was found necessary. Factors that affect durability were identified and a clear procedure for its evaluation was developed. The proposed method, instead of giving precise information on the service life, allows different construction systems to be compared.

2.4. DEGRADATION AGENTS AND MECHANISMS IN THERMAL MORTARS

There are several degradation mechanisms that affect the durability of construction materials and particularly renders. ISO 15686-1 (ISO 2011) presents a summary of the most relevant degradation mechanisms in building materials, taking into account nature and class, which are shown in Table 18.

The classification presented in ISO 15686-1 is applied to different materials, so it is necessary to define the most relevant degradation mechanisms applied to exterior rendering systems and the agents that affect the durability of the referred systems.

Table 18 – Categories of degradation agents in terms of nature and class (ISO 2011).

Nature	Class	Examples
Mechanical agents	Gravity	Snow loads, rainwater loads
	Forces and imposed or restrained deformations	Ice formation, expansion and contraction, land slip, creep
	Kinetic energy	Impacts, sand storm, water hammer
	Vibrations and noises	Tunnelling, vibration from traffic or domestic appliances
Electromagnetic agents	Radiation	Solar or ultraviolet radiation, radioactive radiation
	Electricity	Electrolytic reactions, lightning
	Magnetism	Magnetic fields
Thermal agents	Extreme levels or fast alterations of temperature	Heat, frost, thermal shock, fire
Chemical agents	Water and solvents	Air humidity, ground water, alcohol
	Oxidizing agents	Oxygen, disinfectant, bleach
	Reducing agents	Sulphides, ammonia, agents of combustion
	Acids	Carbonic acid, bird droppings, vinegar
	Alkalis (bases)	Lime, hydroxides
	Salts	Nitrates, phosphates, chlorides
	Chemically neutral	Limestone, fat, oil, ink
Biological agents	Vegetable and microbial	Bacteria, moulds, fungi, roots
	Animal	Rodents, termites, worms, birds

Note: In general, the origin of degradation agents outside the building is the atmosphere or the ground, whereas internally the origin is either occupancy or design and installations.

Batchelor, Loh and Chandrasekaran (2011) grouped several degradation mechanisms considering the following four distinct categories:

- Direct mechanical action: wear and fatigue, rupture and deformation;
- Heating or radiation: thermal degradation and high radiation energy;
- Presence of chemical agents: corrosion, oxidation, softening, embrittlement, biochemical and biological agents;
- Combination of two or more of the previously presented mechanisms (such as wear in corrosive or chemically active environments).

Focusing on the particular degradation of mortars, some studies present the possible degradation mechanisms and the responsible agents for this degradation. According to Addleson (1992) and Aguiar, Cabrita and Appleton (2002), the main causes of degradation on renders are organized as presented in Table 19.

Table 19 – Degradation mechanisms of mortars, according to Addleson (1992) and Aguiar, Cabrita and Appleton (2002).

Nature	Agents
Water action	Humidity
	Ice
	Soluble salts
Biological action	Algae
	Fungi and lichens
	Various plants
	Bacteria
	Small size animals
Mechanical action	Shrinkage
	Wind
	Temperature
	Substrate deformation
	Accidental actions
Human action	Technology
	Maintenance
	Tourism
	Vandalism
	Pollution

Palomo et al. (2000) stated in their work, that degradation occurs by joint action of different mechanisms (physical, chemical, mechanical, biological, etc.), which difficult the classification of degradation processes. However, the degradation processes more frequently observed in historical mortars are presented:

- Dissolution and leaching of the components of hydraulic mortars;

- Interaction of the mortars with the atmospheric pollutants;
- Crystallization of soluble salts;
- Effect of freeze-thaw cycles;
- Expansive reactions;
- Volume changes due to thermal variations or water presence;
- Deterioration due to biological causes.

Water is presented as one of the most relevant degradation agents of mortars, promoting the action of other agents, namely freeze-thaw, salts crystallization and various biological agents. Flores-Colen, Brito and Freitas (2005) analysed anomalies in mortars, with or without paint, highlighting cracks, slurry, detachments, soiling, differences in tone and biological colonization, that originate stains, being in most cases associated with the presence of moisture.

Considering the different mortar binders, degradation mechanisms also act in different ways. For example, lime-based mortars, with or without pozzolans addition, and higher porosity are substantially more permeable compared to hydraulic lime-based and cement mortars. Thus, the amount of water, which circulates in their interior, is higher and, consequently, higher quantities of soluble salts are observed. Also due to its higher permeability, these mortars have greater evaporation, so the risk of salts crystallization is also higher. As regards the mechanical strength, less favourable results are verified compared to hydraulic cement, thus presenting a greater risk when subjected to salts crystallisation pressure. According to Sousa, Pereira and Brito (2005) the larger the pores, the lower the crystallization pressure. As such, the lime-based mortars could present less mechanical degradation, because the formation of crystals inside the pores does not produce excessive pressure, due to the bigger pores dimension. However, the degradation of lime-based mortars due to salt crystallization consists of an important issue, especially in historical buildings (Borges, Santos Silva and Veiga 2014; Fragata, Rosário Veiga and Velosa 2016; do Rosário Veiga et al. 2010). The degradation of lime-based mortars in historical buildings, after rehabilitation, are highly related to the application of coatings with low water vapour permeability, which creates incompatibility between the old and new materials (Gonçalves de Carvalho, Flores-Colen and Faria 2015). Considering the different classifications, Table 20 presents a summary of the studies on mortar degradation mechanisms. It reflects the fact that most of the agents act together, being water one of the agents with the highest influence on the degradation of mortars.

Table 20 – Summary of the studies on mortar degradation mechanisms nature.

Nature/ Author	(ISO 2011)	(Batchelor et al., 2011)[1]	(Addleson 1992) and (Aguiar, Cabrita and Appleton 2002)[2]	(Palomo et al. 2000)[3]
Mechanical	X	X	X	X
Electromagnetic	X			
Thermal	X	X		X
Chemical	X	X		X
Biological	X		X	X
Water			X	X
Human			X	X

1 The author stresses the occurrence of a combination of more than one different mechanism at the same time, such as mechanical action together with chemical action;
2 Temperature action is classified as a mechanical action and the soluble salts as a water action;
3 The author classifies according to the agents, being the nature adapted to this classification.

One of the most influential factors in mortars degradation is the porous structure (open porosity and pore size distribution). Open porosity reflects the interconnected pores, which allow water transport, and the pore size distribution, influencing the amount that is transported. The impact that the porous structure has on the durability of a material is more severe depending on the degradation agents that it is subjected to. The higher the amount of evaporated water during the production of a mortar, the higher the resulting porosity in the hardened material, and thus the lower the mechanical strength and the potential durability of this material, compared to a material with lower porosity. Fig. 12 presents a schematic representation of the cement paste porous network, identifying the different pore types – capillary, micro and macropores.

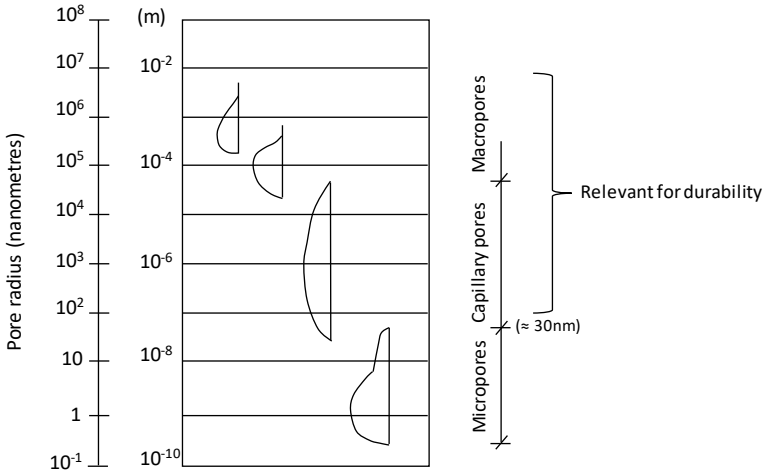

Fig. 12 – Porous net distribution according to Setzer (CEB 1992).

The porous structure, particularly the capillary network, has a very high impact on mortars durability, since that capillary network is continuous, allowing water circulation, while the macropores are often isolated. In general, the way degradation agents penetrate the material depends on the transport mechanisms through the porous network, namely, the permeability and capillary water absorption (Coutinho 1998). However, the difference between the porosity of a material and its permeability should be noted. Increasing the porosity of a material tends to increase the permeability, which affects its durability since it creates more favourable conditions for the penetration of aggressive agents inside the material. The permeability is related to the flow through the porous network, whereas the porosity corresponds to the pores, not necessarily interconnected. As such, depending on the porous network, materials with different porosity and permeability could be obtained, as presented in Fig. 13.

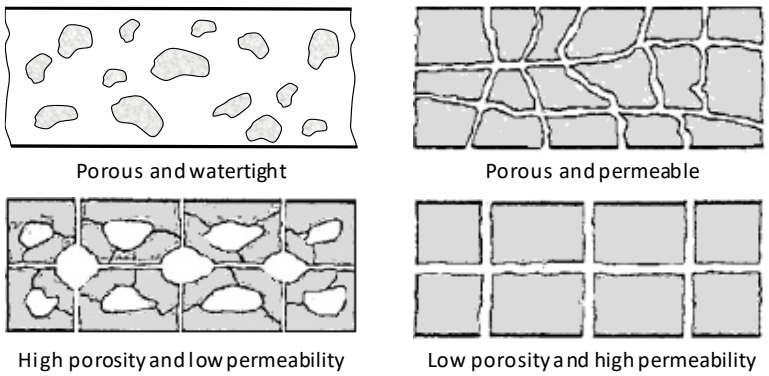

Fig. 13 – Porous net: porosity vs. permeability (Concrete Society 1987).

2.5. DURABILITY ASSESSMENT

2.5.1. PRINCIPLES AND STANDARDS

The durability assessment of renders depends on the nature of the materials and the degradation mechanisms to which the materials are subjected. In general, the durability assessment could be carried out taking into account the following approaches (Lewry and Crewdson 1994):

- Benchmark tests: usually accelerated ageing tests;
- Reference materials/Comparative tests: used to calibrate the test equipment and the test materials: simulate the service environment by accelerating or intensifying the environmental factors;
- Environmental/Stress testing;
- Site testing: natural exposure or "in situ" monitoring.

EN 998-1 (CEN 2010) standard provides durability evaluation according to the standard test method presented in EN 1015-21(CEN 2002a) but does not present any requirements for thermal mortars. The EN 998-1 standard also defines freeze-thaw tests, applied to one-coat mortars, according to the EN 1015-21, and for the remaining mortars provides an assessment taking into account the actual "in situ" conditions. As such, standardized methodologies to evaluate the durability of thermal renders are not available.

2.5.2. ACCELERATED AGEING

The relevance of each degradation mechanism depends on the climate as well as on the building materials and the correspondent resistance to the climatic conditions. In general, it is difficult to simulate all the degradation mechanism and the way they interact together. In fact, in most of the research studies, such as in 2.5.4, only temperature and moisture effects are simulated to perform the long-term ageing of building materials. Solar radiation is another of the most studied degradation mechanisms (Berardi and Nosrati 2018; Haillant 2011; Jelle and Nilsen 2011), using UV (ultra-violet) radiation.

According to (Escobar and Meeker 2006), "acceleration" is not a defined concept and could have various definitions. In " Concepts in Accelerated Testing – Design for Reliability" (Crowe and Feinberg 2001), the concept of accelerated testing is " to compress time and accelerate the failure mechanisms in a reasonable test period so that product reliability can be assessed". In general, the definitions imply the time to go quicker, to obtain reliable information more rapidly.

The acceleration factor (A_F), for a given time period, is expressed by equation (1) (Jelle 2012).

$$A_F = \frac{C_{lab}}{C_{nat}}, \quad (1)$$

Where C_{lab} corresponds to the rate under laboratory test conditions and C_{nat} at natural conditions.

The acceleration could be performed through several methods, such as the increase of the rate of use and the level of stress of the testing equipment. Knowing that a large part of the materials is sensitive to more than one degradation mechanism, the combination of models should be applied. However, when the failure mechanisms are complex and have many variables the implementation of the physical model, by extrapolation, may not be useful, since these models are applied for well-known mechanisms. In these situations, where the degradation mechanisms are highly complex, the application of empirical

acceleration models is more adequate, since they use available data to evaluate and compare to the resulting deterioration (Escobar and Meeker 2006).

Physical and chemical reactions, that are affected by temperature and/or humidity, are normally easily determined by existing models (Crowe and Feinberg 2001).

For example, the chemical degradation processes increase exponentially with increasing temperature, as expressed by the Arrhenius reaction rate (see equation (2)).

$$Rate = B \cdot exp\left(\frac{-E_A}{K_B T}\right) \tag{2}$$

Where B is the constant that characterizes the product failure mechanism and test conditions, E_A is the activation energy of the failure mode, in electron-volts (eV), K_B is the Bolzmann's constant ($8.617 \times 10^{-5} eV/K$) and T is the temperature in Kelvin (K).

Materials and components that operate at high temperatures, in high moisture environments, could be modelled by a relationship between the Arrhenius equation (equation (2)) and the Peck's model, presented in equation (3).

$$Ln\left(t_f\right) = C + \frac{-E_A}{K_B T} - hLn(\varphi) \tag{3}$$

Where t_f is the time to fail, in hours, C is a general constant, h is the humidity constant and φ the relative humidity in (%).

Both temperature and relative humidity should be presented for natural and test conditions.

In these degradation processes, to calculate the acceleration factor, the activation energy must be determined for a specific failure mode, which could be obtained through existing data or experimental tests. However, it is a very difficult parameter to obtain.

Knowing that a substantial part of the materials is subjected to temperature cyclic actions, the most used model to relate the thermal expansion and contraction to the thermal stresses is the Coffin-Manson model described in equation (4). The failure is caused by fatigue, owing to the cyclic stresses.

$$Ln\left(N_f\right) = C - KLn(\Delta T) \tag{4}$$

Where N_f is the number of cycles to failure and K is the temperature cycle exponent.

It was verified, that most of the developed studies, in which these models are applied, refer to electronic components since they have fewer variables and combination of failure mechanisms. In addition, several data of the constant values and activation energy are given (Cui 2005; Haillant 2011).

Considering building materials, these models are applied in the case of simulating solar radiation incidence, using UV radiation as referred before. However, some of the used values are estimated from other previous works, or simplifications are used. This fact may introduce generalized errors, due to the fact that the building materials and the systems could have completely different properties, even for similar materials. The Technical Report TR 010 (EOTA 2004) provides a calculation method for the determination of the radiation and exposure time to be used for artificial weathering, in the cured

assembled system of a liquid applied roof waterproofing kit, which could provide guidelines to adjust the method to other building materials.

The work developed in CIB W080, presented in the state of the art report "Accelerated laboratory test procedures and the correlation between laboratory tests and service life data" (Bruno Daniotti and Cecconi 2010) contributed to increase the knowledge on the durability assessment methodologies, though several studies developed in different research groups. Daniotti, Spagnolo and Paolini (2008) analysed climatic data to define an accelerated ageing procedure for reference service life evaluation. A specific ageing cycle should be performed, considering the specific conditions of a material/system application (as defined in Guidance Document 3 (EOTA 1999)). However, owing the difficult to reproduce all the effects, the most representative cycle may be the assertive choice. The authors state that there exist three different ways of pre-designing ageing cycles, namely:

- Existing standards: existing hygrothermal tests could be assumed as the first hypothesis;
- Climatic data analysis: statistical analysis of existing climatic data combined with the determination of the main degradation mechanisms;
- Preliminary degradation model: based on a preliminary degradation simulation model.

In that way, it is possible to simulate the variability of climatic parameters in a specific area, as performed by Donatelli et al. (2017).
Regarding the thermal rendering systems, the approach developed by Daniotti, Spagnolo and Paolini (2008) seems to be the most adequate and reliable path to achieve the main goal of the current thesis.

2.5.3. STANDARD PROCEDURES OF DURABILITY ASSESSMENT

According to EN 1015-21 (CEN 2002a), the durability of one-coat renders, before and after ageing cycles, is evaluated through water permeability and adhesion tests. The accelerated ageing cycles proposed by the standard are heating-freezing and humidification-freezing cycles. Before testing the samples should be conditioned for 28 days at 20±2 °C of temperature and 65±5 % of relative humidity. Table 21 presents the referred standard accelerated ageing series. After conditioning, the first series, composed of four cycles, is performed. Before starting the second series, the sample remains 48 hours in the reference conditions (20±2 °C of temperature and 65±5% of relative humidity).

Table 21 – Accelerated ageing series, according to EN 1015-21 (CEN 2002a).

Series	Procedure	Temperature (ºC)	Duration (h)	Cycles
1st	Heating	Infrared 60±2ºC	8h±15min	4
	Freezing	-15±1ºC	15h±15min	
Storage	T= 60±2ºC and RH=65±5%			
2nd	Humidification	Immersion T_{amb}	8h±15min	4
	Freezing	-15±1ºC	15h±15min	

Regarding ETICS, the durability assessment is defined in ETAG 004 (EOTA 2013), as shown in Table 22 and Table 23. Before and after carrying out the ageing procedures some tests are performed, such as impact resistance, bond strength tests and capillary water absorption.

Table 22 – Accelerated ageing series of ETICS performed on the rig, according to ETAG 004 (EOTA 2013).

Series	Procedure	Temperature (ºC)	Duration (h)	Cycles
1st	Heat	70	3	80
	Rain	15 (1 l/m^2.min)	1	
2nd	Drainage	-	2	-
3rd	Conditioning	10-25	48	-
4th	Heat	50	8	5
	Cold	-20	16	

Table 23 – Accelerated ageing series of ETICS performed on small scale samples, according to ETAG 004 (EOTA 2013).

Procedure	Thawing		Freezing		Cycles
	Temperature (ºC)	Duration (h)	Temperature (ºC)	Duration (h)	
Freeze-thaw	Water immersion at 23±2ºC	8	-20	16	30

Other standard durability assessment methodologies, based on freeze-thaw ageing, are presented in Table 24.

Table 24 – Other relevant standard durability assessment methodologies, based on freeze-thaw ageing, applied on mortars.

Standard	Conditioning	Freezing		Thawing		Cycles
		Temperature (ºC)	Duration (h)	Temperature (ºC)	Duration (h)	
Cahier 2669-4 (CSTB 1993)	Same methodology as defined in EN 1015-21 (CEN 2002a)					
RILEM MS-A.4 (RILEM 1998)	Cure at 20±2ºC e 95±5% RH	-15	5	1st T_{room} 2nd Drying oven (25±2 ºC)	30min 24h	25

Regarding other degradation mechanisms of mortars, applied in specific conditions or climates, the following standards are described.

The standard ISO 9227:90 (ISO 2006) evaluates the relative corrosion resistance of mortars exposed to marine or industrial environments by means of a salt spray at a high temperature The samples are placed in an enclosed salt spray chamber, filled with a continuous indirect saline mist atmosphere with 50 g/l of a standardized 5% solution of NaCl at 35 ºC for 30 days. The major effect of such environments,

where the temperature is an important factor, is the diffusion of chloride ions into the cementitious mixtures that can produce detrimental effects.

The behaviour of mortars in the presence of aqueous solutions of sodium hydroxide can be tested according to the ASTM C1260-14 (ASTM 2008b). This test is intended to determine the existence of potential reactions between the cement and the aggregate and the cement and polymeric foam that substitutes the aggregate in the manufacture of mortars. This reactivity entails the formation of gels that expand in the presence of humidity, producing cracks and differential movements and with it, a drastic hardness reduction.

2.5.4. NON-STANDARDIZED PROCEDURES OF DURABILITY ASSESSMENT OF NON-TRADITIONAL MORTARS

In addition to the existing standard procedures, several studies of durability assessment of innovative mortars were carried out by different authors. A synthesis is presented in Table 25 in order to deepen the existing knowledge and to evaluate other non-standard tests, regarding the accelerated ageing by heat-cold cycles.

Table 25 – Non-standardized accelerated ageing hygrothermal cycles.

Author	Conditioning	Procedure	T (ºC)	Duration (h)	Cycles	Testing (before and after ageing)
Puertas et al. (2003)	Curing 28 days	Immersion	21	18	50	Impact resistance/ Compressive and flexural strength
		Heat	70±5	6		
Gonçalves da Silva (2004)	1day –Tamb 3h – 80ºC	Cold	20	12	416	Compressive and flexural strength
		Heat	50	12		
Ferrándiz-Mas and García-Alcocel (2013)	Immersion at 20±5ºC – 28days	Heat	60	6	25	Compressive strength
		Cold	20	18		
Hannawi and Prince-Agbodjan (2015)	-	Heat	65	12	40	Compressive and flexural strength
		Cold	20	12		

Puertas et al. (2003) found that ageing cycles promote an increase of the resistance to fracture on specimens incorporating polypropylene fibres. However, the opposite effect on cement mortars without the addition of fibres was observed. Gonçalves da Silva (2004) analysed the durability of a mortar with cement matrix and epoxy or polyester resin and carried out a comparison between these two mixtures. Comparing the mechanical strength before and after the accelerated ageing, the flexural strength of the mortar with epoxy addition was slightly lower than the other one with polyester resin, after ageing and comparing with the obtained results before ageing. With regard to compressive strength, the product with epoxy resin showed much lower values than with polyester resin also after ageing. Ferrándiz-Mas and García-Alcocel (2013) analysed the durability of a mortar with cement matrix and EPS addition (by partial replacement of cement). After applying the heat-cold cycle it was found that the addition of EPS produced a positive effect on the compressive strength of the test specimens subjected to the heat-cold cycles. The specimens with a higher dosage of EPS revealed superior durability. Hannawi and Prince-Agbodjan (2015) found that after heat-cold cycles the compressive and flexural strength increased, which may be due to the formation of new hydrates compounds during the cycles.

Gonçalves da Silva (2004) also performed accelerated ageing with variable relative humidity cycles (see Table 26). The author verified that the compressive strength did not show a significant variation after ageing, for both mortars with the addition of polyester and epoxy. The results confirm that accelerated ageing mechanisms are complex and difficult to correlate with changes in mechanical properties.

Table 26 – Accelerated ageing cycles with relative humidity variation.

Author	Conditioning	Dry period		Wet period		T (ºC)	Cycles	Testing (before and after ageing)
		RH (%)	Duration (h)	RH (%)	Duration (h)			
Gonçalves da Silva (2004)	1 day – T_{amb} 3h – 80ºC	20	12	90	12	40	(10000/24)h	Compressive and flexural strength

Standard procedures were not used in the previous works.

The freeze-thaw mechanism is one of those that cause the highest damages in mortars. Table 27 presents several freeze-thaw cycles applied to non-traditional mortars, developed in research studies.

Puertas et al. (2003) found that mortars incorporating activated slags present greater stability to freeze-thaw action, increasing their mechanical resistance, compared to mortars incorporating fly ash or cement. The inclusion of polypropylene fibres did not promote an improvement in performance after the accelerated ageing cycles. Degirmenci and Yilmaz (2009) verified that the addition of 10-15% of diatomite (in replacement of cement) increased the compressive strength after freeze-thaw cycles. This fact could be a result of the filler diatomite effect on the mortar. On the contrary, Bocca and Grazzini (2012) verified a decrease in compressive strength after ageing. According to ČSN 72 2452 (ČSN 1968), Vejmelková et al. (2012) classified the different samples as being resistant or not to freezing. Only the lime-metakaolin based mortar, with higher purity, and a commercial mortar were classified as freeze-resistant. Wang and Meyer (2012) found that when performing the accelerated ageing procedure defined in ASTM C666/C666M-03 (ASTM 2008a) to mortars with different percentages of high impact polystyrene addition, the dynamic modulus did not change, even after 300 cycles of ageing. Ferrándiz-Mas and García-Alcocel (2013) verified that the addition of EPS improved or maintained the durability of the mortar, since the EPS absorbs some of the crystallization pressure of the ice, contributing to the reduction of damages. Di Bella et al. (2014) obtained, as expected, a reduction in mechanical strength, especially in the flexural strength, after accelerated ageing, for the three types of lime-based mortar evaluated: with the addition of polypropylene, sisal and kenaf fibres. This resistance decrease can be explained by the action of the absorbed water that freezes when subjected to low temperature, increasing in volume within the pores. That fact produces cracking and loss of cohesion in the mortar. The thermal shocks and the action of the infrared radiation did not promote significant changes in the specimens during the heat-cold cycles, being the main cause of degradation the freeze-thaw cycles, due to the humidification and subsequent action of negative temperatures with the formation of ice. Hannawi and Prince-Agbodjan (2015) found that after the freeze-thaw cycles the mechanical strength decreased, which may be due to the degradation of the specimens due to cracking and emergence of voids.

A study of the evaluation of the durability of ETICS, through service life prediction, is presented by Norvaišiene et al. (2013) that performed an accelerated ageing cycle for this purpose, which is presented in Table 28.

Table 27 – Freeze-thaw cycles presented in several research studies.

Author	Conditioning	Freezing		Thawing		Cycles	Standard	Testing (before and after ageing)
		T (ºC)	Duration (h)	T (ºC)	Duration (h)			
Puertas et al. (2003)[1]	Cure 28 days	-20	3	Immersion at T_{amb}	0.5	50	–	Compressive and flexural strength
Degirmenci and Yilmaz (2009)	Immersion at 23±2ºC – 28days	-20	4	Immersion at T_{amb}	4	25	–	Compressive strength
Bocca and Grazzini (2012)	–	-15	25[3]	60	25[3]	8	–	Compressive strength and elastic modulus
Vejmelková et al. (2012)	–	-20±3ºC	4	Immersion at 20ºC	2	15	ČSN 72 2452	Compressive and flexural strength
Wang and Meyer (2012)	Water saturation until testing	4 to -18ºC	2 a 5 h (≥20% time)[4]	Immersion: -18 to 4ºC	2 to 5 h (remaining time)	Dependent on material and tests	ASTM C666/C666M-03	Dynamic modulus
Ferrándiz-Mas and García-Alcocel (2013)	Immersion at 15±5ºC – 48h	-15	18	Immersion at 15ºC	6	25	Adapted from UNE 67028 EX:1997	Compressive strength
Di Bella et al. (2014)[2] 1st Series	25±2ºC and 55±5% – 48 dias	-15±1ºC	15h±15min	Infrared radiation 60±2ºC	8h±15min	4	Adapted from EN 1015-21	Compressive and flexural strength
Di Bella et al. (2014)[2] 2nd Series	20±2ºC and 65±5% – 48h	-15±1ºC	15h±15min	Immersion at T_{amb}	8h±15min	4		
Hannawi and Prince-Agbodjan (2015)	24h saturation	-20	12	Immersion at 20ºC	12	60	–	Compressive and flexural strength

[1] The cycle is repeated twice a day, being the test pieces immersed in water for the remaining 17 hours;

[2] Between freezing and thawing periods the specimen must be placed at 25 ± 2ºC and 55 ± 5% for 30 min; thawing is the first ageing procedure;

[3] The total duration of the cycle is 25h, evolving from 60ºC to -15ºC, and vice versa;

[4] The duration of each period depends on how long the centre of the specimen reaches the temperature limits.

Table 28 – Accelerated ageing daily cycle defined by Norvaišiene et al. (2013).

Description	Air temperature (ºC)	Procedure	Duration (h)
Rain	+20	Humidification	7
Cold	-10	Freezing	3 (decreasing)
			6 (constant)
Heat	+40	Drying	4 (increasing)
			6 (constant)

The rain-cold-heat cycle presented was intended to reproduce during 16 days the real effect of one-year climate exposure. Therefore, the experimental results were evaluated after 16 and 32 days, simulating 1 and 2 years of ageing, respectively. It was found that increasing the thickness of the glass fibre mesh allows an improvement in impact strength, but also leads to the increase of the moisture content of the outer layer of the system.

2.6. SYNTHESIS OF THE CHAPTER

Mortars, as already mentioned above, consist of one or more binders mixed with aggregates and water. The nature of binders and aggregates has become increasingly diverse, taking into account applicable requirements. However, some materials continue to have a significant presence in the production of mortars, in particular – cement, lime and gypsum. Therefore, binders are materials, which have the ability to bond other materials (aggregates), becoming a cohesive and solid material (Gomes, Pinto and Pinto 2013a).

As from the several studies carried out by the mentioned authors in 2.2.3, it was possible to verify the high interest and the large developments on thermal mortars. The developed studies present materials with different matrices, using more frequently cement, cement and lime, and gypsum. There is a clear trend to obtain new materials, with low density and improved thermal characteristics. However, in general, the lower density, which is also directly related to the increase of the porosity from the porous aggregates, results in a loss of mechanical strength. Also reducing the amount of binder for the incorporation of lightweight aggregates implies a reduction of the mechanical resistance, more relevant in cement-based materials. Concerning the type of aggregates in the production of traditional mortars, sand is the most used. However, in recent years, the use of other types of aggregates has increased, which allows the achievement of materials with enhanced properties at various levels, also with concern for the use of sustainable materials. Materials such as cork, vermiculite, EPS and industrial wastes have been widely used in the production of new mortars. Thus, there is a great variety of materials that can be incorporated into the matrix. The main focus of interest is their low density, low thermal conductivity and origin. This last point has gained great importance due to the interest in developing more sustainable materials from an environmental and energy point of view. Thus, the use of raw materials, such as cork and mineral additions, and wastes, such as EPS and artificial fibres is becoming the key aspect. In addition to the evaluation of the impact of the use of different materials, the content of incorporated lightweight aggregates and the size of the granules were also evaluated. The amount of lightweight aggregate, usually replacing sand, has a significant impact on density and thermal conductivity, resulting in materials with good thermal properties. Regarding the size of the aggregate granules, it also showed to have a great influence, mainly in the hygrothermal properties, due to the voids originated by the

different dimensions of the granules. The interaction between the lightweight aggregate and the binder matrix presented a great influence, mainly in the mechanical strength. Since the decrease of the mechanical strength is one of the most affected properties in this type of materials, many authors tried to overcome this gap. One of the ways is through the incorporation of materials with high mechanical performance, such as synthetic fibres (fibreglass, carbon fibre), industrial wastes containing fibres, or natural wastes, resulting for example from the pruning of cork oaks. Table 29, Table 30 and Table 31 present a summary of the main properties obtained in the research studies for the mortars with enhanced properties, organised according to the type of binder.

Despite the search for new solutions with enhanced hygrothermal performance and easily applicable, such as the thermal rendering systems applied by mechanical spraying, ETICS are still widely used in construction. However, these systems have been presenting, over time, several pathologies and problems related to their intrinsic properties. Moreover, the greater adaptability of the thermal rendering and plastering systems to irregular and curved surfaces and the increase of the water vapour permeability comparing to ETICS are presented as major benefits. The fire resistance is another key aspect, regarding the performance and durability of thermal wall systems, which requires further investigation. Since the present work is focused on the durability assessment regarding especially the hygrothermal and mechanical properties of thermal rendering systems, the fire resistance was not explored. Therefore, the use of more sustainable materials and the development of assessment methodologies are great concernings.

Beyond the mortars and ETICS, there are also hybrid products, which present similar characteristics to thermal mortars, but without the use of binders in their production or in smaller content. These types of products are normally easy to apply (by mechanical spraying), applicable in areas with difficult access, allowing an improvement of the thermal behaviour of buildings. These products already exist as sprayed thermal insulation and emulsions with lightweight aggregates. However, these solutions could be compromised by their unfavourable fire resistance, comparing to thermal mortars.

Developing products and construction systems, taking into account the durability of the materials and the increase in their service life, directly contribute to lower production and accumulation of waste and, consequently, to obtain sustainable materials. Thus, in order to safeguard the built environment, it is necessary to study, analyse and act in order to control and increase the durability of the materials, components and construction elements. The identification of the most frequent degradation mechanisms in materials and components help on the development of control measures to avoid failure. In the case of mortars, such as thermal renders, the main degradation mechanisms are presented in Table 32, based on the Guideline on Durability in Buildings (CSA 2007) and on the Assessment of working life products (EOTA 1999).

The porous structure proved to have a great impact on the hygrothermal performance of mortars since permeability depends on the porous network, its connection, size, shape and distribution of the pores.

The analysis of the existing standardization for the durability assessment of hardened mortars does not allow a consistent evaluation considering non-traditional mortars in general.

With regard to thermal mortars, the experience documented in the literature is reduced. Accelerated ageing tests carried out by several authors do not follow a methodology directly related to actual performance and may not be the most appropriate way of evaluating the material/system. Regardless of the matrix and aggregates used in the mortar, accelerated ageing cycles are performed. A trend regarding temperatures is observed, being the temperature in the freezing period approximately -20°C and in the thawing period carried out at room temperature.

The lack of requirements in EN 998-1 (CEN 2010) and the existing test methodology for one-coat mortars, according to EN 1015-21 (CEN 2002a), does not allow to classify and to show the added value of this type of systems, since they are multi-layer systems and should be evaluated as such. In addition, the gaps in the durability assessment of systems for indoor and outdoor applications should be addressed, as they will not present the same performance. It would be interesting to develop methodologies for evaluating durability taking into account different matrices and types of lightweight aggregates. Directing the durability evaluation to the desired performance will guarantee solutions that are more durable, raising the adequacy of this type of systems to the climate where they will be applied. However, this implies the prior definition of the requirements.

The calculation of acceleration factors requires a wide previous knowledge on the quantification of the periods and rates that origin the failure. As such, a large database containing those parameters are necessary. Since the thermal rendering systems gained importance in the market mainly in the last decade and the existing solutions are quite different between them, the required parameters are difficult to obtain. The pre-design of ageing cycles could be developed in different ways as presented by Daniotti, Spagnolo and Paolini (2008). The combination of the three methods to pre-design the ageing cycles (existing standards, climatic data analysis and preliminary degradation model) may comprehend the collected knowledge and return more accurate results.

Table 29 – Summary of the main properties obtained in the research studies, for cement and lime based thermal mortars.

Authors	Binder	Lightweight aggregate/ %addition	Bulk density (dry) (kg/m^3)	Thermal conductivity (dry) ($W/m.^oC$)	Mechanical properties/ Durability
Šeputyte-Jucike et al. (2014)	Cement (10%) and lime (4%)	EPSC/ 1.25l/kg	620	0.13	Class CSI (compression strength = 0.4 N/mm^2)
Dylewski and Adamczyk (2014)	Cement and lime	Bims granules	334	0.068	Class CSII (compression strength = 1.84 N/mm^2) Adhesion = 0.46 N/mm^2
		EPS	200	0.070	Compression strength ≥ 0.5 N/mm^2 Adhesion ≥ 0.08 N/mm^2
Brites, Frade and Santos (2014)	White cement and hydrated lime	EPS	294	0.0774	Compression and flexural strength of 0.5 MPa and 0.3 MPa, respectively, and Young modulus = 216 MPa.
			227	0.0559	Compression and flexural strength of 0.3 MPa and 0.5 MPa, respectively, and Young modulus = 159 MPa.
	Hydraulic and hydrated lime	EPS	285	0.0627	Compression and flexural strength of 0.3 MPa and 0.2 MPa, respectively, and Young modulus = 164 MPa.
	White cement and hydrated lime	Expanded glass	544	0.1286	Compression and flexural strength of 5.0 MPa and 2.0 MPa, respectively, and Young modulus = 2173 MPa.
Vale et al. (2014)	Lime and cement	EPS/100%	237	0.06	Tensile and compression strength of 0.21 MPa and 0.36 MPa, respectively, and Young modulus = 70 MPa.
	Lime and cement	Cork/70-80%	432	0.10	Tensile and compression strength of 0.77 MPa and 1.25 MPa, respectively, and Young modulus = 620 MPa.
	Natural hydraulic lime	Cork	642	0.14	Tensile and compression strength of 1.13 MPa and 2.10 MPa, respectively, and Young modulus = 1160 MPa.
Sousa, Frade and Santos (2014)	Natural hydraulic lime	Cork	600	0.1	Compression and flexural strength of 0.78 MPa and 0.4 MPa, respectively, Young modulus <600 MPa and adhesion = 0.1 MPa (to brick masonry).

Table 30 – Summary of the main properties obtained in the research studies, for cement and lime-based mortars.

Authors	Binder	Lightweight aggregate/ %addition	Bulk density (dry) (kg/m^3)	Thermal conductivity (dry) (W/m.ºC)	Mechanical properties/ Durability
Degirmenci and Yilmaz (2009)	Cement	Diatomite/ >5%	≈2150	-	Reached minimum requirements Increase of the compression strength, after freeze-thaw cycles
Ferrándiz-Mas and García-Alcocel (2013)	Cement	Granulated EPS+PSA/ 60%+30%	920	≈0.48	Class CSI
		Powder EPS+PSA/ 60%+30%	1230	≈0.52	Class CSII
Brás, Leal and Faria (2013)	Cement	Cork	1450-1550	≈0.50	Decrease of the flexural strength with the cork % addition (≈ linear proportion)
		EPS		0.70	Better mechanical strength compared to cork-based mortars
Panesar and Shindman (2012)	Cement	Cork / 10% (0,5-1mm)	≈2100*	1.04*	Decrease of the compressive strength and Young modulus
Cherki et al. (2014b)	White cement	Cork	≈850	≈0.305	Bulk density ≈ 2x less than the control mortar
Çavdar (2012)	Cement	Artificial fibres	910 (polypropylene fibres) - 2680 (glass fibres)	-	Increase of the mechanical properties at high temperatures
Braga, de Brito and Veiga (2012)	Cement	Concrete/15%	1815	-	Compression and flexural strength of 8.6 MPa and 2.7 MPa, respectively.
Oliveira, de Brito and Veiga (2013)	Cement	Glass powder/20%	1830	-	Compression and flexural strength of 7.7 MPa and 2.7 MPa, respectively, and Young modulus = 12.5 GPa.
Tittarelli (2013)	Cement	Hydrophobic material-GRP/ 0,5-5/	-	0.620	Increase of the compressive and flexural strength

Authors	Binder	Lightweight aggregate/ %addition	Bulk density (dry) (kg/m^3)	Thermal conductivity (dry) ($W/m.^oC$)	Mechanical properties/ Durability
Velosa and Veiga (2008)	Lime	Metakaolin	-	-	Compression and flexural strength of 1.3 MPa and 0.4 MPa, respectively, and Young modulus = 3000 MPa.
Faria, Silva and Flores-Colen (2012)	Lime	Metakaolin	-	-	Compression and flexural strength of 0.23-0.24 MPa and 0.05 MPa, respectively.
Vejmelková et al. (2012)	Lime	Metakaolin/20%	1767	0.731	Increase of the compressive and flexural strength

*Results obtained for the concrete-cork composite.

Table 31 – Summary of the main properties obtained in the research studies, for gypsum-based mortars.

Authors	Lightweight aggregate/ %addition	Bulk density (dry) (kg/m^3)	Thermal conductivity (dry) ($W/m.^oC$)	Mechanical properties/ Durability
Hernández-Olivares et al. (1999)	Cork (Winter pruning)/ 20%	578-864	0.126-0.200	Compression and flexural strength of 2.27 MPa and 2.26 MPa, respectively; Increase of the compressive strength, using winter cork from pruning e soils cleaning; Increase of both compressive and flexural strength, using glass fibre.
Cherki et al. (2014a)	Cork / 2,5-5mm to 8-12,5mm	472.32-447.32	0.124-0.101	-
Maia et al. (2015)	Cork	600	0.11	Adhesion = 0.2 MPa (to brick masonry) and 0.1 MPa (to concrete), with cohesive fracture.
Melo et al. (2012)	Vermiculite	877	0.30	-
	EVA (industrial waste)	847	0.26	-
de Oliveira et al. (2012)	Vermiculite/ 15%	920	-	Compression and flexural strength of 3.3 MPa and 2.5 MPa, respectively; Optimum% of vermiculite=20%
	EVA/ 15%	928	-	Compression and flexural strength of 3.2 MPa and 1.8 MPa, respectively; Optimum% of vermiculite=12.5%
Martias et al. (2013)	Vermiculite/ 5-25%	≈ 1000-500	0.46-0.27	Increasing %vermiculite highly increases the porosity, but reduces Young modulus.
Abidi et al. (2015)	Vermiculite/ 5-25%	-	0.45-0.23	Increase in the porosity (51-74%)
	Perlite/ 5-25%	-	0.35-0.16	Increase in the porosity (57-76%)
	Cement/ 5-25%	-	0.53-0.52	Constant porosity (42%)

Authors	Lightweight aggregate/ %addition	Bulk density (dry) (kg/m^3)	Thermal conductivity (dry) (W/m.ºC)	Mechanical properties/ Durability
Gutiérrez-González et al. (2012a)	Polyamide powder-gypsum/ 0,5-1 to 4-1	1190 to 751	0.2624 to 0.1397	Great loss of mechanical strength (%waste should be at most equal to %gypsum); Compressive strength (Ratio 1/1) ≈ 1 MPa; Decrease of the adhesion for high waste contents, but with cohesive fracture (Ratio 1/1 ≈ 6 MPa)
Gutiérrez-González et al. (2012b)	Polyurethane foam-gypsum/ 0,5-1 to 4-1	1258 to 535	0.316 to 0.104	Halving of the compressive and flexural strength, with 1/1 ratio (6,58MPa and 2,59MPa)

Table 32 – Summary of the degradation mechanisms, actions, agents, failures and conditions of failure occurrence on mortars.

Degradation mechanisms	Action(s)	Agent(s)	Failure(s)	Conditions for the occurrence
Freeze-thaw	Thermal/Mechanical/Chemical	Temperature/Ice/Water/Solar radiation	Disintegration Appearance	High moisture content during freeze-thaw, aggravated by chlorides and lack of drainage
Alkali-aggregate reaction	Chemical	Lime/Hydroxides	Expansion followed by disintegration	Silica or dolomite aggregates in the presence of moisture
Leaching of lime	Chemical	Lime/Hydroxides	Efflorescence Mortar disintegration	Vapour transfer and permeability
Biological attack	Biological	Moulds/Fungi	Strength Disintegration	Contact with sewage (acids generation)
Shrinkage	Thermal/Mechanical	Temperature/Solar radiation	Cracks Damages in adjacent components	High water/cement ratio
Temperature fluctuations	Thermal/Mechanical	Temperature/Solar radiation	Cracks	Large areas and hot climates

3. EXPERIMENTAL CHARACTERISATION OF THERMAL RENDERING AND PLASTERING SYSTEMS

3.1. MATERIALS AND EXPERIMENTAL METHODOLOGY

3.1.1. INTRODUCTION

One of the most important steps of the present work is the determination of the properties for the characterisation of the hygrothermal and mechanical performance of each studied material. In that sense, an extensive laboratory test campaign was implemented, enabling the evaluation of selected industrial thermal render systems. The main goal of the experimental campaign is the attainment of accurate results that will be used as input to numerical simulation. The relevance of those properties lies in the attainment of reliable simulation results that help on the study and development of a specific durability assessment methodology. Knowing the effective properties of each material that constitutes the thermal render systems allows the understanding of the main degradation mechanisms of this type of materials and more precise representation of their action.

Hence, to obtain practical results, a partnership with the Portuguese mortars industry was made. The selected thermal render systems correspond to commercial solutions. Four leading manufacturers contributed with thermal rendering systems, which are different between them, enabling a representative sample.

3.1.2. SELECTED THERMAL RENDERING AND PLASTERING SYSTEMS

Eight different materials, constituting four different rendering and plastering systems, were tested. Each system (S) consists of a thermal render/plaster (TR) and a finishing render/plaster (C). The selected materials for this study are described in Table 33 and shown in Fig. 14 to Fig. 17. Each system (S) is provided by a different manufacturer, implying that detailed knowledge of the formulations is not available owing to the industrial confidentiality of the materials available on the market.

Table 33 – Constituent materials of the studied thermal rendering and plastering systems.

Thermal rendering/plastering system	Render/ plaster/ Coating	Binders	Aggregates
S1	TR1	Lime	EPS and special additives
	C1	Natural hydraulic lime, cement, pozzolans and polymers	Mineral fillers, synthetic fibres and resins
	Organic coating (S1)	Mineral fillers, resins in aqueous dispersion, pigments, and specific additives (antifungals and others)	
S2	TR2	Mixed binders	EPS and specific additions
	C2	Hydraulic binders	Mineral fillers, synthetic fibres and resins
	Coating (S2)	Synthetic paint	
S3	TR3	Gypsum	Cork and special additives
	C3	Gypsum	Mineral fillers and special additives
S4	TR4	Lime	Mineral fillers, cork
	C4	Lime	Mineral fillers

a) b) c)

Fig. 14 – Photographs of: a) TR1; b) C1 and c) S1.

a) b) c)

Fig. 15 – Photographs of: a) TR2; b) C2 and c) S2.

a) b) c)

Fig. 16 – Photographs of: a) TR3; b) C3 and c) S3.

a) b) c)

Fig. 17 – Photographs of: a) TR4; b) C4 and c) S4.

In the case of manufacturers 3 and 4, the thermal plastering/rendering system consists only of the thermal plaster/render and the finishing plaster/render. Manufacturer 1 finishes the thermal rendering system by applying an organic coating consisting of mineral fillers, resins in aqueous dispersion, pigments, and specific additives (antifungals and others) (TR1+C1+coating). In addition, Manufacturer 2 finishes with a synthetic paint (TR2+C2+coating). Some of the thermal renders also have special additives in their formulation, which introduce air into the mixture. If the kneading time is exceeded, the combination of the amount of water and mechanical spraying could result in materials with a large number of air voids, beyond the intrinsic porosity of the lightweight aggregates (Sequeira et al. 2016). It is important to refer that the specimens produced to test the adhesive strength and impact resistance of Manufacturers 1 and 2 have, within the finishing render, a glass fibre mesh.

To be admitted in the tests, all the materials had to be guaranteed for adequate applicability by mechanical spraying and workability according to the industrial partner standards. The focus of the tests was therefore on the performance of the hardened products.

The selected tests covered different aspects that can be relevant for the hygrothermal and thermo-mechanical performance evaluation of thermal rendering systems, such as physical, thermal, hygric and mechanical properties of the materials. The experimental campaign included the tests listed in Table 34 and the procedures are described in the following sections. Each test was performed by taking into account the adequacy to the materials/systems and correspondent procedures. The TRs were tested for almost all the considered properties since they are the core material and they have a higher relevance in the system behaviour. The systems as a whole, however, were only tested for emissivity, capillary absorption using the ETAG 004 procedure, vapour diffusion, adhesion and impact resistance as these were the properties that would be influenced by the combination and thickness of layers.

Table 34 – Materials/specimens and corresponding experimental tests and standards.

Material properties	Test standard	Specimens dimensions (mm)	Specimen quantity (from each manufacturer)		
			TR	C	S
Dry bulk density	FE Pa 44 (LNEC 2015b)	40x40x40	3	3	*
Open porosity			3	3	*
Thermal conductivity (dry)	EN 12667 (CEN 2001)	300x300x30	2	*	*
Thermal conductivity (dry and moisture function)	ISO 8894-2 (ISO 2007)	210x210x20	2	2	*
Emissivity	ASTM C 1371-04a (ASTM 2010)	210x210x20	3	3	3
Capillary water absorption	EN ISO 15148 (ISO 2002)	100x100x200	3	3	*
Water absorption	ETAG 004 (EOTA 2013)	210x210x20	*	*	3
Moisture storage function	EN ISO 12572 (ISO 2000b)	100x100x20	3	3	*
Water vapour permeability	EN ISO 12571 (ISO 2000a)	210x210x20	3	*	3
Dynamic elastic modulus	EN 14146 (CEN 2004a)	160x40x40	3	3	*
Flexural and compressive strength	EN 1015-11 (CEN 1999)	160x40x40	3	3	*
Adhesion strength	EN 1015-12 (CEN 2000b)	500x600x20	5	*	5
Impact resistance	EN 13497 (CEN 2002b)	500x600x20	5	*	5

* Non-applicable

3.1.3. EXPERIMENTAL METHODS TO DETERMINE THE PHYSICAL AND HYGROTHERMAL PROPERTIES

3.1.3.1. Introduction

Some of the presented test procedures imply the determination of the dry mass m_0 of the specimens. To achieve that, the specimens are placed in a drying chamber (WTC Binder model as shown in Fig. 18) at 70ºC, excepting the gypsum-based materials, which are dried at 50ºC.

a) b)

Fig. 18 – a) Drying chamber WTC Binder; b) Placement of the specimens in the drying chamber.

3.1.3.2. Density, porosity and pore size distribution

The bulk density, real density, and open porosity tests were performed by hydrostatic weighing according to the test report FE Pa 44 "Determination of open porosity and bulk and real densities" (LNEC 2015a). Three cubic specimens (measuring 40 mm per side) of each material (thermal render and finishing render) were prepared and conditioned. The test begins by placing the specimens in a desiccator for 24 h in vacuum conditions. After this procedure, the samples were immersed for another 24 h. The hydrostatic and immersed weights were then registered. The equipment and test set are presented in Fig. 19.

Open porosity, P_0, is the ratio between the volume of open pores and the apparent volume of a specimen, in percentage, as presented in equation (5).

$$P_0 = \frac{m_s - m_0}{m_s - m_h} \times 100 \tag{5}$$

Where m_0 is the dry mass, m_h the immersed mass and m_s the saturated mass, in [kg].

The dry bulk density, ρ [kg/m^3], is the ratio between the dry mass and the apparent volume, shown in equation (6).

$$\rho = \frac{m_0}{m_s - m_h} \times \rho_{rh} \tag{6}$$

Where ρ_{rh} corresponds to the water density.

The real density, ρ_r [kg/m^3], is obtained through the equation (7).

$$\rho_r = \frac{m_0}{m_{0-} m_h} \times \rho_{rh} \tag{7}$$

a) b)

Fig. 19 – a) Desiccator and vacuum device; b) Hydrostatic weighing.

The microstructure and pore structure were studied using an optical microscope Olympus SZH10, as demonstrated in Fig. 20. These tests were performed in LNEC (National Laboratory for Civil Engineering) in the Building Coatings and Thermal Insulation Unit.

The pore size distribution and matrix properties were determined by mercury intrusion porosimetry (MIP) and helium pycnometry (HP) method using Quantachrome Poremaster device, with low (0.2-80 psia) and high (20-60,000 psia) pressure stations and pore size range of 1100-0.0036 μm. This test procedure was performed by the Laboratory for Process Engineering, Environment, Biotechnology and Energy (LEPABE) in the Faculty of Engineering of University of Porto (FEUP).

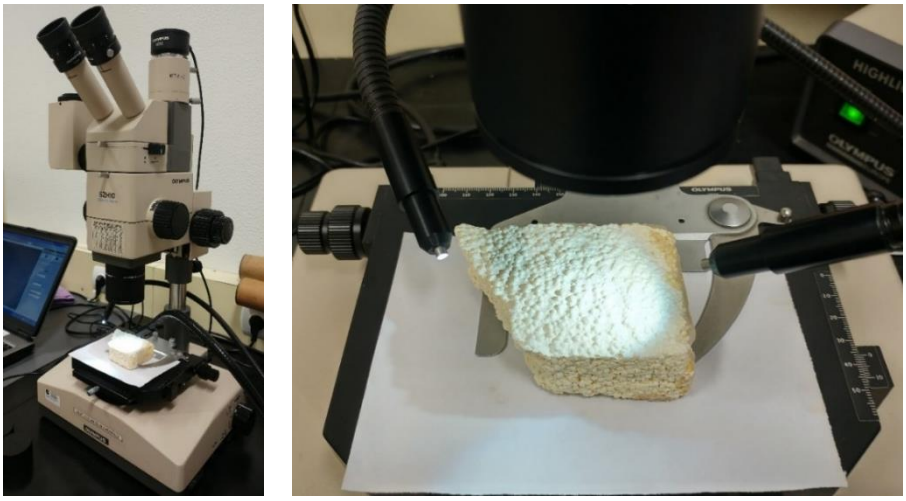

a) b)

Fig. 20 – a) Optical microscope Olympus SZH10; b) Zoom of the specimen area.

3.1.3.3. Thermal conductivity

The thermal conductivity measurement was performed by two different methods:

- Guarded Hot Plate Method (GHP): for dry state samples;
- Hot-wire Method (HW): for samples with different moisture content values.

The guarded hot plate method is based on the European standard EN 12667:2001 "Thermal performance of building materials and products – Determination of thermal resistance by means of guarded hot plate and heat flow meter methods – Products of high and medium thermal resistance " (CEN 2001). Two samples of each thermal render measuring 300x300x30 mm were tested in parallel, using a Holometrix GHP-300 (see Fig. 21 and Fig. 22).

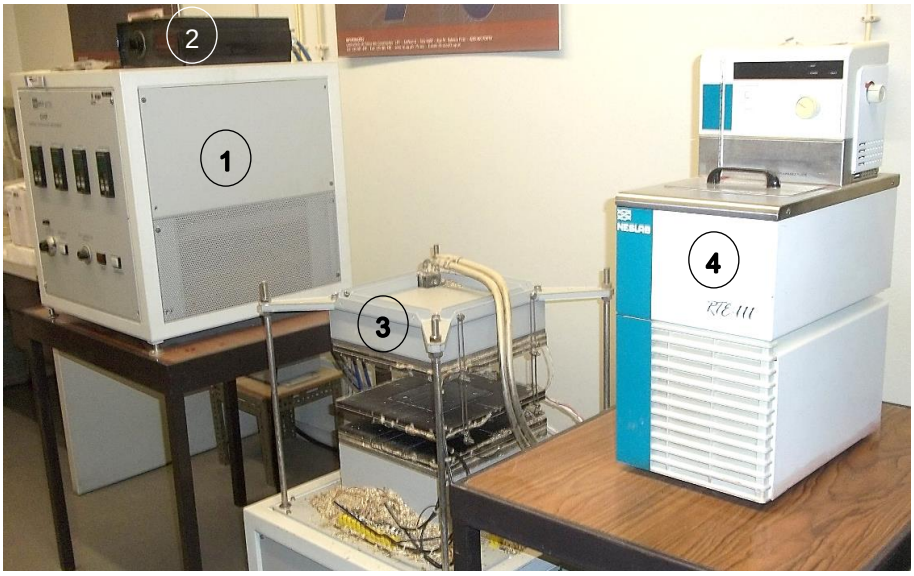

Fig. 21 – Holometrix GHP-300: 1) Temperature control; 2) Data acquisition; 3) Test specimens container; 4) Cooling device.

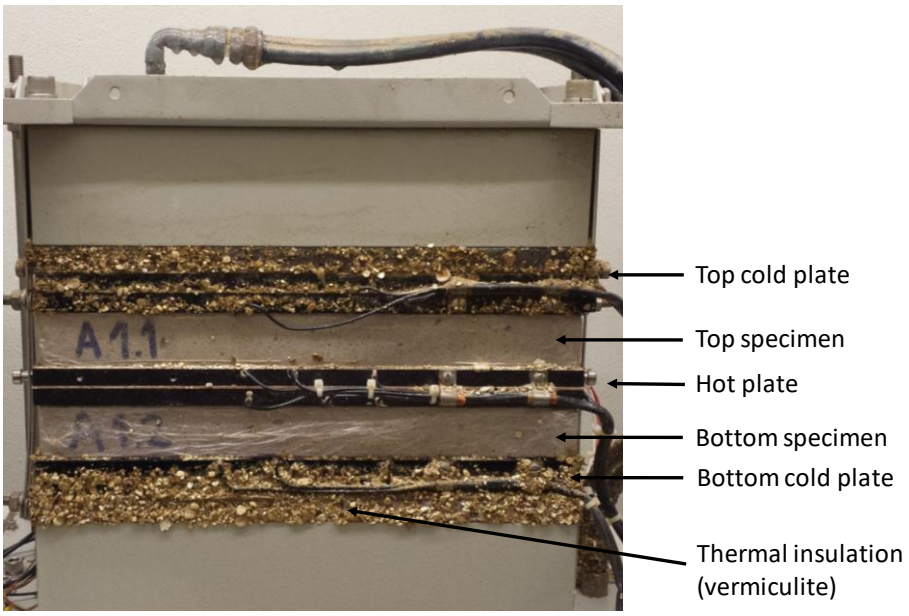

Fig. 22 – Test specimens container.

The hot-wire method (parallel) is a dynamic measuring procedure based on the measurement of the temperature increase at a certain location and at a specified distance from a linear heat source embedded between two test pieces. The test was conducted based on ISO 8894-2:2007 "Refractory materials – determination of thermal conductivity – Part 2: Hot-wire method (parallel)" (ISO 2007) to determine the thermal conductivity moisture dependence, using a CT-Metre (see Fig. 23) and testing in parallel two samples of 210×210x20 mm, using a "anneau" probe (see Fig. 24).

Fig. 23 – CT-Metre equipment: hot-wire method.

Fig. 24 – Detail of the used "anneau" probe connected to the CT-Metre.

These tests procedures were performed at the Laboratory of Building Physics (LFC – CONSTRUCT) in the Faculty of Engineering of University of Porto (FEUP).

3.1.3.4. Emissivity

Emissivity measurements were performed with an emissometer Model AE1 Emittance Measurements using a Port Adapter Model AE-ADP, at LFC, in accordance with the standard ASTM C1371 − 04a "Standard Test Method for Determination of Emittance of Materials Near Room Temperature Using Portable Emissometers" (ASTM 2010). Three test specimens of 210×210x20 mm were used. This test method uses a differential thermopile emissometer. It comprises one thermopile that is covered with a black coating and one that is covered with a reflective coating, for total hemispherical emittance

measurements. The detector thermopiles are heated in order to provide the necessary temperature difference between the detector and the surface. An adapter for measuring low thermal conductivity materials was used. Since the samples are larger than the heat sink, a fan was applied, to guarantee that the samples and the high emittance standard are at the same temperature (D&S 2011) (see Fig. 25).

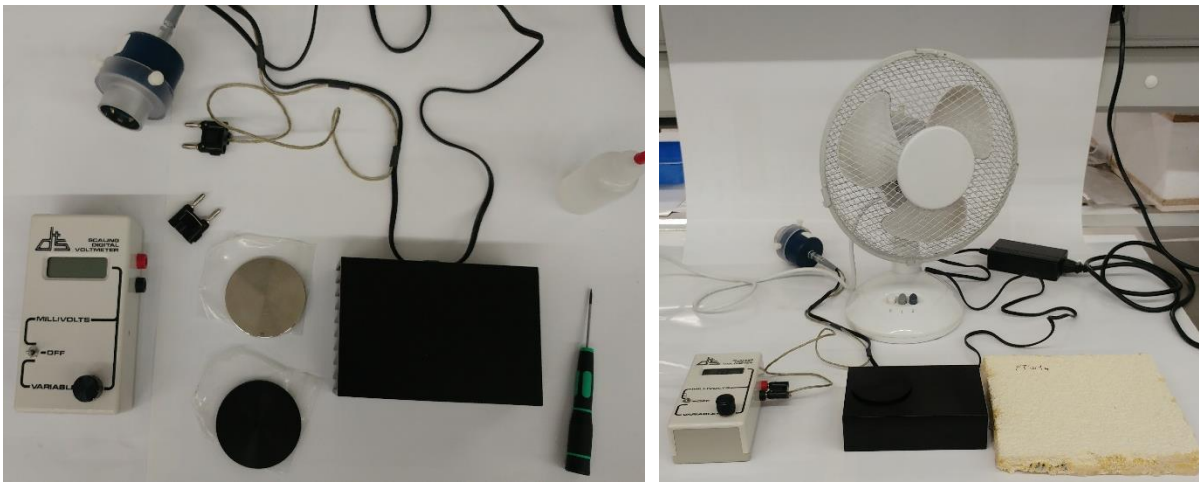

Fig. 25 – Emissometer Model AE1 Emittance Measurements, using a Port Adapter Model AE-ADP.

3.1.3.5. Capillary water absorption

The capillary water absorption test allows the determination of the water absorption coefficient, based on the European standard EN ISO 15148:2002 "Hygrothermal performance of building materials and products – Determination of water absorption coefficient by partial immersion" (ISO 2002). Three specimens of each material of 100×100x200 mm were prepared and the side faces sealed, at LFC. The test consists in placing a surface of each test specimen in contact with water, as demonstrated in Fig. 26, and afterwards register the mass variation due to capillary rise as a function of time.

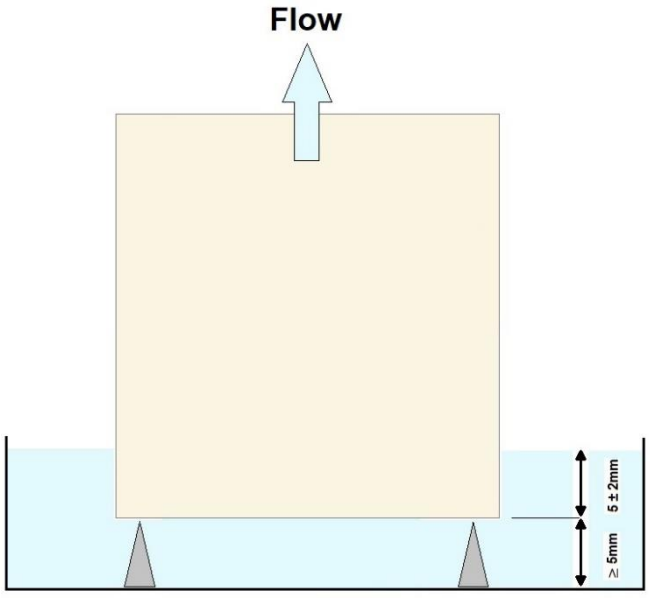

Fig. 26 – Specimen placement for capillary absorption determination according to EN ISO 15148.

Before the test, the specimens are conditioned at room conditions (temperature and relative humidity), until a constant mass is reached. When the test begins, the specimens are placed in contact with water and weighed at approximately 5 minutes, 20 minutes, 1 hour, 2 hours, 4 hours, 8 hours and 24 hours after the beginning of the test. Another weighing is performed between 8 and 24 hours.

The mass variation (Δm_t [kg/m^2]) as a function of time and water contact area, allows the calculation of the water absorption coefficient, A_w. According to EN ISO 15148 (ISO 2002), two distinct ways of calculation of the water absorption coefficient may be used, depending on the trend of the curves, obtained by the mass variation as a function of the square root of time. A linear trend is classified as Type A and the water absorption coefficient calculated by equation (8).

$$A_w = \frac{\Delta m'_{tf} - \Delta m'_{ti}}{\sqrt{t_f}} \tag{8}$$

Where $\Delta m'_{tf}$ is the value of Δm_t on the straight line at time t_f, in general 24h, $\Delta m'_{ti}$ is the Δm_t value at the beginning of the test in [kg/m^2] and $\sqrt{t_f}$ corresponds to the square root of test total time, in seconds, generally 24h. If liquid water on the top surface is observed, the resulting graph shows a straight line with a sudden decrease in slope. In this case, the water absorption coefficient can be calculated with a value of t_f less than 24 hours, when the liquid water appears on the top surface.

When the trend is a curve, it is classified as Type B and the water absorption coefficient calculated by equation (9).

$$A_w = \frac{\Delta m_{tf}}{\sqrt{t_f}} \tag{9}$$

Where Δm_{tf} is the value of Δm_t at time t_f, in general 24h.

According to EN 998-1 (CEN 2010), the water absorption coefficient of thermal mortars should be less than or equal to 5 x 10^{-2} kg/m^2.s^{0,5}.

To determine the capillary absorption of the thermal rendering system, the ETAG 004 (EOTA 2013) procedure was performed. Three specimens of each material of 210×210×20 mm were prepared and the edges of the samples, including the insulation product, were sealed against water penetration. The test consists of a previous ageing of the samples, with wetting-drying cycles, and subsequent immersion with the rendered face downwards, to a depth of 2 to 10 mm. The ageing consists of three cycles of:

- 24 h immersion in a water bath (tap water), with the immersion of the rendered face samples downwards, to a depth of 2 to 10 mm;
- 24 h drying at (50±5ºC).

After the ageing, the specimens should be conditioned during at least 24 h at (23±2ºC) temperature and (50±5%) of relative humidity. The test comprises the following stages:

The samples are weighed after 3 minutes immersion in the bath (reference mass) and then after 1 hour and 24 hours. Prior to the second and subsequent weighing, water adhering to the surface of the sample is removed with a damp sponge cloth.

- Weighing after immersion for 3 minutes – m_{ref};
- Weighing after immersion for 1 hour – m_{1h};
- Weighing after immersion during 24 hour – m_{24h}.

The water absorption of the systems is calculated for 1 hour (see equation (10)) and 24 hours (see equation (11)).

$$A_{1h} = \frac{m_{1h} - m_{ref}}{\mathrm{A}} \tag{10}$$

$$A_{24h} = \frac{m_{24h} - m_{ref}}{\mathrm{A}} \tag{11}$$

Where A corresponds to the face area of the specimens.

3.1.3.6. Moisture storage function

The moisture storage function describes the moisture content, $w(\varphi)$, of a porous material in both hygroscopic and over-hygroscopic range. An approximation to the moisture storage function can be defined using points in both ranges (Künzel 1995).

The determination of moisture content values on the hygroscopic range was based on ISO 12571: 2000 "Hygrothermal performance of building materials and products - Determination of hygroscopic sorption properties" (ISO 2000a). The test was conducted in a climatic chamber Vötsch VC 4034, in LFC, at two relative humidity values, 80% and 90%, at constant temperature (23±0.5°C), for test specimens of 100x100x20 mm (see Fig. 27). In the over-hygroscopic range, free water saturation was determined by immersion of the test specimens and hydrostatic weighing according to FE Pa 44 "Determination of open porosity and apparent and real densities" (LNEC 2015a), as explained in 3.1.3.2.

a) b)

Fig. 27 – a) Climatic chamber Vötsch VC 4034; b) Placement of the specimens for the determination of the moisture storage functions.

The test results are expressed by the equation (12), calculating the representative values of the equilibrium between the moisture content – w – and relative humidity – φ.

$$w(\varphi) = \frac{m_{w(\varphi)} - m_0}{m_0} \quad (12)$$

Where $m_{w(\varphi)}$ is the mass of the specimen, in equilibrium with the ambience, and m_0 the mass of the dry specimen.

3.1.3.7. Water vapour permeability

The water vapour permeability test was based on ISO 12572:2000 – "Hygrothermal performance of building materials and products. Determination of water vapour transmission properties" (ISO 2000b). Six specimens of each material (thermal render and thermal render system) of 210×210×20 mm were tested under two different ranges of relative humidity differences across the sample: wet cup and dry cup, in a climatic chamber, in LFC (see Fig. 28-(a)). The chamber – Fitoclima 3600 EDTU – presents controlled conditions: 23±0.3°C and 50%±3% relative humidity. The effective relative humidity in the cup test is obtained by using a $CaCl_2$ compound (φ = 0% for the dry-cup test) and a KNO_3 solution compound (φ = 94%±0.6% for the wet-cup test), as described in Table 35.

Table 35 – Water vapour permeability test conditions.

Test method	Normalized conditions (ºC/%φ)	Effective temperature (ºC)	Effective relative humidity (%)	
			Climatic chamber	Cup test
Dry cup	23/0-50	23±0.3	50±3	0
Wet cup	23/50-93	23±0.3	50±3	94±0.6

Prior to testing, all the specimens are preconditioned in the climatic chamber at 23 °C and 50% of relative humidity. After stabilisation, the specimens are placed in metallic test cups, with the referred conditions, and the sides of the specimens are sealed with paraffin wax, as shown in Fig. 28-(b).

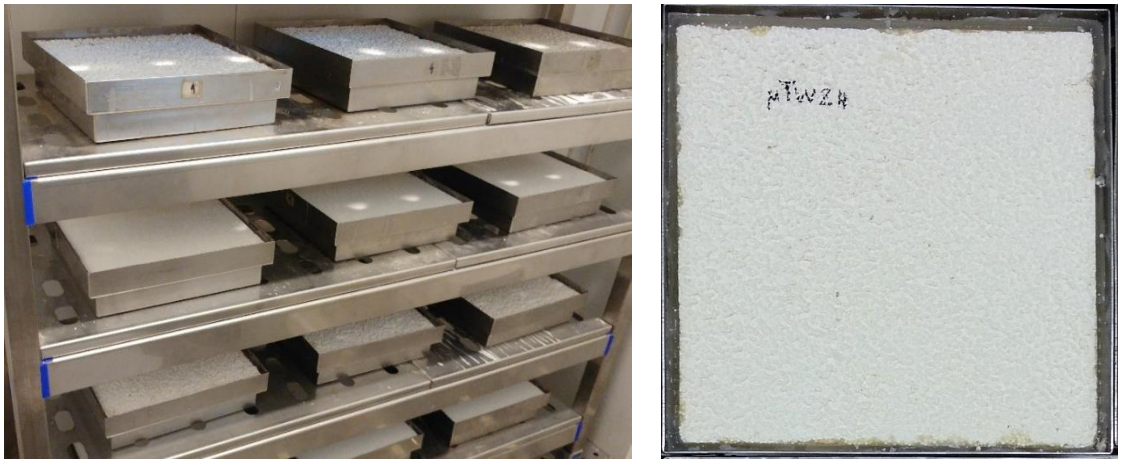

(a) (b)

Fig. 28 – a) Placement of the specimens in the climatic chamber; b) Sealing of the sides of the specimen with paraffin wax, in a metallic cup.

The two test conditions – dry and wet cup – allow evaluating the water vapour permeability as a function of the relative humidity. The test results are:

- Water vapour flow rate through specimen – G, in kg/s;
- Density of water vapour flow rate – g, in kg/(m^2·s);
- Water vapour permeance – W_p, in kg/(m^2·s·Pa);
- Water vapour permeability – δ_p, in kg/(m·s·Pa);
- Water vapour resistance factor – μ, dimensionless;
- Water vapour diffusion-equivalent air layer thickness – s_d, in metres.

In addition, according to EN 998-1 (CEN 2010), the water vapour resistance factor of thermal renders should be less than 15.

3.1.4. EXPERIMENTAL METHODS TO DETERMINE THE MECHANICAL PROPERTIES

3.1.4.1. Dynamic elastic modulus

The dynamic elastic modulus can be determined by a non-destructive test, measuring the fundamental resonance frequency, carried out according to the norm EN 14146 – "Natural stone test methods. Determination of the dynamic elastic modulus of elasticity (by measuring the fundamental resonance frequency) (CEN 2004a), using the ZRM Zeus 2005 equipment, at LNEC. The referred standard preconizes two different methods to determine the fundamental resonance frequency: one based in the continuous excitation and the other one based on the instantaneous excitation of the specimens. Both methods consist of vibrating the specimen using longitudinal, flexural or torsional vibrations and then record the resonance frequency. The experimental setup is demonstrated in Fig. 29-a), placing the electric pulse generator in one face of the specimen and in the opposite a receptor transducer, as shown in Fig. 29-b).

a) b)

Fig. 29 – a) Equipment for the determination of the dynamic elastic modulus; b) Longitudinal measurement.

The dynamic elastic modulus calculated by equation (13).

$$E_d = 4 \times 10^{-6} \times l^2 \times F_L^2 \times \rho \quad (13)$$

Where l is the length of the specimen , in [m], F_L is the longitudinal fundamental resonance frequency, in [Hz] and ρ the dry bulk density, in [kg/m^3].

3.1.4.2. Flexural and compressive strength

The flexural and compressive strength of mortars is determined by the EN 1015-11 – "Methods of test for mortar for masonry - Part 11: Determination of flexural strength and compressive strength of hardened mortar" (CEN 1999). Fig. 30 presents the testing equipment (press, load cell, etc.) used for the flexural and compressive strength determination, ETI-HM-S from PROETI, at LNEC.

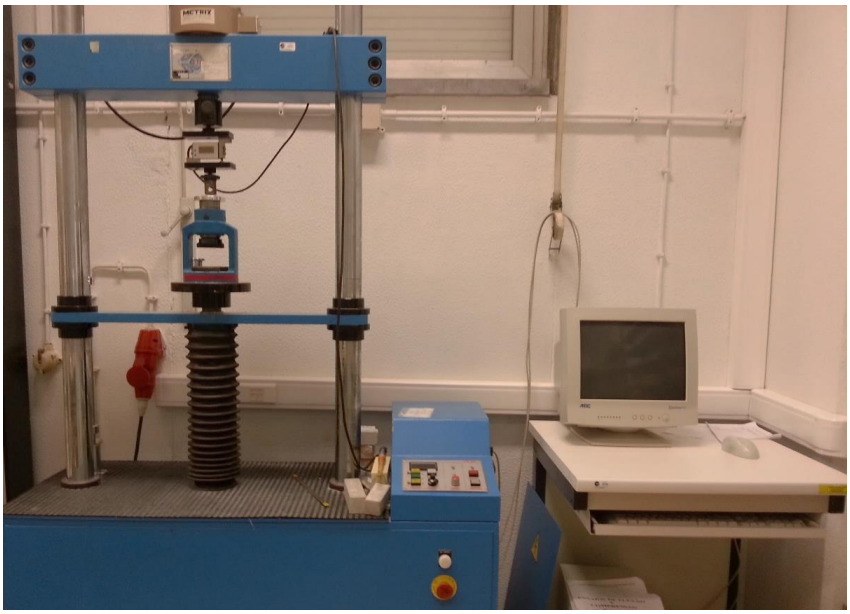

Fig. 30 – Testing equipment for flexural and compressive strength determination.

According to this standard, the flexural strength is determined by applying a three-point load on a prismatic specimen, measuring 160x40x40 mm, until failure takes place. The compressive strength is determined on the two parts of the specimen resulting from the flexural strength test. Thermal renders required a load cell of 2 kN and the finishing renders of 200 kN.

A uniform load in the range of 10 N/s to 50 N/s is used to perform the flexural strength test so that the failure occurs within 30 to 90 seconds (see Fig. 31-a)). The maximum applied load – F – needs to be recorded, in [N]. Equation (14) presents the calculation of the flexural strength R_{flex}, in [N]:

$$R_{flex} = 1.5 \times \frac{F l_{flex}}{b_{flex} d_{flex}^2} \tag{14}$$

Where l_{flex} is the distance between the axes of the support rollers in [mm], b_{flex} is the width and d_{flex} is the depth of the specimen in [mm].

The prisms resulting from the flexural strength test shall be prepared for the compressive strength test so that the specimen has a cubic and solid shape. The specimen shall be aligned so that the load is being applied to the whole width of the face in contact with the platens. A uniform load in the range of 50 N/s to 500 N/s, so that the failure occurs within 30 to 90 seconds, shall be applied. (see Fig. 31-b)). The compressive strength is given by the ratio between the maximum force applied to the specimen and the cross-sectional area.

a) b)

Fig. 31 – a) Flexural strength test; b) Compressive strength test.

3.1.4.3. Adhesive strength

The adhesive strength test is performed based on the EN 1015-12 – "Methods of test for mortar for masonry – Part 12: Determination of adhesive strength of hardened rendering and plastering mortars on substrates" (CEN 2000b) and for gypsum-based materials the EN 13279-2 – "Gypsum binders and gypsum plasters - Part 2: Test methods" (CEN 2004b). According to EN 1015-12, the adhesive strength is determined as the maximum tensile stress applied by a direct load perpendicular to the surface of the rendering mortar on a substrate and is obtained by the quotient between the failure load, in [N] and the test area, in [mm^2]. The test was performed at LFC using a testing machine – Proceq DY-216 – to apply the tensile load by means of a square pull-head (50x50 mm) glued to the test area (with epoxy resin) (see Fig. 32). Despite the EN 1015-12 indicating circular pull-heads, the test was performed using square pull-heads, due to the great disturbance of the core drilling machine and the lower strength of the thermal mortars.

a) b)

Fig. 32 – a) Testing machine Proceq DY-216; b) Testing machine attached to the glued pull-head.

Masonry units were selected as test substrates and produced rectangular panels, with an area around 500x600 mm^2 since it is a widely used substrate. The adhesion of a 2 cm thickness thermal mortar (usual thickness for a single layer) to the substrate was tested. In addition, the thermal render systems were also tested, as shown in Fig. 33.

Fig. 33 – Samples used to determine the adhesive strength of a thermal render system (left) and a thermal render itself (right).

Before glueing the pull-heads, 5 test specimen pre-cuts should be performed, using an angle grinder, with controlled cutting depth, until the substrate.

A tensile load perpendicular to the test area, at a uniform rate, shall be applied. The loading rate was defined according to the expected adhesive strength of the material, as demonstrated in Table 36. The thermal renders usually present low adhesive strength, lower than 0.2 N/mm^2.

Table 36 – Loading rate related to the expected adhesive strength.

Expected adhesive strength (N/mm^2)	Loading rate	
	(N/s)	(N/mm^2.s)
< 0.2	5	0.003
0.2 até 0.5	25	0.013
0.5 to 1.0	100	0.050
> 1.0	200	0.100

In addition to the calculation of the adhesive strength, the fracture pattern may be identified. Three facture patterns are described in EN 1015-12:

- Adhesion fracture at the interface between mortar and substrate: test value equals the adhesive strength;
- Cohesion fracture in the mortar itself: the adhesive strength is greater than the test value;
- Cohesion fracture in the substrate material: the adhesive strength is greater than the test value.

Adhesion fractures in the glueing are considered as a non-acceptable result.

The test procedure according to the EN 13279-2, regarding the gypsum-based materials, is similar to the one presented in EN 1015-12. Regarding the ETAG 004, the bond strength between the substrate and the insulation material should be at least 0.25 MPa, in dry conditions. Analysing the bond strength between the insulation and the adhesive material, also in dry conditions, the adhesive ruptures or cohesive ruptures (in the adhesive) should present strength of at least 0.08 MPa and the cohesive ruptures in the insulation of at least 0.03 MPa.

3.1.4.4. Impact resistance

The resistance to impact is based on the EN13497 – "Thermal insulation products for building applications - Determination of the resistance to impact of external thermal insulation composite systems (ETICS)" (CEN 2002b). The guided fall of 2 steel balls method was performed at LFC.

This method uses 2 steel balls for obtaining two impact energies:

- 2 J: with a steel ball of (500±5) g falling from a height of (408±1) mm;
- 10 J: with a steel ball of (1000±10) g falling from a height of (1020±1) mm.

According to the EN13497, the qualitative analysis consists of evaluating the visible damages. The following are considered as damages:

- The reinforcement has become visible;
- The finishing material or the base coat has visibly delaminated;
- The base coat with the reinforcement has been perforated.

In addition to the qualitative analysis, the mean diameter of the dent is measured (five dents). The test samples have the same characteristics as the used for the adhesive strength test.

ETAG 004 also foresees the hard body impact evaluation. In that way, three categories, which attest the adequacy of the systems to the possible uses, are defined (EOTA 2013):

- Category I: accessible zones (at ground level) and vulnerable to hard body impacts but not subjected to abnormally rough use;
- Category II: possible impacts in public locations, where the height of the system application will limit the size of the impact or at lower levels where the access to the building is controlled;
- Category III: zone not likely to be damaged by normal impacts caused by people or by thrown or kicked objects.

Depending on the qualitative analysis resulting from the hard body impacts, the systems could be classified as Category I to III and consequently applied in different places.

3.2. EXPERIMENTAL RESULTS

3.2.1. PHYSICAL AND HYGROTHERMAL PROPERTIES

3.2.1.1. Density, porosity and pore size distribution

The density and open porosity measured by hydrostatic weighing and MIP/HP methods are presented in Table 37 and Table 38, respectively.

Table 37 – Density and open porosity measured by hydrostatic weighing method.

Mortar	Bulk density * (kg/m^3)	Density* (kg/m^3)	Open porosity* (%)
TR1	208.7±1.36	319.7±6.23	34.7±0.88
TR2	406.2±6.94	563.3±2.42	27.9±1.36
TR3	659.5±5.44	1334.1±23.61	50.6±1.25
TR4	1476.6±9.86	1765.9±10.56	16.4±0.17
C1	1197.0±8.54	1892.9±5.38	36.8±0.43
C2	1357.3±17.20	1908.9±1.88	28.9±0.84
C3	1261.4±2.52	2034.2±5.18	38.0±0.19
C4	1595.2±7.82	2246.7±7.47	29.4±0.12

* Results presented as (average ± standard deviation)

Table 38 – Density and open porosity measured by MIP/HP method.

Mortar	Bulk density * (kg/m^3)	Density* (kg/m^3)	Open porosity* (%)
TR1	266.6.±15.68	484.7±0.00	37.6±11.45
TR2	594.7±61.07	1029.3±0.00	48.2±3.97

* Results presented as (average ± standard deviation)

From the hydrostatic weighing method, thermal renders TR1 and TR2 present lower density than TR3. Because the bulk density of EPS is lower than that of cork (by ~90%), the results are consistent. Thermal render TR1 also has special additives that could be the cause of almost half of the reduction in density compared to TR2. The presented results are similar to the values presented in previous studies. The authors in (Dylewski and Adamczyk 2014; Brites, Frade and Santos 2014; Vale et al. 2014) tested lime-cement-based mortars with different proportions of EPS and the results are similar to those for TR1. TR2 probably has a lower proportion of EPS. In terms of TR3 bulk density, the results are in accordance with the studies (Hernández-Olivares et al. 1999; Cherki et al. 2014a; Vale et al. 2014) on gypsum–cork mortars. Finishing renders have similar density values despite the different binders. In addition, it was found that open porosity was approximately 30%, with the exception of TR3 (~50%). TR4 presents a very high density for a thermal rendering, which according to (Veiga 2010) should be less than 600 kg/m^3. In this case, the bulk density more than doubles the obtained value for TR3 (also with cork addition). This fact is in accordance with the low porosity compared to the other thermal renders.

Fig. 34 to Fig. 37 present the optical microscope images of the studied systems. All images were captured using 0.7× resolution lens.

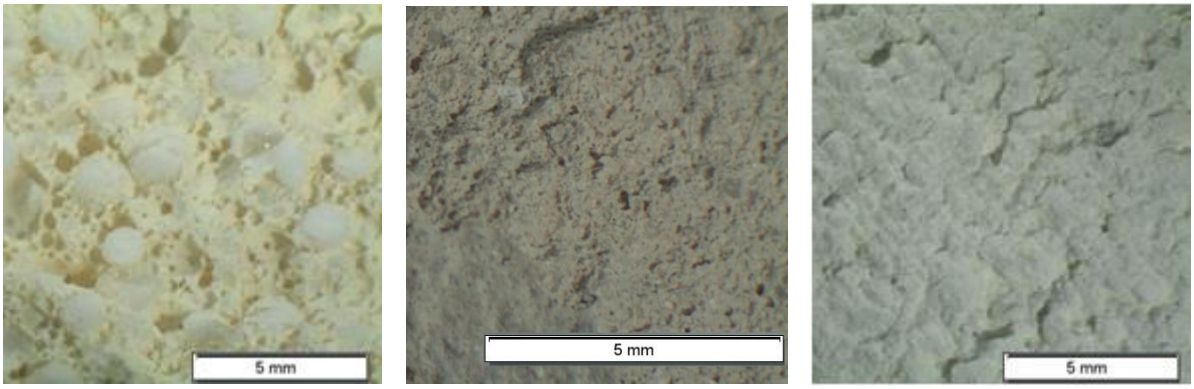

a) b) c)

Fig. 34 – Optical microscope images: a) TR1; b) C1; c) Finishing coating of S1.

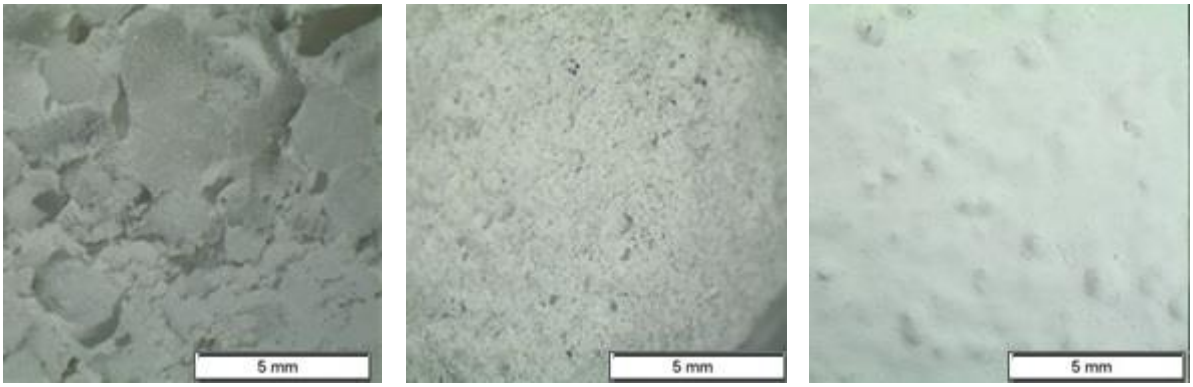

a) b) c)

Fig. 35 – Optical microscope images: a) TR2; b) C2; c) Finishing coating of S2.

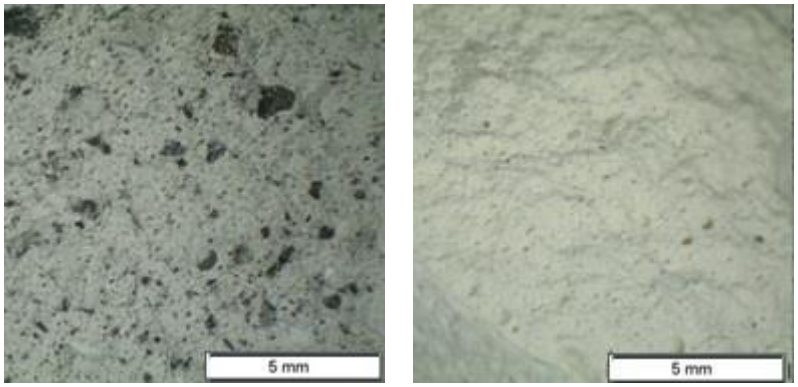

a) b)

Fig. 36 – Optical microscope images: a) TR3; b) C3.

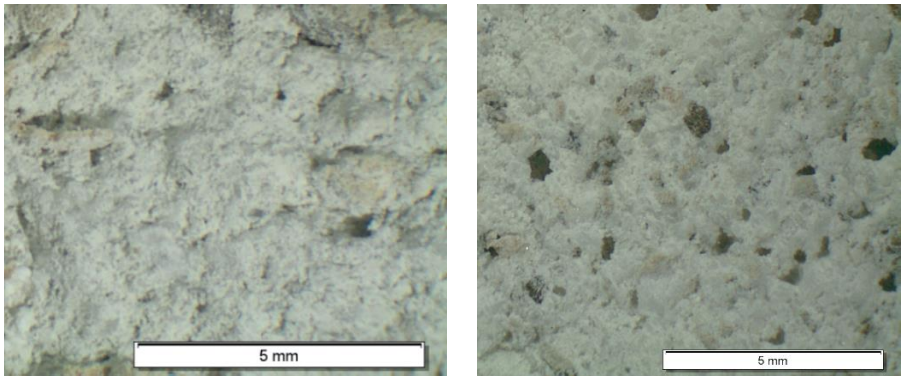

a) b)

Fig. 37 – Optical microscope images: a) TR4; b) C4.

Considering that thermal renders TR1 and TR2 have low density, large closed pores are expected (a fact supported by optical microscope images in Fig. 34 and Fig. 35), related to the EPS that correspond to a very significant volume. Because of their closed pores, bulk density decreases but open porosity, which is not influenced by that type of pore, does not increase. The obtained results presented in Table 38 are supported by the microscope images, such as TR4, which presents a compact microstructure. In comparing thermal renders with finishing renders, it is clear from the microscope images that the former have larger pores and a more complex porous network. Fig. 38 shows the mercury intrusion porosimetry results. The specific pore volume of thermal render TR1 is higher than that of TR2. In addition, the pore size distribution curves reveal that TR1 has a higher volume of large pores than does TR2, which has a greater pore size distribution. The peak at ~8 µm stands out in Fig. 38-b) for both mortars, which could correspond to the interior size of EPS granules. According to the IUPAC classification (Rouquerol et al. 1994), both thermal renders have no micropores. TR2 presents fewer macropores than TR1, which contribute to the low bulk density. The pore size distribution, in the smaller range of pores, is in accordance with the porosimetry of the binders: macropores are typical of lime binders whereas mesopores are present in hydraulic matrixes. Capillary porosity is assumed to have a major effect on the transport process. Pore sizes from 0.01 to 0.05 µm are referred to as medium capillaries and those from 0.05 to 10 µm are classified as large capillaries. Above 10 µm, pores are classified as air voids (Pipilikaki and Beazi-Katsioti 2009). Capillary pores are highly interconnected and, in the case of lime-based mortars, like TR1, porosity is further influenced by the carbonation of Ca(OH)2 to CaCO3, which represents a 10% volume increase (Papanyianni and Stefanidou 2001).

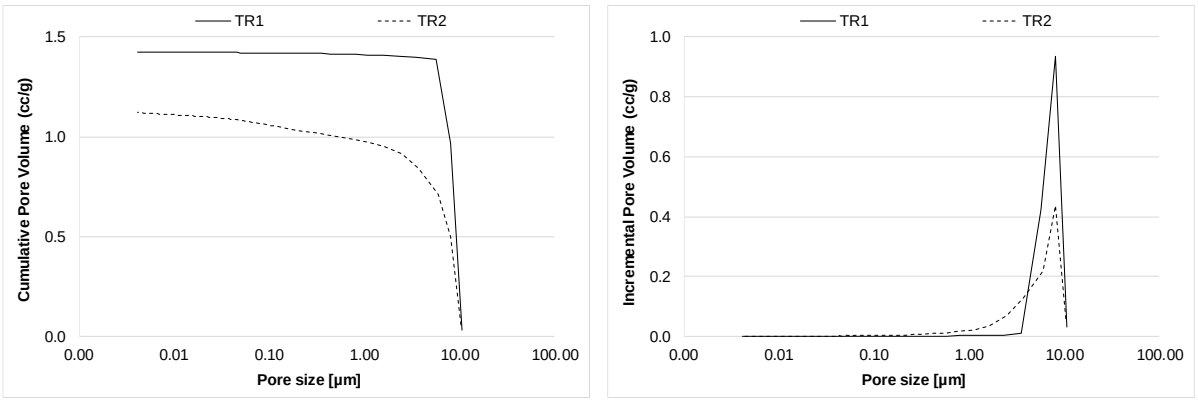

a) b)

Fig. 38 – Pore size distributions of TR1 and TR2: a) Cumulative pore volume and b) Incremental pore volume.

3.2.1.2. Thermal conductivity and emissivity

The results of thermal conductivity obtained by the two selected methods and the results of emissivity are presented in Table 39.

Table 39 – Thermal conductivity and emissivity at dry state.

Property	λ (GHP)*	λ (HW)*	ε*
Material	$\lambda_{10.dry}$ (W/m.ºC)	$\lambda_{20.dry}$ (W/m.ºC)	(-)
TR1	$0.049\pm3.129\times10^{-5}$	$0.050\pm6.325\times10^{-4}$	$0.88\pm1.000\times10^{-2}$
TR2	$0.078\pm1.400\times10^{-5}$	$0.077\pm7.071\times10^{-4}$	$0.88\pm0.000\times10^{0}$
TR3	$0.134\pm1.816\times10^{-5}$	$0.140\pm1.095\times10^{-3}$	$0.89\pm5.774\times10^{-3}$
TR4	$0.259\pm1.956\times10^{-4}$	—	$0.92\pm5.196\times10^{-2}$
C1	—	$0.220\pm3.761\times10^{-3}$	$0.90\pm5.774\times10^{-3}$
C2	—	$0.370\pm7.721\times10^{-3}$	$0.87\pm0.000\times10^{0}$
C3	—	$0.292\pm5.014\times10^{-3}$	$0.88\pm0.000\times10^{0}$
C4	—	$0.431\pm9.342\times10^{-3}$	$0.87\pm0.000\times10^{0}$
S1	—	—	$0.92\pm0.000\times10^{0}$
S2	—	—	$0.91\pm5.774\times10^{-3}$

* Results presented as (average ± standard deviation)

Since TR4 presented a thermal conductivity (measured by the GHP method) above 0.2 W/(m·ºC), this material could not be classified as a thermal render according to EN 998-1 (CEN 2010). In addition, the high bulk density is not expectable for a thermal render. As such, the materials from the Manufacturer 4 were not further evaluated.

Comparing the two test methods shows that thermal renders present similar thermal conductivity, with a strong correlation (R^2=0.9973), as demonstrated in Fig. 39. However, the hot-wire method leads to higher standard deviations than the guarded hot plate method. As can be seen, and as expected, the lightweight aggregates produce a positive effect on decreasing thermal conductivity, when compared to traditional cement or lime-based mortar ($\lambda \approx$ 1.3-1.8 W/(m·ºC)) or gypsum plaster ($\lambda \approx$ 0.40-0.57 W/(m·ºC)) (D&S 2011).

Binders and additives have a significant effect on the results of thermal renders TR1 and TR2 that have EPS as a lightweight addition. The results are in accordance with the studies previously cited (Dylewski and Adamczyk 2014; Brites, Frade and Santos 2014; Vale et al. 2014) in the case of lime- and cement-based mortars with EPS addition and with studies (Hernández-Olivares et al. 1999; Cherki et al. 2014a; Vale et al. 2014) on gypsum–cork mortars.

Heat transfer takes place not only by conduction but also by convection and radiation. Consequently, the thermal conductivity of lightweight porous materials is certainly affected by bulk density but also by porosity and pore structure, which could present large heterogeneity (Júlio et al. 2016a). Fig. 40 presents an exponential correlation, which was obtained between dry bulk density and thermal conductivity in the dry state (R^2=0.9717). Also in (Gomes et al. 2017), the authors have found an

exponential correlation between these two properties. As expected, the difference between thermal renders and finishing renders is clear.

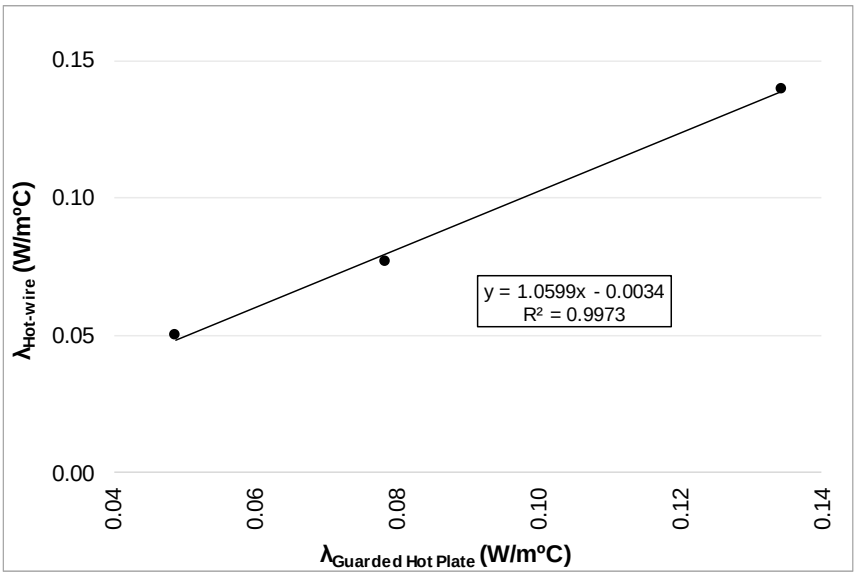

Fig. 39 – Correlation between Guarded Hot Plate and Hot-Wire methods to determine thermal conductivity, in the dry state.

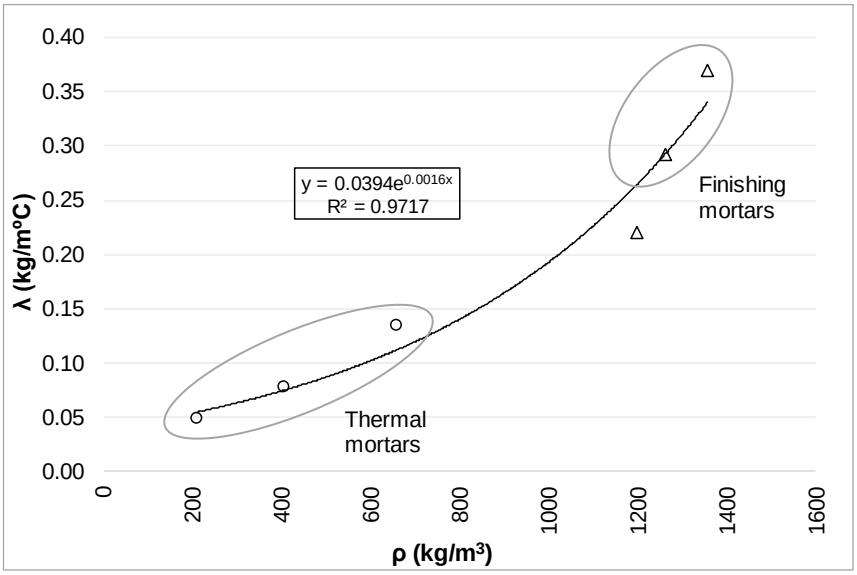

Fig. 40 – Thermal conductivity as a function of bulk density.

The dependence of the thermal conductivity on moisture content was studied by several authors (Toman and Černý 2001; Grunewald 2000; Gomes et al. 2017) and can be numerically determined by equation (15) (IBP 2016).

$$\lambda_w = \lambda\left(1 + b\frac{w}{\rho}\right) \tag{15}$$

Where λ_w is the thermal conductivity of the moist material and λ is the thermal conductivity of the dry material [W/m.ºC], w is the water content [kg/m^3], ρ is the bulk density of the dry material [kg/m^3] and b is the moisture-induced thermal conductivity supplement [%/M.-%]. This supplement corresponds to how many percent the thermal conductivity increases per mass percent of moisture (Künzel 1995).

Fig. 41 analyses the relation between thermal conductivity and moisture content of the studied thermal renders.

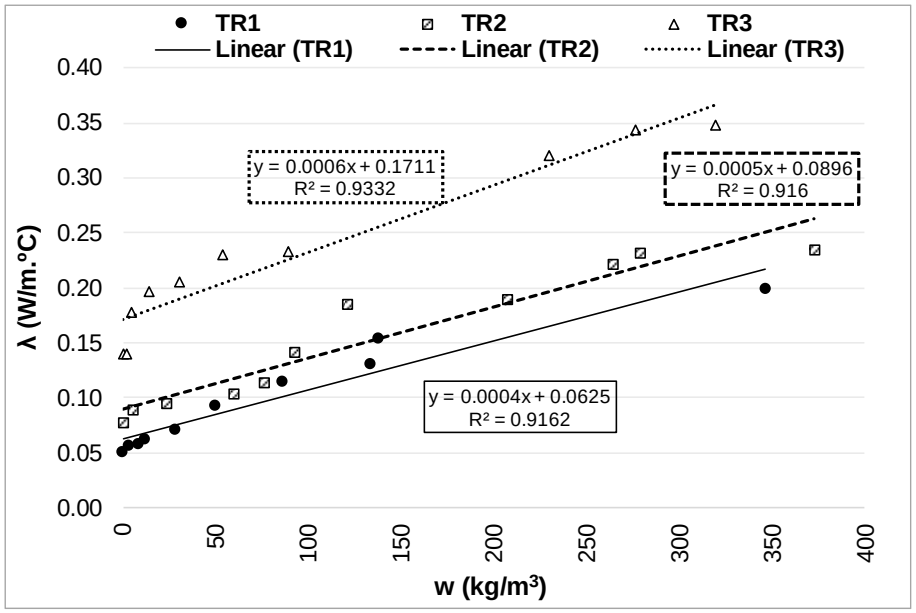

Fig. 41 – Thermal conductivity as a function of moisture content.

As it can be seen, the thermal renders exhibit similar behaviour, as indicated by the similar trend of the linear regressions. As expected, TR3 presents a higher linear slope – m-value ($m1$ = 0.0006, $m2$ = 0.0005, and $m3$ = 0.0004), so thermal conductivity increases at a higher rate than in the other materials. The linear regression of TR3 is presented to highlight this fact because this material has a distribution closer to a logarithmic regression, owing to its behaviour in the hygroscopic range. However, it is possible that the inclusion of cork as a lightweight aggregate has reduced the ability of gypsum-based mortars to absorb water because the slope of the linear regression is very close to those of the other analysed renders. This could be due to suberin in cork composition, which is a hydrophobic substance (Pereira 2007). TR1 and TR2, which have the same aggregate, present almost equal linear regression slopes. Several authors observed in their experimental tests a linear correlation between thermal conductivity and moisture content of different mortars such as lightweight renders (Gomes et al. 2017; Mňahončáková et al. 2006).

The emissivity values for both thermal renders and coatings are similar (with low variability) and are in accordance with the measurements performed in (Barreira et al. 2015). It can be concluded that the materials have a high emissivity. Moreover, the coatings actually increased the emissivity of the finished surface, which means that the finishing coating reflects more energy than the finishing render.

3.2.1.3. Capillary absorption

The capillary water absorption of the analysed materials is presented in Table 40. Regarding the whole system, the capillary absorption coefficient is presented for a 24h test duration.

Table 40 – Capillary absorption coefficient results.

Property	A_w (ISO 15148)*		A_w (ETAG 004)*
Material	(kg/m^2.s$^{0.5}$)	Graph type	(kg/m^2.s$^{0.5}$)
TR1	$2.96\text{x}10^{-2}\pm1.289\text{x}10^{-3}$	B (convex curve)	—
TR2	$1.42\text{x}10^{-2}\pm1.016\text{x}10^{-3}$	B (convex curve)	—
TR3	$2.82\text{x}10^{-1}\pm1.414\text{x}10^{-4}$	A (liquid water on the top)	—
C1	$6.45\text{x}10^{-3}\pm2.121\text{x}10^{-4}$	A (straight line)	—
C2	$1.61\text{x}10^{-2}\pm1.225\text{x}10^{-4}$	B (convex curve)	—
C3	$2.10\text{x}10^{-1}\pm1.485\ \text{x}10^{-3}$	A (liquid water on the top)	—
S1	—	—	$1.56\ \text{x}10^{-3}\pm6.589\text{x}10^{-4}$
S2	—	—	$2.19\text{x}10^{-3}\pm2.115\text{x}10^{-4}$
S3	—	—	$2.68\text{x}10^{-2}\pm1.340\text{x}10^{-5}$

* Results presented as (average ± standard deviation)

The different behaviour of gypsum-based materials in terms of capillary absorption stands out (see Fig. 42) of an order of magnitude comparing to thermal renders TR1 and TR2. Finishing renders C1 and C2 that have hydraulic binders in their composition present a similar behaviour, but with capillary absorption coefficient variation of an order of magnitude between each material (TR1<TR2<TR3). The results for the gypsum-based materials show that they have a strong capillary network, which enables rapid water percolation (confirmed in Fig. 42 by horizontal lines that correspond to saturation – water on the top of the specimen).

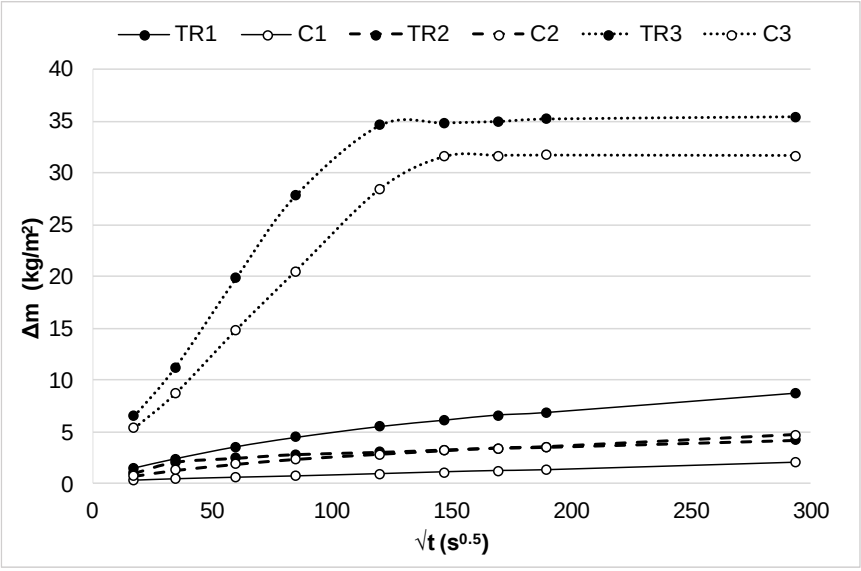

Fig. 42 – Capillary absorption as a function of the square root of time.

According to the EN 998-1 (CEN 2010), TR1 is classified as W1, as required to the thermal renders. TR2, C1 and C2 are W2 since the capillary absorption coefficient is lower than 0.2 $kg/m^2.min^{0.5}$. The gypsum-based renders are very capillary materials and could not be classified as renders for exterior applications.

Regarding the results obtained with the ETAG 004 method, the thermal rendering system S1 has less water absorption, which is in accordance with the C1 water absorption coefficient. Additionally, this system includes an organic coating on the outer surface that has resins and special additives. This creates a more efficient barrier against water absorption compared to the synthetic paint used in S2 (see Fig. 43-b)). Again, S3 presents a completely different behaviour comparing to S1 and S2, as it can be seen in Fig. 43-a).

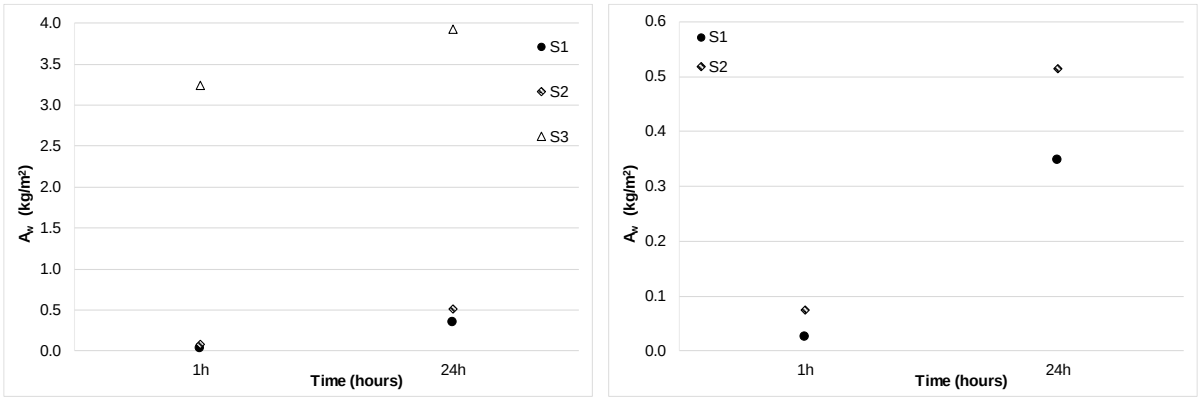

(a) (b)

Fig. 43 – Capillary absorption obtained according to ETAG 004 for: a) S1, S2 and S3 and b) Detailed results of S1 and S2.

In addition, the variability of coating thickness should be taken into account when analysing the different properties.

3.2.1.4. Moisture storage function

The moisture storage function of the analysed materials in equilibrium with the three different ambiences – 80% (w_{80}) and 90% (w_{90}) of relative humidity and saturated (w_f) – is presented in Table 41.

As expected, the moisture storage functions of gypsum-based materials have a higher capability of water adsorption (at free water saturation point). At 80% of relative humidity, TR3 and C3 present similar values, lower than the other analysed materials.

Table 41 – Moisture storage function results.

Property	w_{80}*	w_{90}*	w_f*
Material	(kg/m³)	(kg/m³)	(kg/m³)
TR1	2.5±1.22	8.0±0.52	346.5±6.95
TR2	9.5±0.14	20.3±0.41	278.7±18.26
TR3	2.0±0.08	5.6±0.05	504.2±16.34
C1	9.1±0.14	30.0±0.07	366.6±6.79
C2	5.6±0.50	19.7±0.41	288.3±11.95
C3	2.7±0.08	4.7±0.06	378.8±2.43

* Results presented as (average ± standard deviation)

3.2.1.5. Water vapour permeability

The water vapour permeability has been determined using both dry-cup and wet-cup arrangements. The measurements were performed not only in the thermal render samples but also in samples of the complete systems. Table 42 presents the water vapour resistance factor of the thermal renders/plaster and the water vapour diffusion-equivalent air layer thickness of the thermal renders/plaster and the systems as well. Since the water vapour resistance factor is a characteristic of each material when testing the permeability of the whole system the equivalent air layer thickness should be the analysed property.

Table 42 – Water vapour permeability for dry and wet cup tests.

Property	μ* (-)		s_d* (m)	
Mortar	Dry Cup	Wet Cup	Dry Cup	Wet Cup
TR1	11.7±0.40	9.3±0.59	0.26±0.01	0.20±0.02
TR2	12.7±2.00	10.4±1.39	0.27±0.04	0.22±0.04
TR3	7.1±0.19	6.5±0.66	0.15±0.01	0.14±0.01
S1	—	—	0.61±0.24	0.49±0.03
S2	—	—	0.42±0.04	0.29±0.08
S3	—	—	0.21±0.00	0.18±0.00

* Results presented as (average ± standard deviation)

The water vapour resistance factor of the thermal renders is in accordance with the EN 998-1 requirement – $\mu \leq 15$, for both dry and wet cups. Gypsum-based materials present higher vapour permeability, which highlights their potential for interior application. The finishing coating of S1 has a great influence in the obtained results since it confers high resistance to water vapour transfer comparing to S2, for similar results in TR1 and TR2.

Thermal rendering system S1 exhibits a large standard deviation. This is possibly due to the thickness variation of finishing layers, which has a significant effect on water vapour permeability results (where,

in this specific case, the layer is thicker). Even with controlled processes, the application on the site can be highly affected by workmanship quality. The water vapour diffusion equivalent air thickness of the finishing coat (finishing render and coating of systems S1 and S2) will be analysed as one single layer, $s_{d,C}$, and for both dry and wet-cup tests, will be determined by equation (16) (Ramos, Delgado and de Freitas 2010).

$$s_{d,S} = s_{d,air,i} + s_{d,TR} + s_{d,C} + s_{d,air,e} \quad (16)$$

Where $s_{d,S}$ is the vapour diffusion thickness of the whole system, $s_{d,air,i}$ is that of the interior surface, $s_{d,TR}$ is that of the thermal render, and $s_{d,air,e}$ is that of the exterior surface [m].

In (Worch 2004), the author experimentally determined the surface vapour diffusion thickness of building materials and suggested 0.015 m for the interior surface and the application of equation (17).

$$s_{d,air,e} = \frac{1}{67 + 90v}, \quad (17)$$

Which depends on wind speed, v, for the exterior surface.

The tests were conducted in a climatic chamber, with air speed of ≈ 9 m/s, so the vapour diffusion thickness of the exterior surface was 0.007 m. By applying equation (16), the average, $s_{d,C}$ values correspond to 0.33, 0.14, and 0.04 m for C1, C2, and C3, respectively, for the dry-cup test. By applying the same equation to wet-cup test values, the average $s_{d,C}$ values are 0.27, 0.05, and 0.02 m for C1, C2, and C3, respectively. Dry-cup and wet-cup tests present very similar water vapour diffusion thicknesses. However, for system S2, the effect of higher relative humidity conditions (wet-cup test) is observed by the clear reduction of the water vapour thickness (≈ 64% variation).

3.2.2. MECHANICAL PROPERTIES

3.2.2.1.Dynamic elastic modulus

The dynamic modulus test was carried out in the thermal and finishing renders/plaster, which results are presented in Table 43.

Table 43 – Dynamic elastic modulus results.

Property	E_d*
Material	(MPa)
TR1	104±6.9
TR2	482±55.7
TR3	719±15.5
C1	3821±489.3
C2	3351±73.4
C3	3515±54.6

* Results presented as (average ± standard deviation)

As expected, the thermal renders are more flexible than the finishing coatings. The lower dynamic modulus of elasticity of the thermal renders may contribute to the absorption of significant dimensional variation of the wall, in opposition to a traditional render.

3.2.2.2.Flexural and compressive strength

The flexural and compressive tests were carried out in the thermal and finishing renders/plaster. The results are presented in Table 44.

Table 44 – Flexural and compressive strength results.

Property	R_{flex}*	R_{comp}*
Material	(MPa)	(MPa)
TR1	0.34±0.045	0.26±0.026
TR2	0.61±0.085	0.91±0.168
TR3	0.45±0.101	0.56±0.067
C1	3.01±0.520	5.78±0.718
C2	2.11±0.156	3.48±0.360
C3	2.07±0.102	3.94±0.321

* Results presented as (average ± standard deviation)

In general, the compressive strength is higher than the flexural strength, except for TR1, which may be due to the higher amount of EPS particles that have higher compressibility and higher enclosed porosity, as shown in Fig. 44, which contribute to higher ductility and hence to improved tensile strength.

a) b)

Fig. 44 – Specimens after the compressive strength test: a) TR1 and b) TR2.

Concerning the compressive strength, TR2 and TR3 are classified as CSI, according to EN 998-1 (CEN 2010), while TR1 does not fit in the requirements. This fact points out the importance to adequate the requirements to the system as a whole.

3.2.2.3.Adhesive strength

The average results obtained for the adhesive strength in the thermal renders/plaster and in the thermal rendering and plastering systems are presented in Table 45. Table 46 to Table 51 present the single values and fracture patterns in the five specimens of each material.

Table 45 – Adhesive strength: average results.

Property	Adhesive strength*
Material	(MPa)
TR1	0.10±0.025
TR2	0.22±0.020
TR3	0.33±0.073
S1	0.14±0.014
S2	0.18±0.041
S3	0.22±0.092

* Results presented as (average ± standard deviation)

Considering only the obtained value for the adhesive strength, the systems did not present, in general, a high performance. Regarding ETAG 004, TR3 is the only material that fit the requirement, analyzing the adherence between substrate and insulation (at least 0.25 MPa in dry conditions), but the results are not too distant from the threshold. Regarding the requirements in terms of bond strength between the insulation and the adhesive, the values are quite low. As such, the thermal mortars and related systems present an adhesive strength in line with the ETAG 004 requirements. In addition, the adhesive strength value is not enough to evaluate the adhesion resistance of a material, since the obtained fracture patterns indicate other fragilities of the material. As such, it is observed in the following tables that the systems are more cohesive than the thermal mortars. TR1 mortar shows a surface, which presents low roughness and consequently an adhesive interface. Gypsum-based materials evidenced embrittlement of their structure, which results in higher variability.

Table 46 – Adhesive strength and fracture patterns obtained in TR1.

Property	Adhesive strength	Fracture pattern	
Material	(MPa)	Description	Photograph
1	0.12	50% adhesion/ 50% cohesion	
2	0.09		
3	*	60% adhesion/ 40% cohesion	
4	0.12		
5	0.07	70% adhesion/ 30% cohesion	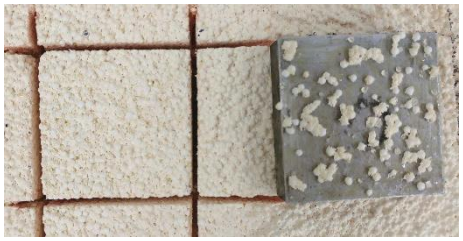
Average	0.10	58% adhesion (TR-glue interface)/ 42% cohesion in the TR itself	
St. Deviation	0.025		

* not valid

Table 47 – Adhesive strength and fracture patterns obtained in TR2.

Property	Adhesive strength	Fracture pattern	
Material	(MPa)	Description	Photograph
1	0.24	10% adhesion/ 90% cohesion	
2	0.21	100% cohesion	
3	0.24		
4	0.22	5% adhesion/ 95% cohesion	
5	0.19		
Average	0.22	4% adhesion (between TR-substrate interface)/ 96% cohesion in the TR itself	
St. Deviation	0.020		

Table 48 – Adhesive strength and fracture patterns obtained in TR3.

Property	Adhesive strength	Fracture pattern	
Material	(MPa)	Description	Photograph
1	0.40	5% adhesion (TR-substrate interface)/ 95% cohesion	
2	0.22	20% adhesion (TR-glue interface)/ 80% cohesion	
3	0.29		
4	0.3	10% adhesion (TR-glue interface)/ 90% cohesion	
5	0.39	15% adhesion (TR-glue interface)/ 85% cohesion	
Average	0.33	14% adhesion/ 86% cohesion in the thermal render itself	
St. Deviation	0.073		

Table 49 – Adhesive strength and fracture patterns obtained in S1.

Property	Adhesive strength	Fracture pattern	
Material	(MPa)	Description	Photograph
1	0.16	100% cohesion	
2	0.14		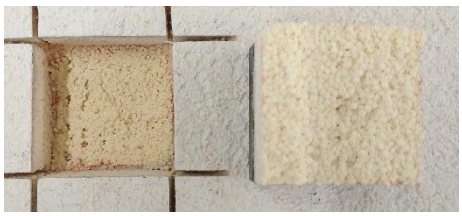
3	0.13		
4	0.12		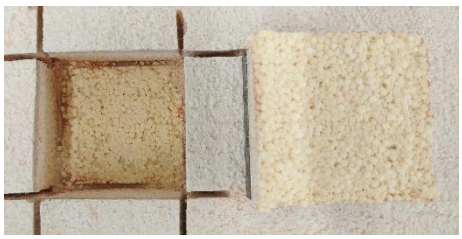
5	0.15		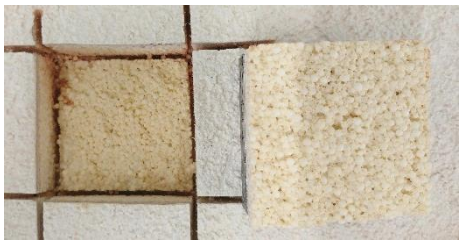
Average	0.14	100% cohesion in the TR itself	
St. Deviation	0.014		

Table 50 – Adhesive strength and fracture patterns obtained in S2.

Property	Adhesive strength	Fracture pattern	
Material	(MPa)	Description	Photograph
1	0.18	100% cohesion	
2	0.19		
3	0.11		
4	0.20		
5	0.21		
Average	0.18	100% cohesion in the TR itself	
St. Deviation	0.041		

Table 51 – Adhesive strength and fracture patterns obtained in S3.

Property	Adhesive strength	Fracture pattern	
Material	(MPa)	Description	Photograph
1	0.10	50% adhesion(TR-C interface)/ 50% cohesion in the C itself	
2	0.20		
3	0.27	10% adhesion (TR-substrate)/ 90% cohesion in the TR itself	
4	0.20		
5	0.35	5% adhesion (TR-substrate)/ 95% cohesion in the TR itself	
Average	0.22	25% adhesion/ 75% cohesion	
St. Deviation	0.092		

3.2.2.4.Impact resistance

The average results obtained for the dent diameter of the hard body impact in the thermal renders/plaster and in the thermal rendering and plastering systems are presented in Table 52.

Table 52 – Dent diameter of the hard body impact: average results.

Impact energy	2J*	10J*
Material	(mm)	(mm)
TR1	30.1±1.92	40.7±1.12
TR2	25.4±1.00	35.6±1.24
TR3	19.8±1.29	26.7±0.61
S1	17.8±1.45	29.5±1.04
S2	18.4±0.99	27.3±1.25
S3	19.6±0.50	26.2±0.80

* Results presented as (average ± standard deviation)

As expected, the 10J impact implies greater damages than the 2J impact. The systems S1 and S2 promote a significant improvement on the hard body impact since the dent dimensions are considerably reduced (≈ 40% and 28% for 2J and 28% and 23% for 10J, TR1-S1 and TR2-S2 respectively). However, the additional layer C3 did not contribute to increasing the impact resistance, since the dent diameter is almost the same for both TR3 and S3. This fact may be due to the existence of a glass fibre mesh in the systems S1 and S2, which confers an improved performance to hard body impact comparing to gypsum-based system S3. Despite the similarity between TR3 and S3, these materials present in most cases (with the exception considering the systems for 2J energy impact) lower dent values than the other systems from manufacturers 1 and 2.

Table 53 to Table 55 present the single values and fracture patterns in the five specimens for each material.

As it can be observed, the 2 Joule energy impact only produces a slight depression both in the thermal renders as in the systems. Although, as previously referred, the absence of a reinforcement mesh allows the cracking of the finishing render C3 for both 2J and 10J energy impact, while in S1 and S2 this only happens in the 10J impact. The finishing coating of S1 is more flexible than the other coatings, which is reflected by less micro cracking. However, when that happens, the coating shows pronounced cracks, as it can be seen in S1.1-10J.

Table 53 – Visual observation of the dent obtained by hard body impact in TR1 and S1.

Material	TR1		S1	
Impact energy	2J	10J	2J	10J
1		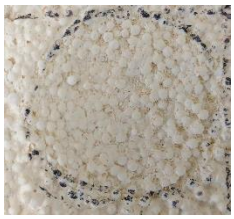		
2	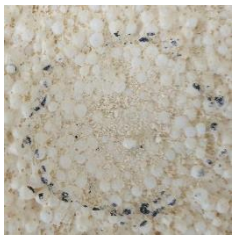			
3	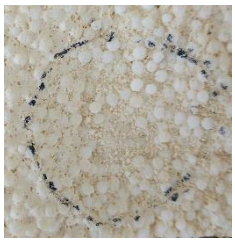			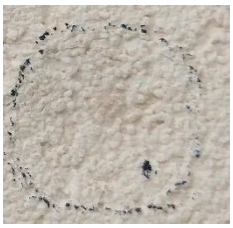
4				
5				
Visual observation	Slight depression	Bigger depression; EPS particles crushing	Slight depression	Cracks on the coating

Table 54 – Visual observation of the dent obtained by hard body impact in TR2 and S2.

Material	TR2		S2	
Impact energy	2J	10J	2J	10J
1				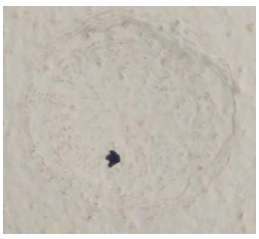
2				
3				
4				
5				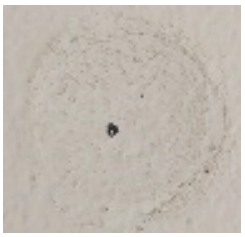
Visual observation	Slight depression	Bigger depression; EPS particles crushing	Slight depression	Circular cracking on the coating

Table 55 – Visual observation of the dent obtained by hard body impact in TR3 and S3.

Material	TR3		S3	
Impact energy	2J	10J	2J	10J
1			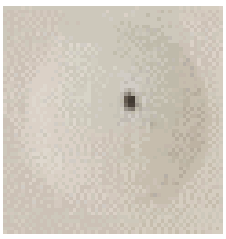	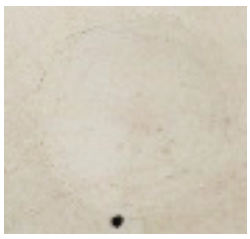
2			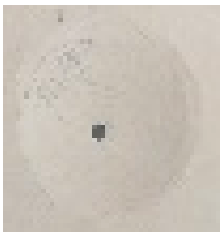	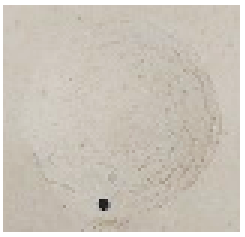
3			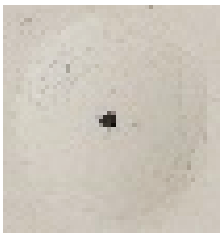	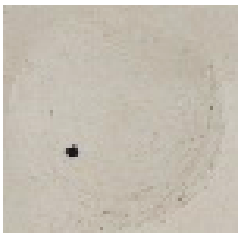
4			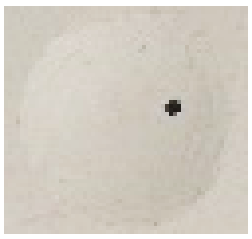	
5			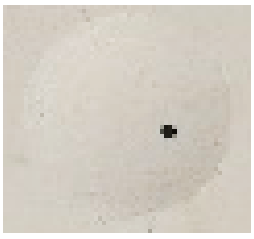	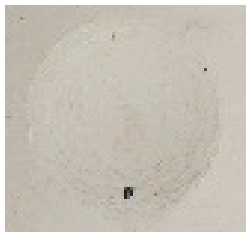
Visual observation	Slight depression	Bigger depression; Segregation of the cork particles crushing	Circular cracking on the coating	Circular cracking on the coating

Regarding the ETAG 004 classification, an adaptation to the thermal rendering systems is presented in Table 56.

Table 56 – Thermal rendering systems classification according to hard body impact, based on the ETAG 004 requirements.

Impact energy	2J	10J	Category
S1	Rendering not penetrated		III
S2	Rendering not penetrated		III
S3	Rendering not penetrated	Rendering not penetrated; delamination	III

All the systems fit the requirements to be classified as Category III.

3.2.3. SUMMARY

The four studied thermal render systems presented different properties that resulted in differentiated hygrothermal behaviour. Since the studied materials were expected to present enhanced thermal performance, two of the most important properties – density and the thermal conductivity – were analysed.

TR1 and TR2, despite the same lightweight aggregate addition (EPS), present a wide variation in material properties that affect the hygrothermal simulation results. TR1 and TR2 are classified as T1 and TR3 is classified as T2 by EN 998-1 (CEN 2010), and the bulk density is within the recommended range: <600 kg/m^3 (Veiga 2010), in contrast to TR4. Thermal render TR4 presents a high thermal conductivity and bulk density (higher than 0.2 W/(m·ºC) and 600 kg/m^3, respectively), which do not allow the material to be classified as a thermal render according to EN 998-1 (CEN 2010) and Veiga (2010). As such, the materials from the Manufacturer 4 were discarded for further evaluation.

Regarding the relation between thermal conductivity and bulk density in the dry state, an exponential correlation with a high correlation coefficient (R^2=0.9869) was obtained. As expected, the difference between thermal renders and finishing renders is clear. Despite the differences among the thermal renders, thermal conductivity, as a function of water content, has a similar linear development (approximated slopes), being more evident for thermal renders with the same addition (EPS). However, TR3 has a quicker initial increase, because the gypsum binder leads to higher water absorption. Several authors have developed different approaches to measure the effective thermal conductivity as a function of temperature and pressure. Pore size has been shown to have a significant impact on thermal conductivity (Reichenauer, Heinemann and Ebert 2007; Zhao, Zhang and He 2009). For a particle and pore size of 0.1–10 μm, solid–gas coupling and pore and particle microstructures have a significant effect on the heat transfer (Zhao et al. 2012; Swimm et al. 2009). The pore size distribution of thermal renders TR1 and TR2 is in the same range, and therefore the solid–gas coupling effect on the heat transfer could lead to a variation of the effective thermal conductivity for high-pressure values.

The low-density results are not directly correlated with porosity (either open or enclosed pores), as presented in Fig. 45. For thermal renders with the addition of materials with high enclosed porosity (especially EPS), a linear correlation between density and porosity was not found. The high rate of mesopores results in higher water absorption coefficients, owing to their capillary network. Both thermal renders with EPS addition present the same behaviour: The higher the bulk density, the lower the open

porosity and capillary absorption coefficient. This was already expected given the presented pore structure results. Again, the gypsum-based material displays distinct results.

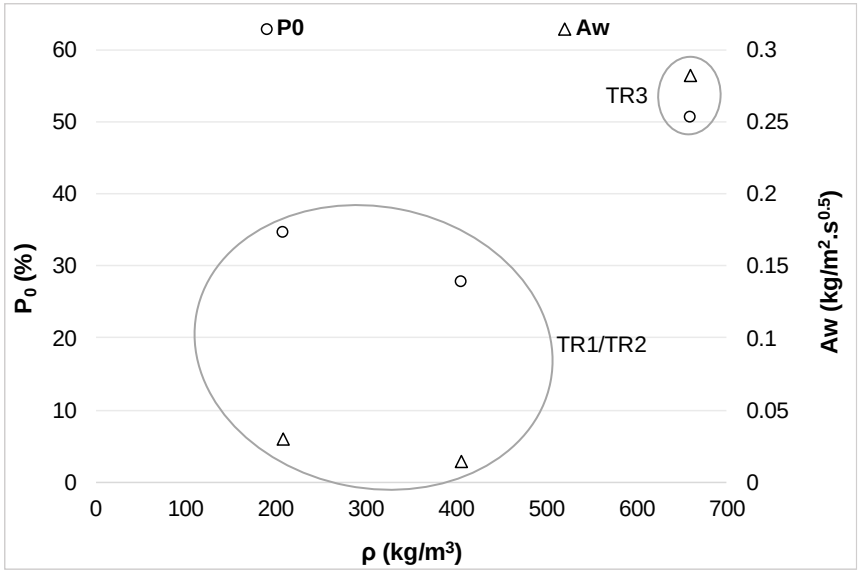

Fig. 45 – Dry bulk density as a function of the open porosity and capillary water absorption coefficient, considering the analysed thermal mortars.

Since the liquid transport presents an important role in the hygric behaviour of thermal renders, the liquid moisture coefficients were analysed. The liquid moisture diffusivity for suction (D_{ws}) describes the capillary uptake of water when the imbibing surface is fully wetted. The moisture diffusivity for redistribution (D_{ww}) describes the spreading of the imbibed water when the wetting is finished, no new water is taken up any more and the water present in the material is redistributing. Since the redistribution is a slower process (taking place in the small capillaries with their high flow resistance), the corresponding liquid transport coefficient is generally lower than the coefficient for suction (Krus 1996). The equation (18) gives an approximation of the liquid transport coefficient for suction by the relation with water absorption coefficient (A_w).

$$D_{ws}(w) = 3.8 \cdot \left(\frac{A_w}{w_f}\right)^2 \cdot 1000^{\left(\frac{w}{w_f}-1\right)} \tag{18}$$

Where w is the moisture content and w_f the free water saturation in [kg/m³].

Fig. 46 and Fig. 47 present the liquid transport coefficient for suction as a function of the moisture content for the studied thermal renders.

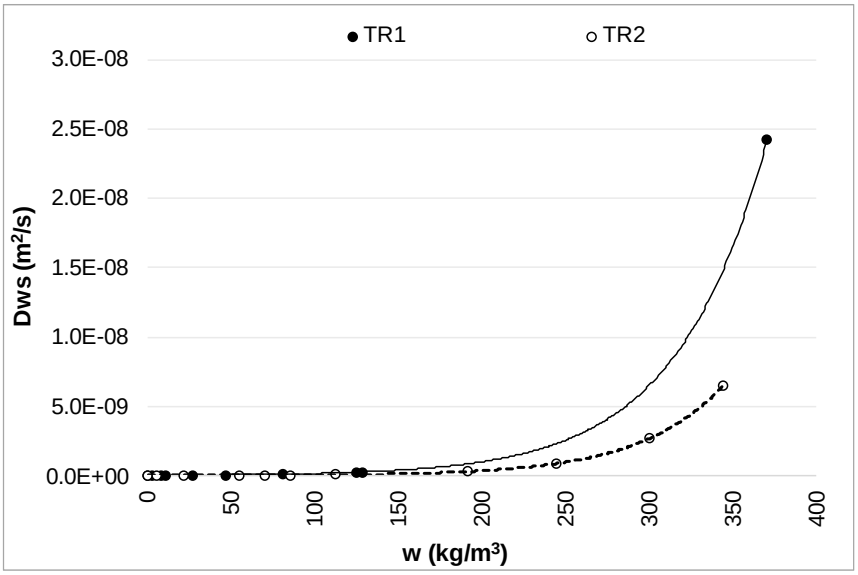

Fig. 46 – Liquid transport coefficient for suction as a function of the moisture content, in TR1 and TR2.

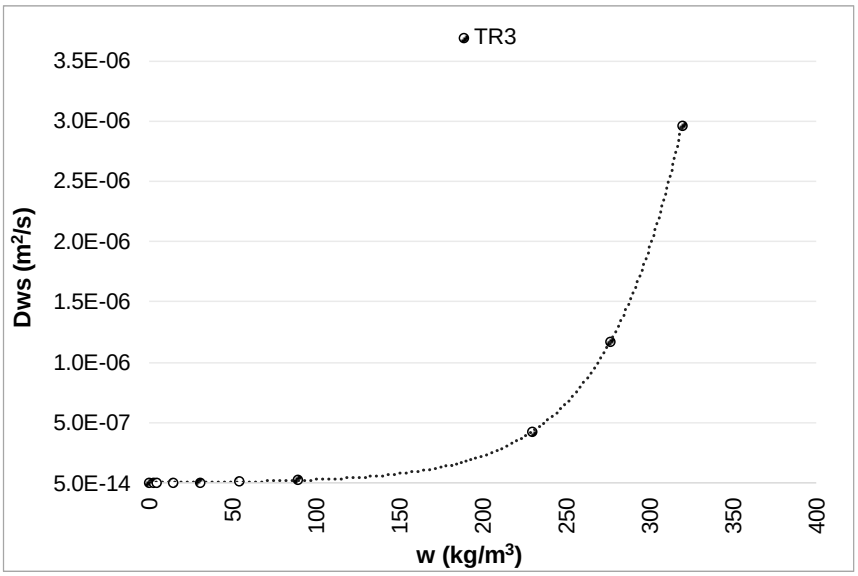

Fig. 47 – Liquid transport coefficient for suction as a function of the moisture content, in TR3.

Observing Fig. 46 and Fig. 47, the thermal renders TR1 and TR2 present a lower liquid transport coefficient for suction than TR3, being TR2 one order of magnitude lower than TR1. A cement-lime mortar (similar matrix to TR1 and TR2) has a liquid transport coefficient for suction around 10^{-10} to 10^{-7} and a current gypsum plaster of $10^{-8.5}$-$10^{-5.5}$ (IBP 2014). Therefore, the analysed materials present a lower liquid transport coefficient for suction, which is an added value in terms of capillary water uptake.

Analysing the mechanical behaviour of the studied materials, as expected the thermal renders present low mechanical resistance compared to traditional cement and lime-based mortars (Vale et al. 2014; Soares, Flores-Colen and Brito 2017; Costigan and Pavía 2018). However, they are more flexible than the studied finishing renders and other current renders (Oliveira, de Brito and Veiga 2015; Kabeer and Vyas 2018). The lower dynamic modulus of the thermal renders contributes to the absorption of significant dimensional variation of the wall, in opposition to a traditional render. Concerning the

compressive strength, TR2 and TR3 are classified as CSI, according to EN 998-1 (CEN 2010), while TR1 does not fit in the requirements. This fact points out the importance to adequate the requirements to the system as a whole.

Figures Fig. 48 and Fig. 49 present the relation between some of the measured mechanical properties with the bulk density. As regards the thermal renders, the higher the density the higher the dynamic modulus. The finishing renders present the opposite trend: the higher the density the lower the dynamic modulus. In terms of compressive and flexural strength the higher the bulk density the higher resistance, only for the non-based gypsum materials (TR1 and TR2).

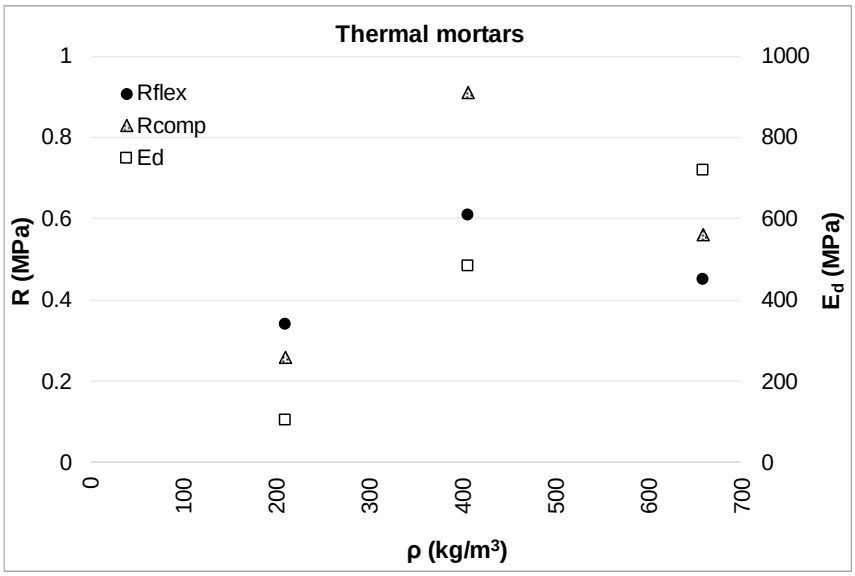

Fig. 48 – Dynamic modulus, compressive and flexural strength as a function of the bulk density, in the thermal mortars (TR1, TR2 and TR3).

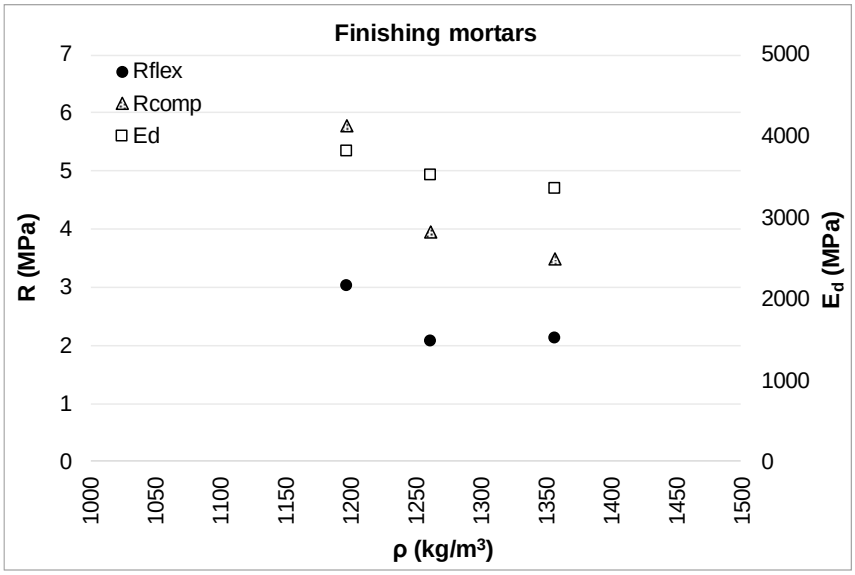

Fig. 49 – Dynamic modulus, compressive and flexural strength as a function of the bulk density, in the finishing mortars (C1, C2 and C3).

Considering the adhesive strength, the thermal renders usually present lower resistance comparing to traditional renders, especially in the case of materials with EPS addition. Comparing to a traditional ETICS, the thermal renders/plaster and related systems present similar results or even better (LNEC 2018). However, the amount of binder in the mixture leads to a significant variation in the obtained values, which could vary between 0.035 MPa (Kabeer and Vyas 2018) to 1.7 MPa (Skoczylas and Rucińska 2018), considering cement-based mortars. The amount of aggregate also has a great influence in the mechanical strength, since a variation of 2% of cork addition (5 to 7%), in a gypsum-based plaster, promotes a decrease of 2.62-1.68 MPa on the compressive strength (Vasconcelos et al. 2013) and around 78% and 67% higher than the presented for the thermal render TR3.

The thermal render systems present an improved behaviour, in terms of fracture pattern, since high percentages of cohesive fractures are obtained (highlighting the 100% cohesive fracture of S1 and S2). Being the adhesive strength conditioned by the tensile strength of the thermal renders/plaster (weakest materials), the results show that the real adhesive strength is greater than the measured values. Gypsum-based materials evidenced embrittlement of their structure, which results in higher variability. TR3 presents a slightly higher adhesive resistance comparing the obtained for a gypsum plaster by Doleželová, Krejsová and Vimmrová (2018). Incorporating PCMs in the mixture, the adhesive strength increases, but in the same order of magnitude (Silva et al. 2018).

Analysing the hard body impact, the existence of a glass fibre mesh in the systems S1 and S2 promotes a significant improvement since the dent dimensions are considerably reduced (≈40% and 28% for 2J and 28% and 23% for 10J, TR1-S1 and TR2-S2 respectively). Traditional renders present much lower dent, comparing to these thermal renders (Lalic 2017). Additionally, the same study presents similar results to the analysed thermal renders. Despite the similarity between TR3 and S3, these materials present in most cases (with the exception of the systems for 2J energy impact) lower dent values than the other systems from manufacturers 1 and 2. Fig. 50 presents the dent diameter as a function of the bulk density (dry state), for both 2J and 10 J energy impact, in the thermal renders.

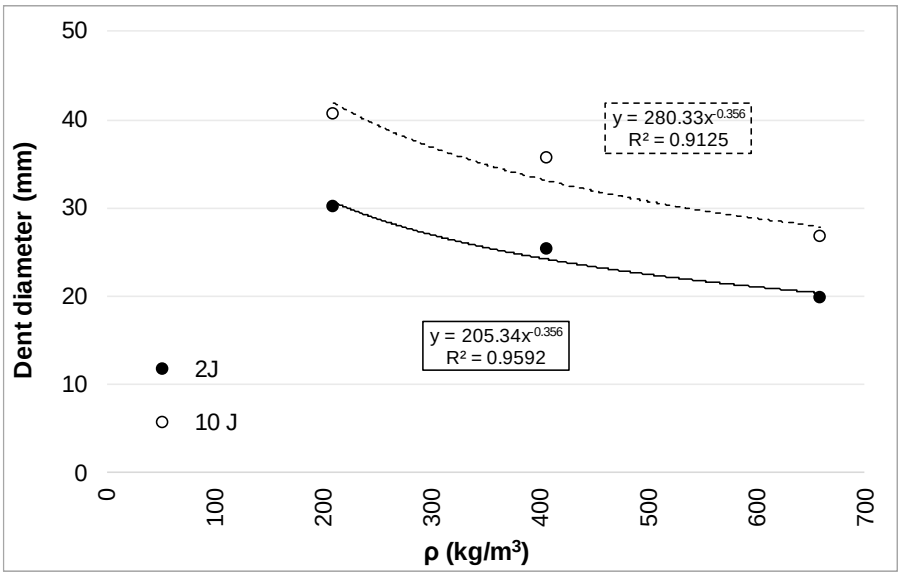

Fig. 50 – Dent diameter obtained by the hard body impact as a function of the bulk density, in the thermal mortars (TR1, TR2 and TR3).

The relation is reflected by an exponential regression with a high correlation between the two measured properties. For both tested impact energies, the higher the bulk density the lower the dent diameter. The high porosity (such as enclosed pores) of TR1 and TR2 leads to less compact material, contrary to TR3, which has less enclosed porosity (as verified in 3.2.1.1), and the cork addition contributes to an improved behaviour to the impact. Regarding the ETAG 004 requirements, all the systems can be classified as Category III (defined as the lowest defined category concerning impact).

Generally, the mechanical properties of the thermal renders/plaster and related systems are in line with the ETICS, highlighting the importance of evaluating the systems as a whole.

A summary of the mechanical and hygrothermal properties of the studied materials is presented in Table 57 and Table 58.

Table 57 – Summary of the mechanical properties of the studied materials (average values).

Property/ Material	TR1	TR2	TR3	C1	C2	C3	S1	S2	S3
E_d (MPa)	103	482	719	3821	3351	3515	—	—	—
R_{flex} (MPa)	0.34	0.61	0.45	3.01	2.11	2.07	—	—	—
R_{comp} (MPa)	0.26	0.91	0.56	5.78	3.48	3.94	—	—	—
Adhesive strength (MPa)	0.10	0.22	0.33	—	—	—	0.14	0.18	0.22
Dent diameter (2J impact) (mm)	30.1	25.4	19.8	—	—	—	17.8	18.4	19.6
Dent diameter (10J impact) (mm)	40.7	35.6	26.7	—	—	—	29.5	27.3	26.2

Table 58 – Summary of the hygrothermal properties of the studied materials (average values).

Property/ Material	TR1	TR2	TR3	C1	C2	C3	S1	S2	S3
ρ (kg/m^3)	208.7	406.2	659.5	1197.0	1357.3	1261.4	—	—	—
ρ_r (kg/m^3)	319.7	563.3	1334.1	1882.9	1908.9	2034.2	—	—	—
P_0 (%)	34.7	27.9	50.6	36.8	28.9	38.0	—	—	—
λ (W/m^{o}C)	0.049	0.078	0.134	0.220	0.369	0.292	—	—	—
λ_w (W/m^{o}C)	0.199	0.235	0.348	—	—	—	—	—	—
ε (-)	0.88	0.88	0.89	0.9	0.87	0.88	0.92	0.91	—
A_w (ISO 15148) (kg/m^2.s$^{0.5}$)	2.96x10^{-2}	1.42x10^{-2}	2.82x10^{-1}	6.45x10^{-3}	1.61x10^{-2}	2.10x10^{-1}	—	—	—
A_w (ETAG 004) (kg/m^2.s$^{0.5}$)	—	—	—	—	—	—	1.56x10^{-3}	2.19x10^{-3}	2.68x10^{-2}
w_{80} (kg/m^3)	2.5	9.5	2.0	9.1	5.6	2.7	—	—	—
w_{90} (kg/m^3)	8.0	20.3	5.4	30.0	19.7	4.7	—	—	—
w_f (kg/m^3)	346.5	278.7	504.2	366.6	288.3	378.8	—	—	—
μ (dry-cup)	11.7	12.7	7.1	—	—	—	—	—	—
μ (wet-cup)	9.3	10.4	6.5	—	—	—	—	—	—
s_d (dry-cup)	0.26	0.27	0.15	0.33*	0.14*	0.04*	0.61	0.42	0.21
s_d (wet-cup)	0.20	0.22	0.14	0.27*	0.05*	0.02*	0.49	0.29	0.18

*Estimated in 3.1.3.7

4. NUMERICAL SIMULATION OF DEGRADATION MECHANISMS

4.1. FRAMEWORK

The numerical simulation of degradation mechanisms is one of the strategies to predict the performance of building elements, systems or materials and prevent their early degradation.

In the present work, it is intended to carry out a set of simulations that can support the analysis of the hygrothermal and thermo-mechanical behaviour of thermal rendering systems. The analysis of the specific degradation mechanisms and damages in the thermal rendering systems, obtained by numerical simulation, will help on the definition of a durability assessment methodology applicable to these systems in particular. In that way, to evaluate the impact of realistic scenarios of thermal render systems application, reliable data should be used. The previously measured properties will be used as an input to the numerical simulations to achieve that purpose.

To analyse the hygrothermal and thermo-mechanical performance of the studied thermal rendering systems, two simulation tools were selected.

An overview of hygrothermal numerical simulation tools applied to building physics is described in Delgado et al. (2010) and López et al. (2017). According to Barreira (2010) and Barreira et al. (2013), WUFI Pro software, based on the EN 15026 (CEN 2007), has demonstrated several advantages on the simulation of a thermal insulation multilayer system such as ETICS, which principles of application are similar to those of the studied thermal rendering systems. This one-dimensional model for heat and moisture transport was developed by the *Fraunhofer* Institute for Building Physics (IBP 2016) WUFI is a hygrothermal simulation software that performs dynamic simulations of coupled heat and moisture transfer and is based on advanced knowledge of vapour diffusion and liquid transport in building materials. The input geometry, boundary conditions and detailed material properties allow a realistic calculation of the transient behaviour of a multilayer component (Künzel and Kiessl 1996). Taking into account the referred documents, WUFI Pro was selected to perform the hygrothermal simulation, being highlighted some of its advantages:

- The detailed calculation model, which includes the capillary liquid transport and the explicit radiative balance (ERB), with measured material properties, contributing to a more realistic approach;
- The large and complete database, with reliable materials properties and weather data files;
- The analysis of façade multilayer systems, constituted of porous materials, supported by several studies (Ramos et al. 2009; Barclay, Holcroft and Shea 2014; Cascione et al. 2017; Künzel, Schmidt and Holm 2002; Zillig, Lenz and Krus 2003);
- The protocol between the Fraunhofer Institute (IBP) and LFC/FEUP.

Considering the analysis of the thermo-mechanical performance, several simulation tools, using the Finite Element Method (FEM), are available. ADINA, ANSYS, ANSYS+CivilFEM, Abaqus/CAE, COMSOL and DIANA FEA are examples of FEM simulation tools applied to civil engineering.

Dassault Systémes Abaqus is a finite element simulation tool, which allows performing different types of analysis of several problems, including non-structural such as heat transfer, thermo-mechanical analysis, electrical and acoustic areas (Dassault Systemes 2015b). Abaqus has been widely applied to mechanical processes, but also to heat transfer analysis. Bedon et al. (2018) studied high-performance systems as an alternative to traditional curtain-walls for building façades. Pan, Gu and Sun (2015) and Farooqi and Sheikh (2005) perform numerical analysis of the thermo-mechanical behaviour of composite materials. Zhou, Wong and Lau (2014) studied the performance of the building envelope, in particular, a new concrete wall with the inclusion of a gypsum plaster in the interior. Also, Pereira (2008) and Sousa (2009) analyse the thermal effect in masonry walls through Abaqus FEM simulation. Taking into account the existing knowledge, the Abaqus simulation tool was selected to perform the thermo-mechanical analysis.

Knowing that the material properties determined in Chapter 3 will be used as an input to a more realistic numerical simulation, Table 59 presents which measured properties will be used in each simulation tool.

Table 59 – Relation between experimentally measured properties and their application as input data in simulation programs.

Experimental test/Sub-chapter	WUFI Pro input	ABAQUS input
Density and porosity/3.2.1.1	Bulk density (dry)	Bulk density (dry)
Density and porosity/3.2.1.1	Open porosity	—
Thermal conductivity/3.2.1.2	Thermal conductivity (dry)	Thermal conductivity (dry)
Thermal conductivity/3.2.1.2	Thermal conductivity (moisture-dependent)	—
Emissivity/3.2.1.2	Emissivity	—
Capillary absorption/3.2.1.3	Water absorption coefficient	—
Density and porosity/3.2.1.1 Capillary absorption/3.2.1.3	Liquid transport coefficient (suction)	—
Moisture storage function/3.2.1.4	Reference water content (80%)	—
Density and porosity/3.2.1.4	Free water saturation	—
Water vapour permeability/3.2.1.5	Water vapour resistance factor	—
Dynamic elastic modulus/ 3.2.2.1	—	Dynamic modulus

4.2. HYGROTHERMAL IMPACT ON FAÇADES WITH THERMAL RENDERING AND PLASTERING SYSTEMS APPLICATION

4.2.1. MODELLING PRINCIPLES

High moisture levels result in higher heat losses and risk of early degradation. To evaluate this type of problems, different authors use the WUFI Pro software simulating materials with a complex porous structure. Cascione et al. (2017) studied the hygrothermal behaviour of opaque building envelopes,

evaluating condensation and also durability. Barclay, Holcroft and Shea (2014) compared the moisture values obtained by the WUFI Pro simulation and the laboratory measurements in the hygrothermal performance of buildings and concluded that they had a very close fit. Also, Sehizadeh and Ge (2016) used WUFI Pro to simulate the durability performance of residential wall assemblies taking into account the impact of future climates.

WUFI Pro software is, therefore, a simulation tool of simultaneous moisture and heat transfer of building envelopes. It allows realistic hygrothermal simulations of several constructive elements and differentiated climatic conditions, through one-way analysis, at transient state. The main objective is to calculate the temperature, relative humidity and moisture content in the simulated materials that constitute the constructive component. WUFI Pro has an extensive database on material properties and climates (about 150 cities in Europe, North America, South America, Oceania and Japan). The WUFI Pro 5.3.4 version was used in the present work.

In order to simulate the hygrothermal behaviour of the building element, it is necessary, in advance, to provide the following data:

- Geometry and assembly;
- Orientation, inclination and height;
- Hygrothermal properties of the materials;
- Outdoor and indoor climate conditions;
- Surface transfer coefficients;
- Initial conditions of temperature and relative humidity.

In terms of the heat transfer calculation, WUFI Pro takes into account the:

- Thermal conduction;
- Short-wave solar radiation;
- Enthalpy flows through moisture movement with phase change;
- Night-time long-wave radiation cooling (with complete climate data files).

Convective heat transport is not considered, due to the difficulty to quantify it and to the fact that it rarely is one-dimensional (IBP 2016).

Regarding the moisture transport mechanisms, WUFI Pro includes, in the vapour phase, the vapour diffusion and, in the liquid phase, the capillary conduction and surface diffusion. The input of the boundary conditions for each time step includes meteorological data, such as temperature, relative humidity, driving rain and radiation. In addition, the indoor climate has to be defined.

WUFI Pro provides several hygrothermal outputs over time, particularly:

- Total water content of the studied constructive element;
- Water content in layer (in every single layer);
- Temperature, relative humidity and dewpoint temperature in the exterior and interior surfaces, but also in defined monitor positions of the constructive element;
- Isopleths (plotting of the surface temperature of each time step against the corresponding relative humidity) in the exterior and interior surfaces, but also in defined monitor positions of the constructive element.

Based on the input data, WUFI Pro uses the hygrothermal calculation models for each element of the envelope, through mass balance (moisture), (see equation (19)), and energy conservation (heat), see equation (20)) (Künzel 1995).

$$\frac{dw}{d\varphi} \cdot \frac{\partial \varphi}{\partial t} = \nabla \left(D_\varphi \cdot \nabla \varphi + \delta_p \cdot \nabla (\varphi \cdot p_{sat}) \right) \tag{19}$$

$$\frac{dH}{dT} \cdot \frac{\partial T}{\partial t} = \nabla \cdot (\lambda_w \cdot \nabla \mathrm{T}) + h_v \cdot \nabla \left(\delta_p \cdot \nabla (\varphi \cdot p_{sat}) \right) \tag{20}$$

Where w is the water content [kg/m^3], φ is the relative humidity [-], t is the time [s], D_φ is the liquid conduction coefficient [kg/(m.s)], δ_p is the water vapour permeability [kg/(m.s.Pa)], p_{sat} is the water vapour saturation pressure [Pa], H is the total enthalpy [J/m^3], T is the temperature [ºC], λ_w is the thermal conductivity of the moist material [W/(m.ºC)] e h_v is the evaporation enthalpy of water [J/kg].

Analysing equation (19), the first member expresses the moisture storage function. The two terms on the second member present the liquid transfer as moisture-dependent and vapour transfer as independent of water content. In terms of the heat balance in equation (20), which takes into account the moisture influence on the heat storage capacity and the heat conduction, the storage term appears on the left and the term for heat conduction and latent heat transport by vapour diffusion on the right. A fully implicit finite volume method is applied to the transport equations discretization, which are coupled with an iterative process (Krus, Nouidui and Sedlbauer 2009).

For the hygrothermal calculation process, specific material properties are indispensable – basic material data – and other properties are complementary. The basic material properties are the bulk density, the porosity, the specific heat, the thermal conductivity and the water diffusion vapour resistance factor, at dry state. The complementary material properties are moisture dependent (IBP 2016):

- Moisture content, as a function of relative humidity;
- Liquid transport coefficients for suction and redistribution, as a function of the moisture content;
- Thermal conductivity, depending on the moisture content;
- Water vapour diffusion resistance factor, as a function of relative humidity.

One of the most important properties for assessing the heat and moisture transfer through the materials is its moisture storage function. When moisture transport properties such as the adsorption curve or water vapour permeability are known, the hygric performance of a building material or a building element composed of several materials could be optimized. The coating material properties become of major importance to reproduce reliable hygrothermal simulations that could help on the decision of materials and systems selection for envelope components (Maia, Ramos and Veiga 2016; Maia, Ramos and Veiga 2018b).

WUFI Pro software could approximate this function from the reference water content, which corresponds to the moisture content at a relative humidity of 80% (w_{80}) and moisture content at free saturation (w_f), which is the moisture storage function at a relative humidity of 100%. Due to the air voids in the enclosed pore structure, the free saturation is less than the maximum water content (w_{max}), which is determined by the porosity. Fig. 51 present a typical moisture storage function of building materials, as a function of relative humidity.

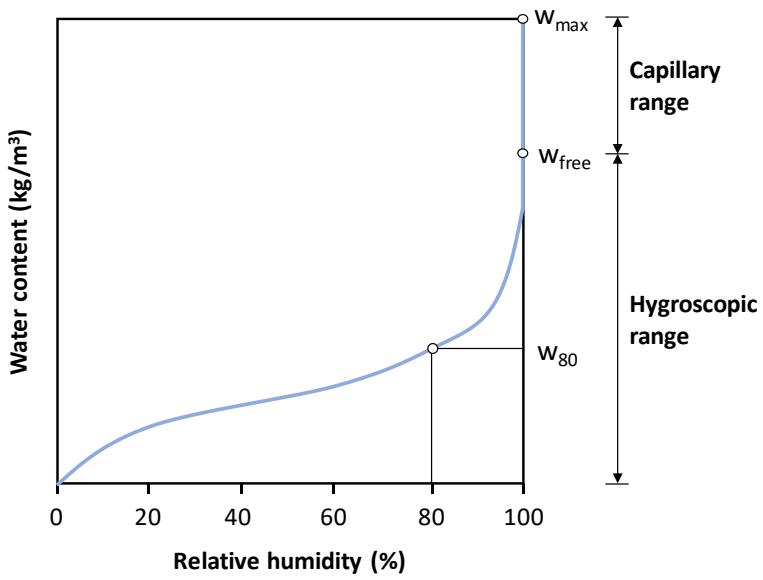

Fig. 51 – Typical moisture storage function of building materials, as a function of the relative humidity (IBP 2016).

For most materials, the approximation of the moisture storage function is determined using equation (21).

$$w(\varphi) = w_f \cdot \frac{(b' - 1) \cdot \varphi}{b' - \varphi} \tag{21}$$

Where $w(\varphi)$ is the moisture content corresponding to the relative humidity φ [kg/m^3], w_{free} is the moisture content at free saturation and b' the approximation factor. This approximation factor must be greater than one and can be determined from the equilibrium water content at 80% of relative humidity by substituting the correspondent values in equation (21) (Künzel 1995).

Another predominant mechanism of moisture transport in porous materials is the capillary transport, described in equation (22).

$$g_w = -D_w(w) \cdot grad\ w \tag{22}$$

Where g_w is the liquid transport flux density [kg/(m^2.s)], w the moisture content and D_w the liquid transport coefficient [m^2/s].

The liquid transport coefficient for suction (D_{ws}) describes the capillary uptake of water when the imbibing surface is fully wetted. In the context of building physics, this describes rain on a façade or an imbibition experiment. The liquid transport coefficient for redistribution (D_{ww}) describes the spreading of the imbibed water when the wetting is finished, no new water is taken up any more and the water present in the material is redistributing. In a building component, this corresponds to the moisture migration in the absence of rain. Since the redistribution is a slower process (taking place in the small capillaries with their high flow resistance), the corresponding liquid transport coefficient is generally lower than the coefficient for suction. The equation (18) in chapter 3.2.3 gives an approximation of the liquid transport coefficient for suction by the relation with water absorption coefficient.

The dependence of the thermal conductivity as a function of moisture content is defined by equation (15) in sub-chapter 3.2.1.2, and presents a great impact in the hygrothermal behaviour.

Additional analysis to the common outputs is obtained by the WUFI Postprocessor (IBP 2016), which analyses the hourly temperatures and heat flows resulting from the full transient simulation, taking into account the real hygrothermal conditions in the construction (see equation (23)).

$$U = \frac{-Q}{\Delta T} \tag{23}$$

Where Q is the heat flow density through the component [W/m^2] and ΔT the monthly mean value of temperature difference between indoor and outdoor air temperature [ºC].

The results include the effects of:

- Variable material properties: variable moisture content on the thermal conductivity;
- Additional thermal transport processes: latent heat transport by vapour flows;
- Additional heat sources: solar radiation;
- Parameters depending on environmental conditions: wind-dependent surface transfer coefficients.

The night-time overcooling is a phenomenon frequently disregarded in most of the hygrothermal simulations. However, it could be of major influence and become a hygrothermal hazard as it increases the risk of algae growth in façades (Barreira and de Freitas 2013; Barreira et al. 2013). If overcooling occurs, the radiative heat flow is lost from the surface towards the sky, while the convective heat flux flows from the (warmer) ambient air towards the (cooler) surface. In that way, overcooling must be simulated by removing the radiation part from the heat transfer coefficient and the long-wave radiation exchange must be computed separately from convective heat exchange. WUFI Pro simulates this phenomenon by combining short and long-wave radiation exchange into a radiation balance (ERB) (see equation (24)). A positive net radiation results in heating the surface and a negative value causes cooling.

$$I = a \cdot I_s + \varepsilon \cdot I_l - I_e \tag{24}$$

Where I is the net radiation at the component surface [W/m^2], a the short-wave radiation absorptivity of the surface [-], I_s the short-wave solar radiation [W/m^2], ε the long-wave emissivity of the surface [-], I_l the long-wave counterradiation [W/m^2] and I_e the long-wave emission of the surface [W/m^2].

Being the most radiation parameters obtained by experimental measurements (excepting the long-wave emission, which depends on the temperature of the component surface via the Stefan-Boltzman equation), uncertainty results may occur. In that way, accurate radiation data are required. WUFI Pro provides a wide range of reliable climate data containing all the required parameters for the explicit radiative balance.

Regarding the previous knowledge and the WUFI simulation capabilities, the simulation of combined heat and moisture transport processes, in a transient state, allows evaluating early degradation risk. As such, the knowledge of the temperature profiles across the wall and the water content, in the more vulnerable materials, allow the determination of the effective thermal transmission coefficients and consequent durability evaluation.

4.2.2. SIMULATION MODEL AND INPUT DATA

As referred before, WUFI software can be used to evaluate the hygrothermal impact of realistic scenarios of thermal render systems.

To evaluate their performance and application possibilities, systems S1 (lime-based thermal render with EPS addition) and S2 (thermal render with mixed binders and EPS addition) were considered as exterior insulation solutions, while S3 (gypsum-based thermal plaster with cork addition) was considered as interior insulation. This is due to the fact that gypsum based materials have high water absorption, as it was shown in 3.2.1.3, but especially to their solubility in water (Klimchouk 2000; Hong et al. 2018), The hygrothermal performance of thermal rendering systems was also compared with an ETICS application, on the exterior wall. The configuration of the walls considered in the simulations included a 6-cm-thick thermal render, as this would be a feasible application of these materials.

The influence of climate on the performance of these systems was analysed by simulating the application in three different European cities. These locations were chosen to perform a representative analysis of different European climatic conditions, taking into account different locations: Porto (P) (southern Europe), Nancy (N) (central Europe), and Oslo (O) (northern Europe). The locations were selected to apply a hygrothermal load with differentiated average outdoor temperature values combined with wind-driven rain. The selection of these specific cities was also made by considering the availability of detailed climatic data required for the intended evaluation, using ERB. Although Oslo would not be a typical location for the application of this constructive solution, it was considered to enhance the range of climatic conditions and to provide comparative data. The counterradiation sum of the three cities is 2912.4, 2782.1 and 2641.4 k Wh/m^2.year, respectively, and the normal rainfall totals are 1201, 613, and 605 mm/year for Porto, Nancy, and Oslo, respectively. Fig. 52, Fig. 53 and Fig. 54 present the solar radiation and driving rain distribution, according to the orientation, in Porto, Nancy and Oslo, respectively.

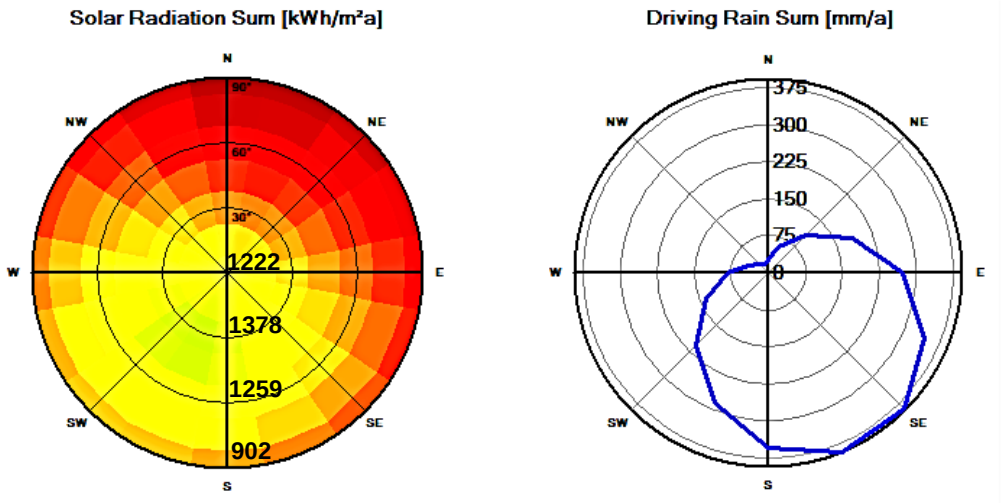

Fig. 52 – Solar radiation and driving rain sum, depending on the orientation: Porto climate (IBP 2016).

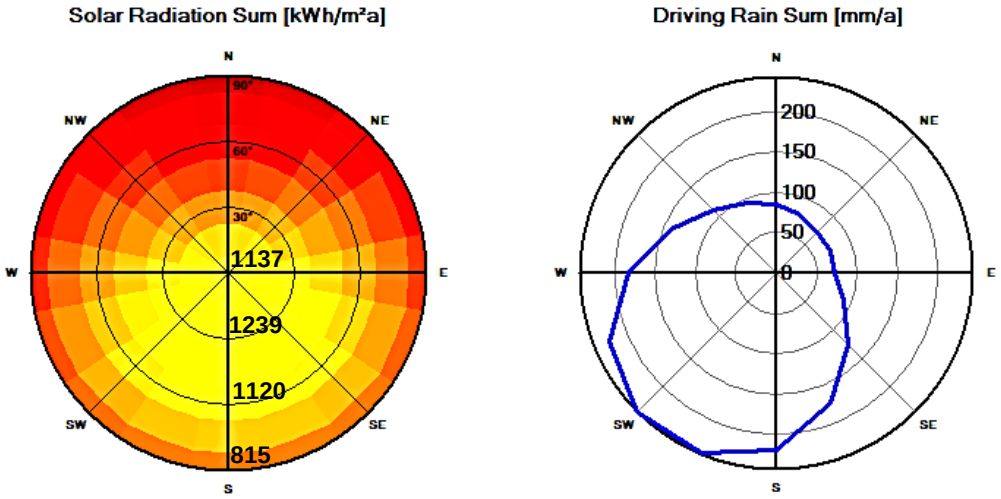

Fig. 53 – Solar radiation and driving rain sum, depending on the orientation: Nancy climate (IBP 2016).

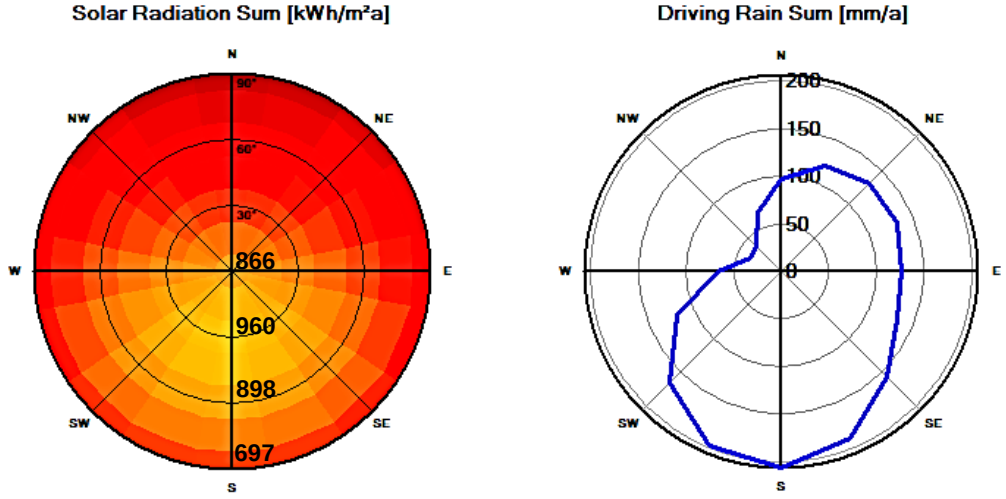

Fig. 54 – Solar radiation and driving rain sum, depending on the orientation: Oslo climate (IBP 2016).

Fig. 55 and Fig. 56 present the temperature and vapour pressure distribution of the exterior air, respectively. The average outdoor temperatures of the three cities are 15.4ºC (P), 9.2ºC (N), and 6.8ºC (O), and the average outdoor vapour pressure is 1290 Pa (P), 1004 Pa (N), and 851 Pa (O).

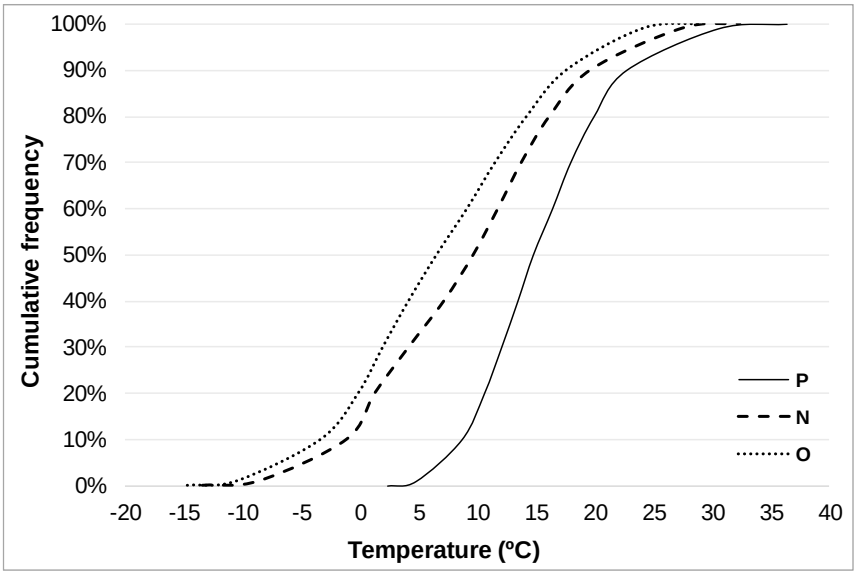

Fig. 55 – Cumulative frequency of exterior air temperature in Porto, Nancy and Oslo.

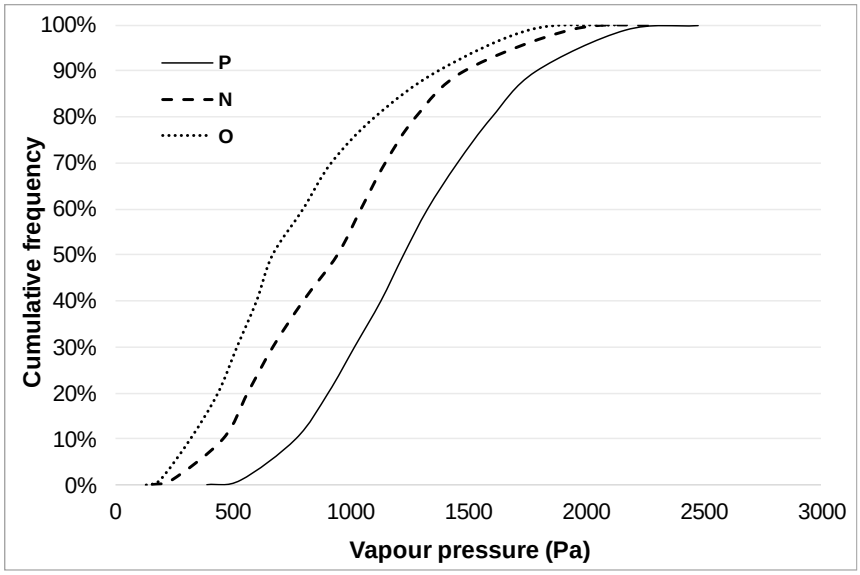

Fig. 56 – Cumulative frequency of exterior air vapour pressure in Porto, Nancy and Oslo.

The target U-values of the walls were established in connection with each country's regulations (Porto: 0.3 W/(m^2·ºC) (Government of Portugal 2013), Nancy: 0.2 W/(m^2·ºC) (Ministère de l'Égalité des Territoires et du Logement 2012), and Oslo: 0.18 W/(m^2·ºC)) (Ministry of Local Government and Modernisation 2017). The thickness of the aerated concrete block layer was adapted to achieve the reference U-value in Porto, being 26 cm for combination with system S1, 32.5 cm with system S2, 38 cm with system S3, and 22 cm in the simulation where ETICS was considered. Fig. 57 and Fig. 58 present the configuration of the wall models with exterior and interior thermal insulation system application.

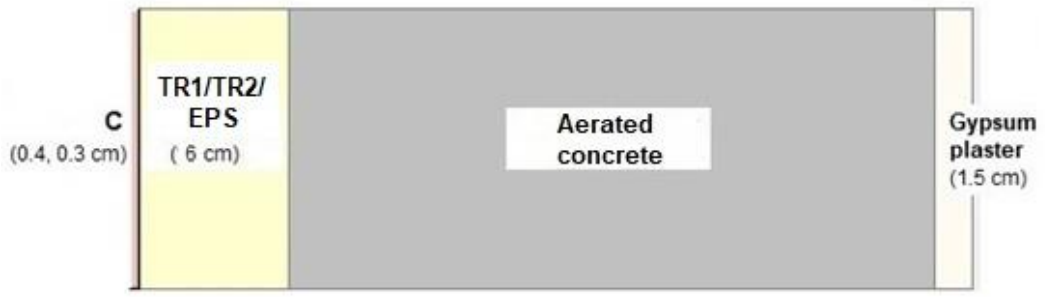

Fig. 57 – Model configuration: application of thermal rendering system (exterior surface).

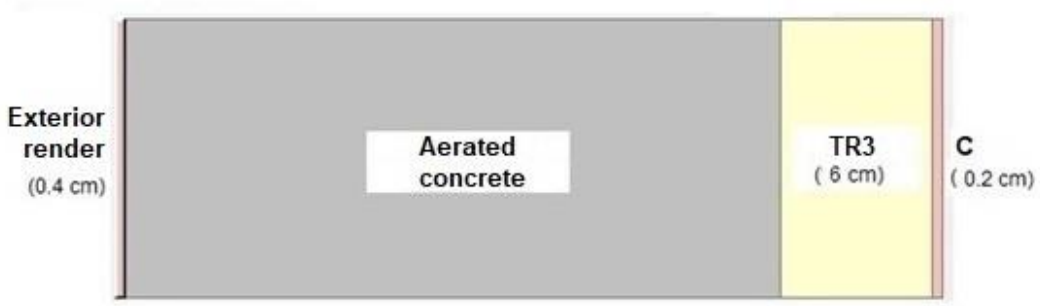

Fig. 58 – Model configuration: application of thermal plastering system (interior surface).

The measured properties of thermal renders and finishing renders were used for a more realistic simulation of the thermal rendering systems. Table 60 to Table 63 present a summary of the input data of the thermal rendering and plastering systems S1 (TR1+C1), S2 (TR2+C2) and S3 (TR3+C3) and ETICS.

The WUFI Pro database provided the properties (see Table 124 in ANNEX 1 – WUFI Pro database materials) for substrate (see Fig. 209-a)), exterior cement-based render, for S3 simulations (see Fig. 209-b)), interior gypsum-based plaster, for S1 and S2 simulations (see Fig. 210-a)), and EPS for the ETICS (see Fig. 210-b)) (IBP 2016). To the ETICS simulation, it was adopted the finishing render and coating from system S1.

Two solar absorption coefficients were selected: 0.27 (white render) and 0.80 (dark render). The four solar orientations were considered, providing direct and non-direct solar radiation exposure. The rain was considered because of its high influence on the durability of the render systems. The wind-driven rain calculation was performed according to ASHRAE 160 for a medium exposure category and a building height of <10 m. The simulated wall was considered below a low-sloped roof (ASHRAE 2009). No water penetration resulting from defects was considered in the simulations.

The interior climate was defined according to EN 15026 (CEN 2007), considering normal moisture load (indoor temperature ranging between 20-25ºC and relative humidity between 30-60%).

The simulation period, of all the simulation scenarios, corresponds to one year.

Therefore, a total of 96 hygrothermal simulations, taking into account the different referred parameters, were performed. ANNEX 2 – Simulation scenarios presents all the scenarios and associated configurations.

Table 60 – Input data in WUFI Pro: Measured material properties of system S1.

Classification	Property	TR1	C1
Basic properties	ρ (kg/m³)	208.7	1197.0
	P_0 (%)	34.7	36.8
	c (J/kg.ºC)[a]	1000	900
	λ (W/mºC)	0.049	0.220
	μ (dry-cup)	11.7	82.0[b]
Complementary properties	w_{80} (kg/m³)	2.47	9.06
	w_f (kg/m³)	346.52	366.58
	A_w (kg/m².s$^{0.5}$)	0.0296	0.0065
	λ_w (W/mºC)	Fig. 41	No
	D_{ws} (m²/s)	Fig. 46	Generated[c]
Surface transfer coefficients	ε (-)	—	0.92

[a]WUFI Pro Database (IBP 2016)
[b]Calculated according to $\mu_c = s_{d,C}/e_C$ (in 3.2.1.5)
[c]Generated curve by WUFI Pro calculation (IBP 2016)

Table 61 – Input data in WUFI Pro: Measured material properties of system S2.

Classification	Property	TR2	C2
Basic properties	ρ (kg/m³)	406.2	1357.3
	P_0 (%)	27.9	28.9
	c (J/kg.ºC)[a]	1000	900
	λ (W/mºC)	0.078	0.370
	μ (dry-cup)	12.7	46.0[b]
Complementary properties	w_{80} (kg/m³)	9.48	5.64
	w_f (kg/m³)	278.72	288.25
	A_w (kg/m².s$^{0.5}$)	0.0142	0.0161
	λ_w (W/mºC)	Fig. 41	No
	D_{ws} (m²/s)	Fig. 46	Generated[c]
Surface transfer coefficients	ε (-)	—	0.91

[a]WUFI Pro Database (IBP 2016)
[b]Calculated according to $\mu_c = s_{d,C}/e_C$ (in 3.2.1.5)
[c]Generated curve by WUFI Pro calculation (IBP 2016)

Table 62 – Input data in WUFI Pro: Measured material properties of system S3.

Classification	Property	TR3	C3
Basic properties	ρ (kg/m³)	659.5	1261.4
	P_0 (%)	50.6	38.0
	c (J/kg.ºC)[a]	1000	850
	λ (W/mºC)	0.134	0.292
	μ (dry-cup)	7.1	19[b]
Complementary properties	w_{80} (kg/m³)	2.03	2.65
	w_f (kg/m³)	504.15	378.80
	A_w (kg/m².s$^{0.5}$)	0.282	0.210
	λ_w (W/mºC)	Fig. 41	No
	D_{ws} (m²/s)	Fig. 47	Generated[c]
Surface transfer coefficients	ε (-)	—	0.91

[a]WUFI Pro Database (IBP 2016)
[b]Calculated according to $\mu_c = s_{d,C}/e_C$ (in 3.2.1.5)
[c]Generated curve by WUFI Pro calculation (IBP 2016)

Table 63 – Input data in WUFI Pro: Material properties of simulated system ETICS.

Classification	Property	EPS	C1
Basic properties	ρ (kg/m³)	15.0	1197.0
	P_0 (%)	95.0	36.8
	c (J/kg.ºC)[a]	1500	900
	λ (W/mºC)	0.040	0.220
	μ (dry-cup)	30.0	82.0[b]
Complementary properties	w_{80} (kg/m³)	No	9.06
	w_f (kg/m³)	No	366.58
	A_w (kg/m².s$^{0.5}$)	No	0.0065
	λ_w (W/mºC)	Fig. 210-b)	No
	D_{ws} (m²/s)	No	Generated[c]
Surface transfer coefficients	ε (-)	—	0.92

[a]WUFI Pro Database (IBP 2016)
[b]Calculated according to $\mu_c = s_{d,C}/e_C$ (in 3.2.1.5)
[c]Generated curve by WUFI Pro calculation (IBP 2016)

4.2.3. HYGROTHERMAL PERFORMANCE INDEXES

A deepened knowledge of the hygrothermal performance and related durability of thermal rendering and plastering systems could be assessed by hygrothermal simulation, defining for this purpose a set of hygrothermal indexes.

The definition of hygrothermal performance indexes enables the application of a durability assessment methodology to thermal rendering and plastering systems, by comparing them and highlighting the main causes of potential hygrothermal degradation.

Taking into account the simulation potential of WUFI Pro and the main degradation mechanisms in rendering systems, the temperature (exterior surface and difference between the thermal render surfaces), the thermal transmission coefficient of the system, the water content in the thermal render layer and condensation potential (on the exterior surface) were defined as hygrothermal performance indexes.

The surface temperatures and profiles across the wall allow evaluating the system integrity, due to the thermal induced stresses by the temperature variation. On the one hand, high-temperature variation in the surface contributes to the cracking of the coating, which allows the water to easily penetrate in the inner layers. A high-temperature variation across the surface layers also promotes different stresses and consequently contribute to the incompatibility of displacements of the distinct layers that constitute the thermal system.

The water action has a significant impact in the thermal performance of thermal rendering and plastering systems since the water content in the thermal render/plaster layer highly influences the thermal conductivity and consequently the thermal transmission coefficient. As such, the annual effective thermal transmission coefficient and the water content in the thermal render/plaster layer present an important role in the durability of thermal rendering and plastering systems.

Beyond the temperature and water content, the exterior surface condensation, originated by overcooling, is a concerning hygrothermal hazard that influences the durability of the thermal systems due to the algae growth. This pathology was mainly detected in thermal systems, such as ETICS (Barreira and de Freitas 2013; Barreira et al. 2013). In contrast to the interior condensation, exterior condensation is less dependent on the whole building performance but highly dependent on the physical and hygrothermal properties of the façade materials.

Research works developed in the course of the PhD (Maia, Ramos and Veiga 2016, 2017, 2018a; Maia, Ramos and Veiga 2018b) help on the definition and development of the hygrothermal performance indexes and the hygrothermal analysis, which are described in the following sub-chapters.

4.2.3.1.Temperature

As previously referred, the temperature influence and its distribution in thermal insulation systems represent a relevant indicator of the thermal performance. To evaluate the effect of temperature, the following performance indexes were calculated from the hourly values obtained in the one-year simulation of selected scenarios:

- Tse – Maximum exterior surface temperature;
- ΔTse – Temperature amplitude of the exterior surface;
- $\Delta T_{interface}$ – Temperature amplitude of the interface surface between the thermal render/plaster and the substrate;
- ΔT_{TR} – Maximum temperature difference between the thermal render/plaster layer surfaces.

A schematic representation of the referred temperature indexes is presented in Fig. 59.

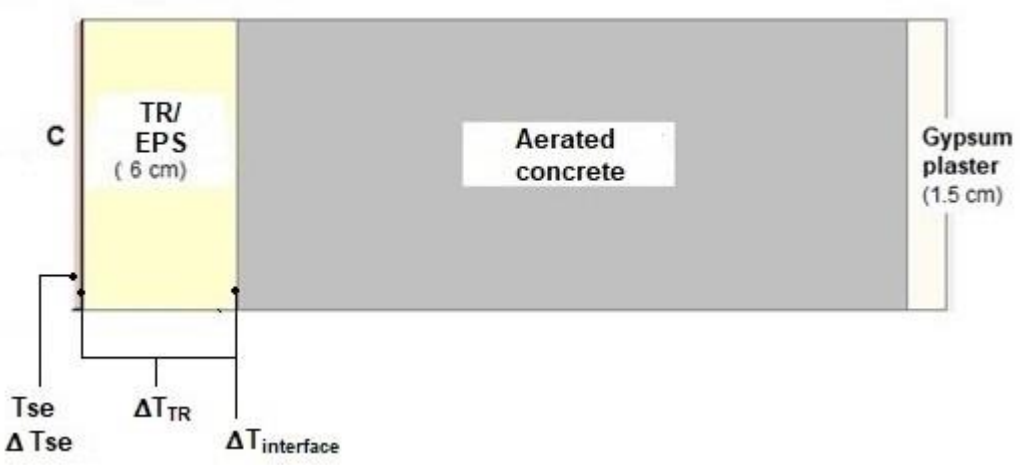

Fig. 59 – Schematic representation of the temperature indexes.

Since the solar radiation is higher in the south and west orientations, the temperature indexes will be analysed only for these two orientations. However, the results for all the four orientations are presented in ANNEX 3 – Temperature . Table 64 to Table 67 present the obtained temperature indicators in 46 simulation scenarios, considering south and west orientations.

Table 64 – Temperature indicators obtained in system S1, for the south and west orientations.

Climate	Porto				Nancy				Oslo			
Orientation	South		West		South		West		South		West	
CP	0.27	0.8	0.27	0.8	0.27	0.8	0.27	0.8	0.27	0.8	0.27	0.8
Tse (ºC)	36.7	46.5	40.7	64.5	34.5	45.2	35.7	49.7	32.6	44.8	32.8	45.1
ΔTse (ºC)	35.8	45.4	39.8	63.5	48.8	59.3	50.0	63.8	48.5	60.6	48.7	61.0
$\Delta T_{interface}$ (ºC)	35.4	44.9	39.3	62.4	48.3	58.7	49.5	63.1	48.0	59.9	48.3	60.4
ΔT_{TR} (ºC)	9.7	17.0	13.0	31.4	15.2	20.2	15.2	20.2	20.4	20.4	20.4	20.4

Table 65 – Temperature indicators obtained in system S2, for the south and west orientations.

Climate	Porto				Nancy				Oslo			
Orientation	South		West		South		West		South		West	
A	0.27	0.8	0.27	0.8	0.27	0.8	0.27	0.8	0.27	0.8	0.27	0.8
Tse (ºC)	36.4	46.1	40.3	63.8	34.1	44.6	35.2	49.0	32.3	44.3	32.6	44.7
ΔTse (ºC)	35.4	44.9	39.3	62.7	48.2	58.5	49.4	63.0	48.0	60.0	48.4	60.5
$\Delta T_{interface}$ (ºC)	35.1	44.5	39.0	61.9	47.8	58.0	48.9	62.4	47.7	59.5	48.1	60.1
ΔT_{TR} (ºC)	9.2	16.6	12.0	28.9	14.3	20.2	14.3	18.7	19.2	19.2	19.2	19.2

Table 66 – Temperature indicators obtained in ETICS, for the south and west orientations.

Climate	Porto				Nancy				Oslo			
Orientation	South		West		South		West		South		West	
A	0.27	0.8	0.27	0.8	0.27	0.8	0.27	0.8	0.27	0.8	0.27	0.8
Tse(ºC)	36.8	46.6	40.9	64.9	34.7	45.4	35.9	49.9	32.8	45.0	32.9	45.2
ΔTse(ºC)	36.0	45.6	40.0	63.9	49.1	59.6	50.3	64.2	48.8	61.0	49.0	61.2
$\Delta T_{interface}$ (ºC)	35.7	45.2	39.7	63.1	48.7	59.1	49.9	63.6	48.4	60.4	48.6	60.7
ΔT_{TR} (ºC)	11.1	16.3	12.7	30.3	18.0	19.2	17.7	19.6	20.4	20.4	20.4	20.4

Table 67 – Temperature indicators obtained in S3, for the south and west orientations.

Climate	Porto				Nancy				Oslo			
Orientation	South		West		South		West		South		West	
A	0.27	0.8	0.27	0.8	0.27	0.8	0.27	0.8	0.27	0.8	0.27	0.8
Tse (ºC)	36.1	45.5	39.8	62.8	33.6	43.8	34.8	48.0	32.0	43.7	32.4	44.2
ΔTse (ºC)	35.2	44.3	38.7	61.5	47.3	57.1	48.7	61.7	47.7	59.3	48.1	59.9
$\Delta T_{interface}$ (ºC)	7.9	7.9	7.9	8.4	10.7	11.0	10.9	11.5	10.7	11.4	10.8	11.5
ΔT_{TR} (ºC)	2.3	2.1	2.2	2.1	4.5	4.2	4.6	4.4	4.4	4.4	4.4	4.4

For a more comprehensive analysis, some of the results were plotted. Fig. 60 presents the values of the maximum exterior surface temperature, considering the white and dark coatings, respectively.

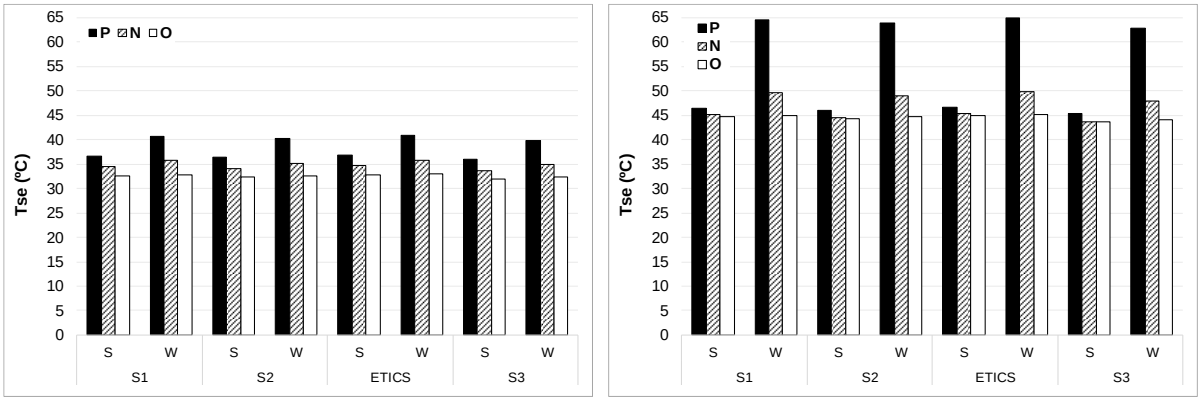

Fig. 60 – Maximum exterior surface temperature (Tse), considering south and west orientation and solar absorption of: a) 0.27 and b) 0.80.

The exterior surface temperature (Tse) was mainly affected by the location and the solar absorption coefficient. As expected, higher temperatures were observed in lower latitudes for a higher solar absorption coefficient. Tse was not significantly sensitive to the type of exterior insulation system (S1, S2 or ETICS). The influence of the wall orientation is quite significant since the temperature difference between the south and west orientations is relevant. That difference is emphasized by the higher solar absorption coefficient. Porto shows the highest increase (almost 20 ºC), on surface temperature,

regarding south and west orientation, since it also presents higher solar radiation values, especially in southwest orientation, comparing to Nancy and Oslo.

Fig. 61 and Fig. 62 present the 99th percentile and maximum temperatures, respectively, the difference between the thermal render layer surfaces ($\Delta T_{interface,}$) considering the white and dark coating, respectively.

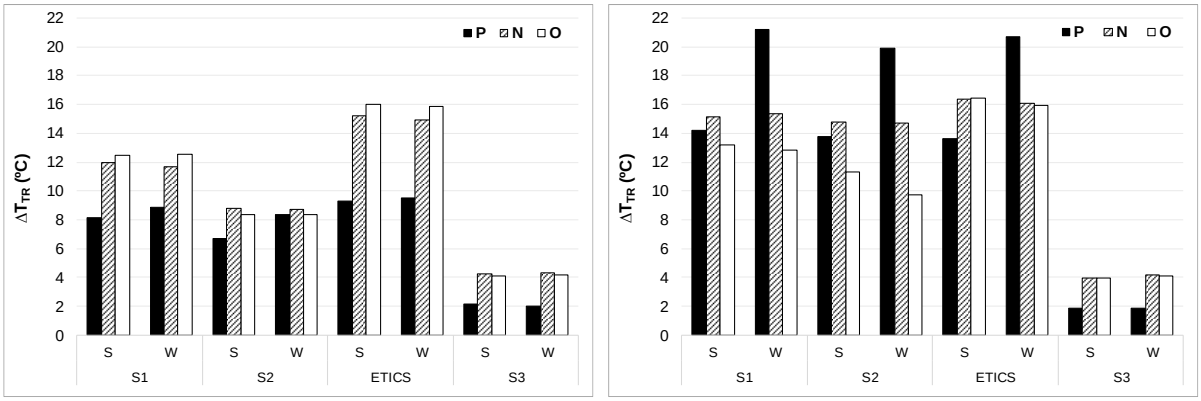

a) b)

Fig. 61 – 99th percentile of the temperature difference between the thermal render layer surfaces (ΔT_{TR}), considering south and west orientation and solar absorption of: a) 0.27 and b) 0.80.

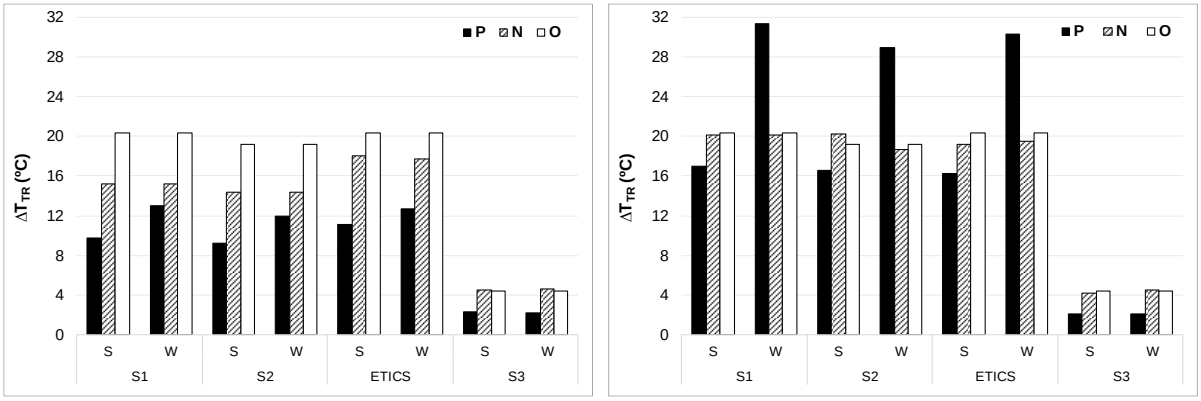

a) b)

Fig. 62 – Maximum temperature difference between the insulation layer surfaces (ΔT_{TR}), considering south and west orientation and solar absorption of: a) 0.27 and b) 0.80.

Regarding Fig. 61, the temperature difference of the 99th percentile between thermal render surfaces (ΔT_{TR}) was demonstrated to be more sensitive to the type of system, which, combined with different exposure conditions, led to different variation patterns. For lower solar absorption, systems S1 and S2 reached ΔT_{TR} values that could be up to 4ºC lower than the ones found in ETICS in comparable scenarios. However, observing Fig. 62-a), the different systems result in similar temperature differences among them. The peak values in both analysis are observed in winter months. Regarding the higher solar absorption, thermal rendering systems and ETICS presented similar behaviour and peak values could be observed in both winter and summer months. This means that the higher the temperature the lower the influence of the system characteristics. When a transient behaviour becomes dominant, thermal renders will give a higher temperature difference owing to their lower thermal diffusivity (d), comparing

to ETICS. This property describes how quickly a material, under transient heat conduction, reacts to a change in temperature and is given by equation (25) (Hagentoft 2001). This means that the thermal renders/plasters take more time to reach a new equilibrium condition.

$$d = \frac{\lambda}{\rho c} \tag{25}$$

Where λ is the thermal conductivity (dry state) [W/m.ºC], ρ is the dry bulk density [kg/m^3] and c is the specific heat [J/kg.ºC].

Therefore, increasing the solar absorption coefficient decreases the temperature difference between the systems (excluding S3). Despite the decrease of the influence of the material properties at high temperatures, with low solar absorption coefficients, the effect of the thermal inertia can be observed. The thermal effusivity (e) (or heat storage capacity) is the ability of the materials to absorb heat (Hagentoft 2001) (see equation (26)).

$$e = \sqrt{\lambda \rho c} \tag{26}$$

The higher the thermal conductivity and the density, the higher the thermal effusivity and the ability to absorb the heat flux, as shown in Fig. 63. It is clear, however, that thermal renders can be submitted to relevant temperature differences across their thickness, leading to thermal induced stress. Regarding the wall orientation, significant differences are observed when the dark coating is applied, especially in Porto (as observed in exterior surface temperatures).

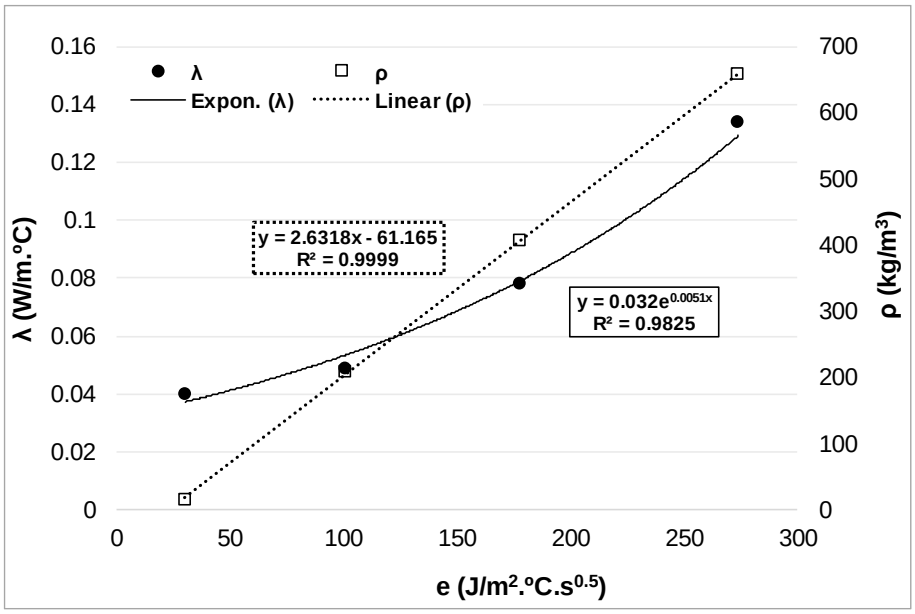

Fig. 63 – Thermal effusivity as a function of thermal conductivity and density, for the studied thermal renders/plaster and EPS.

4.2.3.2.Thermal transmission coefficient

The thermal transmission coefficient (U-value) helps on the analysis of the thermal performance of building components. In this specific case, the wall U-values were determined taking into account the

several material properties and their dependence on the moisture content. The thermal renders present different hygric behaviour, being widely affected by the moisture distribution. To a better comparison among the studied systems, the ratio between average (U_{av}) and reference (U_{ref}) U-value were calculated. This ratio takes into account the local requirements (reference U-value), highlighting possible hygrothermal risk when the ratio is bigger than 1 (see Table 68 to Table 71).

Table 68 – Thermal transmission indexes obtained in system S1.

α	Climate	Porto				Nancy				Oslo			
	Orientation	N	S	E	W	N	S	E	W	N	S	E	W
0.27	$U_{av}/U_{ref,\ annual}$	1.19	1.12	1.18	1.07	1.09	1.06	1.04	1.06	1.10	1.10	1.08	1.06
	$U_{av}/U_{ref,\ winter}$	1.14	1.11	1.18	1.12	1.07	1.08	1.07	1.09	1.09	1.14	1.11	1.08
	$U_{av}/U_{ref,\ summer}$	1.23	1.13	1.19	0.98	1.12	1.04	1.01	1.04	1.08	1.05	1.04	1.03
0.80	$U_{av}/U_{ref,\ annual}$	1.01	0.71	0.91	0.67	0.95	0.80	0.81	0.84	0.97	0.88	0.90	0.88
	$U_{av}/U_{ref,\ winter}$	1.09	0.83	1.07	1.00	1.04	1.00	1.03	1.05	1.08	1.10	1.09	1.07
	$U_{av}/U_{ref,\ summer}$	0.92	0.55	0.75	0.21	0.84	0.59	0.54	0.60	0.83	0.64	0.70	0.66

It is possible to observe the effect of increasing the solar absorption coefficient, which results in lowering the U_{av}/U_{ref} ratio and the hygrothermal risk. This fact is more evident in the summer season and in the lower latitudes (Porto), due to the high solar radiation in these areas. The higher the solar radiation the higher the temperature and consequently the drying process, which contributes to reducing the effective U-value.

Table 69 – Thermal transmission indexes obtained in system S2.

α	Climate	Porto				Nancy				Oslo			
	Orientation	N	S	E	W	N	S	E	W	N	S	E	W
0.27	$U_{av}/U_{ref,\ annual}$	1.19	1.12	1.18	1.07	1.09	1.06	1.04	1.06	1.10	1.10	1.08	1.06
	$U_{av}/U_{ref,\ winter}$	1.14	1.11	1.18	1.12	1.07	1.08	1.07	1.09	1.09	1.14	1.11	1.08
	$U_{av}/U_{ref,\ summer}$	1.23	1.13	1.19	0.98	1.12	1.04	1.01	1.04	1.08	1.05	1.04	1.03
0.80	$U_{av}/U_{ref,\ annual}$	1.02	0.73	0.92	0.67	0.96	0.81	0.81	0.85	0.98	0.88	0.90	0.88
	$U_{av}/U_{ref,\ winter}$	1.09	0.84	1.07	1.01	1.04	1.01	1.03	1.05	1.08	1.08	1.08	1.06
	$U_{av}/U_{ref,\ summer}$	0.92	0.58	0.77	0.20	0.85	0.60	0.54	0.61	0.84	0.66	0.70	0.66

Table 70 – Thermal transmission indexes obtained in system ETICS.

α	Climate	Porto				Nancy				Oslo			
	Orientation	N	S	E	W	N	S	E	W	N	S	E	W
0.27	U_{av}/U_{ref}, annual	1.17	1.07	1.14	1.05	1.06	1.01	1.01	1.02	1.09	1.03	1.04	1.03
	U_{av}/U_{ref}, winter	1.12	1.03	1.11	1.09	1.02	1.01	1.02	1.02	1.05	1.03	1.04	1.03
	U_{av}/U_{ref}, summer	1.23	1.11	1.18	0.98	1.10	1.02	1.00	1.02	1.13	1.02	1.04	1.02
0.80	U_{av}/U_{ref}, annual	1.00	0.68	0.88	0.64	0.93	0.77	0.78	0.81	0.95	0.82	0.87	0.85
	U_{av}/U_{ref}, winter	1.07	0.79	1.01	0.98	1.00	0.94	0.99	0.99	1.03	0.99	1.02	1.02
	U_{av}/U_{ref}, summer	0.92	0.53	0.75	0.16	0.83	0.56	0.52	0.57	0.85	0.62	0.69	0.65

Table 71 – Thermal transmission indexes obtained in system S3.

α	Climate	Porto				Nancy				Oslo			
	Orientation	N	S	E	W	N	S	E	W	N	S	E	W
0.27	U_{av}/U_{ref}, annual	1.18	1.15	1.20	1.07	1.09	1.07	1.03	1.07	1.08	1.08	1.06	1.05
	U_{av}/U_{ref}, winter	1.13	1.13	1.19	1.11	1.05	1.08	1.05	1.08	1.07	1.10	1.07	1.06
	U_{av}/U_{ref}, summer	1.22	1.16	1.21	0.98	1.13	1.08	1.00	1.06	1.08	1.06	1.04	1.03
0.80	U_{av}/U_{ref}, annual	1.01	0.75	0.93	0.67	0.95	0.81	0.80	0.85	0.96	0.87	0.89	0.87
	U_{av}/U_{ref}, winter	1.07	0.86	1.09	0.99	1.03	1.01	1.01	1.04	1.06	1.05	1.05	1.04
	U_{av}/U_{ref}, summer	0.91	0.58	0.78	0.20	0.85	0.60	0.52	0.61	0.82	0.65	0.69	0.65

For a better understanding of the evolution over the course of the year, the monthly ratios of U_{av}/U_{ref} are presented in Fig. 64 to Fig. 66.

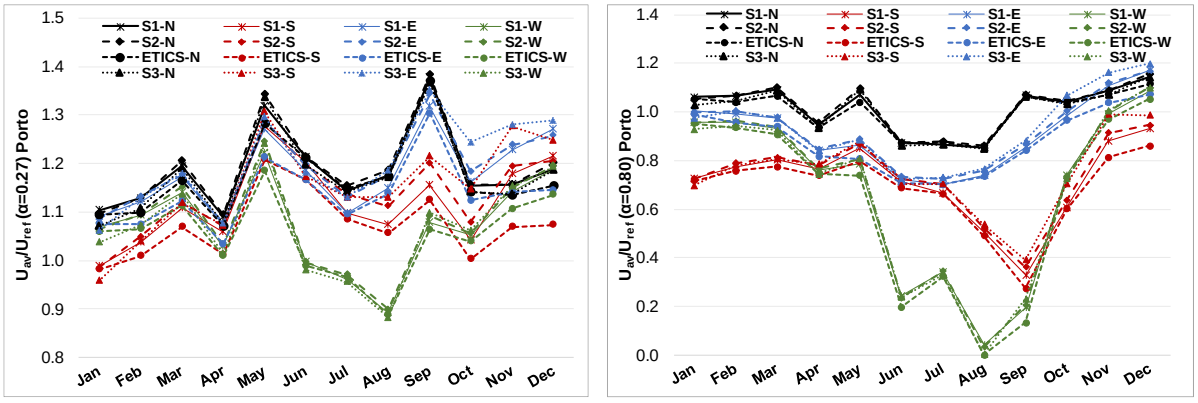

a) b)

Fig. 64 – Monthly ratio between average and reference U-value in Porto, considering the 4 orientations (N, S, E, W) and solar absorption of: a) 0.27 and b) 0.80.

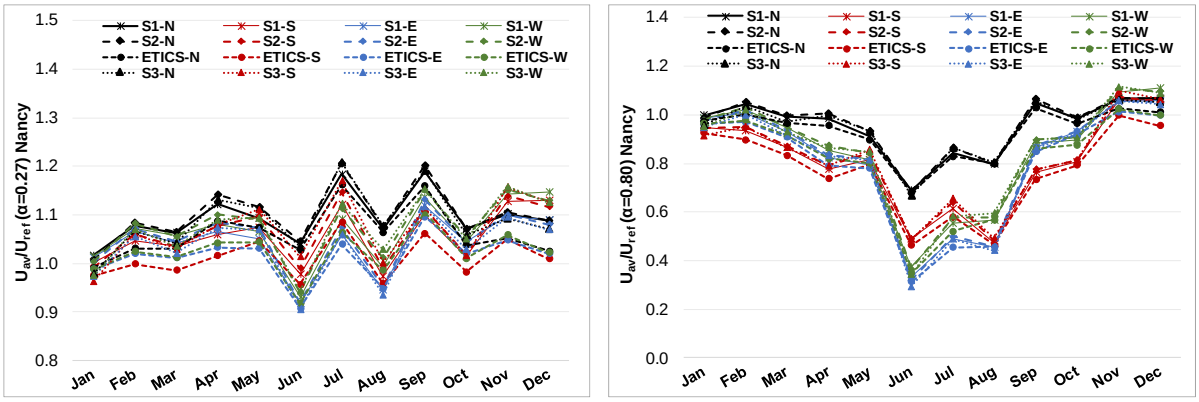

a) b)

Fig. 65 – Monthly ratio between average and reference U-value in Nancy, considering the 4 orientations (N, S, E, W) and solar absorption of: a) 0.27 and b) 0.80.

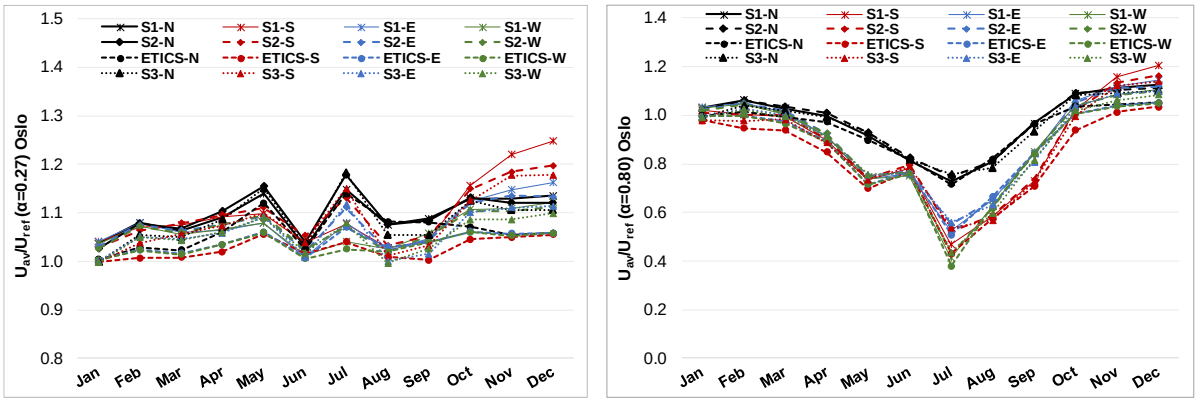

a) b)

Fig. 66 – Monthly ratio between average and reference U-value in Oslo, considering the 4 orientations (N, S, E, W) and solar absorption of: a) 0.27 and b) 0.80.

The darker coating application, considering the four wall orientations, reduced the hygrothermal impact (lower U_{av}/U_{ref}), especially in the summer season. Generally, the darker coating reduces the differences between the different systems. The lighter coating implies a lower drying process, increasing the water content and consequently the average U-value, compromising the hygrothermal performance of the whole system. In general, ETICS application results in a reduction of the hygrothermal impact, owing to its hygrothermal properties. In Porto, which has a mild temperature and high relative humidity, the application in the north façade leads to an increase of the hygrothermal risk, because the presented ratio is higher for both solar absorption coefficients. However, in the summer, it is possible to observe the solar effect resulting from the lowering of the U index, especially in Porto for the darker coating applied to the west façade. In addition, the presented ratio is lower and similar for the different systems in the summer months, while in the colder months they exhibit different behaviours, especially in the low latitude climate, for the orientations with higher solar exposition.

4.2.3.3.Water content

As previously referred, the water content could lead to a harmful impact in thermal systems, by increasing the thermal transmission, since different hygric properties, such as the water absorption and

vapour permeability, result in different amount of retained water. Materials with high water absorption contribute to high water content. This problem could be emphasized if combined with low vapour permeability coatings, contributing to the increase of the water content in the material. Fig. 67 to Fig. 69 present the monthly water content in the insulation layer (TR1, TR2, EPS and TR3) of the studied systems for all the simulated scenarios.

It is possible to observe the different behaviour of the studied systems. S1 and especially S2 present a higher water content in the thermal render comparing to ETICS and S3. EPS has a completely different behaviour in terms of hygric performance compared to the thermal renders, owing to its constitution and hygric properties, so these need to be taken into account. As expected, EPS presents a very low water content variation, because it is an almost impermeable material. Thermal render TR3 also presented a very low water content when applied in the conditions of system S3 (interior application). As such, the water content in these layers is reduced, as it can be seen in ANNEX 4 – Water content indicators in Fig. 211 to Fig. 214.

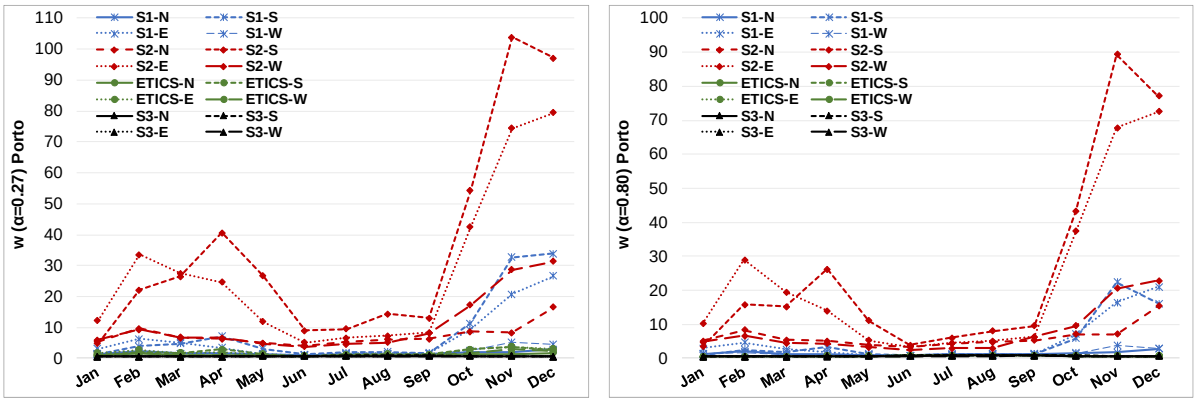

a) b)

Fig. 67 – Monthly water content in the insulation layer in Porto, considering the 4 orientations (N, S, E, W) and solar absorption of: a) 0.27 and b) 0.80.

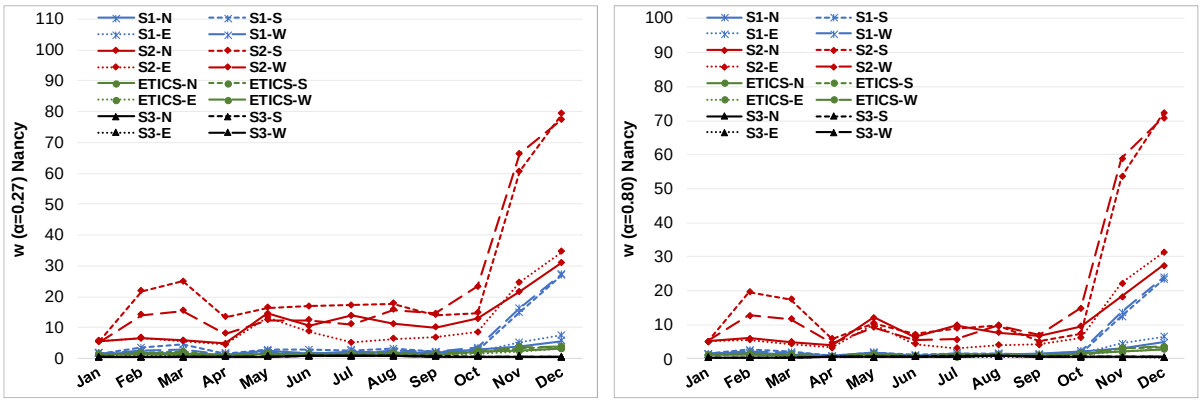

(a) (b)

Fig. 68 – Monthly water content in the insulation layer in Nancy, considering the 4 orientations (N, S, E, W) and solar absorption of (a) 0.27 and (b) 0.80.

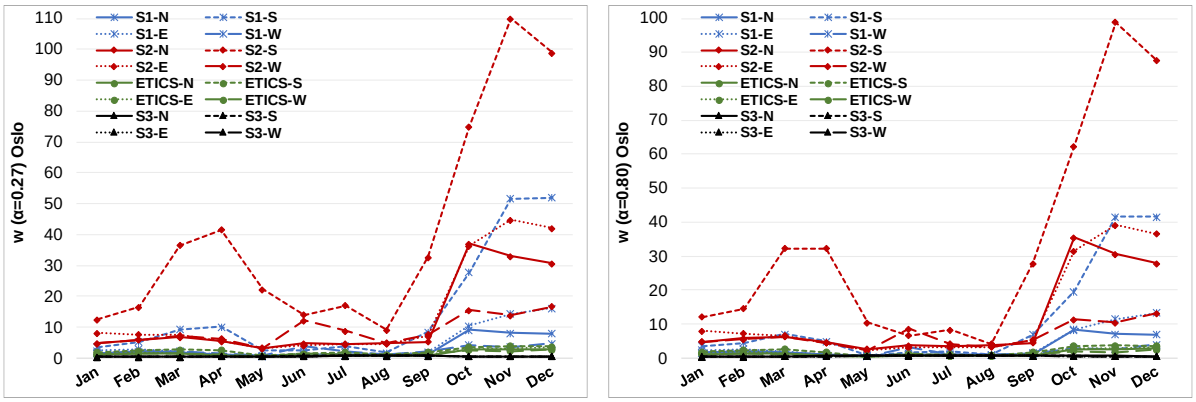

a) b)

Fig. 69 – Monthly water content in the insulation layer in Oslo, considering the 4 orientations (N, S, E, W) and solar absorption of: a) 0.27 and b) 0.80.

The box-plots of water content variation in the thermal render layer were assessed with the hourly values of that parameter also obtained in one-year simulation of selected scenarios. Fig. 70 to Fig. 73 present the water content in the thermal render layer of systems S1 and S2, considering the 4 orientations, the 3 climates (Porto – P, Nancy – N and Oslo – O) and the two solar absorption coefficients.

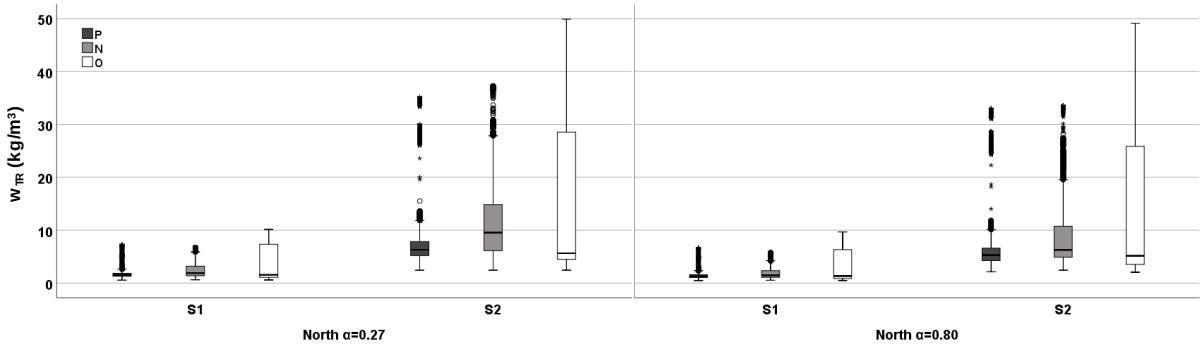

Fig. 70 – Box-plot of the water content in the thermal render layer of S1 and S2 with solar absorption of 0.27 and 0.80, in the north façade.

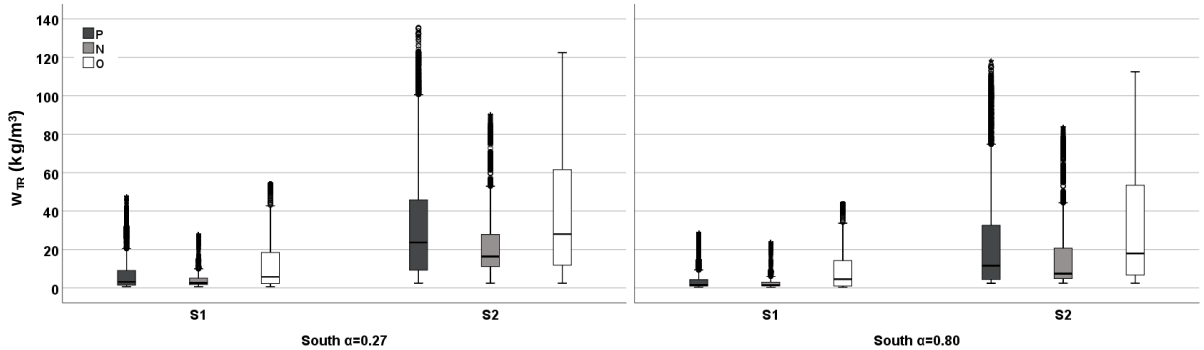

Fig. 71 – Box-plot of the water content in the thermal render layer of S1 and S2 with solar absorption of 0.27 and 0.80, in the south façade.

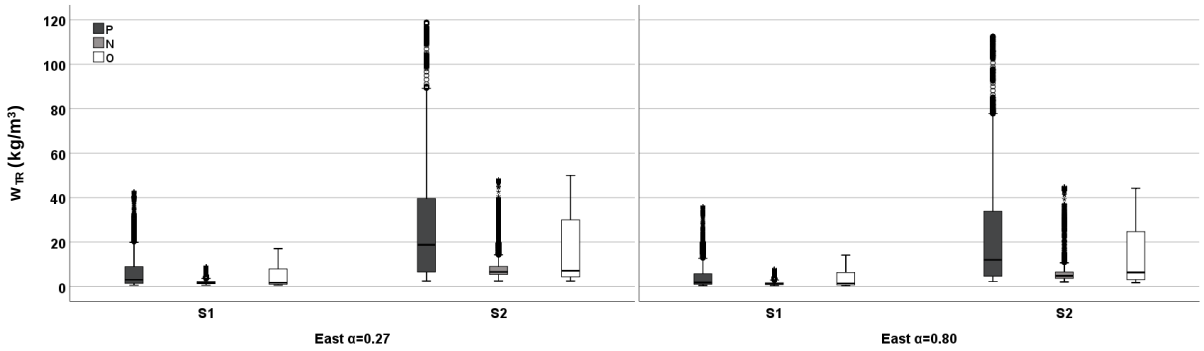

Fig. 72 – Box-plot of the water content in the thermal render layer of S1 and S2 with solar absorption of 0.27 and 0.80, in the east façade.

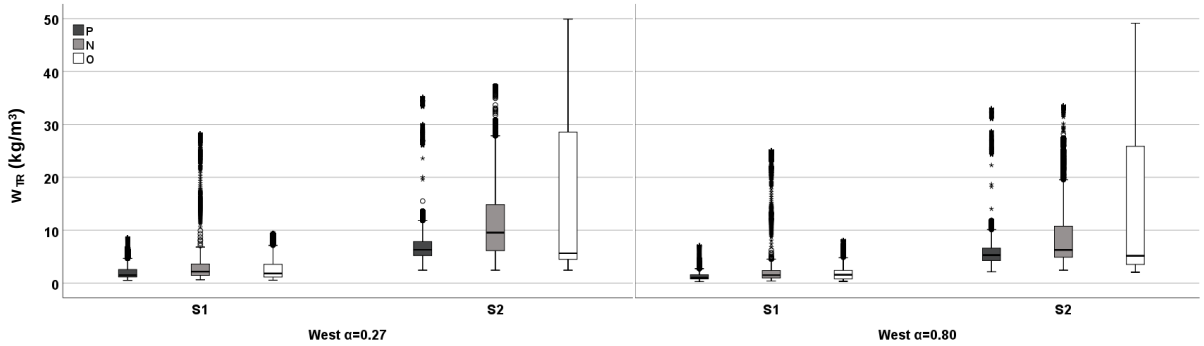

Fig. 73 – Box-plot of the water content in the thermal render layer of S1 and S2 with solar absorption of 0.27 and 0.80, in the west façade.

The drying process was clear when applying the darker coating, because the water content is lower and presents less dispersion. It is also noted the rain effect by the water content increase in the orientations with higher rain incidence. Therefore, Porto presents higher water content in the thermal render in the south and east, Nancy in the south and west and Oslo in the south orientation.

TR1 and TR2 present very different behaviours. Despite the lower water absorption coefficient of TR2, the S2 coating has higher capillary absorption than S1's. Therefore, the low absorption of the S1 coating led to lower water content in the thermal render layer, in contrast to S2, for both solar absorption coefficients. Although the w_{TR}/w_f average values in both systems are ≤17% (see Fig. 74). The maximum values are ≤16% for S1 and around 13-45% for S2, depending on the location (see Fig. 75).

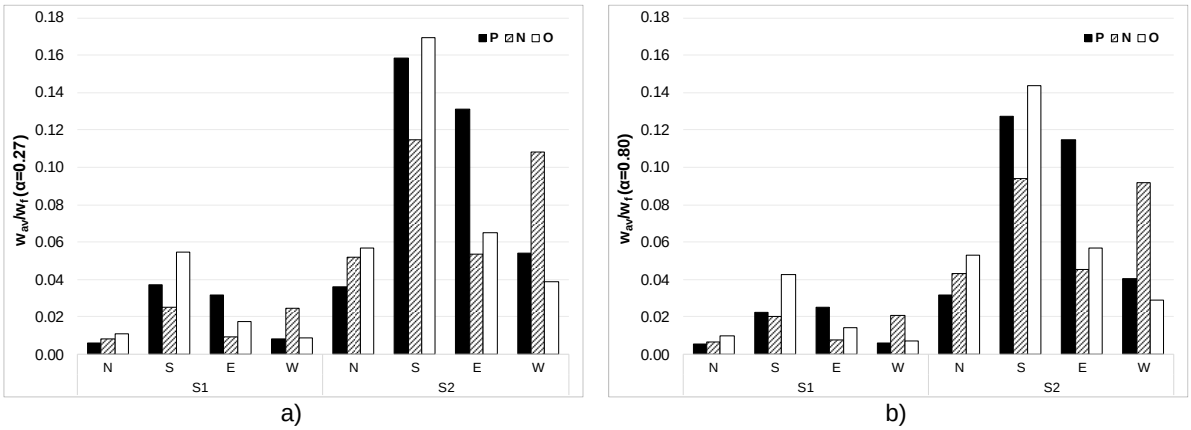

Fig. 74 – Ratio between the average water content and the free water saturation in the TR, considering the 4 orientations (N, S, E, W) and solar absorption of: a) 0.27 and b) 0.80.

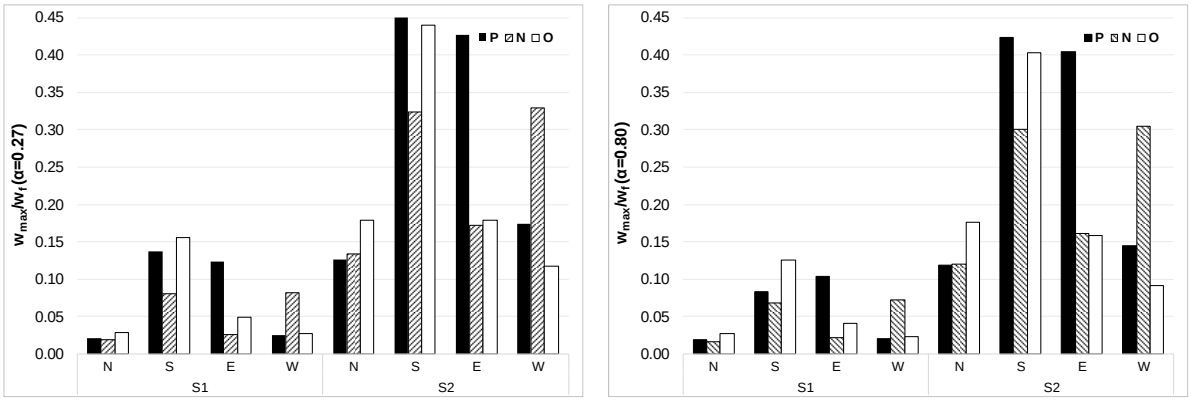

Fig. 75 – Ratio between the maximum water content and the free water saturation in the TR, considering the 4 orientations (N, S, E, W) and solar absorption of: a) 0.27 and b) 0.80.

In both cases, the south orientation led to higher water content values, since it is the orientation with higher rain frequency. The differences between TR1 and TR2 are also evident. The box-plots of the ratio between the water content and the free water saturation in the TR1 and TR2 are presented in ANNEX 4 – Water content indicators in Fig. 215 to Fig. 218.

4.2.3.4. Condensation risk

The focus was set on this specific pathology because algae growth on the exterior surface of the façade is linked to system performance and, in contrast to interior condensation, is less dependent on the whole building performance. The risk of condensation on the exterior surface of the façade was assessed through the quantification of the condensation potential (Zheng et al. 2004). This potential represents the difference between the water vapour partial pressure in the air and the water vapour saturation pressure on the surface, calculated by equation (27).

$$CP = P_v(air) - P_{sat}(surface) \tag{27}$$

Where $P_v(air)$ is the water vapour partial pressure in the air close to the surface and $P_{sat}(surface)$ is the water vapour saturation pressure on the surface. Positive values of the potential imply condensation.

Another way to explore the condensation risk consists in quantifying the number of hours that a façade is exposed to 100% of relative humidity (Ramos et al. 2014).

The condensation risk indexes are presented in Table 72, being the condensation potential presented in Fig. 76, to a quicker analysis.

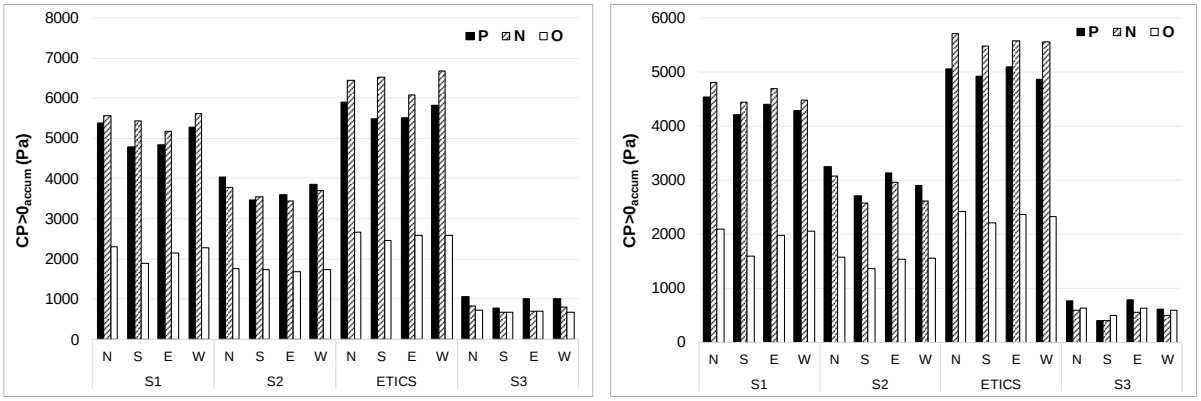

a) b)

Fig. 76 – Accumulated positive condensation potential considering the 4 orientations (N, S, E, W) and solar absorption of: a) 0.27 and b) 0.80.

Despite the better hygrothermal performance highlighted in the previous paragraphs, ETICS presented a higher condensation risk when compared to S1 and S2. The thermal effusivity, a measure of the ability of materials to exchange thermal energy with its surroundings, as a function of $[\lambda.\rho]$, explains the observed values (as demonstrated before with equation (26)). The higher the thermal conductivity and the density, the higher the thermal effusivity and the ability to absorb or dissipate heat flux. This provides a heat supply to the surface, reducing the periods of overcooling during night-time. This means that thermal renders can represent a lower risk of algae growth, when compared to ETICS, because of their higher mass. When the thermal insulation system is applied in the interior in the case of S3, this greatly reduces the condensation risk because the exterior layers have a higher thermal capacity. The application in the north façade leads to an increase of the condensation potential, especially in Porto, which is in accordance with the results obtained in 4.2.3.2. Again, the darker coating contributes to increase the hygrothermal performance by reducing the condensation potential.

Table 72 – Condensation potential indexes.

S	α	Climate	Porto				Nancy				Oslo			
		Orientation	N	S	E	W	N	S	E	W	N	S	E	W
S1	0.27	$CP > 0$	5397.2	4776.0	4831.1	5281.1	5556.2	5438.4	5187.5	5607.0	2310.0	1890.3	2138.3	2281.5
		$\varphi = 100\%$	0.0	0.0	0.0	0.0	7.0	1.0	6.0	2.0	24.0	2.0	20.0	20.0
	0.80	$CP > 0$	4533.7	4202.6	4411.1	4277.7	4807.0	4437.7	4687.3	4486.3	2083.4	1587.2	1973.6	2045.4
		$\varphi = 100\%$	0.0	0.0	0.0	0.0	6.0	0.0	5.0	1.0	19.0	1.0	19.0	16.0
S2	0.27	$CP > 0$	4038.2	3476.6	3608.1	3855.7	3779.1	3532.7	3445.9	3689.2	1749.5	1740.7	1690.0	1738.2
		$\varphi = 100\%$	0.0	0.0	0.0	0.0	0.0	0.0	0.0	0.0	4.0	0.0	0.0	0.0
	0.80	$CP > 0$	3250.2	2708.7	3121.2	2897.5	3066.0	2569.4	2953.8	2603.1	1565.7	1350.6	1526.0	1560.7
		$\varphi = 100\%$	0.0	0.0	0.0	0.0	0.0	0.0	0.0	0.0	4.0	0.0	0.0	0.0
ETICS	0.27	$CP > 0$	5891.8	5498.9	5515.9	5836.2	6437.1	6514.3	6092.5	6667.1	2674.1	2454.7	2589.3	2578.1
		$\varphi = 100\%$	0.0	3.0	5.0	0.0	9.0	8.0	8.0	8.0	32.0	23.0	29.0	22.0
	0.80	$CP > 0$	5049.8	4931.3	5087.0	4872.9	5702.1	5485.3	5577.6	5558.4	2418.0	2212.1	2354.9	2313.3
		$\varphi = 100\%$	0.0	0.0	3.0	0.0	9.0	8.0	8.0	8.0	23.0	21.0	24.0	18.0
S3	0.27	$CP > 0$	1069.7	776.9	1018.9	998.8	838.6	670.4	709.0	806.1	718.4	669.4	702.3	669.1
		$\varphi = 100\%$	0.0	0.0	0.0	0.0	0.0	0.0	0.0	0.0	0.0	0.0	0.0	0.0
	0.80	$CP > 0$	765.1	393.4	775.8	611.0	588.5	395.0	546.4	484.6	622.0	492.0	620.1	588.1
		$\varphi = 100\%$	0.0	0.0	0.0	0.0	0.0	0.0	0.0	0.0	0.0	0.0	0.0	0.0

4.2.4. SUMMARY

In simulations of thermal render systems applied on an exterior surface, TR2 exhibits a higher water content than TR1, despite the lower capillary absorption coefficient of TR2. This highlights the importance of the whole system analysis because the C1–S1 water absorption coefficient is much lower than that of C2–S2. Thermal plastering system S3, owing to its high water absorption, should not be applied on the exterior surface. Besides, gypsum products are usually not intended for exterior applications because of their high solubility in liquid water. The application of finishing coatings with low water absorption on these gypsum-based plasters could enhance their application. However, possible defects in the application and future damage (e.g., cracks) would allow the degradation agents to act directly upon the thermal plaster, compromising its durability.

A higher water content in the thermal render layer contributes to an increase of hygrothermal risk, as can be seen in S2 by the ratio between the average and the reference U-values for the different scenarios, in contrast to ETICS, which usually exhibits very low water content and consequently lower hygrothermal risk. The hygrothermal properties of the materials could lead to a completely different performance despite the compliance of the U-value requirements for each country, which reinforces the importance of hygrothermal evaluation of the whole system. Porto, for example, presented higher hygrothermal risk regarding the north façade, with higher U_{av}/U_{ref} and condensation potential values. However, Nancy and Oslo present a lower variation in the 4 orientations, because the solar radiation and rain are lower compared to that of Porto. The lower the solar radiation and total rain, the lower the variation of the hygrothermal indicators considering the 4 orientations and the 4 systems. The façades exposed to a higher incidence of rain and radiation are subjected to higher hygrothermal induced damages.

Interior thermal insulation systems can offer better performance when applied in mild climates, such as Porto because they result in lower thermal stresses (owing to the low surface temperature differences) and also in a reduction of the condensation potential, which is more severe in that type of climate. However, in colder climates, such as Nancy and Oslo, the higher façade U-value compromises thermal performance. Nevertheless, it still could be an alternative to increase thermal resistance, when the exterior insulation application is not feasible.

For exterior thermal insulation systems, the analysed ETICS showed good performance, in general, but it was better for colder climates because hygrothermal risk are diminished compared to the thermal rendering systems (lower effective U-value and water content). For warmer and more humid climates, the enhanced hygric properties, such as the capillary absorption and the vapour permeability of the thermal renders and also the whole system (especially S1) contribute to regulation of the humidity and to compatibility with the masonry substrate (which is typical in southern Europe). Another relevant finding was the improved behaviour of the thermal rendering systems comparing to the simulated ETICS, regarding the condensation potential. The higher thermal effusivity of TR's, reduces the night-time overcooling periods on the surface, leading to a lower risk of algae growth in thermal rendering systems.

Beyond the properties of thermal insulation systems, the solar absorption coefficient has a significant impact on the hygrothermal behaviour because it contributes to the reduction of hygrothermal risk. However, it promotes an increase of thermal stresses, especially in warmer climates with high solar radiation, such as Porto. In contrast, for climates with low solar radiation, a high solar absorption coefficient constitutes a good way to increase the hygrothermal performance.

The definition of hygrothermal performance indexes allows to a better comprehension of the degradation mechanisms and consequently the hygrothermal risk and associated durability.

In terms of thermal action, the temperature fluctuation may have a significant impact, due the high variation, especially using darker coatings. The colour has demonstrated a greater impact, concerning thermal degradation, than the different material properties, which promote slight differences between the studied systems. The façade orientation also has a significant impact in the thermal performance, since orientation with high solar radiation incidence results in higher temperature variations. As such, the durability assessment methodology should be established regarding these worst-case situations.

The water action showed a significant impact on the increase of the hygrothermal risk in both the thermal render/plaster and the whole system, by increasing the effective U-value. The higher water content in the thermal render/plaster was observed in the orientation with higher amount of rain incidence on the façade (south orientation), for systems with higher water absorption. This fact points out the importance of analysing the effect of rain incidence in climates with greater frequency, regarding the worst façade incidence. The capillary absorption, especially of the outer layers, has a considerable impact in the performance of the whole system since higher capillary absorption coatings imply a greater water content in the thermal render/plaster. Consequently, the outer layers play an important role in the durability assessment of façade systems.

The simulation of three different climates and exterior/interior application allow verifying the different action of the degradation mechanisms in each thermal system. As such, the durability evaluation taking into account different degradation levels contributes to optimizing the application of thermal rendering and plastering systems.

4.3. THERMO-MECHANICAL IMPACT ON FAÇADES WITH THERMAL RENDERING AND PLASTERING SYSTEMS APPLICATION

4.3.1. MODELLING PRINCIPLES

The behaviour of a system depends on its geometry, material properties, initial boundary conditions and loads, which can be highly complex by analytical resolution. Therefore, numerical methods, namely the discretization methods, such as the Finite Element Method (FEM), are one of the most used methods to solve this type of problems. FEM is a fundamental and indispensable piece in the modelling and simulation of advanced engineering systems in the most diverse areas, namely in buildings.

The Finite Element Method allows solving heat transfer problems, namely when thermal action induces stresses – thermo-mechanical action. Several principles are considered for the numerical resolution of differential equations of the formulated problem, such as Newton's second law, mass conservation, energy conservation, etc. The basic premise of FEM is that the solution of a studied area can be analytically modelled or approximated by an assembly of discrete elements. One of the advantages of FEM is the possibility to formulate the problem in different ways (Huebner et al. 2001), namely:

- Direct approach: applied to more basic problems, using algebraic matrices;
- Variational approach: applied to simpler to more complex geometry, using variations calculations, such as the principle of minimum potential energy;
- Weighted residuals approach: applied also to non-structural problems, such as heat transfer and fluid mechanics, through the derivation of the material properties.

According to Liu and Quek (2003), numerical modelling procedure using FEM consists of four distinct phases:

- Geometry modelling;
- Definition of the mesh (discretization process);

- Material properties specification;
- Specification of initial boundary conditions and loads.

According to Fish and Belytschko (2007), FEM consists of dividing an object in finite elements, connected by nodes, which create a mesh of finite elements. FEM could be applied in five different steps, focused on the development of the equations:

- Pre-processing: subdivision of the problem domain into finite elements;
- Formulation of the element: development of equations applied to the elements;
- Assembly: obtention of the equations of the complete system, through the single element equations;
- Resolution of the equation system;
- Post-processing: outputs determination, such as stresses and strains, and visualization.

In an easier way, it is possible to highlight the three most relevant steps:

- Pre-processing: discretization of the problem, selection of the interpolation functions and derivation of the elements equations;
- Analysis: Definition of the boundary conditions, calculation and solution of the equations system;
- Post-processing: presentation of results after processing.

Solid objects and structures are subject to loads and forces creating stresses, generally non-uniform, which lead to deformations or displacements. The relations between them are fundamental for the modelling, simulation and design of engineering systems.

Stresses are established as strains rate magnitude, transmitted node to node, in a solid subject to external actions, and applied to constitute the equilibrium conditions at a node of a solid (in three-dimensional space). As such, six stress (σ) components are checked, in a node of a solid, and defined as stress tensor which can be written as follows:

$$Stress\ tensor\ \sigma^T = \{\sigma_{xx}\ \sigma_{yy}\ \sigma_{zz}\ \sigma_{yz}\ \sigma_{xz}\ \sigma_{xy}\} \tag{28}$$

In the Theory of Elasticity the relationship between stresses and strains, for not very high loads, is in general linear or linearisable, for most of the materials used in structures, and the deformations are also considered linear, during part of the loading. The constitutive equation that establishes a relation between the stress (σ) and the strain (ε_S) of a material of a solid element, with elastic behaviour in anisotropic materials i,s generally the Hooke's Law, presented in equation (29).

$$\sigma = k\varepsilon_S \tag{29}$$

Where k is a matrix of constants which depends on the Young's modulus, Poisson's ratio and shear modulus, considering isotropic materials.

One common way to induce stresses in buildings is through thermal action by the heat transfer. This could be such a complex problem to model and, consequently, to predict future events. Elements have embodied energy, which heat flow can occur by conduction, convection and radiation mechanisms. Knowing that heat flows from the higher temperature to the lower temperature area, which promotes molecular interaction, thermal conduction is seen as a relevant mechanism in solids and the thermal conductivity as an important material property. The conductive heat transfer, at a steady state, could be expressed by the Fourier's law (see equation (30) (McCarthy 2018).

$$\frac{Q\prime}{A} = -\lambda \frac{dT}{dx} \tag{30}$$

Where Q' is the heat transfer [W], A is the area [m^2], λ is thermal conductivity [W/(m.ºC)] and T is the temperature [ºC].

Considering one-dimensional heat transfer, in walls composed of different materials, the y direction is assumed infinite. Consequently, the heat source and heat exchanges are independent of y direction. In addition, due to the infinite length of the wall, the convection in x direction is not considered (only the conduction process is assumed), as expressed by equation (31).

$$\lambda A \frac{d^2T}{dx^2} + q = 0 \tag{31}$$

Where λ is the thermal conductivity A is the cross-section area and T is the temperature. The first term of the equation (31) corresponds to the conduction process and the term q to the heat source.

Abaqus software, from *Dassault Systémes*, is a thermo-mechanical simulation tool that allows reproducing heat transfer problems, using the finite element method (Dassault Systemes 2015b).

The thermo-mechanical simulation envisaged in this work the determination of stresses induced by hygrothermal action in walls with thermal rendering systems. It is of major importance to choose the best analytic process applicable to this specific case. Abaqus allows to analyse several actions, providing the following analysis types (Dassault Systemes 2015a):

- Stress/strain static analysis;
- Stress/strain dynamic analysis;
- Transport analysis in steady-state behaviour;
- Heat transfer and stress analysis by thermal action;
- Fluid dynamic analysis;
- Electromagnetic analysis;
- Coupled pore fluid flow and stress analysis;
- Mass diffusion analysis;
- Acoustic and impact analysis;
- Structural analysis in aquatic environment.

Taking into account the main goal of the present sub-chapter, the most appropriate analysis type is the "Heat transfer and stress analysis by thermal action". This analysis procedure allows the simulation of different heat transfer problems, such as:

- Heat transfer (dissociated analysis): heat transfer problems, which involve conduction, convection and radiation. Temperature is calculated without knowing the stress/strain state;
- Sequentially coupled thermal-stress analysis: if the stress/strain depend on the temperature action, but no inverse dependency exists; it should be first performed a heat transfer analysis and then the resulting data should be used for the stress analysis;
- Fully coupled thermal-stress analysis: to solve simultaneously stress/strain and temperature fields, when thermal and mechanical actions affect each other.

Therefore, the thermo-mechanical action could be simulated through dissociated and coupled analysis.

The coupled thermo-mechanical analysis is performed by the combination of, at first, thermal analysis and then, the stress/strain mechanical analysis. Two main steps constitute this process:

- Determination of the temperature distribution by heat transfer-thermal analysis;
- Determination of the stresses and strains induced by the previously determined temperature distribution.

Being the temperature distribution on the wall provided by experimental tests and hygrothermal simulation, a sequentially coupled thermal-stress analysis will be used. In that way, this analysis requires the existence of elements with both temperature and displacement degrees of freedom in the model. As such, in a 3D modelling, the suitable finite element is a continuum three-dimensional solid element with 8-node trilinear displacement and temperature, designated as C3D8T (C – continuous element; 3D – three-dimensional constituted by 8 nodes; and T – thermal action analysis).

Abaqus comprises three distinct parts:

- Modelling: model configuration and definition of the geometry and the materials;
- Analysis: model simulation;
- Visualization: simulation results.

Each part is constituted by different modules, which allow the software to create the object, specify the actions to which it is subjected and apply the FEM to analyse the stresses. As such, Abaqus comprises the following modules:

- Part: create the part geometry (rigid or flexible);
- Property: definition of the material properties;
- Assembly: create one or more instances through the parts of the model; position parts for initial configuration;
- Step: selection of the analysis type and output requests;
- Interaction: Define contact and other interactions between the different parts, and assign them to the steps in the analysis history;
- Load: definition of the applied loads and boundary conditions;
- Mesh: split the assembly into meshable regions and assign the selected finite element mesh type to it;
- Job: running the simulation jobs; monitor the analysis jobs.

4.3.2. SIMULATION MODEL AND INPUT DATA

As referred before, Abaqus uses the finite element method, which allows a coupled thermal-stress (temperature-displacement). Since the effect of the temperature variation, in the thermal render layer, is of great importance, a coupled temperature-displacement analysis was performed in the present work. The Abaqus/CAE – Simulia (Dassault Systemes 2015b) were used.

Three different cases were studied:

- 1st analysis: Influence of the temperature variation in the thermal render layer surfaces, according to the results obtained by hygrothermal simulation in 4.2.3.1;
- 2nd analysis: Influence of the thermal shock in the exterior surface, resulting from an abrupt decrease of temperature;
- 3rd analysis: Influence of the substrate in the development of stresses in the thermal render system.

A 3D model of 2.5x3.0 m^2 was designed. The choice of these dimensions is linked to further work, developed in 5.4. Boundary constraints, in terms of displacements and rotations, were defined:

- Displacements in x*yz* axis blocked: base of the wall;
- Displacements in z axis blocked: top and sides of the wall.

Fig. 77 presents the schematic 3D model used in the thermo-mechanical simulation, corresponding the front layer to the exterior surface. The models presented in Fig. 77-a) and in Fig. 77-b) have the same configuration as presented in Fig. 57 and Fig. 58, respectively.

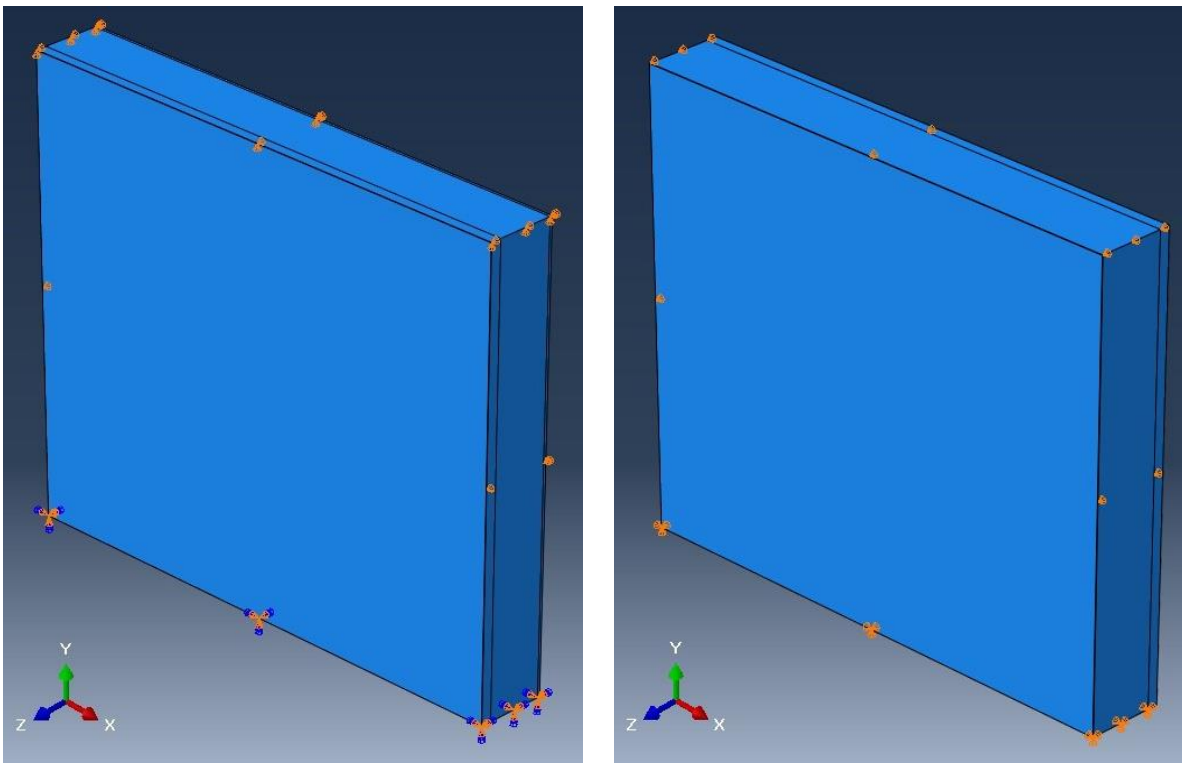

a) b)

Fig. 77 – Schematic representation of the 3D simulation model with: a) Exterior insulation application (S1, S2 and ETICS); b) Interior insulation application (S3).

The material properties used as input for the thermo-mechanical simulation were obtained by the experimental tests (density, thermal conductivity and elastic modulus of ther thermal rendering and plastering systems, in chapter 3), in the WUFI Pro Database (IBP 2016) (specific heat and basic properties of the substratesa and interior plaster) and bibliography references (ESCSI 2007; Zeng et al. 2012; A Silva et al. 1999; Ang and Wang 2004) (thermal expansion coefficient and Poisson's ratio), as presented in Table 73.

Table 73 – Material properties used in the thermo-mechanical simulation.

	Thickness (m)	ρ (kg/m³)	λ (W/m.ºC)	a' (x10⁻⁶/ºC)	E (MPa)	c (J/kg.ºC)	υ (-)
C1	0.004	1197.0	0.2202	9.6	3820.6	900	0.17
TR1	0.060	208.7	0.0487	9.0	103.5	1000	0.20
C2	0.003	1357.3	0.3700	9.6	3351.4	900	0.17
TR2	0.060	406.2	0.078	9.0	482.2	1000	0.20
C3	0.002	1261.4	0.2920	9.6	3515.4	850	0.34
TR3	0.060	659.5	0.1340	9.0	718.9	1000	0.20
EPS	0.060	15.0	0.040	50	2.0	1500	0.12
Aerated concrete	0.26/0.325/ 0.22/0.38[1]	600.0	0.1400	10.8	2125	850	0.20
Brick masonry	0.15	650	0.55	4.5	1600	850	0.25
OSB[2]	0.025	630	0.12	7.0	7500	850	0.15
Interior plaster	0.015	850.0	0.2000	17	3500	850	0.20
Exterior render	0.004	1310.0	0.8700	9.6	5918	850	0.20

[1]S1/S2/ETICS/S3; [2]OSB: Oriented Strand Board.

Since the focus of the first analysis is in the effect of large temperature variation in the thermal render layer, only the west orientation will be considered, as it presents the higher variations (as shown in 4.2.3.1). Table 74 presents the surface temperature constraints, which were assumed in each simulation scenario. Due to the similarity of some scenarios, considering the two solar absorption coefficients (0.27 and 0.80), only one scenario was simulated. This fact is observed in Oslo, where only the lower solar absorption influence was analysed, and considering S3, due to the interior insulation application. In order to guarantee the equilibrium of the entire system, an initial temperature of 20 ºC was set.

The temperature profile of each simulation scenario is presented in Fig. 78 to Fig. 84.

Table 74 – Boundary constraints of the 1st analysis: surface temperature.

System	α (-)	Input	Temperature (ºC)		
			Porto	Nancy	Oslo
S1	0.27	$T_{se,TR}$	40.3	2.4	-3.5
		$T_{si,TR}$	27.3	17.7	16.9
		T_{si}	20.0	20.0	20.0
	0.80	$T_{se,TR}$	63.6	49.1	—
		$T_{si,TR}$	32.2	28.9	
		T_{si}	20.0	20.0	
S2	0.27	$T_{se,TR}$	40.1	2.8	-3.5
		$T_{si,TR}$	28.1	17.2	16.9
		T_{si}	20.0	20.0	20.0
	0.80	$T_{se,TR}$	63.2	38.0	—
		$T_{si,TR}$	34.3	19.3	
		T_{si}	20.0	20.0	
ETICS	0.27	$T_{se,TR}$	40.6	-13.9	-3.5
		$T_{si,TR}$	27.9	3.8	16.9
		T_{si}	20.0	20.0	20.0
	0.80	$T_{se,TR}$	64.2	49.5	—
		$T_{si,TR}$	33.9	29.9	
		T_{si}	20.0	20.0	
S3	0.27	$T_{se,TR}$	18.8	14.0	14.2
		$T_{si,TR}$	21.0	18.6	18.7
		T_{se}	14.5	-7.4	-6.2

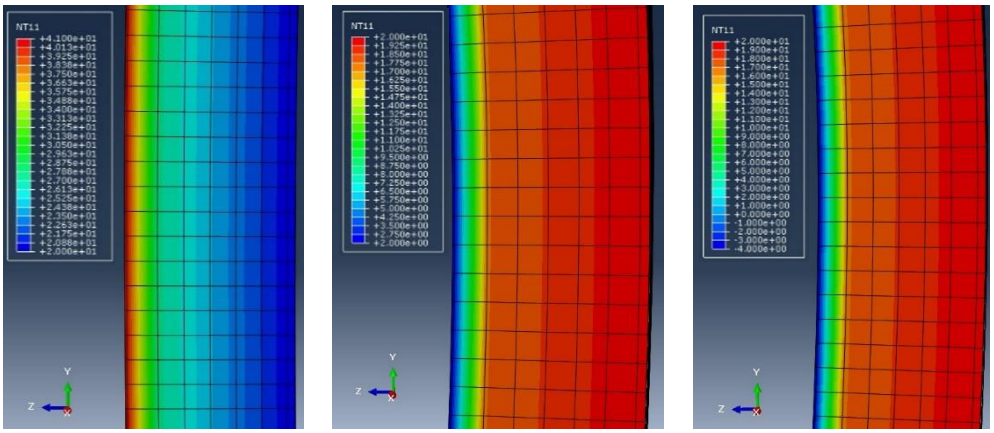

a) b) c)

Fig. 78 – Temperature profile in S1, considering a solar absorption coefficient of 0.27, in: a) Porto; b) Nancy; c) Oslo.

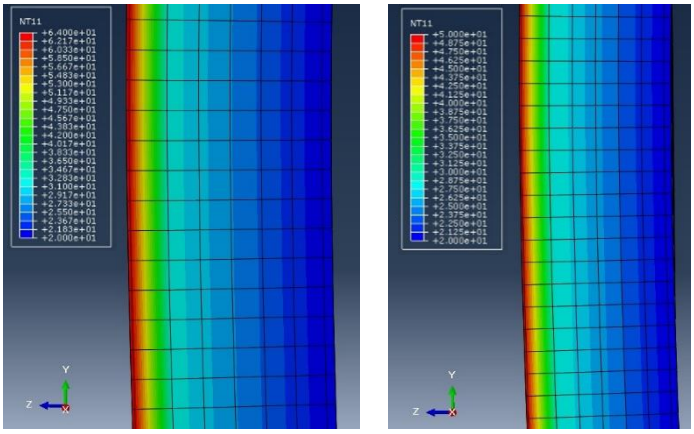

a) b)

Fig. 79 – Temperature profile in S1, considering a solar absorption coefficient of 0.80, in: a) Porto; b) Nancy.

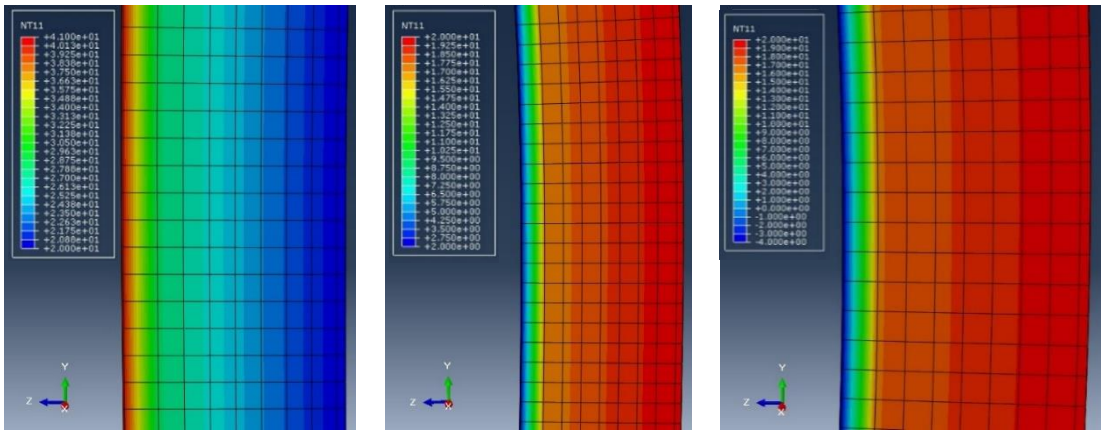

a) b) c)

Fig. 80 – Temperature profile in S2, considering a solar absorption coefficient of 0.27, in: a) Porto; b) Nancy; c) Oslo.

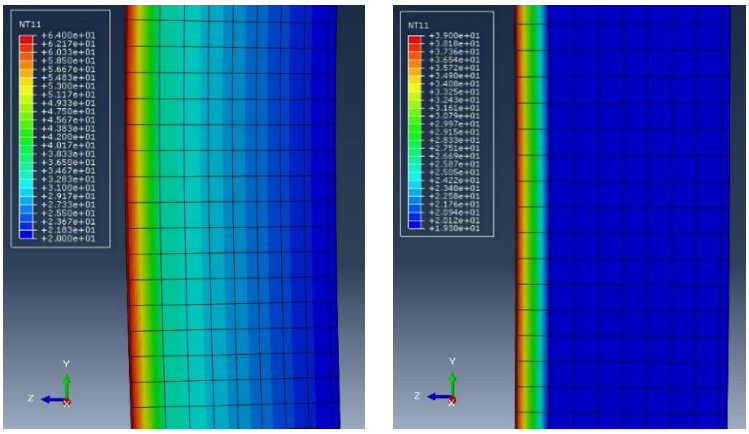

a) b)

Fig. 81 – Temperature profile in S2, considering a solar absorption coefficient of 0.80, in: a) Porto; b) Nancy.

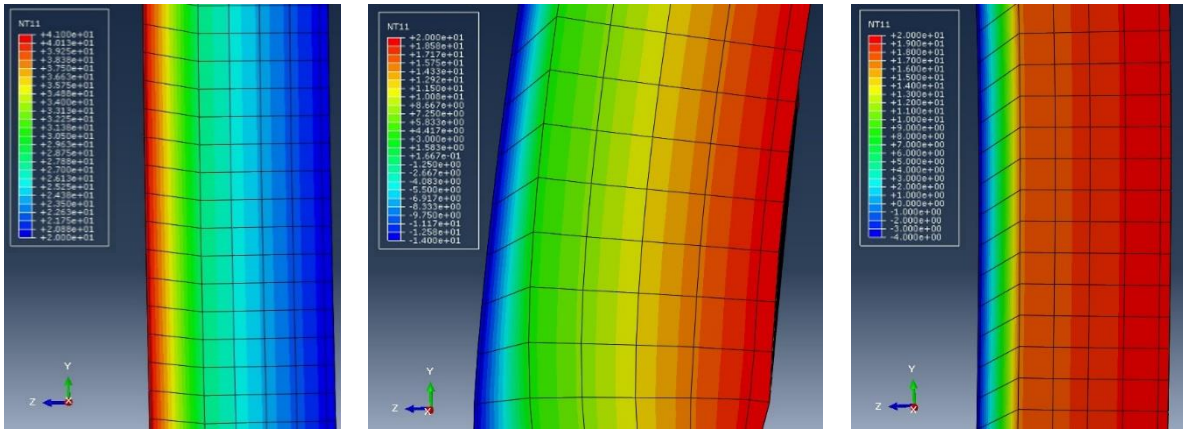

a) b) c)

Fig. 82 – Temperature profile in ETICS, considering a solar absorption coefficient of 0.27, in: a) Porto; b) Nancy; c) Oslo.

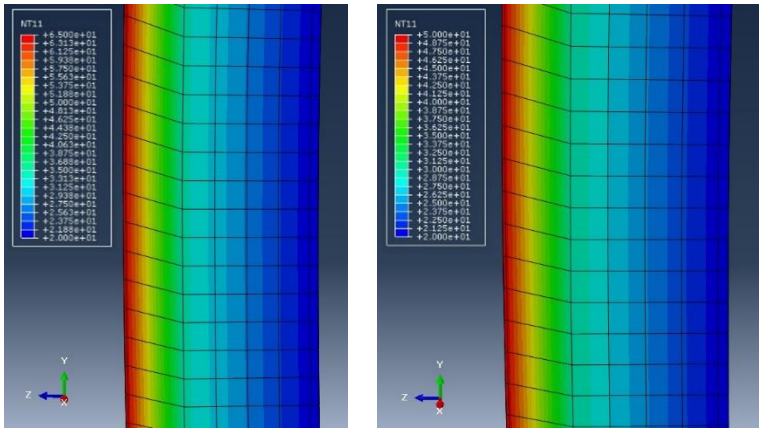

a) b)

Fig. 83 – Temperature profile in ETICS, considering a solar absorption coefficient of 0.80, in: a) Porto; b) Nancy.

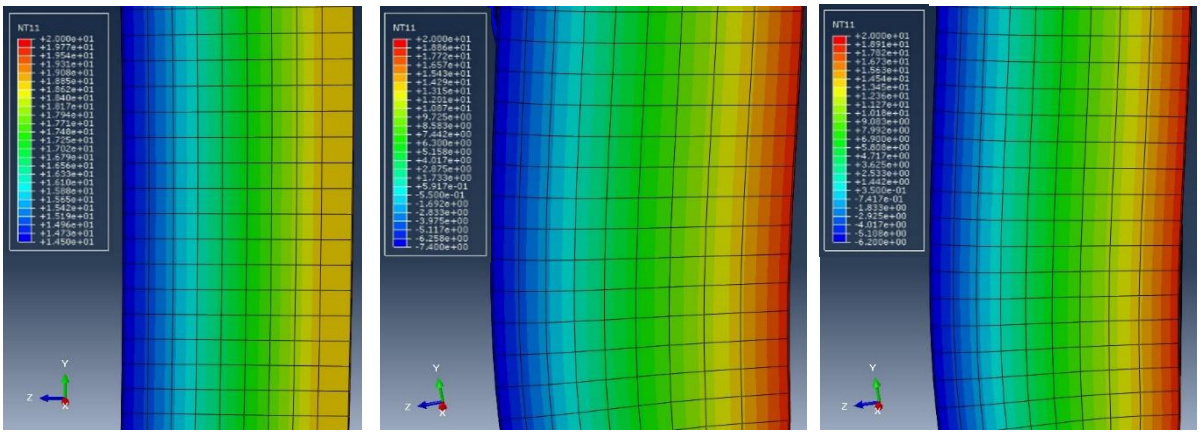

a) b) c)

Fig. 84 – Temperature profile in S3, considering a solar absorption coefficient of 0.27, in: a) Porto; b) Nancy; c) Oslo.

In the case of the second analysis, an abrupt decrease of exterior surface temperature was studied. The incidence of rain in the façades following warm periods, when the wall could reach high surface temperatures, lead to a fast decrease of temperature and consequently to an increase in the thermal stresses. In that way, an initial exterior surface temperature of 70ºC and a decrease to 15ºC was analysed. These values are in accordance with previous measurements performed in ETICS, where the finishing render and coating of the system S1 was applied, considering darker coatings (Sá 2018) and included in ETAG 004 (EOTA 2013). The referred analysis is a first step to understand the effect of the rain incidence in façades since it will be further developed in 5.4. The deepening of this phenomenon is of major importance, since the hygrothermal simulation, performed with WUFI Pro, did not take into account the façade cooling by cold rain water (IBP 2016).

For the last analysis, the influence of the application on different supports was evaluated. The aerated concrete block masonry, used in the previous simulations, was compared and replaced by a common ceramic brick masonry layer and an oriented strand board (OSB). The effect of the thermal shock (abrupt decrease of temperature 70 to 15 ºC) with the different substrates combined with S1 is analysed. The material properties are described in Table 73.

4.3.3. INFLUENCE OF THE TEMPERATURE VARIATION IN THE THERMAL RENDER/PLASTER LAYER SURFACES

The temperature influence and its distribution in thermal insulation systems represent a relevant indicator of the thermo-mechanical performance of the whole façade. The thermal impact on the thermal render layer is analysed in terms of higher principal stresses, strains and displacements.

Due to the expansion and contraction of the different layers, the tensile and compressive stresses, strains and displacements, in the three surfaces of the thermal system (exterior surface, C-TR and TR-substrate surfaces) are evaluated. The thermal expansion and contraction of the wall resulted in typical deformed shapes regarding the thermal load. Fig. 85 presents the non-deformed shape of the wall and Fig. 86 to Fig. 88 show the typical deformed shape, corresponding the front face to the exterior side (excepting S3, which corresponds to the interior side). In addition, the distribution of typical principal stresses is also shown. The results are presented considering half wall.

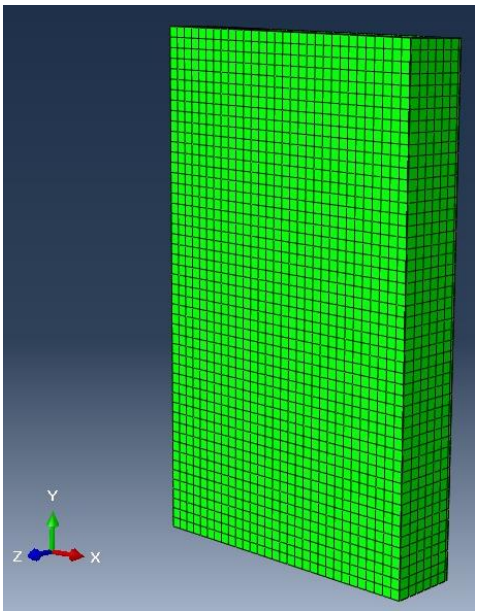

Fig. 85 – Non-deformed shape of half wall.

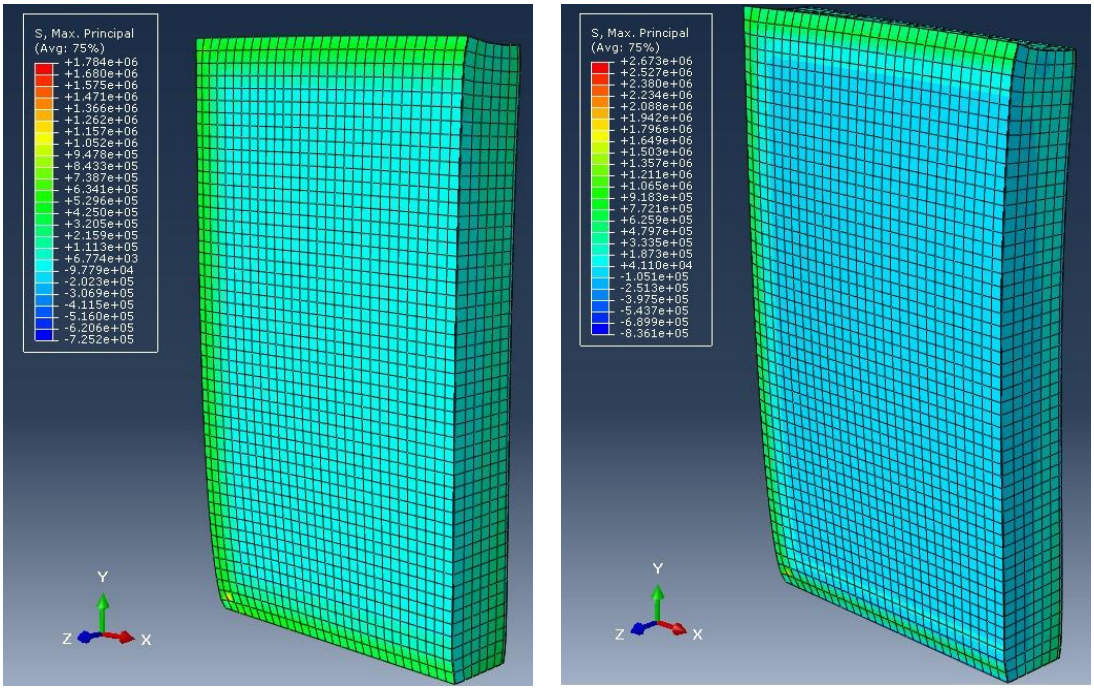

a) b)

Fig. 86 – Typical deformed shape in Porto, using S1, S2 and ETICS, considering a solar absorption coefficient of: a) 0.27; b) 0.80.

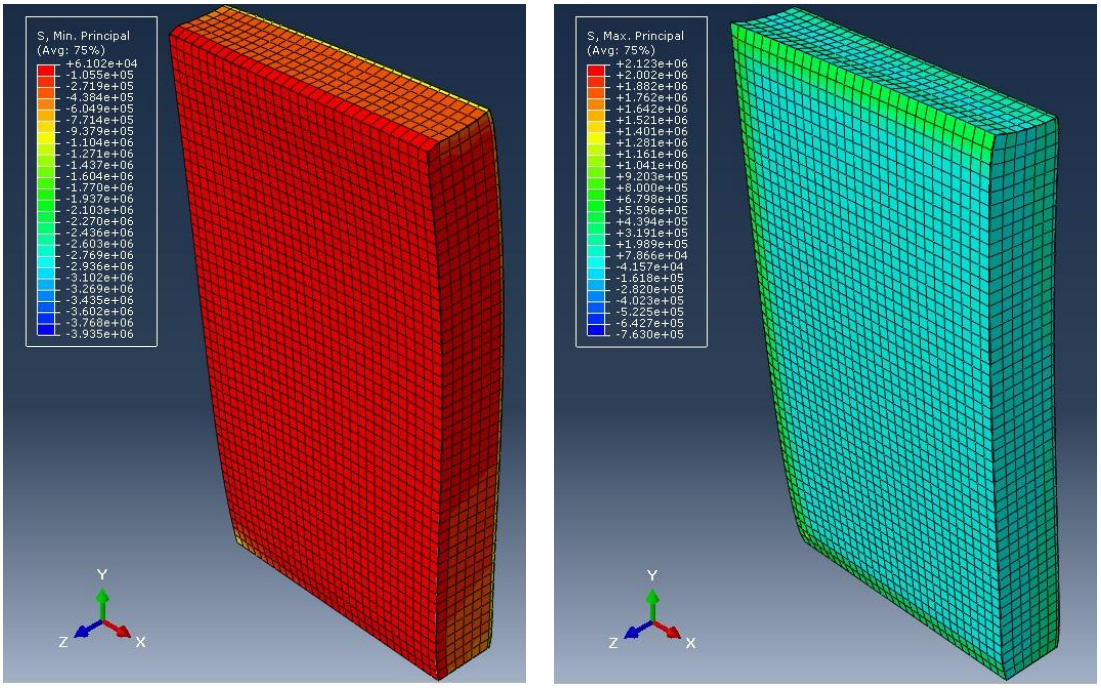

a) b)

Fig. 87 – Typical deformed shape in Nancy and Oslo, using S1, S2 and ETICS, considering a solar absorption coefficient of: a) 0.27; b) 0.80.

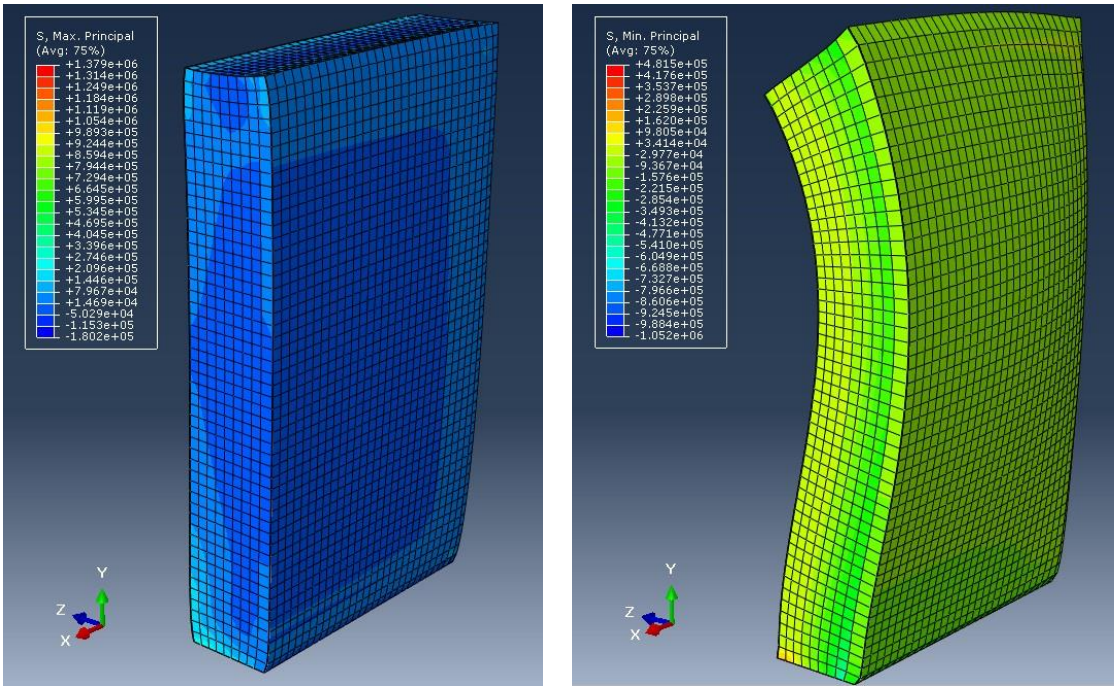

a) b)

Fig. 88 – Typical deformed using S3 in: a) Porto; b) Nancy and Oslo.

Table 75 presents the principal stresses in the thermal rendering system interfaces, considering a central node of the façade since it disregards the effect of the contour constraints. The tensile and compressive stresses are represented as positive and negative values, respectively. The stresses are presented in the inner side of the finishing render/plaster layer (C-inner), in the interface of the finishing render/plaster between the thermal render/plaster (C-TR) and in the interface of the thermal render/plaster between the substrate layers (TR-substrate).

As expected, the temperature effect (increase or decrease) promotes expansion and contraction of the different materials, resulting in tensile and compressive stresses, respectively. This fact highlights the importance of adapting the façade systems to each climate since the thermal stresses are highly dependent on the thermal loads. As such, the application of coatings with completely different solar absorption presents a great impact.

In Porto, where the solar radiation presents higher influence, the increase of the solar absorption of the façade led to much higher tensile stresses. In addition, the resulting strains due to the high thermal induced stresses (dark coating) are greater, promoting considerably different strains in each layer, as shown in Fig. 89. The white coating produced, as expected, much lower strains and less variation between the different layers (using the same scale). This means that using darker colours the compatibility between the different layers could be compromised. In both cases, the finishing render presents higher strains than the thermal render.

Table 75 – Principal stresses obtained by temperature variation in the thermal rendering and plastering system interfaces in a central node of the façade.

System	Solar absorption coefficient	Climate	C (inner) (Pa)	C-TR (Pa)	TR-Substrate (Pa)
S1	0.27	Porto	-267.7	157.3/-48.7	129.3/-1461.0
		Nancy	406.8	-686.3/78.2	-343.5/-35246.3
		Oslo	498.6	-774.3/103.0	-391.4/-38281.5
	0.80	Porto	-659.9	609.6/-132.8	380.8/-3842.9
		Nancy	-409.4	317.0/-81.0	216.8/-2368.1
		Oslo	—	—	—
S2	0.27	Porto	-185.8	57.5/-331.3	367.9/-1141.4
		Nancy	165.2	-336.0/645.5	-757.7/-37939.2
		Oslo	202.8	-362.0/736.2	-847.0/-40286.4
	0.80	Porto	-443.2	433.2/-1176.3	1296.2/-3599.8
		Nancy	9.2	171.6/-113.3	10246.1/-175.5
		Oslo	—	—	—
ETICS	0.27	Porto	-234.7	241.6/209.9	269.3/-1603.8
		Nancy	684.0	-2295.1/-1667.0	-1739.5/7725.6
		Oslo	514.3	-1222.3/-1915.2	-1953.9/-39373.9
	0.80	Porto	-669.6	1005.8/852.9	985.0/-5153.6
		Nancy	-392.0	501.4/434.8	523.5/-2914.1
		Oslo	—	—	—
S3	0.27	Porto	-191.6	123.1/-426.1	468.2/-1449.0
		Nancy	224.2	-417.9/845.0	-952.2/-40275.0
		Oslo	274.5	-449.3/961.9	-1066.2/-48746.4

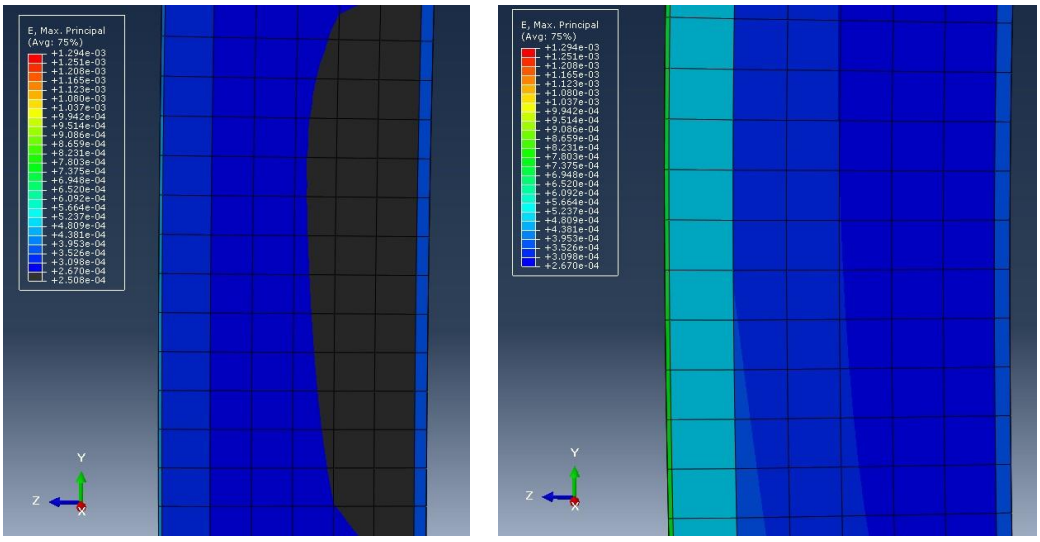

a) b)

Fig. 89 – Maximum strains obtained in Porto with S1, for a solar absorption coefficient of: a) 0.27; b) 0.80.

S1 and ETICS presented a similar increase (around 4 times), while S2 increases more than 7 times. Despite the three referred systems are submitted to similar temperature variation, the thermal induced stresses are different, evidenced the effect of the thermal conductivity: lower thermal conductivity of TR1 and EPS lead to a lower variation of thermal stresses. As already observed in 4.2.3.1 thermal renders and EPS present low thermal effusivity and consequently heat storage, which supports the lower stresses comparing to the other studied systems.

Observing the results in Nancy and Oslo, when the façade is submitted to a temperature decrease (lower solar absorption coefficient), the compressive stresses are dominant, since the interior surface presents higher temperatures than the exterior and thermal render surfaces. As such, the thermal render is subjected to higher compressive stresses than in warmer climates and a consequent crush of the porous structure. As shown in Fig. 90, the thermal render layer is subjected to strains with opposite direction, which corroborates the previous findings.

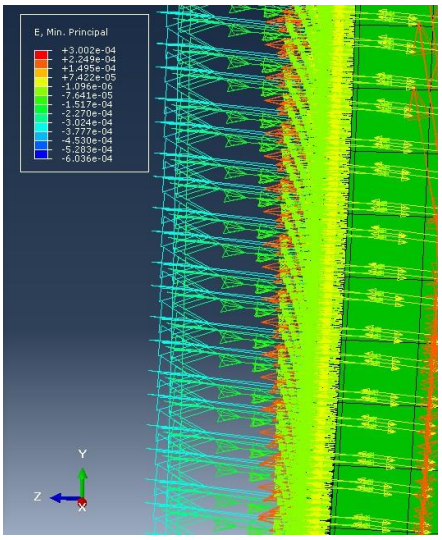

Fig. 90 – Typical minimum principal strains in the thermal rendering system, in Nancy, for a solar absorption coefficient of 0.27, considering exterior application.

Comparing S1, S2 and ETICS the effect of the physical and thermo-mechanical properties of thermal renders (TR1 and TR2) and EPS, such as the density (ρ), porosity (P_0), dynamic elastic modulus (E_d) and thermal expansion coefficient (α') can be observed in Fig. 91.

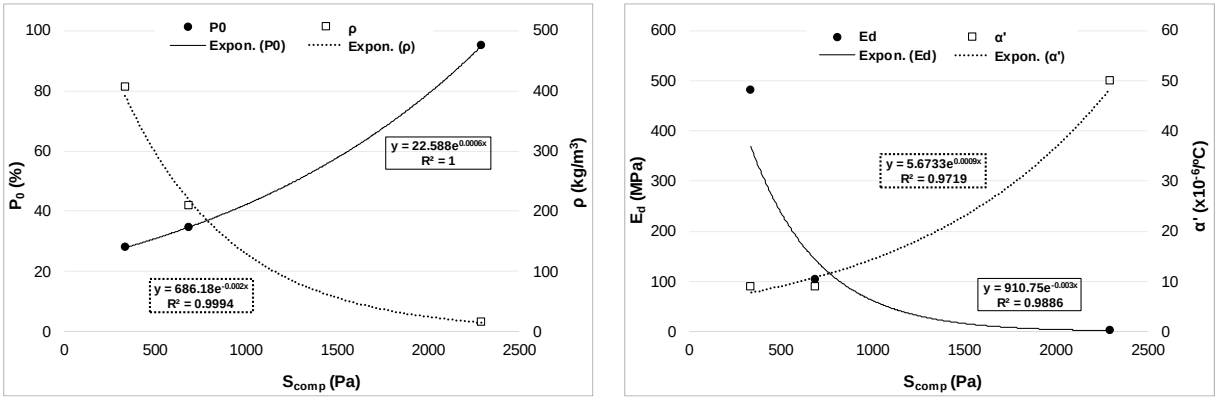

a) b)

Fig. 91 – Compressive stresses as a function of: a) Porosity and density; and; b) Dynamic elastic modulus and thermal expansion coefficient, of TR1, TR2 and EPS.

The higher the porosity and the lower the density, the higher the compressive stresses. Thermal enhanced materials, such as the thermal renders and EPS, usually present low density and high porosity in order to lowering the thermal conductivity. Regarding Fig. 91-b), the lower the dynamic elastic modulus and the higher the thermal expansion coefficient the higher the compressive stresses. As verified in 3.2.2.2, the thermal renders present low mechanical strength, especially low compressive strength, which corroborates the observed tendency.

In general, S3 presents lower compressive stresses than the systems applied as exterior insulation, which was expectable, due to the reduced exposure. However, S2 presents similar compressive stresses to S3, regarding Nancy and Oslo, despite the higher temperature variation which S2 is subjected to. This highlights the capabilities in terms of mechanical behaviour of S2 that result in similar stresses, in the thermal render layer, for greater thermal action. Although, regarding the thermal render-substrate interface, the higher rigidity of TR2 (comparing to TR1 and EPS) results in higher stresses in this particular zone, which may allow the development of cracking in the thermal render.

Table 76 presents the displacements in the thermal rendering system interfaces, regarding the different simulated scenarios. The results are in accordance with the obtained stresses, presented above: the higher the stresses the higher the displacements.

Table 76 – Displacements obtained by temperature variation in the insulation layer in a central node of the façade.

System	Solar absorption coefficient	Climate	C-TR	TR-Substrate
			(m)	(m)
S1	0.27	Porto	4.13×10^{-4}	4.09×10^{-4}
		Nancy	3.43×10^{-4}	3.41×10^{-4}
		Oslo	3.46×10^{-4}	3.43×10^{-4}
	0.80	Porto	4.92×10^{-4}	4.82×10^{-4}
		Nancy	4.38×10^{-4}	4.32×10^{-4}
		Oslo	—	—
S2	0.27	Porto	3.92×10^{-4}	3.88×10^{-4}
		Nancy	3.09×10^{-4}	3.06×10^{-4}
		Oslo	3.10×10^{-4}	3.06×10^{-4}
	0.80	Porto	5.41×10^{-4}	5.31×10^{-4}
		Nancy	3.21×10^{-4}	3.19×10^{-4}
		Oslo	—	—
ETICS	0.27	Porto	4.96×10^{-4}	4.13×10^{-4}
		Nancy	3.89×10^{-4}	4.20×10^{-4}
		Oslo	2.80×10^{-4}	3.88×10^{-4}
	0.80	Porto	7.67×10^{-4}	5.58×10^{-4}
		Nancy	6.29×10^{-4}	4.96×10^{-4}
		Oslo	—	—
S3	0.27	Porto	3.21×10^{-4}	3.19×10^{-4}
		Nancy	2.58×10^{-4}	2.48×10^{-4}
		Oslo	2.52×10^{-4}	2.42×10^{-4}

Generally, the displacements due to expansion were higher than the displacements due to contraction. This may be related to the high rigidity and thickness of the substrate, which restricts more the

contraction displacements than the expansion, which is higher influenced by the thermal system (less rigid and thinner). This is in accordance with the lower displacements in the thermal render-substrate interface. The displacements are similar in both C-TR and TR-substrate interface, except in ETICS, reflecting the higher dimensional variation of EPS, due to its higher thermal expansion coefficient.

4.3.4. INFLUENCE OF THE THERMAL SHOCK IN THE EXTERIOR SURFACE

The present sub-chapter aims to deepen the knowledge of the induced thermal stresses due to thermal shock by the cold rain incidence on a hot surface. Table 77 presents the maximum stresses after the heating and the cooling of the surface and Table 78 the resulting displacements.

Table 77 – Tensile and compressive stresses obtained by thermal shock in a central node of the façade.

System	Tensile stress (Pa)	Compressive stress (Pa)
	T=70 ºC	T=15 ºC
S1	2163.0	-862.1
S2	2023.7	-720.4
ETICS	2596.8	-1674.4
S3	9772.0	-366.2

Table 78 – Displacements obtained by thermal shock in a central node of the façade.

System	Displacements (m)	
	T=70 ºC	T=15 ºC
S1	7.67×10^{-4}	4.54×10^{-4}
S2	8.60×10^{-4}	4.90×10^{-4}
ETICS	9.85×10^{-4}	5.23×10^{-4}
S3	1.03×10^{-4}	5.44×10^{-4}

The typical deformed shape and principal stresses after heating and after the abrupt decrease are shown in Fig. 92.

When heated, the surface expands originating tensile stresses. The higher elastic modulus of C1, comparing to C2, may contributes to increase the stresses, since the dimensional variation is restricted, resulting in lower displacements. However, the results are similar, which reflects the influence of the thermal render. The change in the stress state may lead to cracks in the coating, allowing the climate agents to activate other failure mechanisms in the thermal render. Despite the same exterior coating of S1 and ETICS, the tensile stress obtained in the ETICS is higher, due to the much higher thermal expansion coefficient of EPS than TR1

Since S3 is applied in the interior, the inner side of the exterior coating is analysed. This highlights the fact that the application of rigid coatings will contribute to the increase of the tensile stresses. Otherwise, the compressive stresses are highly reduced, since the adjacent layer is the substrate (rigid material).

However, the internal insulation systems do not contribute to thermal inertia and hence they are not favourable for summer comfort in warm climates.

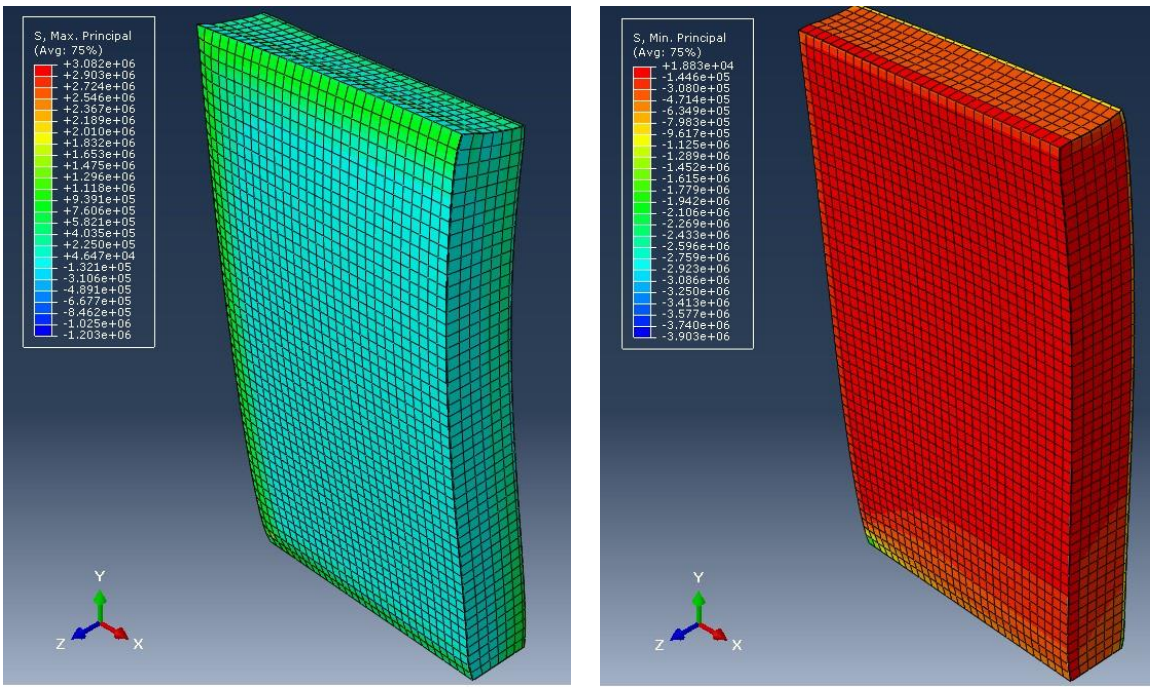

a) b)

Fig. 92 – Typical deformed shape after: a) Heating; b) Abrupt decrease.

In the ETICS, the finishing render surface also presents strains with opposite directions in both heat (70 ºC) and cold (15 ºC) periods, as shown in Fig. 93. This fact may compromise the durability of the entire system, due to the cracking of the finishing render.

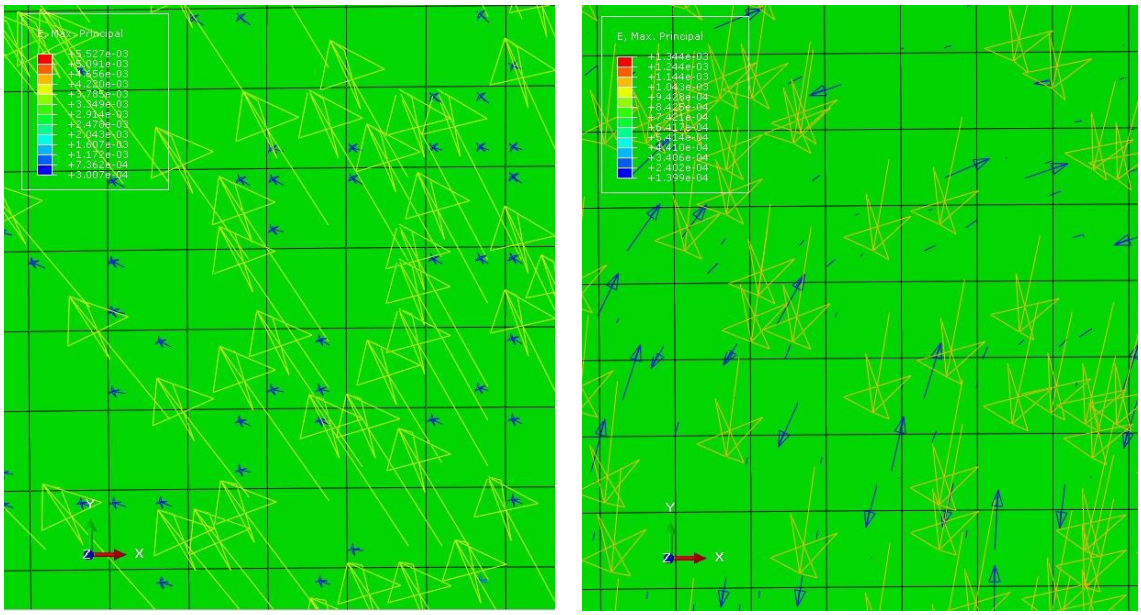

a) b)

Fig. 93 – Strains distribution in the façade surface of ETICS after: a) Heating; b) Abrupt decrease.

Regarding the rigidity of the thermal render/EPS (E_{TR}) and the finishing render (E_C), the higher the difference of rigidity between the two layers the higher the stresses, as shown in Fig. 94. This highlights the importance of compatibility between the adjacent layers in terms of rigidity. In addition, thermal rendering systems may present in this aspect an advance comparing to ETICS, since they present enhanced thermal properties, such as ETICS, but reduced thermal induced stresses.

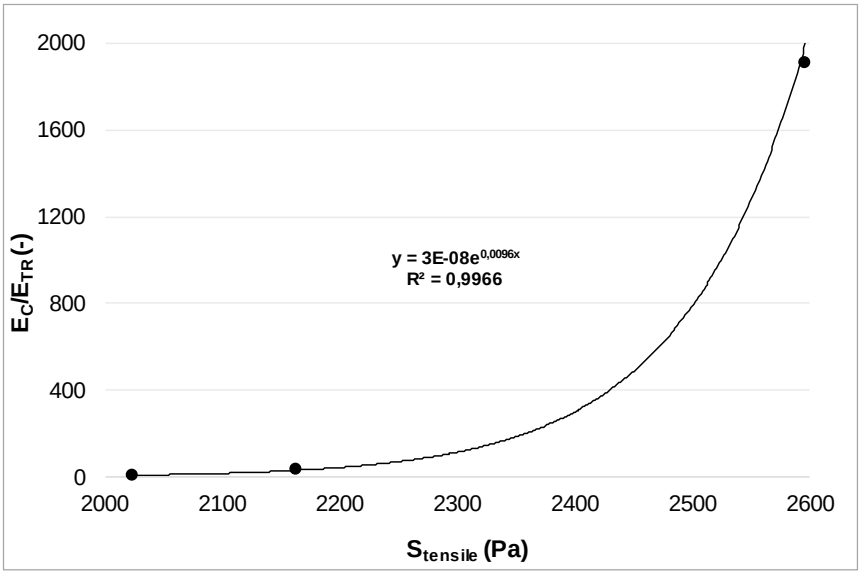

Fig. 94 – Tensile stresses as a function of the ratio between the dynamic elastic modulus of the finishing render (E_C) and the thermal render/EPS (E_{TR}).

Fig. 95 presents the distribution of the tensile stresses in the thermal render layer, after heating in S1 and ETICS. As it can be seen, the thermal render presents a more homogeneous distribution than EPS, which means less stresses difference between the adjacent elements.

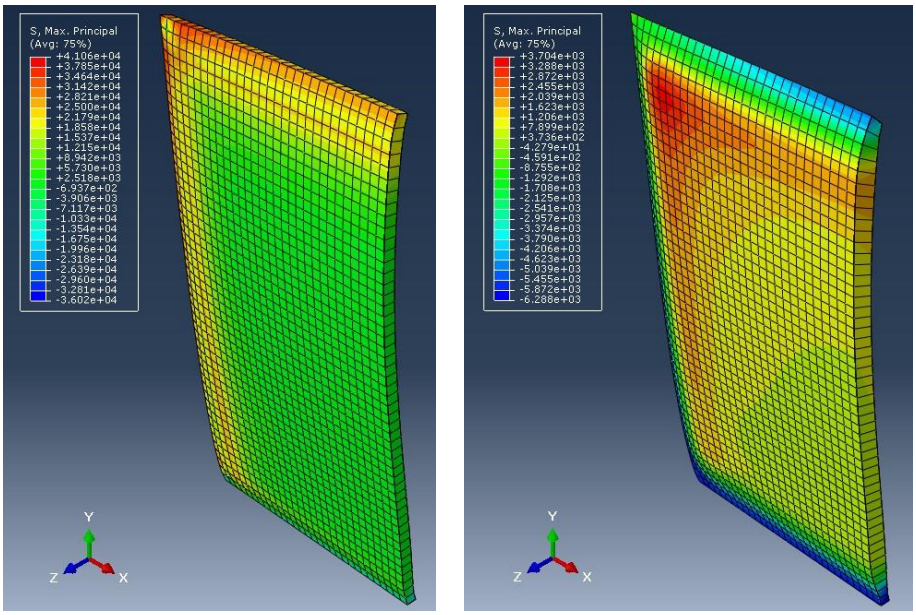

a) b)

Fig. 95 – Distribution of the tensile stresses after heating (70 ºC) in: (a) Thermal render TR1; (b) EPS.

In addition, a good compromise between the different layers of the façade systems, regarding the rigidity and strength, should be taken into account. As such, Fig. 96 and Fig. 97 present the strains profile regarding S1, S2 and ETICS after heating and cooling periods, respectively.

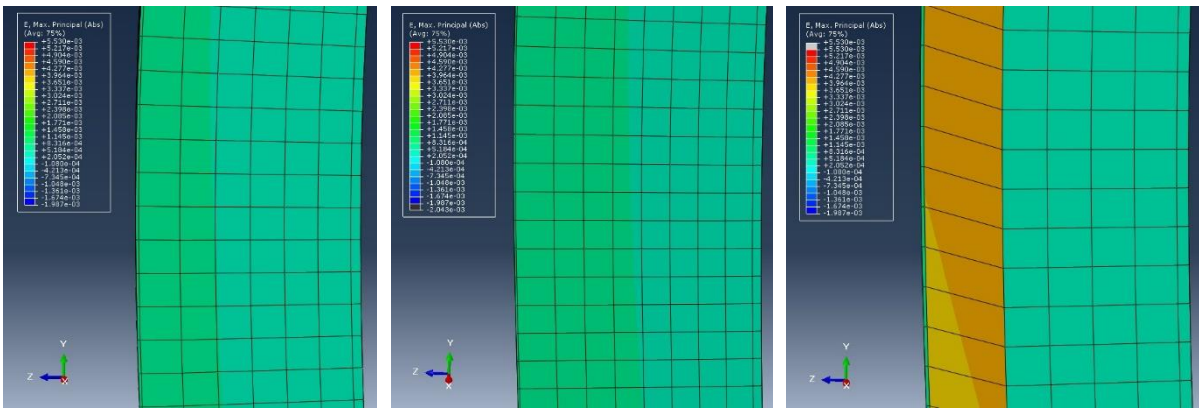

a) b) c)

Fig. 96 – Strains profile after heating (70 ºC) in: a) S1; b) S2 and c) ETICS.

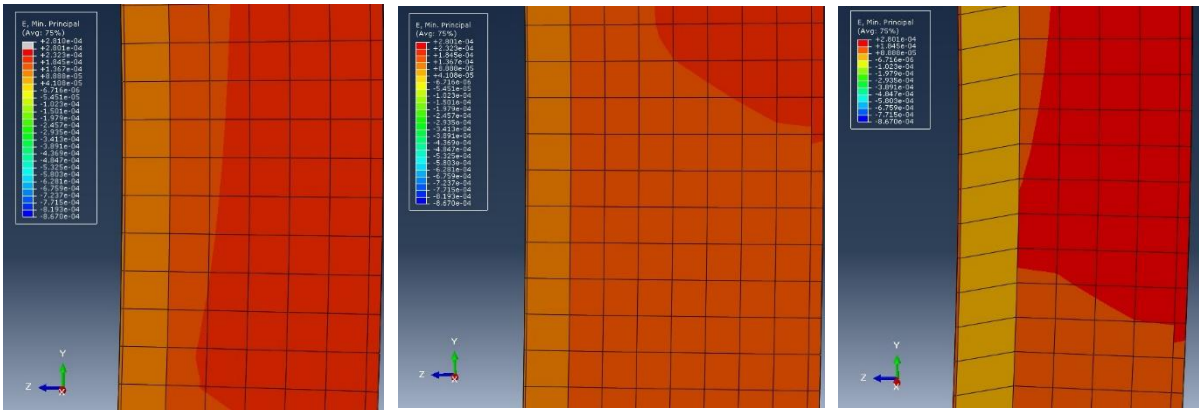

a) b) c)

Fig. 97 – Strains profile after the abrupt decrease of temperature (15 ºC) in: a) S1; b) S2 and c) ETICS.

As demonstrated, the ETICS presented higher variation between the different layers. This is especially verified after the heating period, where the insulation layer has greater values than the adjacent layers. In contrast, the thermal renders present similar strains between the adjacent layers to the thermal render, which provides greater compatibility and consequently less cracking and detachment between the layers.

4.3.5. INFLUENCE OF THE TYPE OF SUBSTRATE

The present sub-chapter presents a brief comparison between different substrates, using aerated concrete blocks, current brick masonry and OSB, with current thicknesses. This allows analysing the effect of using a current support configuration (heavy construction) or using a lightweight substrate, analysing the effect of distinct rigidities. As such, that influence will be analysed using only the thermal rendering system S1.

The typical deformed shape and principal stresses after heating and after the abrupt decrease are shown in Fig. 98 and Fig. 99.

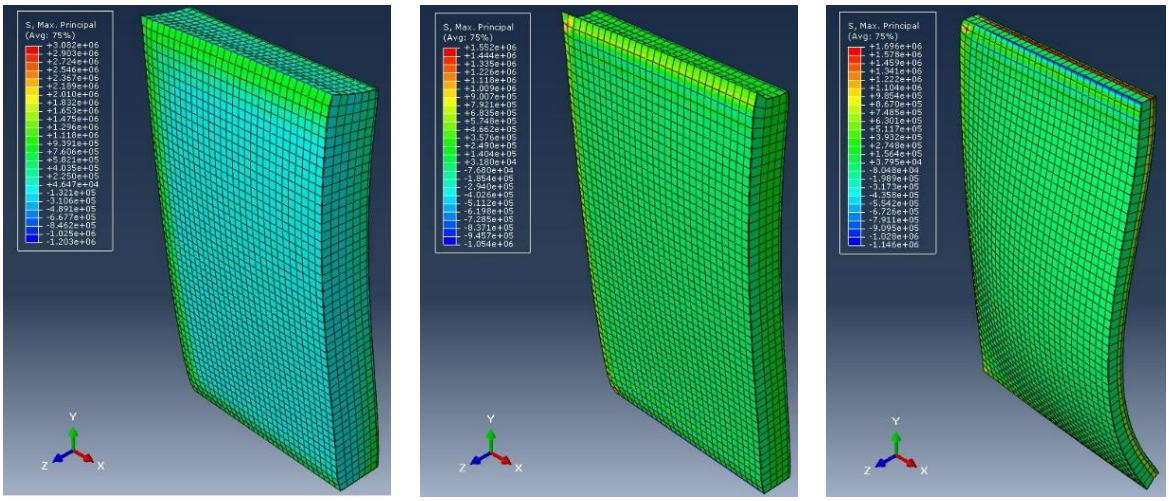

a) b) c)

Fig. 98 – Typical deformed shape after heating, using: a) Aerated concrete; b) Brick masonry; c) OSB.

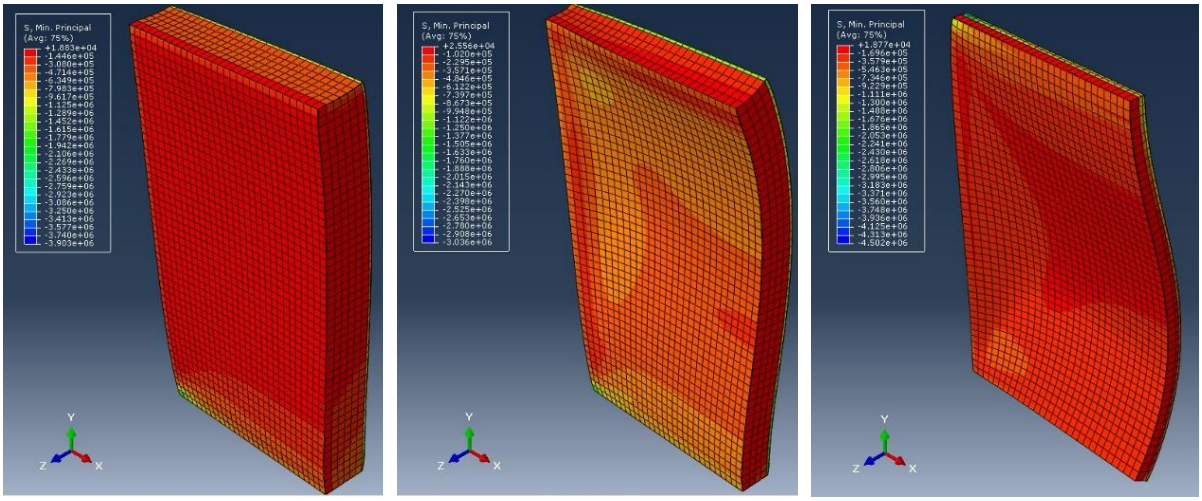

a) b) c)

Fig. 99 – Typical deformed shape after the abrupt decrease, using: a) Aerated concrete; b) Brick masonry; c) OSB.

It can be seen the higher curvature of walls using thinner substrates, especially the OSB, in both expansion and contraction periods. This fact induces higher deformation and the high rigidity of the OSB promotes the increase of stresses, as shown in the following results.

Table 79 and Table 80 present the maximum stresses and displacements, respectively, after heating (70 ºC) and after the abrupt decrease (15 ºC), considering the three different substrates in the thermal render surfaces (exterior and interior), in a central node of the wall.

Table 79 – Tensile and compressive stresses obtained in the thermal render layer surfaces, with different substrates.

Substrate	Tensile stress (ext/int) (Pa)	Compressive stress (ext/int) (Pa)
	T=70 ºC	T=15 ºC
Aerated concrete	2554.7/1363.9	-1332.6/-380.4
Brick masonry	788.2/335.2	-353087.0/-8832.0
OSB	4677.4/849.1	-58432.7/-2021.9

Table 80 – Displacements obtained in the thermal render layer surfaces, with different substrates.

Substrate	Displacements (ext/int) (m)	
	T=70 ºC	T=15 ºC
Aerated concrete	$8.13/7.90 \times 10^{-4}$	$3.68/3.70 \times 10^{-4}$
Brick masonry	$3.46/3.54 \times 10^{-4}$	$3.74/3.57 \times 10^{-4}$
OSB	$9.46/9.25 \times 10^{-4}$	$5.36/5.35 \times 10^{-4}$

The type of substrates showed to have a significant impact on the thermal shock effect in exterior thermal rendering systems.

The low thickness of the OSB and the high rigidity of the panel results in greater displacements in the thermal render layer, in both high and low temperatures (thermal shock). Regarding the tensile stresses, the higher the rigidity of the substrate, the higher the stresses in the thermal render, as shown in Fig. 100.

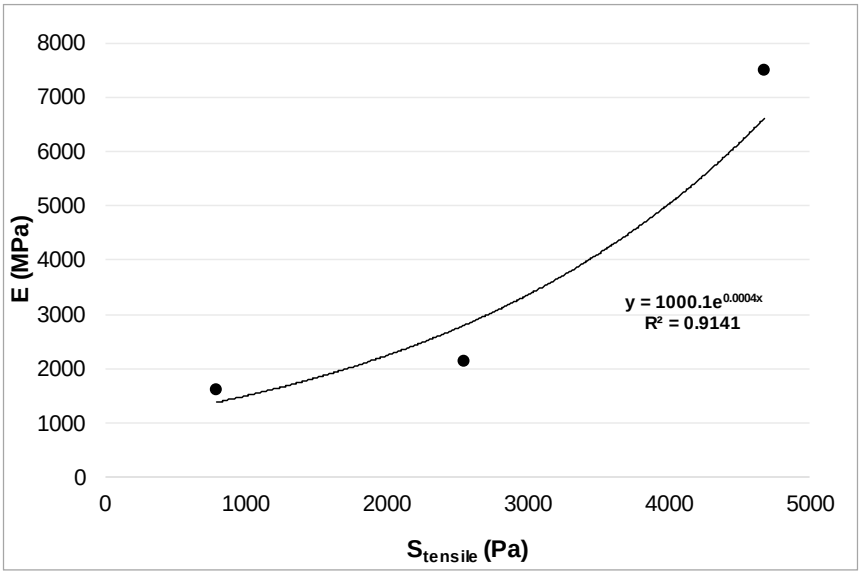

Fig. 100 – Tensile stresses in the TR as a function of the elastic modulus of the substrate.

The aerated concrete and the OSB substrates promote higher displacements, regarding the expansion period, which is in accordance with the higher thermal expansion coefficients, comparing to the brick masonry. In addition, the aerated concrete and OSB substrates promote higher stresses in the inner

surface of the thermal render, as shown in Fig. 101, especially using the aerated concrete, which has the highest thermal expansion coefficient.

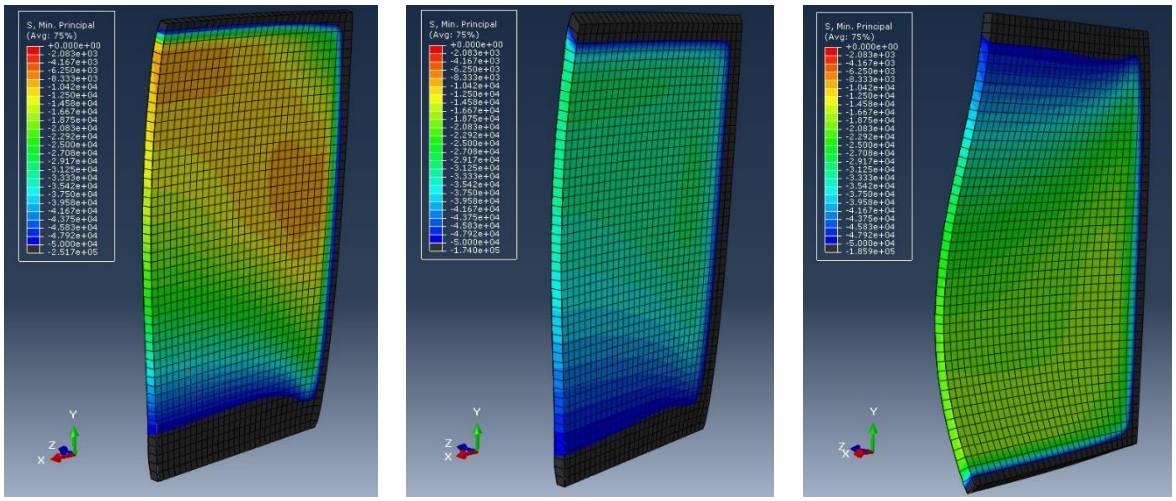

a) b) c)

Fig. 101 – Stresses distribution in the inner surface of the thermal render after heating, using: a) Aerated concrete; b) Brick masonry; c) OSB.

However, analysing the profile of the strains distribution, the aerated concrete substrate resulted in a more homogeneous distribution than brick masonry and OSB, which allows better compatibility between the different layers, as shown in Fig. 102.

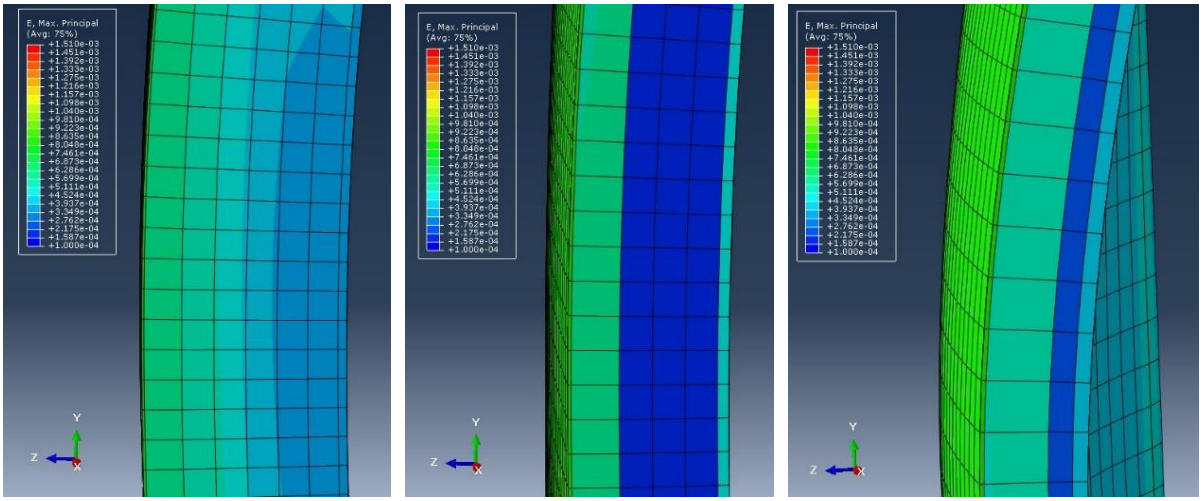

a) b) c)

Fig. 102 – Strains profile after heating, using: a) Aerated concrete; b) Brick masonry; c) OSB.

Observing the contraction period, the displacements are lower and similar using the heavier substrates, which was expected due to the low thickness of the OSB substrate. Regarding the strains profile in Fig. 103, the walls using concrete masonry and OSB resulted in greater strains in the thermal render layer.

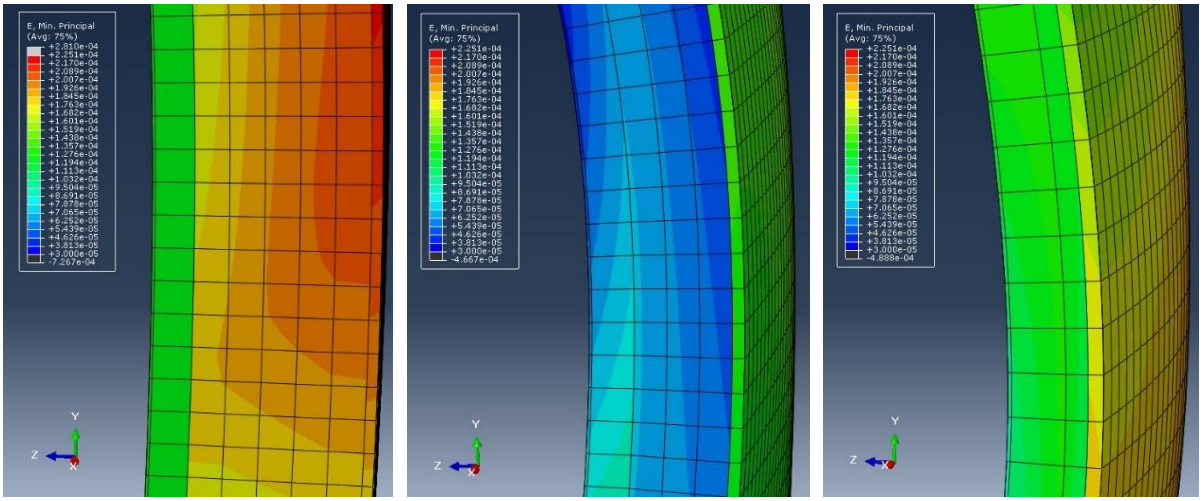

a) b) c)

Fig. 103 – Strains profile after the abrupt decrease, using: a) Aerated concrete; b) Brick masonry; c) OSB.

4.3.6. SUMMARY

The mechanical properties of each layer that constitutes the façade produce quite different stresses and strains. In addition, the contour constraints could induce misleading observations. As such, the results were analysed taking into account a central node of the façade.

The three different analyses allow evaluating the impact of the thermo-mechanical properties of the different layers that constitute the thermal rendering system regarding different thermal loads.

As expected, the increase and decrease of temperature promoted expansion and contraction of the different materials, resulting in tensile and compressive stresses, respectively, in the system. This fact highlights the importance of adjusting the façade systems to each climate since the thermal stresses are highly dependent on the thermal loads. As such, the application of coatings with completely different solar absorption presented a great impact. A tendency was observed from the higher to the lower latitudes, where the solar radiation presents greater influence: higher solar absorption of the façade coating lead to higher tensile stresses. On the other hand, for the higher latitudes, when the façade is submitted to a decrease of temperature, the compressive stresses were dominant. As such, the thermal render was subjected to higher compressive stresses than in warmer climates and a consequent crush of porous structure. Regarding the different thermal rendering systems, applied as exterior insulation, when similar temperature variation is applied, the effect of the thermal conductivity can be observed: lower thermal conductivity values led to a lower variation of the stresses when submitted to higher temperatures. In addition, the low thermal effusivity of thermal renders and EPS and consequently low heat storage supports the obtained lower stresses. The physical properties influence the stress distribution, namely higher porosity and lower density lead to higher compressive stresses. In general, S3 presented lower compressive stresses than the systems applied as exterior insulation, which was expectable. The displacements are similar in both C-TR and TR-substrate interface, excepting in ETICS, reflecting the higher dimensional variation of EPS, due to the higher thermal expansion coefficient.

Regarding the thermal shock effect, the change in the stress state may lead to cracks in the coating, allowing the climate agents to activate other failure mechanisms in the thermal render. The higher elastic modulus of C1, comparing to C2, contributed to increase the stresses, since the dimensional variation was restricted, resulting in lower displacements. Despite the same exterior coating of S1 and ETICS, the tensile stress obtained in the ETICS was higher, due to the much higher thermal expansion coefficient

of EPS than TR1. A quite significant impact of the different rigidities of the thermal rendering system materials was observed: the higher the difference of rigidity between the two layers the higher the stresses, highlighting the importance of compatibility between adjacent layers in terms of rigidity. The application of more rigid coatings contributed to increase the tensile stresses, as performed in S3. In addition, the interior application compromised the thermal inertia of the façade, which is a crucial aspect especially in the summer season (where the expansion occurs more often due to the increase in temperature).

The type of substrate showed to have a significant impact on the thermal shock effect in exterior thermal rendering systems. The low thickness and the high rigidity of the OSB result in higher stresses and displacements in the thermal render layer. As such, less rigid substrates promoted lower tensile stresses in the thermal renders. The aerated concrete and the OSB substrates promote higher displacements, regarding the expansion period, which is in accordance with the higher thermal expansion coefficients, comparing to the brick masonry. Observing the contraction period, the displacements are lower and similar using the heavier substrates, which was expected due to the low thickness of the OSB substrate.

Moreover, a good compromise between the different layers of the façade systems, regarding the rigidity and mechanical strength, should be taken into account. This fact could compromise the durability since the cracking promotes a faster failure of the entire system.

In short, the thermal induced stresses presented a significant impact on the durability of the studied thermal enhanced systems. The different temperature variation resulting from the application in different climates, the specific characteristics of the coatings (such as the colour and the rigidity), the intrinsic properties of the insulation layer (such as the thermal conductivity, thermal expansion coefficient and rigidity) and the type of substrate presented great impact in the thermo-mechanical performance of thermal systems. All these aspects should be taken into account in the development of a durability assessment methodology, applicable to thermal rendering systems, since it may compromise their integrity over time.

5. DURABILITY ASSESSMENT OF THERMAL RENDERING AND PLASTERING SYSTEMS

5.1. FRAMEWORK

Regarding the uneven and high variability of the results, as well as the constraints, obtained with standardized methodologies, the need of a suitable methodology to assess the durability of thermal rendering systems is of great interest, since these materials continue to awaken the interest of the researchers (Borges, Flores-Colen and de Brito 2018; Soares et al. 2018; Westgate, Paine and Ball 2018; Nosrati and Berardi 2018) and the manufacturers (Saint-Gobain Weber 2016; Secil Argamassas 2017; Fassa Bortolo 2017).

The identification of relevant standards for the evaluation of the durability of thermal render systems is one of the most important steps to define the intended assessment. As such, Fig. 104 presents the framework of the durability assessment standards, applicable to renders and multilayer systems with enhanced thermal properties. It highlights one of the motivations of the present thesis, which is the absence of durability assessment methodologies applicable to thermal rendering systems. These systems should be analysed as a whole, since each layer has a significant effect in the system performance, as demonstrated by the numerical simulations presented in Chapter 4. Consequently, the existing procedures, such as the ones provided by EN 1015-21 and ETAG 004 do not allow a feasible durability assessment of thermal rendering and plastering systems.

However, being the referred methodologies applicable to renders and thermal multilayer systems (ETICS), they may be adapted to thermal rendering and plastering systems, since they present some similar characteristics. This adaptation could give reliable data and inputs to the development of durability assessment methodologies directly applicable to thermal rendering and plastering systems.

Being the main goal of the current work the development and implementation of durability assessment methodologies applicable to thermal rendering and plastering systems, a methodological process for the durability assessment was developed, as explained in Fig. 105.

The methodology combines several stages, being the first one the evaluation and adaptation of the referred existing methodologies, presented in 5.2.2 and 5.2.3. The analysis of existing ageing procedures combined with hygrothermal simulation and existing data will result in the development of a new hygrothermal accelerated ageing cycle (presented in 5.3), which will be further implemented to exemplary thermal rendering systems (presented in 5.4). The development of the hygrothermal cycle will focus the South European climate context, using a representative Portuguese climate of the most severe conditions, in terms of temperature fluctuation.

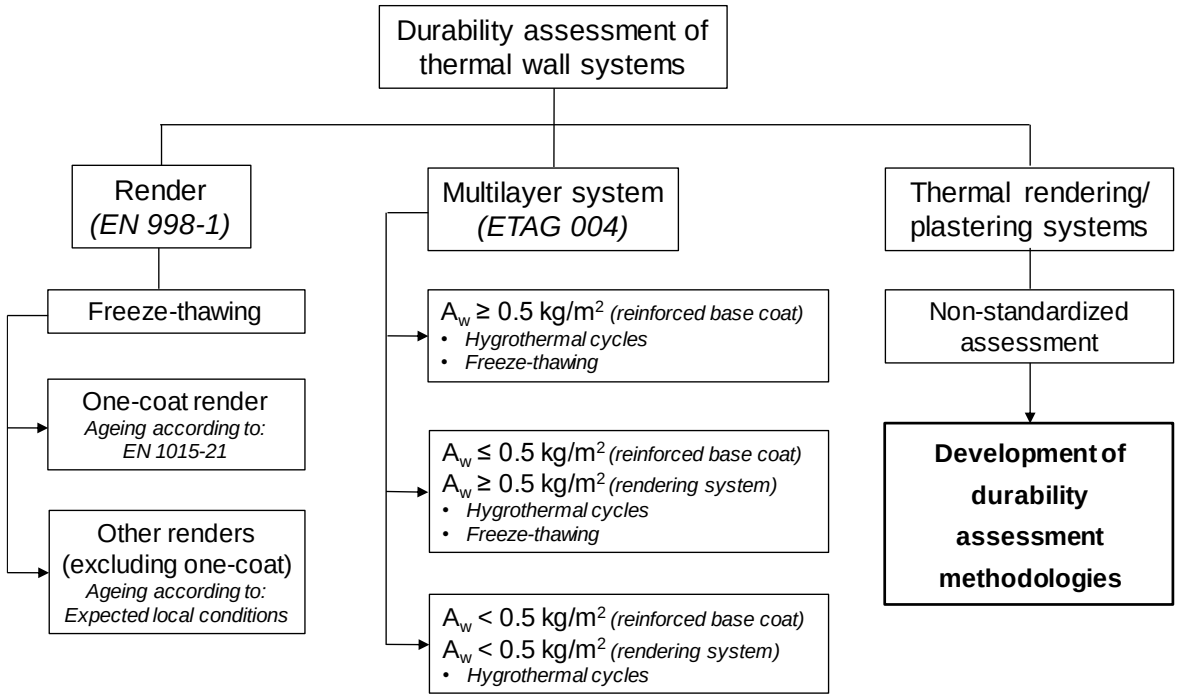

Fig. 104 – Framework of existing durability assessment methodologies, applicable to renders and thermal multilayer systems.

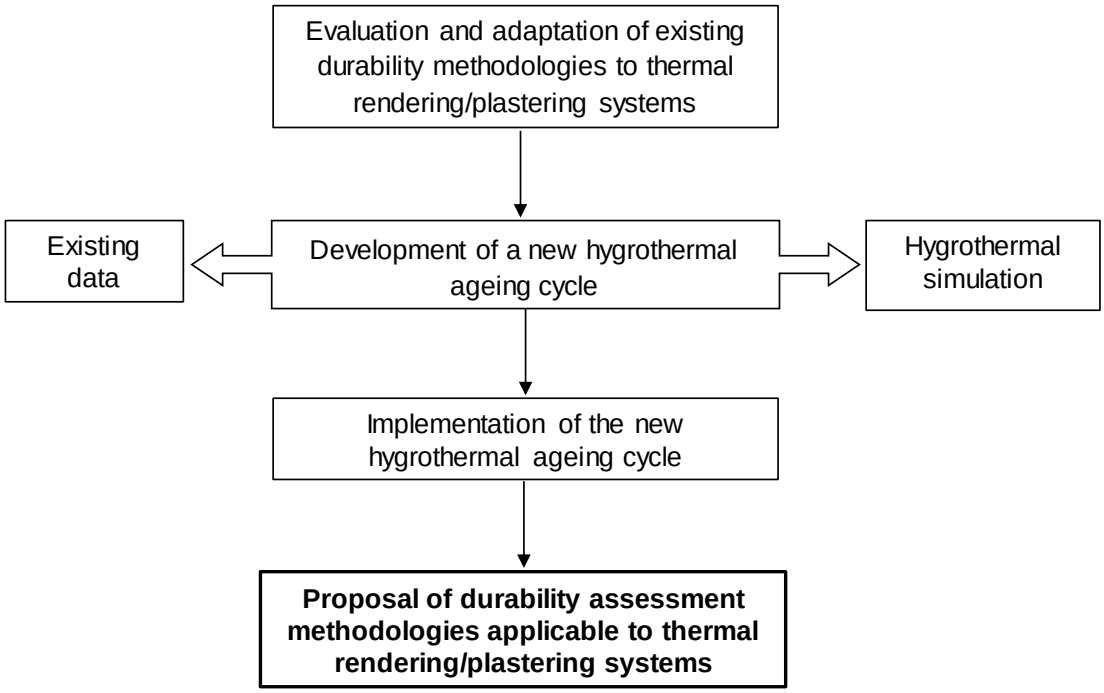

Fig. 105 – Methodological process for the durability assessment of thermal rendering/plastering systems.

Fig. 106 presents the adopted experimental methodology to evaluate the durability assessment of thermal rendering and plastering systems. The first step consists in assessing the thermal renders/plaster themselves and the thermal rendering/plastering systems according to the adaptation of existing

methodologies, such as the envisaged in EN 1015-21 and ETAG 004, using small-scale specimens. The EN 1015-21 methodology includes heating-freezing and humidification-freezing ageing cycles and the ETAG 004 freeze-thawing cycles. The evaluation of the existing procedures will allow understanding the gaps, disadvantages and advantages of implementing such methodologies to thermal rendering and plastering systems. Those findings and adaptation will help on the definition of the whole methodology.

The second step consists in the implementation of a new accelerated ageing hygrothermal cycle adapted to thermal rendering systems, through hygrothermal simulation and the previous knowledge of the existing methodologies.

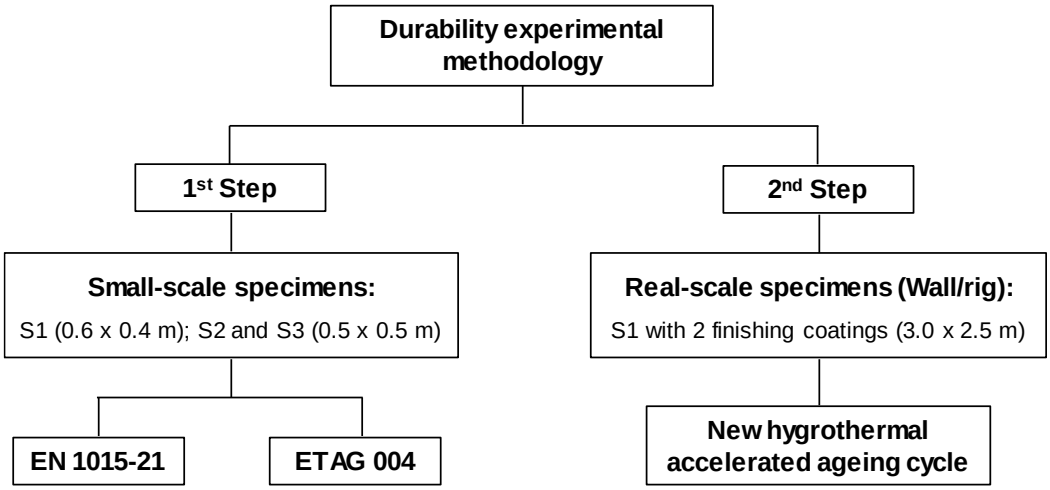

Fig. 106 – Durability experimental methodology.

Being the location, where the system is intended to be applied, one of the main aspects to take into consideration in the durability assessment, the wide range of existing climates should be considered. Regarding the durability assessment in the European context, the application of thermal rendering systems in such different climates should be taken carefully. Since different degradation mechanisms may occur in different climates, an accurate adaptation of the accelerated ageing cycles (heat-cold, heat-rain and/or freeze-thawing cycles) is of highest relevance.

One of the most used climate classifications is Köppen-Geiger. The world climates are classified according to 3 different criterions (Kottek et al. 2006):

- Main climates: equatorial (A), arid (B), warm temperate (C), snow (D) and polar (E);
- Precipitation: desert (W), steppe(S), fully humid (f), summer dry (s), winter dry (w) and monsoonal (m);
- Temperature: hot arid (h), cold arid (c), hot summer (a), warm summer (b), cool summer (c), extremely continental (d), polar frost (F) and polar tundra (T).

Recently, in Benmansour et al. (2014), this classification was re-analysed and optimised as presented in Fig. 107. European climates are generally classified as warm temperate (C) and snow (D), excepting some regions in Spain that are arid (B). Portuguese climate is classified as warm temperate, summer dry and hot/warm summer (south/north of the country).

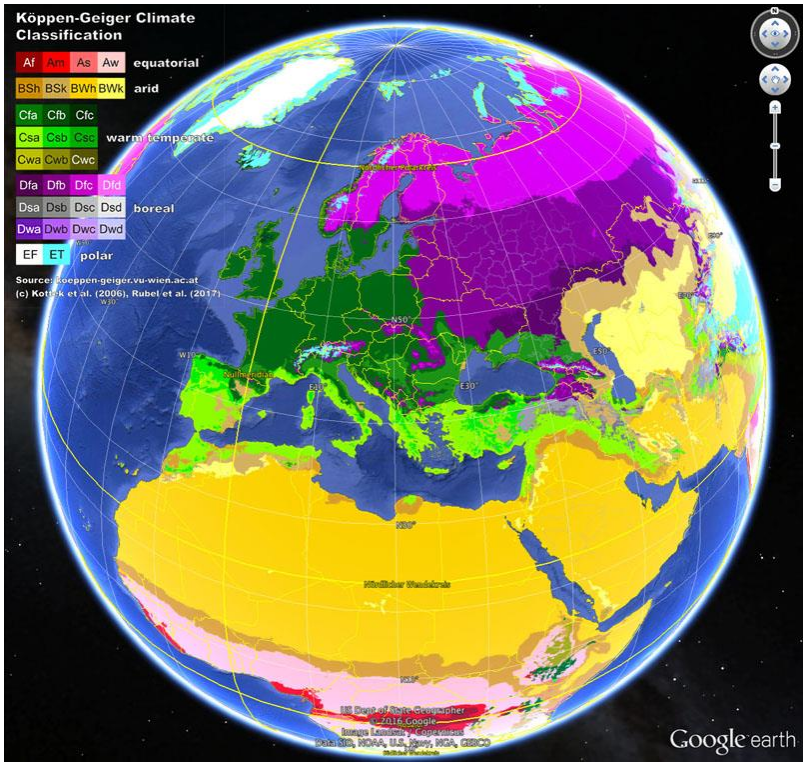

Fig. 107 – Köppen-Geiger climate classification (Benmansour et al. 2014).

The EOTA (1999) Guidance Document presents a simpler approach to classify the European climates, according to the air temperature and the solar energy intensity. The European temperature sub-division is performed according to the winter and summer conditions, resulting in three temperature zones, as shown in Table 81. Regarding the air temperature and the UV radiation, a simple division into moderate and severe climate is applied (see Table 82).

Table 81 – European climatic sub-division according to the air temperature (EOTA 1999)

Zone	Winter	Summer
	Dec/Jan/Feb	Jun/Jul/Aug
A	Cold winters: Several months: T>0ºC (rarely); $T_{daily,av.}$< 0ºC; $T_{min.}$ < -30ºC (may be).	$T_{max.}$ > 30ºC (rarely).
B	Moderate winters: Frequent frosts; 0 < $T_{daily,av.}$< 5ºC; $T_{min.}$ < -20ºC (may be).	$T_{max.}$ > 30ºC (occasionally).
C	Warm winters: Infrequent frosts; $T_{daily,av.}$ > 5ºC.	$T_{max.}$ > 30ºC (frequently); $T_{max.}$ > 40ºC (occasionally).

Table 82 – European climatic sub-division according to the air temperature and UV radiation (EOTA 1999)

Climate	Moderate	Severe
Annual radiation on horizontal surfaces	< 5 GJ/m^2 and	≥ 5 GJ/m^2 and/or
T_{av} (warmest month of the year)	< 22ºC	≥ 22ºC

Regarding the interest in developing a durability assessment applicable to thermal rendering systems, it is important to cover a wide range of climates and, consequently, different degradation mechanisms.

In that way, the temperatures of different European climates, representing a wide range of climates, were analysed, according to the EOTA Guidance Document 003 (EOTA 1999), and presented in Table 83 to Table 85. Table 83 and Table 84 present the analysis of the exterior air temperature during winter and summer, respectively. A tendency from the lower to the higher latitudes is observed, being more representative of zones C to A, respectively. As such, different agents and related degradation mechanisms may have a significant impact on façade systems, such as freeze-thawing, in higher latitude climates, and temperature fluctuations performed by heat-cold temperature variation. Analysing Table 84, severe climates, with higher solar exposition, may present a significant degradation in the façade systems due to the thermal shock in hot surfaces, due to an abrupt decrease of temperature originated by cold rain incidence.

The referred document (EOTA 1999) also classifies the internal environment into four sub-divisions, due to specific conditions to which the buildings are subjected:

- Temperature: heating, non-heating, refrigerating, localised radiation, etc.;
- Humidity: dry or wet conditions;
- Liquid water: permanently wet (e.g. bathrooms);
- Chemicals: cleaning, cooking and special conditions in laboratories, hospitals, etc..

As such, the adaptation of the ageing cycles to the climatic conditions where are intended to be applied is of major importance. That knowledge allows the development of new hygrothermal ageing cycles (presented in 5.3 and further in 5.6.2), which complement the durability assessment methodologies.

The combination of the evaluation of the existing methodologies with the new accelerated ageing cycle allows the definition of durability assessment methodologies applicable to thermal rendering systems, taking into account:

- The intrinsic properties of the materials which constitute the thermal system: relevant properties of the thermal render/plaster and finishing render/plaster;
- The application: interior or exterior;
- The intended location to be applied: climatic zones or environmental conditions;
- The main degradation mechanisms, which represent the ageing procedures to be implemented;
- The durability tests and related requirements.

Fig. 108 summarizes the different stages of the durability assessment methodology and the sequencing between them.

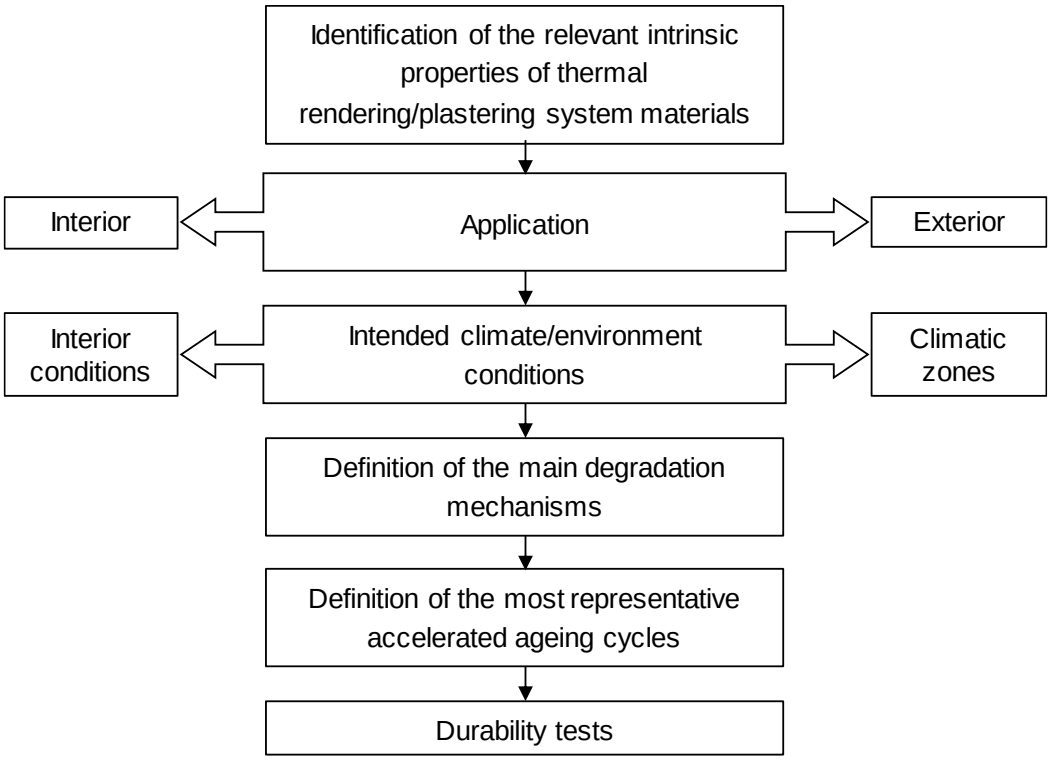

Fig. 108 – Durability assessment methodology.

Table 83 – Classification of European climates according to the air temperature, regarding the % of occurrence in winter

Zone	Winter conditions	Lisbon	Bragança	Marseille	Modena	Vienna	Nancy	Potsdam	Warsaw	Oslo	Tromsoe
—	$T_{e,av.}$	10.3 ºC	7.0 ºC	6.7 ºC	5.1 ºC	1.0 ºC	0.6 ºC	0.9 ºC	-2.0 ºC	-2.2 ºC	-3.6 ºC
A	$T_{e,av}$ (monthly) > 0ºC	100.0%	100.0%	100.0%	100.0%	100.0%	100.0%	100.0%	0.0%	33.3%	0.0%
	$T_{e,av}$ (daily) < 0ºC	0.0%	0.0%	2.2%	1.1%	36.7%	51.1%	32.2%	63.3%	65.6%	76.7%
	$T_{e,min.}$ < -30ºC	0.0%	0.0%	0.0%	0.0%	0.0%	0.0%	0.0%	0.0%	0.0%	0.0%
B	0 < $T_{e,av.}$(daily) < 5ºC	2.2%	12.0%	24.4%	45.6%	46.7%	26.7%	58.9%	31.1%	32.2%	23.3%
	$T_{e,min.}$ < -20ºC	0.0%	0.0%	0.0%	0.0%	0.0%	0.0%	0.0%	0.0%	0.0%	0.0%
C	$T_{e,av}$ (daily) > 5ºC	97.8%	88.0%	73.3%	53.3%	16.7%	21.1%	8.9%	5.6%	2.2%	0.0%

Table 84 – Classification of European climates according to the air temperature, regarding the % of occurrence in summer.

Zone	Winter conditions	Lisbon	Bragança	Marseille	Modena	Vienna	Nancy	Potsdam	Warsaw	Oslo	Tromsoe
—	$T_{e,av.}$	20.5 ºC	22.5 ºC	23.8 ºC	25.0 ºC	19.6 ºC	17.8 ºC	17.2 ºC	17.2 ºC	16.1 ºC	10.8 ºC
A	$T_{e,max}$ (monthly) > 30ºC (rarely)	1.4%	3.7%	1.7%	2.9%	0.3%	0.2%	0.0%	0.0%	0.0%	0.0%
B	$T_{e,max}$ (monthly) > 30ºC (occasionally)	1.4%	3.7%	1.7%	2.9%	0.3%	0.2%	0.0%	0.0%	0.0%	0.0%
C	$T_{e,max}$ (monthly) > 30ºC (frequently)	1.4%	3.7%	1.7%	2.9%	0.3%	0.2%	0.0%	0.0%	0.0%	0.0%
	$T_{e,max}$ (monthly) > 40ºC (occasionally)	0.0%	0.0%	0.0%	0.0%	0.0%	0.0%	0.0%	0.0%	0.0%	0.0%

Table 85 – Classification of European climates according to the average temperature of the warmest month of the year.

	Lisbon	Bragança	Marseille	Modena	Vienna	Nancy	Potsdam	Warsaw	Oslo	Tromsoe
T_{av}	22.0 ºC	23.6 ºC	25.0 ºC	25.9 ºC	20.4 ºC	18.1 ºC	17.9 ºC	17.9 ºC	18.9 ºC	11.0 ºC
Climate	Severe	Severe	Severe	Severe	*	*	*	*	*	*

*Requires the UV radiation calculation

5.2. EVALUATION OF EXISTING METHODOLOGIES OF DURABILITY ASSESSMENT

The first part of the durability assessment consists of the evaluation of existing methodologies, applicable to small-scale samples. These preliminary results will help on the definition of a durability assessment methodology applicable to thermal rendering and plastering systems.

Considering the systems under study, S1 (lime-based thermal render with EPS addition) and S2 (thermal render with mixed binders and EPS addition) will be analysed taking into account a worst-case situation – exterior application – and S3 (gypsum-based thermal plaster with cork addition) without humidification, owing its composition (gypsum-based material).

5.2.1. MATERIALS AND EXPERIMENTAL METHODOLOGY

To analyse the durability of the thermal render itself, the methodology defined in EN 1015-21 will be adapted to each thermal render under study. Two specimens with 2 cm thickness of thermal render and a ceramic brick masonry substrate were prepared. TR1 test specimen has 40x60 cm^2 and TR2 50x50 cm^2 of area, complying with the minimum required face side of 40 cm x 40 cm. Fig. 109 presents the referred test specimens.

a) b)

Fig. 109 – Test specimens for durability tests according to the adapted methodology from EN 1015-21: a) TR1; b) TR2.

To analyse the system as a whole the methodologies defined in EN 1015-21 and in ETAG 004 will be adapted to each thermal render under study. Each system will be tested considering a typical constitution, according to the manufacturers' conditions. Hence, the constitution of the 3 studied systems is presented Fig. 110, Fig. 111 and Fig. 112 and in Table 86 All specimens were applied on ceramic brick masonry. S1 test specimen has an area of 40x60 cm^2 and S2 and S3 50x50 cm^2.

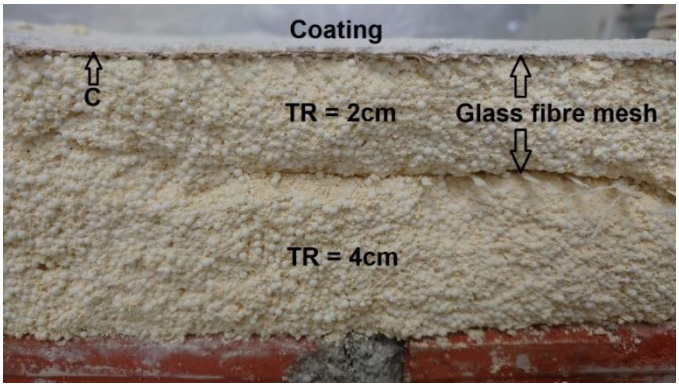

Fig. 110 – Constitution of the thermal rendering system S1 for the durability tests.

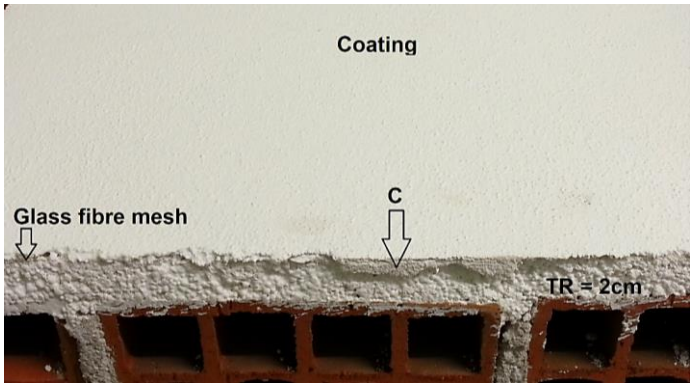

Fig. 111 – Constitution of the thermal rendering system S2 for the durability tests.

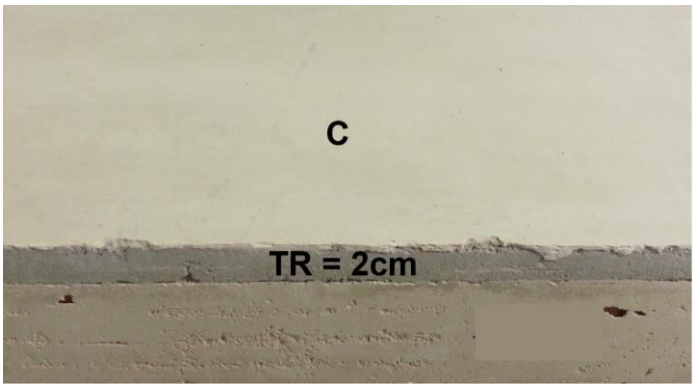

Fig. 112 – Constitution of the thermal plastering system S3 for the durability tests.

Table 86 – Constitution of the thermal rendering and plastering systems for the durability tests.

System	Render/plaster/Coating	Layer properties
S1	TR1	4+2 cm (glass fibre mesh between the layers)
	C1	≈ 4 mm (glass fibre mesh in the render)
	Organic coating (S1-O)	≈ 2 mm
	Mineral coating (S1-M)	≈ 2 mm
S2	TR2	2 cm
	C2	≈ 3 mm (glass fibre mesh in the render)
	Coating	≈ 1 mm
S3	TR3	2 cm
	C3	≈ 2 mm

The constitutions of the selected thermal rendering systems were previously described in 3.1.2. Thermal rendering system S1 will be tested with two different finishing coatings: an organic coating (S1-O), already applied in the previous tests, and another mineral coating (S1-M) consisting of lime, hydraulic binder, mineral fillers, pigments, and specific additives. Observing Fig. 113, the organic coating presents higher roughness than the mineral coating.

a) b)

Fig. 113 – Finishing coatings of thermal render system S1: a) Organic (S1-O); b) Mineral (S1-M).

Thermal renders were tested by adapting the methodology defined in EN 1015-21 (heating-freezing + humidification-freezing), as described in Table 21, in sub-chapter 2.5.3. In that way, TR1 and TR2 were tested by performing the two ageing sequences. Regarding thermal rendering systems, the same procedure is adopted, being S3 evaluated to heating-freezing ageing. S1 and S2 were also evaluated according to the ageing procedures defined in ETAG 004 (freeze-thaw), described in Table 23, applicable to small-scale samples, also presented in sub-chapter 2.5.3.

The heating procedure was performed by using the Solamagic Infra-Red (IR) lamp device (2000 W) (see Fig. 114), while the freezing procedure required the use of a deep freeze cabinet such as the model SMEG EL5=SCO (see Fig. 115). Regarding the humidification/thawing step, a large waterproof container, which kept the rendered surface below a minimum 15 mm water depth, was used (see Fig. 116).

Fig. 114 – Solamagic Infra-Red (IR) lamp device.

Fig. 115 – Deep freeze cabinet SMEG EL5=SCO 50.

a) b)

Fig. 116 – Large waterproof container: a) Side view; b) Interior view.

To analyse the ageing effect, before and after the ageing procedures, liquid water permeability, adhesive strength, impact resistance and microstructure were evaluated. Considering the analysis of the durability of the thermal renders, the impact resistance was not studied, since the behaviour to the impact should be evaluated regarding the whole system. Also, the liquid water permeability was not measured in TR's, since these materials are applied as an internal layer and non-directly exposed to liquid water. In addition, the high porosity and capillary absorption of the thermal renders (comparing to a current render) do not allow to implement these water permeability test procedures, since presents a great amount of water diffusion by the surface (as it can be seen in Fig. 117), distorting the results.

Fig. 117 – Inconclusive thermal render water permeability test.

The adhesive strength and impact resistance tests were performed according to the procedures described in 3.1.4.3 and 3.1.4.4, respectively. The microstructure was observed using the optical microscope Olympus SZH10 shown in Fig. 20.

The liquid water permeability was determined through two distinct methodologies.

One of the methods is based on the water permeability test described in EN 1015-21 (CEN 2002a), which measures the liquid water required to keep a permanent head of 100 mm of water above the rendered surface, using a cone with 100 mm diameter. The cone is bonded to the surface using a water-resistant sealant. The experimental layout is presented in Fig. 118-a). The amount of water necessary to keep the water level constant (100 mm) over 48 h is registered.

The other method is performed using Karsten tubes (LNEC 2002). One of the advantages of this method is its ability to measure horizontal and vertical surfaces. In that way, to future comparison with large-scale tests in walls, this method is performed placing the specimens vertically. The Karsten tube has volume graduation, where 10 ml correspond to 10 cm head of water. After bonding 3 tubes to the rendered surface, each tube is filled with water until 10 mm (0 ml scaling) and the drop in the water level is recorded at regular intervals (see Fig. 118-b)). This allows the exact recording of the amount of water that has penetrated under a pressure of 10 cm height of water per unit of time.

a) b)

Fig. 118 – Water permeability test using the: a) Adapted methodology from EN 1015-21; b) Karsten tubes method.

5.2.2. EXPERIMENTAL RESULTS – ADAPTED METHODOLOGY FROM EN 1015-21

5.2.2.1. Liquid water permeability

The liquid water permeability was measured according to two different methodologies. Table 87 presents the volume of water that penetrates in the systems (V_t), for each presented methodology, at two different time periods. In Fig. 119, the amount of water absorbed along the test period is presented.

Table 87 – Volume of water penetration before (BA) and after (AA) heating-freezing and humidification-freezing ageing cycles.

Experimental method		Cone		Karsten tubes	
V_t (ml/m^2)		24 h	48h	1h	2h
S1-O	BA	44.6	89.1	99.0	141.5
	AA	191.0	216.5	292.4	386.7
S1-M	BA	802.1	1228.7	188.6	334.8
	AA	1082.3	1171.4	980.9	1626.9
S2	BA	445.6	687.5	202.8	292.4
	AA	420.2	573.0	269.0	367.8
S3*	BA	636.6	3934.3	6224.7	—
	AA	2323.7	7754.0	26714.5	—

*Due to the fast water absorption, S3 measurements with the cone method were made after 1h and 5h, rather than 24h and 48h, respectively.

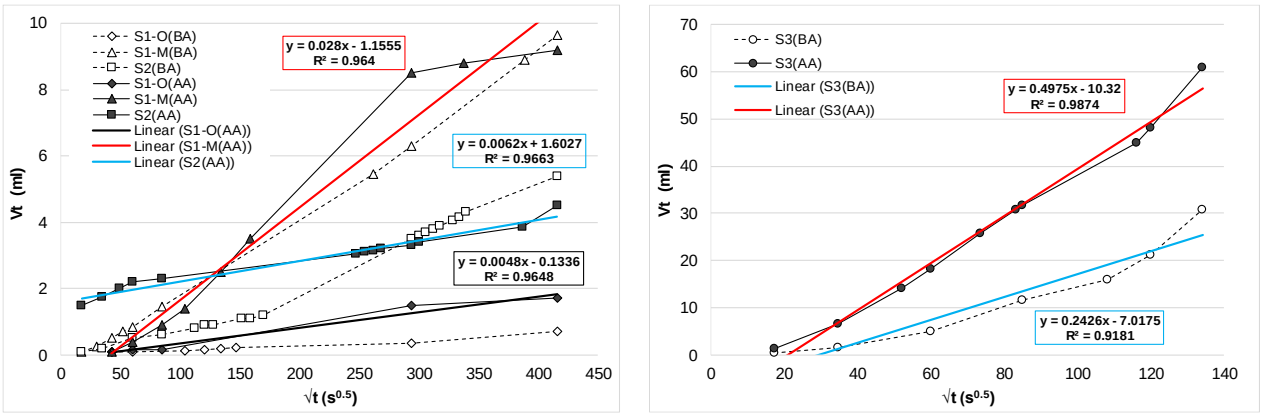

a) b)

Fig. 119 – Water permeability test results using the cone method: a) S1 and S2, after heating-freezing and humidification-freezing ageing cycles; b) S3, after heating-freezing ageing cycles.

Regarding the obtained results, the amount of water that penetrates into the specimen increases after ageing procedures. Nevertheless, S2 presents a slight decrease of the water volume with the cone method, after 1 day, and S1-M only after 42 hours, after ageing, contrasting with the S1-O, which presents higher absorption after ageing, during all the test procedure.

Another clear finding is the differences between the organic and the mineral coating, as the last one presents a much higher water absorption. This fact is in accordance with the characteristics of the

referred coatings, namely the liquid water permeability and the capillary water absorption. Regarding the data provided by the manufacturer, the organic coating is less permeable than the mineral coating, since it is classified as W3 ($\leq$ 0.1 kg/m^2.h$^{0.5}$), according to EN 15824 (CEN 2017), while the mineral coating has a W2 classification (< 0.2 kg/m^2.min$^{0.5}$), according to EN 998-1 (CEN 2010).

In addition and as expected, S3 present a much higher water absorption volume than S1 and S2, presenting a bigger variation after heating-freezing ageing cycles (265% and 97% variation with the cone method after 24h and 48h, respectively). The larger water stain dispersion after 1h of testing for the aged sample is visible in Fig. 120, highlighting the weakening of the system.

a) b)

Fig. 120 – Water distribution in S3, after 1h: a) Before ageing; b) After heating-freezing ageing cycles.

The effect of water in gypsum-based materials can be also observed in Fig. 121. The water action promotes cracking and loss of the finishing plaster material (C3), being visible the thermal render layer (grey colour). This is due to the intrinsic properties of gypsum, which has high capillary absorption and dissolves in water (Klimchouk 2000; Hong et al. 2018).

a) b)

Fig. 121 – Gypsum coating (C3) degradation: a) Detachment and loss of material; b) Cracking and dissolution.

Fig. 122 presents the results of the water permeability tests using the Karsten tubes method.

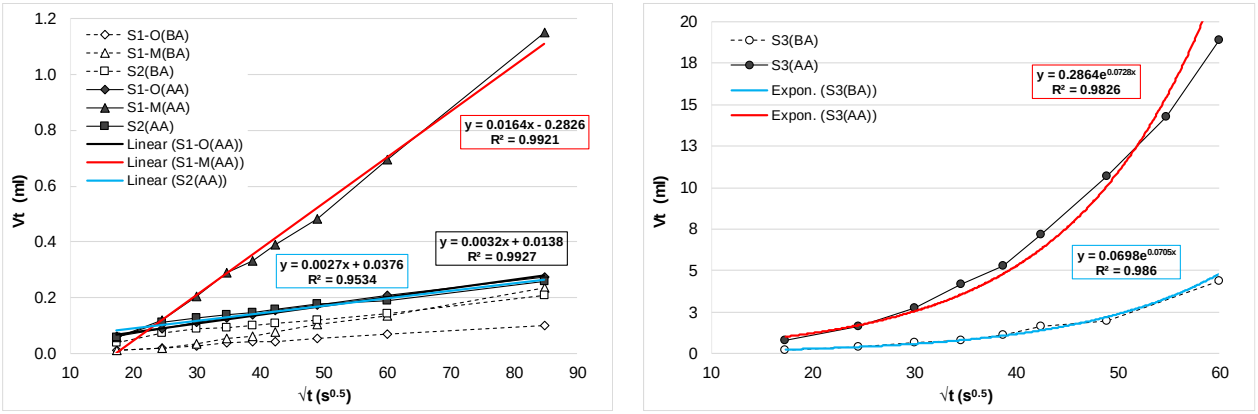

Fig. 122 – Water permeability test results using the Karsten tubes method: a) S1 and S2, after heating-freezing and humidification-freezing ageing cycles; b) S3, after heating-freezing ageing cycles.

Regarding the S1 and S2 thermal rendering systems, a distinct behaviour after ageing is observed: S1-M presents a faster increase of the water absorption than the rest of the specimens, which show a constant increase (similar slope). A linear trend with high correlation ($R^2 > 0.95$) is observed. Regarding S3, a large variation between the non-aged and aged results (329% variation after 1h) is obtained. A strong correlation ($R^2 \approx 0.98$ – exponential trend) is also observed. This finding is not observed using the cone method, which shows irregular trends and, consequently, lower correlation. This could be related to the higher complexity of the cone test method, which introduces higher variability in the obtained results, comparing to the Karsten tubes method. Apparently, the cone method is more suitable to determine the permeability of low absorption materials that combined with the higher pressure than the Karsten tubes, make this test procedure inadequate to thermal rendering systems.

5.2.2.2. Adhesive strength

The adhesive strength to the substrate and the fracture patterns, after ageing, in the thermal renders TR1 and TR2 are presented in Table 88 and Table 89, respectively. In Fig. 123, a comparison between all the specimens of TR1 and TR2 before and after ageing is presented.

Table 88 – Adhesive strength and fracture patterns obtained in TR1, after heating-freezing and humidification-freezing ageing cycles.

Property	Adhesive strength	Fracture pattern	
Measurement	(MPa)	Description	Photograph
1	0.052	30% adhesion/ 70% cohesion	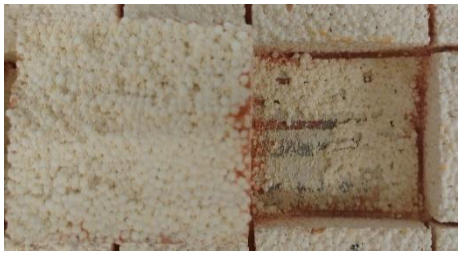
2	0.040	25% adhesion/ 75% cohesion	
3	0.048	100% cohesion	
4	0.072		
5	0.064	10% adhesion/ 90% cohesion	
Average	0.055	13% adhesion (TR-substrate interface) 87% cohesion in the TR itself	
St. Deviation	0.013		

Table 89 – Adhesive strength and fracture patterns obtained in TR2, after heating-freezing and humidification-freezing ageing cycles.

Property	Adhesive strength	Fracture pattern	
Measurement	(MPa)	Description	Photograph
1	0.084	15% adhesion/ 85% cohesion	
2	0.072	50% adhesion/ 50% cohesion	
3	0.076	30% adhesion/ 70% cohesion	
4	0.068		
5	0.100	5% adhesion/ 95% cohesion	
Average	0.080	26% adhesion (TR-substrate interface) 74% cohesion in the TR itself	
St. Deviation	0.013		

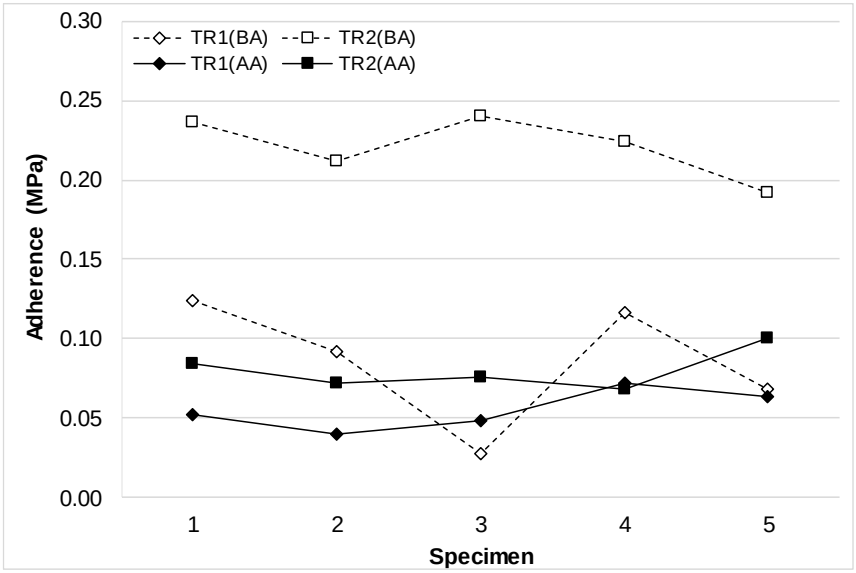

Fig. 123 – Adhesive strength of thermal renders TR1 and TR2 before (BA) and after (AA) heating-freezing and humidification-freezing ageing cycles.

As expected, the ageing produces a quite significant reduction in the adhesive strength. A decrease of 82% and 176% (average value) was observed in TR1 and TR2, respectively. The adhesion of thermal renders is lower than a common cement-based render (Skoczylas and Rucińska 2018), which is emphasized by the ageing. As such, the fracture pattern assumes a very important role, since cohesive ruptures could enhance their mechanical performance. Both thermal renders presented a higher percentage of cohesive fracture in the mortar itself than adhesive fracture between the thermal render and the substrate layers, which is a positive aspect. Regarding the ETAG 004 requirements, the thermal renders fit the adhesion parameters: despite de lower values ($\leq$ 0.08 MPa), especially in TR1, the test results are considered admissible, due to the cohesive rupture in the thermal render itself.

The adhesive strength results, obtained in the studied thermal rendering and plastering systems, are shown in Table 90 to Table 95. Since S1-O and S1-M were not analysed in chapter 3, the adhesive strength before ageing is also presented in Table 90 and Table 92. Fig. 124 and Fig. 125 present a comparison between the different thermal rendering systems, before and after the ageing procedures, considering all the individual values of the specimens and the average adhesive strength, respectively.

Table 90 – Adhesive strength and fracture patterns obtained in S1-O, before ageing.

Property	Adhesive strength	Fracture pattern	
Measurement	(MPa)	Description	Photograph
1	0.064		
2	0.084		
3	0.064	100% adhesion	
4	0.088		
5	0.088		
Average	0.078	100% adhesion (between the TR layers/mesh interface)	
St. Deviation	0.013		

Table 91 – Adhesive strength and fracture patterns obtained in S1-O, after heating-freezing and humidification-freezing ageing cycles.

Property	Adhesive strength	Fracture pattern	
Measurement	(MPa)	Description	Photograph
1	0.060	100% cohesion	
2	0.028	100% adhesion	
3	0.028	100% cohesion	
4	0.024	50% adhesion/ 50% cohesion	
5	0.028	100% adhesion	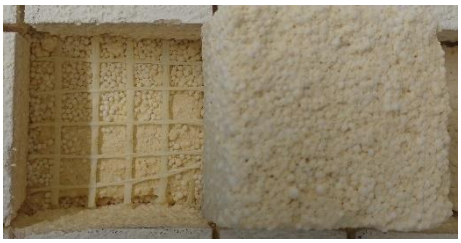
Average	0.034	50% adhesion (between the TR layers/mesh interface) 50% cohesion in the TR itself	
St. Deviation	0.015		

Table 92 – Adhesive strength and fracture patterns obtained in S1-M, before ageing.

Property	Adhesive strength	Fracture pattern	
Measurement	(MPa)	Description	Photograph
1	0.096	100% cohesion	
2	0.056		
3	0.060	100% adhesion	
4	0.084		
5	0.076		
Average	0.074	80% adhesion (between the TR layers/mesh interface)	
St. Deviation	0.017	20% cohesion in the TR itself	

Table 93 – Adhesive strength and fracture patterns obtained in S1-M, after heating-freezing and humidification-freezing ageing cycles.

Property	Adhesive strength	Fracture pattern	
Measurement	(MPa)	Description	Photograph
1	0.036	100% adhesion	
2	0.032	100% cohesion	
3	0.032	100% adhesion	
4	0.044	70% adhesion/ 30% cohesion	
5	0.040	100% adhesion	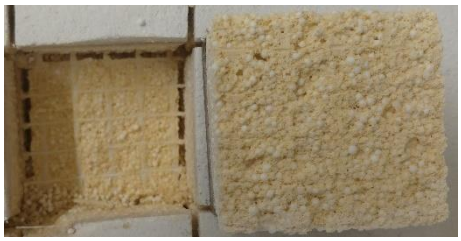
Average	0.037	74% adhesion (between the TR layers/mesh interface)	
St. Deviation	0.005	26% cohesion in the TR itself	

Table 94 – Adhesive strength and fracture patterns obtained in S2, after heating-freezing and humidification-freezing ageing cycles.

Property	Adhesive strength	Fracture pattern	
Measurement	(MPa)	Description	Photograph
1	0.164	30% adhesion/ 70% cohesion	
2	0.156	40% adhesion/ 60% cohesion	
3	0.188	15% adhesion/ 85% cohesion	
4	0.172	50% adhesion/ 50% cohesion	
5	0.172	10% adhesion/ 90% cohesion	
Average	0.170	29% adhesion (TR-substrate interface)	
St. Deviation	0.012	71% cohesion in the TR itself	

Table 95 – Adhesive strength and fracture patterns obtained in S3, after heating-freezing ageing cycles.

Property	Adhesive strength	Fracture pattern	
Measurement	(MPa)	Description	Photograph
1	0.132		
2	0.132	100% cohesion	
3	0.128		
4	0.124	15% adhesion/ 85% cohesion	
5	0.112	100% cohesion	
Average	0.126	3% adhesion (TR-substrate interface)	
St. Deviation	0.008	97% cohesion in the TR itself	

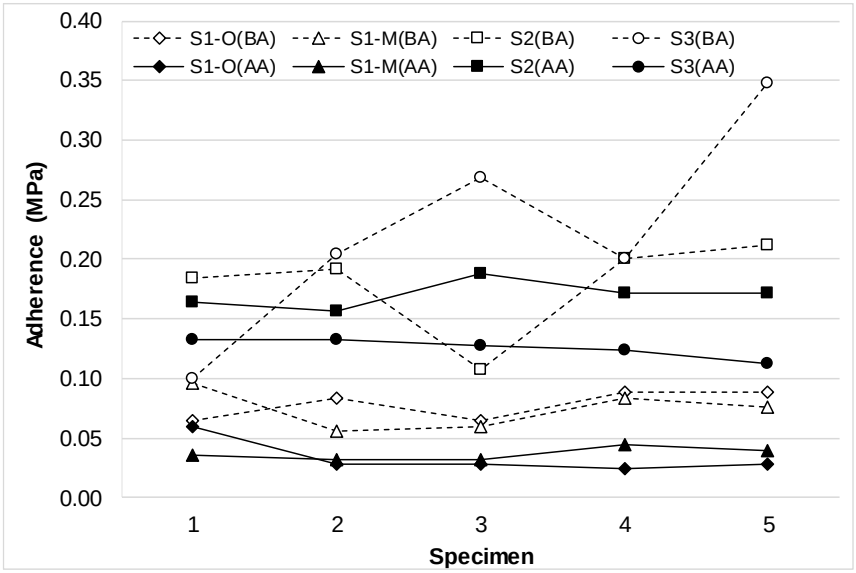

Fig. 124 – Adhesive strength of thermal rendering and plastering systems before (BA) and after (AA) heating-freezing and humidification-freezing ageing cycles.

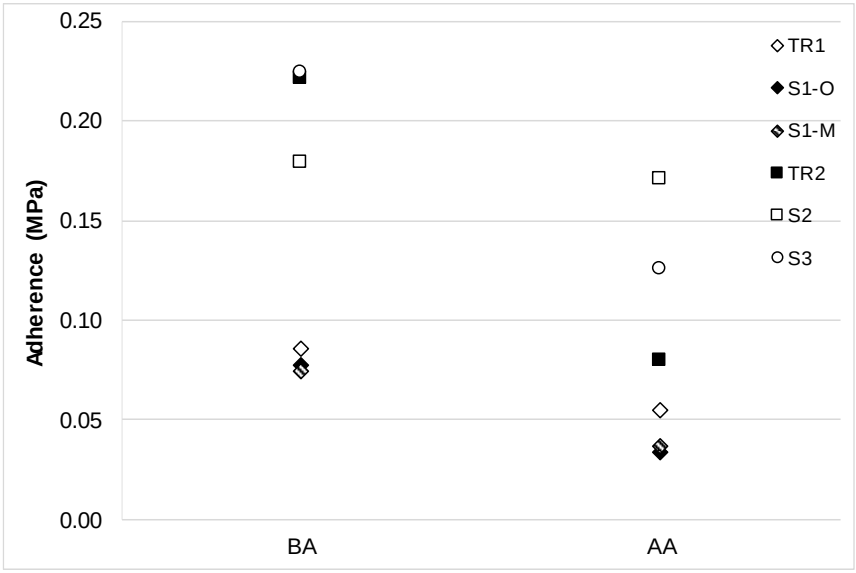

Fig. 125 – Average adhesive strength of thermal renders/plaster and systems before (BA) and after (AA) heating-freezing and humidification-freezing ageing cycles.

A decrease in the adhesive strength after ageing is observed in all the studied systems.

Regarding the results obtained in S1-O and S1-M, before ageing, the resistance is similar for both coatings. However, when comparing these specimens (with 2 layers of thermal render) with the single thermal render layer (see Table 46), a difference of around 82% is observed. The execution of the specimens considering a real application is of major importance in order to reproduce more reliable results. Moreover, the application of 2 layers of thermal render and glass fibre mesh introduces an interface where the fracture could occur (which was verified). In that way, the glass fibre mesh should be well embedded in the thermal render to minimize the interface effect. All these aspects contribute to the decrease of the adhesive strength of S1.

S1-O and S1-M presented very low adhesive strength, after ageing, and the adhesive fractures (between the thermal render and the mesh interface) occurred more frequently. Considering the ETAG 004 requirements, the obtained results were not admissible.

S2 and S3 present an adhesive strength, after ageing, in the same order of magnitude of S1 (2 cm) before ageing. However, S3 should not be compared to the other systems, since the ageing procedure was less severe. Regarding Fig. 124 and Fig. 125, S2 presents a stable behaviour decreasing only 5% after ageing, which highlights the importance of the finishing coating, since TR2 presents a significant decrease after ageing. Despite the short ageing period, the heating-freezing cycles produce a quite significant decrease of the adhesive resistance (around 78%) in S3. This states the importance of an accurate analysis of the durability in all the systems, even in less severe environments (indoor application), without liquid water action (humidification procedure).

5.2.2.3. Impact resistance

The average dent diameter of the hard body impact, in the studied thermal rendering systems, is presented in Table 96 and Fig. 126.

Table 96 – Average dent diameter of the hard body impact, after heating-freezing and humidification-freezing ageing cycles.

Impact energy	2J* (mm)		10J* (mm)	
Procedure	BA	AA	BA	AA
S1-O	21.2±1.64	20.3±1.67	33.0±1.19	37.8±2.32
S1-M	15.7±1.40	19.9±3.19	31.3±1.26	36.1±0.99
S2	18.4±0.99	19.56±1.26	27.3±1.25	28.9±1.36
S3	19.6±0.50	18.7±0.78	26.2±0.80	26.1±0.77

* Results presented as (average ± standard deviation)

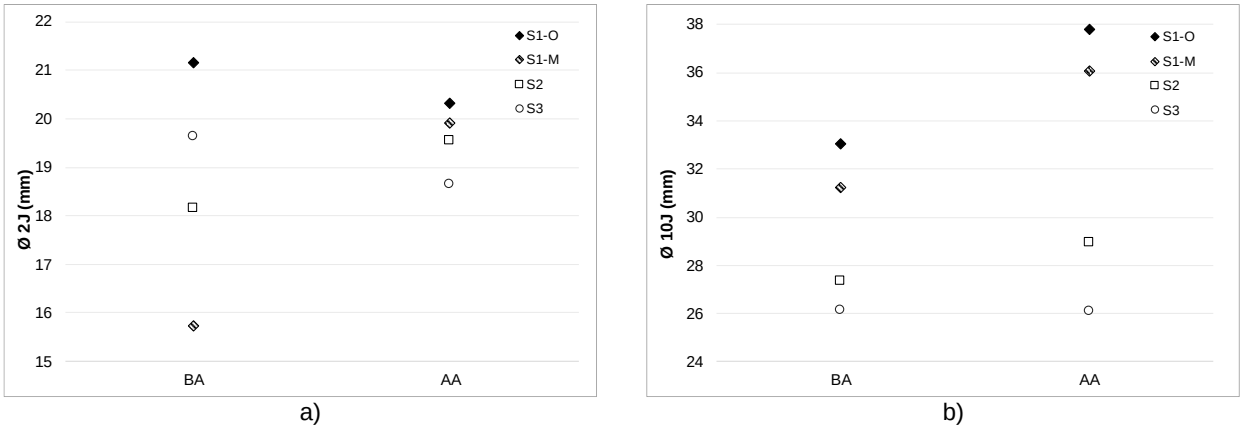

a) b)

Fig. 126 – Average dent diameter before (BA) and after (AA) heating-freezing and humidification-freezing ageing cycles for an impact of: a) 2J; b) 10J.

The two impact energies were performed to analyse different impact types, such as caused by normal traffic and normal use.

Generally, the dent diameter increases after ageing, which was not verified in S1-O and S3. However, that decrease is not significant (≈ 5%) and the precision of the measurements (in millimetres) introduces some variability. This could reveal that, in these systems, the impact resistance remains constant after ageing.

Regarding S1-O and S1-M, the mineral coating presented a lower dent diameter than the organic coating, suggesting a better resistance to the hard body impact. Analysing Fig. 126-b), S1-O and S1-M show a similar performance between them, before and after ageing, but completely different to S2 and S3. This highlights the influence of the systems configuration in the several results. As such, when comparing S1 (with 2 layers of thermal render) with the TR1 (see Table 53 in sub-chapter 3.2.2.4), a difference of around 20% and 12% is observed, for 2J and 10J, respectively, presenting the single layer specimen lower dents. This follows the same observed in 5.2.2.2, noting higher mechanical resistance for the single layer specimen.

Beyond the quantitative analysis, by the dent diameter measurement, qualitative analysis by means of any observed damages was performed. In that way, Table 97 to Table 100 present the damages observed in the different systems, before and after the ageing procedures.

In general, the thermal rendering systems present more damages, like cracking and detachment, after ageing procedures. Again, observing S1-O (with 2 layers of thermal render) and the single thermal render layer (see Table 54 in sub-chapter 3.2.2.4), the damages are smaller in the last one. The lower thickness of the thermal render results in smaller depressions (less deep dents), which could be attributed to the substrate influence. Regarding the organic and mineral coatings influence in the impact resistance, a distinct behaviour is noted. The organic coating results in larger cracks and complete perforation, especially with 10J energy impact. While the mineral coating does not allow perforation, resulting in microcracks. However, higher depressions, detachment and loss of material, with the mineral coating, are observed. The existence of resins in the organic coating could contribute to increase their resistance, by means of decreasing the depressions. However, the cracking generally occurs throughout the coating thickness, which allows a faster water penetration in the system.

S2 presented a significant degradation after ageing, in terms of qualitative observation, such as delamination of the finishing coating, more evident with 10J energy impact.

S3 presented delamination of the finishing plaster (C3) before and after ageing, becoming visible the thermal render (grey colour).

Table 97 – Visual observation of the dent obtained by hard body impact in S1-O, before and after heating-freezing and humidification-freezing ageing cycles.

Impact energy	2J		10J	
Procedure	BA	AA	BA	AA
1				
2	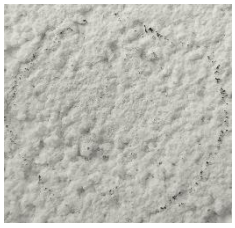			
3				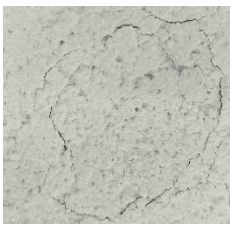
4				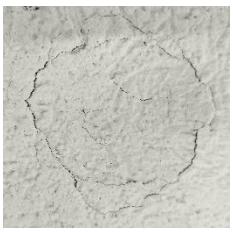
5				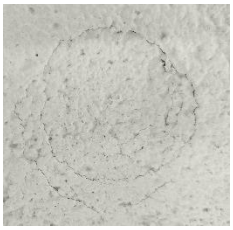
Visual observation	Slight depression	Slight depression; cracks on the coating	Bigger depression; cracks on the coating	Large depression; bigger cracks on the coating

Table 98 – Visual observation of the dent obtained by hard body impact in S1-M, before and after heating-freezing and humidification-freezing ageing cycles.

Impact energy	2J		10J	
Procedure	BA	AA	BA	AA
1				
2			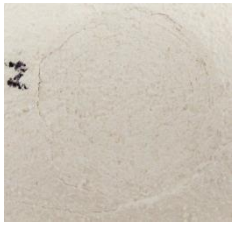	
3				
4				
5				
Visual observation	Slight depression	Slight depression; microcracks on the coating	Bigger depression; cracks on the coating and detachment	Large depression; bigger cracks on the coating

Table 99 – Visual observation of the dent obtained by hard body impact in S2, before and after heating-freezing and humidification-freezing ageing cycles.

Impact energy	2J		10J	
Procedure	BA	AA	BA	AA
1			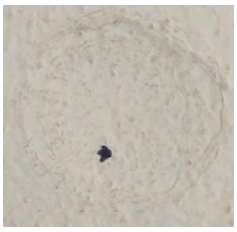	
2				
3				
4			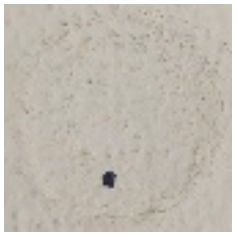	
5				
Visual observation	Slight depression	Circular cracking	Circular cracking	Circular cracking and detachment on the coating

Table 100 – Visual observation of the dent obtained by hard body impact in S3, before and after heating-freezing and humidification-freezing ageing cycles.

Impact energy	2J		10J	
Procedure	BA	AA	BA	AA
1				
2				
3			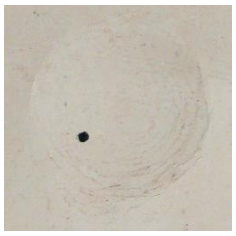	
4				
5				
Visual observation	Circular cracking on the coating	Circular cracking and detachment of the coating	Circular cracking on the coating	Circular cracking and detachment of the coating

Regarding the ETAG 004 classification (EOTA 2013), an adaption to the thermal rendering systems is presented in Table 101.

Table 101 – Thermal rendering systems classification according to hard body impact, based on the ETAG 004 requirements.

Procedure	Before ageing		After ageing		Category
Impact energy	2J	10J	2J	10J	
S1-O	Rendering not penetrated		Rendering perforation		—
S1-M	Rendering not penetrated		Rendering not penetrated; detachment		III
S2	Rendering not penetrated	Rendering not penetrated; delamination	Rendering not penetrated	Rendering not penetrated; delamination	III
S3	Rendering penetration and delamination			Rendering not penetrated	—

S1-M and S2 are the only that meet some requirements, such as non-penetration, while S1-O and S3 were not suitable for categorization. That fact states the importance of carefully analysing the use of the zones where these systems could be applied.

5.2.2.4. Visual observation and porous structure

To complement the durability assessment, an accurate visual observation of the materials and their microstructure is of major importance, since it could highlight and explain the system performance. S1 and S2 did not evidence any critical points or significant coating degradation. However, S3 showed a regular degradation in the finishing plaster (C3), exemplified by the stained frame and delamination as it is shown in Fig. 127.

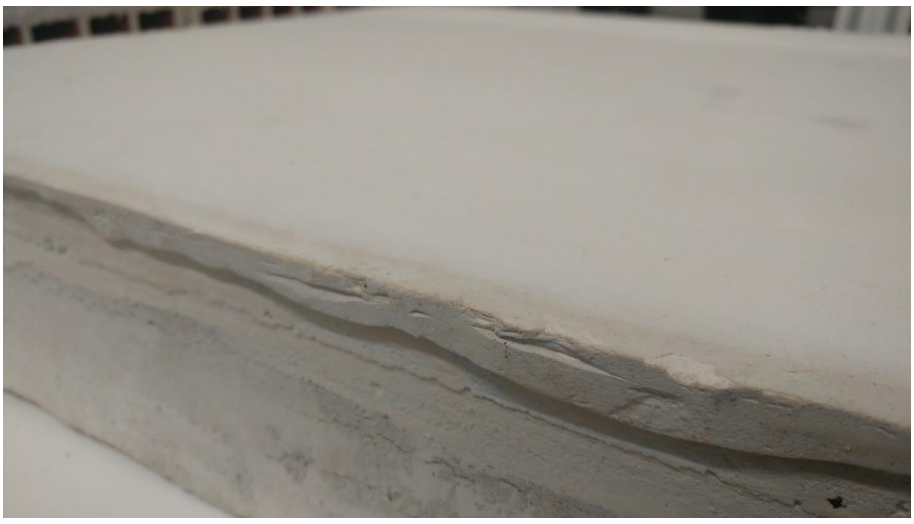

Fig. 127 – Visual observation of S3, after heating-freezing ageing cycles.

To evaluate the effect of the ageing in the several materials, on a microscopic scale, optical microscope images are presented in Fig. 128 to Fig. 134. Fig. 128 and Fig. 132 show the images obtained for the ageing of the thermal render itself, while Fig. 133 and Fig. 134 show the images obtained for the ageing of the whole system.

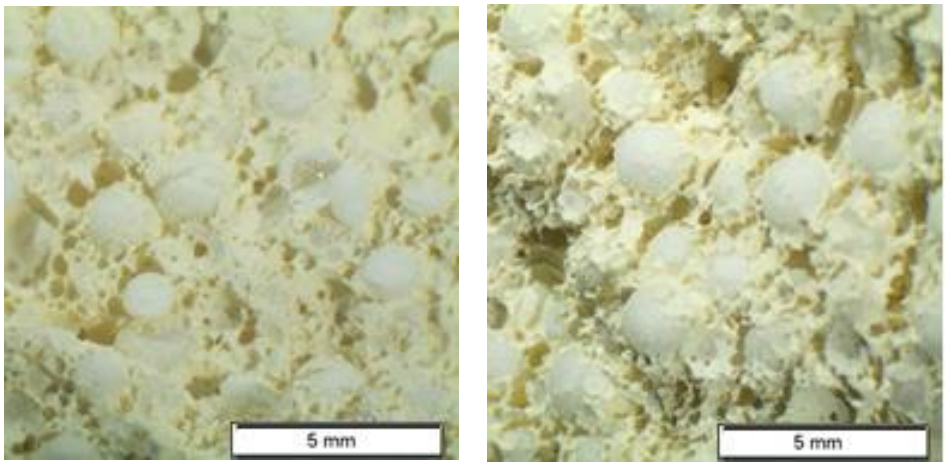

a) b)

Fig. 128 – Optical microscope images of TR1: a) Before ageing; b) after heating-freezing and humidification-freezing ageing cycles.

The heating-freezing and humidification-freezing cycles produced an alteration on the matrix of the thermal render. The water penetration and consequent freeze-thaw action promoted the material expansion and contraction, producing cracks among macropores. In addition, the water action may lead to some loss of binder.

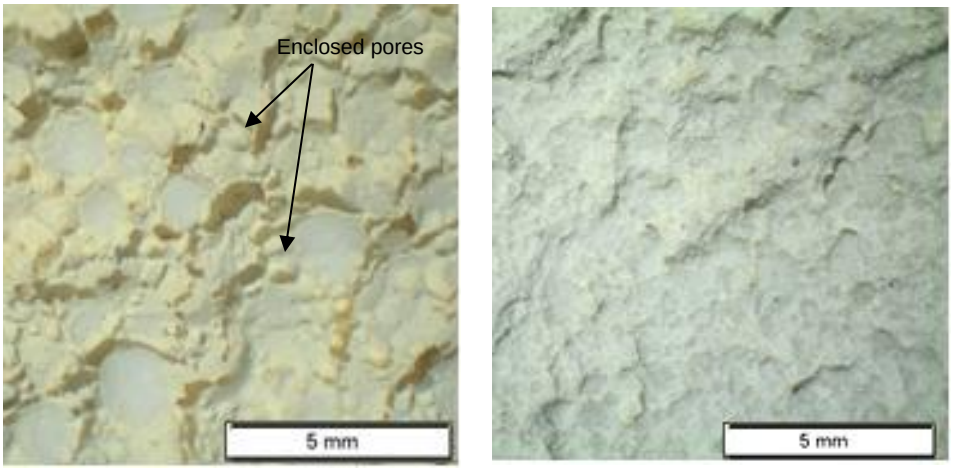

a) b)

Fig. 129 – Optical microscope images of S1-O after heating-freezing and humidification-freezing ageing cycles.

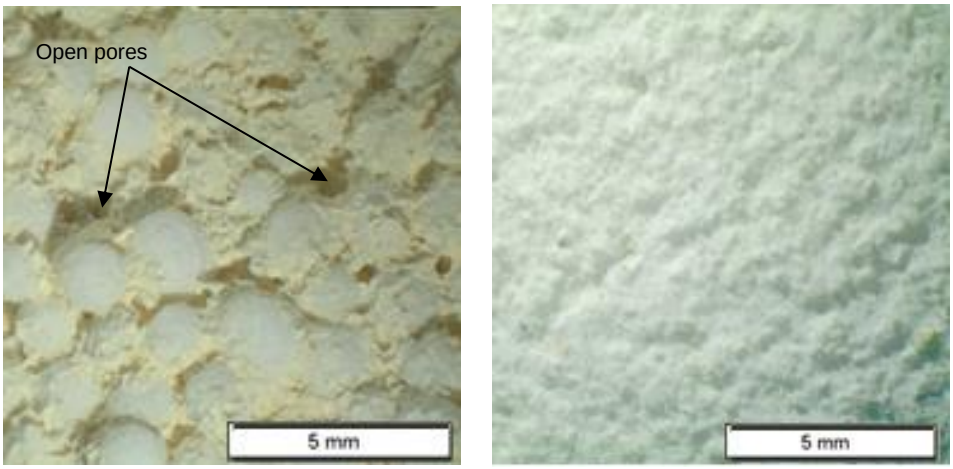

a) b)

Fig. 130 – Optical microscope images of S1-M after heating-freezing and humidification-freezing ageing cycles: a) TR1; b) Mineral coating.

In the thermal render with organic coating, it is possible to observe the enclosed porosity, while with the mineral coating some open pores are visible. In addition, the presence of water seems to be stronger in the TR with the mineral coating, due to matrix alteration (see Fig. 131). This is in accordance with the results obtained in the liquid water permeability (see 5.2.2.1), which shows to be higher with the mineral than the organic coating.

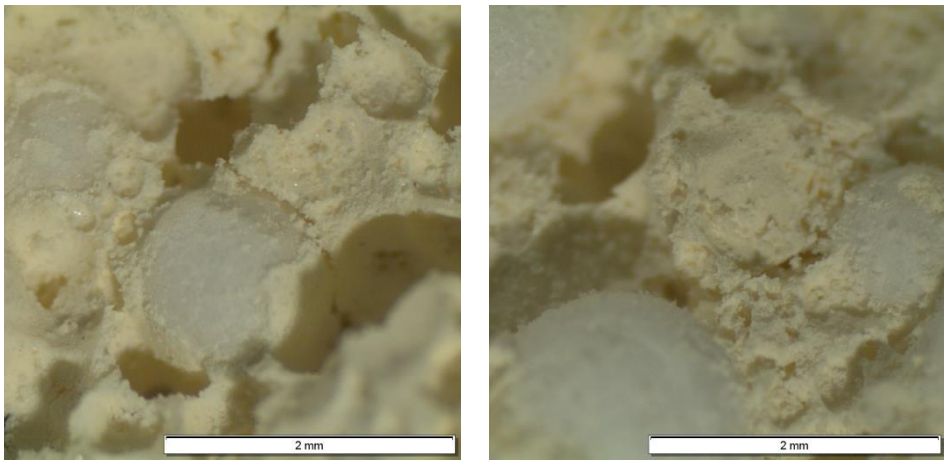

a) b)

Fig. 131 – Optical microscope images of TR1 (2.5x), after heating-freezing and humidification-freezing ageing cycles: a) Organic coating; b) Mineral coating.

a) b)

Fig. 132 – Optical microscope images of TR2: a) Before ageing; b) after heating-freezing and humidification-freezing ageing cycles.

The image obtained in the middle of TR2 shows less open pores after ageing than before. Despite the samples were obtained in the same conditions, the thermal render could present different pores distribution in the specimen and that consideration may not be generalized.

TR2, aged in the whole system, presented a similar aspect to the thermal render aged without finishing. This could mean that even with finishing render and coating the ageing procedure contributes to similar degradation of the material structure. On the other hand, the finishing coating presents several microcracks after ageing.

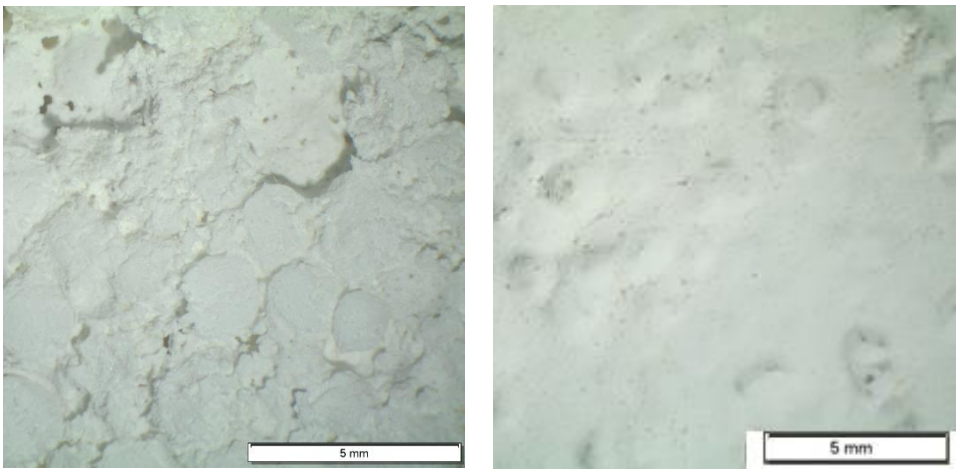

a) b)

Fig. 133 – Optical microscope images of S2 after heating-freezing and humidification-freezing ageing cycles: a) TR2; b) Finishing coating.

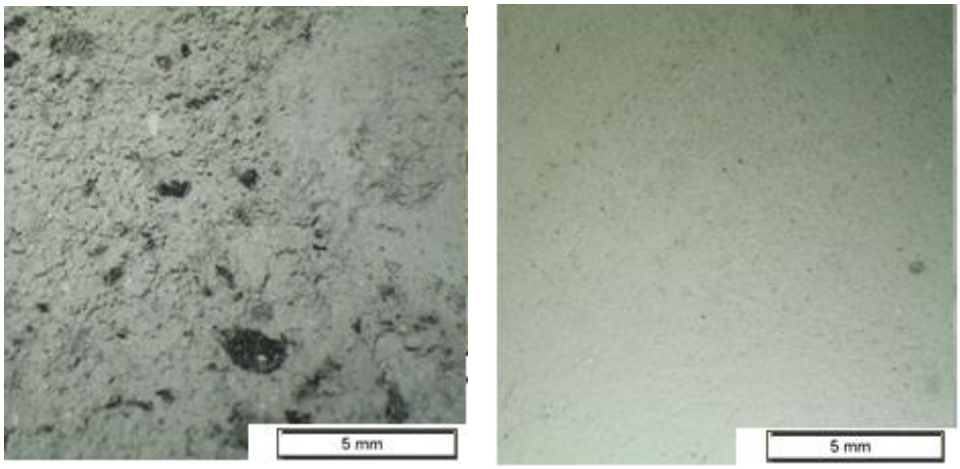

a) b)

Fig. 134 – Optical microscope images of S3 after heating-freezing ageing cycles: a) TR3; b) C3.

S3 did not evidence an alteration of the microstructure, especially in the thermal render, while the finishing plaster showed a brushed aspect.

5.2.3. EXPERIMENTAL RESULTS – ADAPTED METHODOLOGY FROM ETAG 004

5.2.3.1. Liquid water permeability

The liquid water was measured, by two different methodologies, before and after ageing, analysing the effect of freeze-thaw ageing cycles. Table 104 presents the volume of water that penetrates in the systems (V_t), for each presented methodology, at two different time periods. In Fig. 135, the amount of water absorbed along the test period is presented.

Table 102 – Volume of water penetration before (BA) and after (AA) freeze-thaw.

Experimental method		Cone		Karsten tubes	
V_t (ml/m^2)		24 h	48h	1h	2h
S1-O	BA	44.6	89.1	99.1	141.5
	AA	31.8	50.9	146.2	330.1
S1-M	BA	802.1	1228.7	188.6	334.8
	AA	184.6	210.1	245.2	396.1
S2	BA	445.6	687.5	202.8	292.4
	AA	86.6	140.1	183.9	226.4

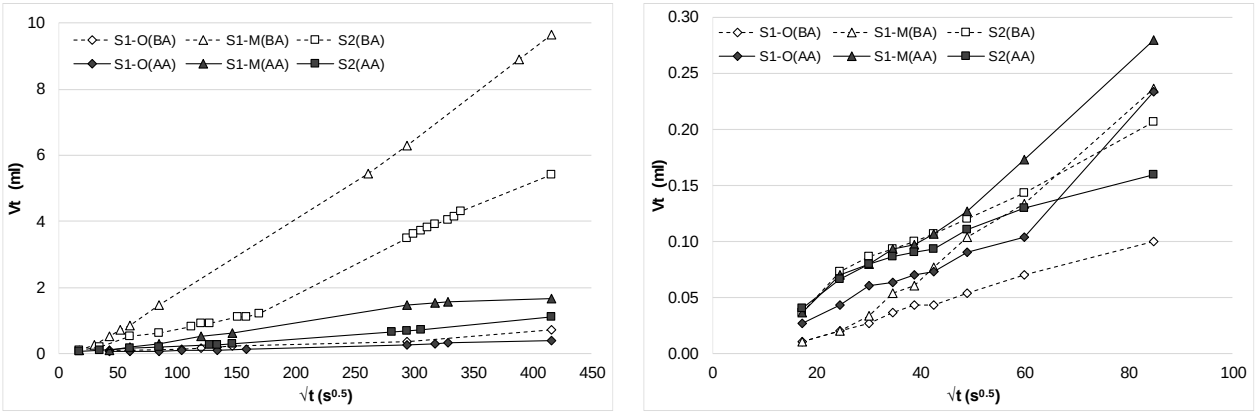

Fig. 135 – Water permeability test results of S1 and S2, after freeze-thaw ageing cycles, using the: a) Cone method; b) Karsten tubes method.

Regarding the obtained results, the amount of water that penetrates into the specimen does not present a clear tendency. Although, in general, the water volume decreases after ageing, contrary to the results obtained in 5.2.2.1. This fact could be related to incomplete drying of the specimens. In addition, the two methods contribute again to the obtaining of different results. The results suggest that the coating presented consolidation, which contributed to the reduction of the water permeability. Since the test area of the Karsten tubes is lower than the cone method, the results after ageing may comprehend areas of lower and greater consolidation, which allowed the differences between both methods. Again, differences between the organic and the mineral coating are observed, presenting the last one a higher amount of water absorption.

5.2.3.2. Adhesive strength

The adhesive strength after freeze-thaw ageing cycles presents a specific behaviour regarding S1. As can be seen in Fig. 136 and Fig. 137, the fractures were mostly adhesive between the thermal render and the finishing render. The severe ageing cycles promote a fast detachment of the layers and the embrittlement of the thermal render.

a) b)

Fig. 136 – Fracture patterns obtained in S1-O, after freeze-thaw ageing cycles: a) Specimens overview; b) Detailed view.

Fig. 137 – Example of the adhesive fractures obtained in S1-M, after freeze-thaw ageing cycles.

Table 103 and Table 104 show the adhesive strength values and the fracture pattern obtained in S1-O and S1-M, respectively, after freeze-thaw ageing cycles.

Table 103 – Adhesive strength and fracture patterns obtained in S1-O, after freeze-thaw ageing cycles.

Property	Adhesive strength	Fracture pattern	
Measurement	(MPa)	Description	Photograph
1	0.0	50% adhesion/ 50% cohesion	
2	0.0	50% adhesion/ 50% cohesion	
3	0.0	100% adhesion	
4	0.0	50% adhesion/ 50% cohesion	
5	0.0	100% adhesion	
Average	0.0	70% adhesion (between the TR-C)	
St. Deviation	0.0	30% cohesion in the TR itself	

Table 104 – Adhesive strength and fracture patterns obtained in S1-M, after freeze-thaw ageing cycles.

Property	Adhesive strength	Fracture pattern	
Measurement	(MPa)	Description	Photograph
1	0.0	100% adhesion	
2	0.0	100% adhesion	
3	0.0	10% adhesion/ 90% cohesion	
4	0.0	20% adhesion/ 80% cohesion	
5	0.0	100% adhesion	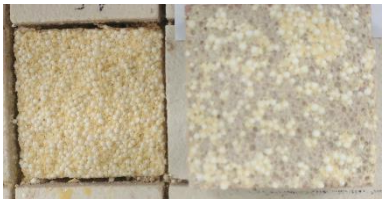
Average	0.0	66% adhesion (between the TR-C)	
St. Deviation	0.0	34% cohesion in the TR itself	

The zero value was due to the detachment of the coating layers at the pre-cut phase, so the pull-off was not even performed. Considering the ETAG 004 requirements, the obtained results were not admissible.

Table 105 presents the adhesive strength and the fracture patterns obtained in S2, after freeze-thaw cycles.

Table 105 – Adhesive strength and fracture patterns obtained in S2, after freeze-thaw ageing cycles.

Property	Adhesive strength	Fracture pattern	
Measurement	(MPa)	Description	Photograph
1	0.144	100% cohesion	
2	0.104	100% cohesion	
3	0.140	100% cohesion	
4	0.148	5% adhesion/ 95% cohesion	
5	0.128	50% adhesion/ 50% cohesion	
Average	0.133	11% adhesion (between the TR-substrate)	
St. Deviation	0.018	89% cohesion in the TR itself	

S2 presents a decrease of around 35% in the adhesive strength, after ageing, and the cohesive fractures in the thermal render itself occurred with a higher rate (89%) than the adhesive fractures between the thermal render and the substrate. Considering the ETAG 004 requirements, the obtained results are admissible.

Fig. 138 shows the comparison between the different systems, before and after ageing.

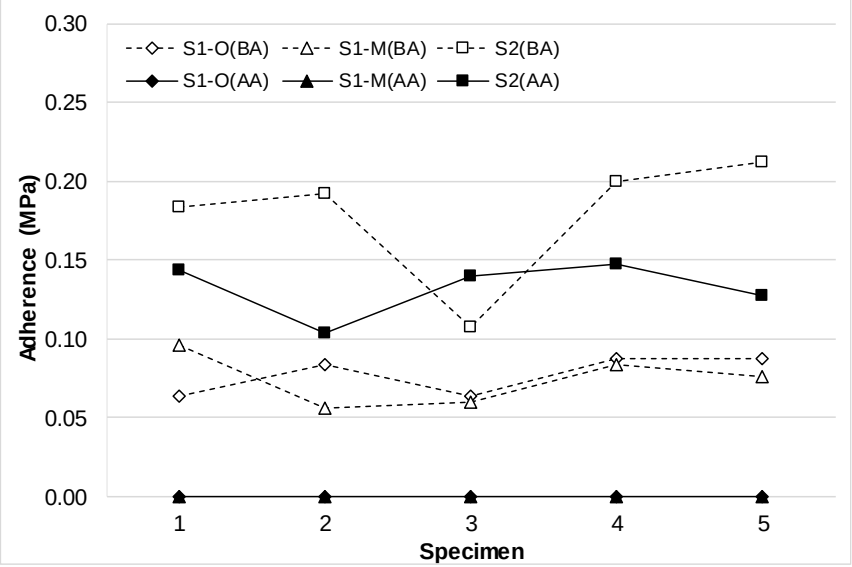

Fig. 138 – Adhesive strength of thermal rendering systems S1-O, S1-M and S2 before (BA) and after (AA) after freeze-thaw ageing cycles.

The results obtained in S1-O and S1-M are quite similar for both coatings, before and after ageing. S2 presents better adhesive resistance than S1, but care should be taken when comparing these two systems (S1 with 2 layers of thermal render and S2 with a single thermal render layer).

5.2.3.3. Impact resistance

The average dent diameter of the hard body impact, in the studied thermal rendering systems, is presented in Table 106 and Fig. 139.

Table 106 – Average dent diameter of the hard body impact, after freeze-thaw ageing cycles.

Impact energy	2J* (mm)		10J* (mm)	
Procedure	BA	AA	BA	AA
S1-O	21.2±1.64	23.5±2.06	33.0±1.19	44.3±2.21
S1-M	15.7±1.40	21.6±1.30	31.3±1.26	34.4±0.63
S2	18.4±0.99	20.1±0.75	27.3±1.25	29.3±1.24

The dent diameter always increases after ageing, mainly in S1 (10-37%), while S2 presents a slight increase (7-9%) and lower dents, which could reveal a higher impact resistance after ageing.

Regarding S1-O and S1-M, the mineral coating presents lower dent diameter than the organic coating, suggesting a better resistance to the hard body impact, such as in 5.2.2.3. Beyond the quantitative analysis, by the dent diameter measurement, qualitative analysis by means of any observed damages is performed.

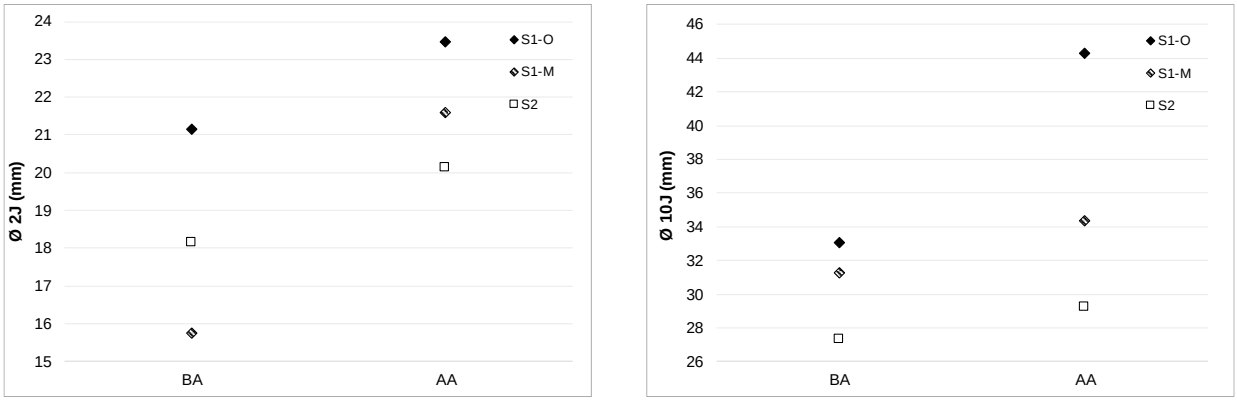

a) b)

Fig. 139 – Average dent diameter before (BA) and after (AA) after freeze-thaw ageing cycles for an impact of: a) 2J; b) 10J.

In that way, Table 107 and Table 108 present the observed damages in the different systems, before and after the ageing procedures.

In general, the thermal rendering systems present more damages, like cracking and detachment, after ageing procedures. Regarding the organic and mineral coatings influence in the impact resistance, a distinct behaviour is again noted. The organic coating results in larger cracks and complete perforation, especially with 10J energy impact. While the mineral coating does not allow perforation, resulting in microcracks. However, higher depressions, detachment and loss of material, with the mineral coating, is observed. It is noted that the depressions are considerably bigger than the obtained in 5.2.2.3, highlighting the effect of a severe ageing cycle.

S2 presents a significant degradation after ageing, in terms of qualitative observation, such as delamination of the finishing coating, more evident with 10 J energy impact.

Table 107 – Visual observation of the dent obtained by hard body impact in S1, after freeze-thaw ageing cycles.

System	S1-O		S1-M	
Impact energy	2J	10J	2J	10J
1				
2				
3				
4				
5				
Visual observation	Slight depression; cracks on the coating	Large depression; rupture/cracks on the coating	Slight depression and detachment of the coating	Large depression; detachment and microcracking of the coating

Table 108 – Visual observation of the dent obtained by hard body impact in S2, before and after freeze-thaw ageing cycles.

Impact energy	2J		10J	
Procedure	BA	AA	BA	AA
1			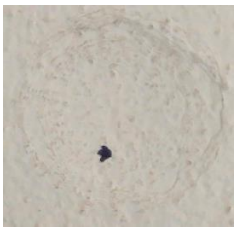	
2		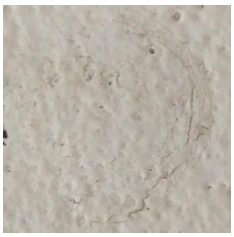		
3				
4			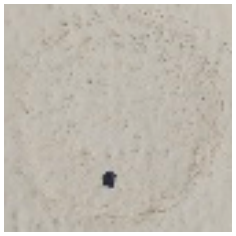	
5			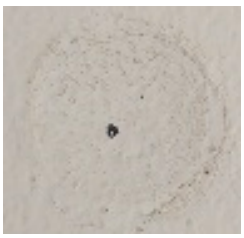	
Visual observation	Slight depression	Slight depression and detachment	Circular cracking	Circular cracking and detachment on the coating

Regarding the ETAG 004 classification (EOTA 2013), an adaptation to the thermal rendering systems is presented in Table 103.

Table 109 – Thermal rendering systems classification according to hard body impact, based on the ETAG 004 requirements.

Procedure	Before ageing		After ageing		Category
Impact energy	2J	10J	2J	10J	
S1-O	Rendering perforation				—
S1-M	Rendering not penetrated		Rendering not penetrated; detachment		III
S2	Rendering not penetrated	Rendering not penetrated; delamination	Rendering not penetrated	Rendering not penetrated; delamination	III

S1-M and S2 are the only that meet some requirements, such as non-penetration, while S1-O was not suitable for categorization.

5.2.3.4. Visual observation and porous structure

To complement the durability assessment, an accurate visual observation of the materials and their microstructure is of major importance, since it could highlight and explain the system performance. The visual observation, before and after ageing, of the coatings S1-O and S1-M are presented in Fig. 140 and Fig. 141, respectively.

a) b)

Fig. 140 – Visual observation of S1-O: a) before; b) after ageing according to ETAG 004 procedure.

a) b)

Fig. 141 – Visual observation of S1-M: a) before; b) after freeze-thaw ageing cycles.

As it can be seen, the two coatings present a darker colour (yellowish colour) after ageing, with stains dispersed in the surface. The higher degradation, comparing to 5.2.2.4, could be related to the severe ageing cycles (freeze-thaw), but also with some critical points found in the specimens. Fig. 142-a) shows some damages in the coating, which may be related to the handling of the specimens during the ageing in the different procedures (freezing and thawing), performed in different equipment. Beyond the coating observation, cracks in the sealant, placed in the sides of the specimen, were found, as demonstrated in Fig. 142-b). This fact could be attributed to the temperature variations during the cycles, which also affect the sealant durability.

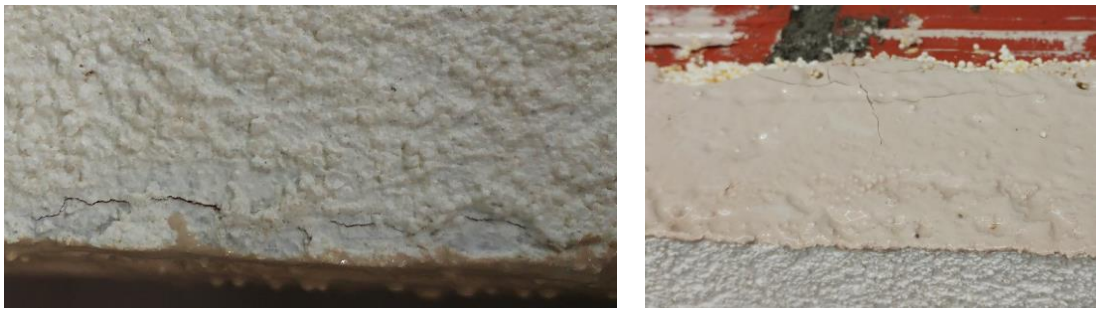

a) b)

Fig. 142 – a) Damage of the coating; b) Cracks on the sealant, after freeze-thaw ageing cycles.

These two damages allow the water to easily penetrate in the inner layers (finishing render and thermal render) resulting in a severe deterioration of the system, such as the adhesive fractures and the embrittlement of the thermal render (see Fig. 143). The degradation of the thermal rendering systems may be distorted by these specific damages, resulting in overstated action.

Fig. 143 – Deterioration of the thermal render layer, after freeze-thaw ageing cycles.

On the other hand, S2 did not evidence any critical points or significant coating degradation.

Fig. 144 to Fig. 146 show the obtained images after the freeze-thaw ageing cycles.

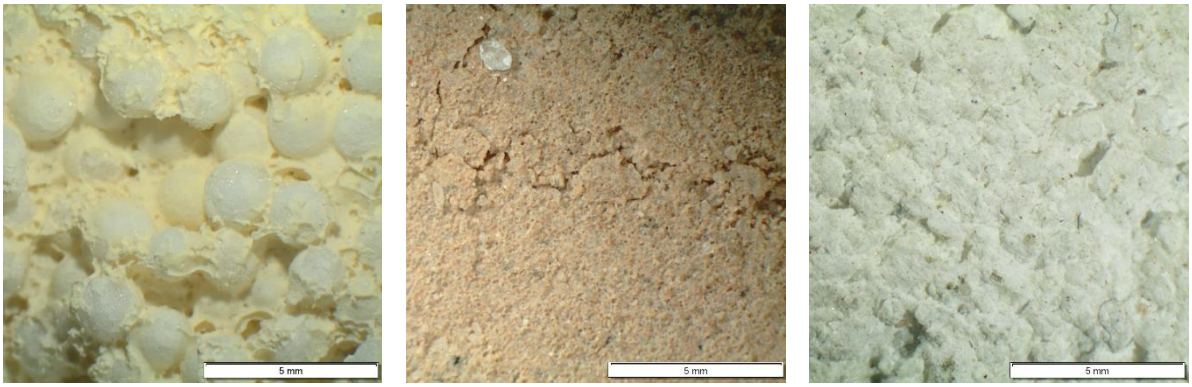

a) b) c)

Fig. 144 – Optical microscope images of S1-O after freeze-thaw ageing cycles: a) TR1; b) C1; c) Organic coating.

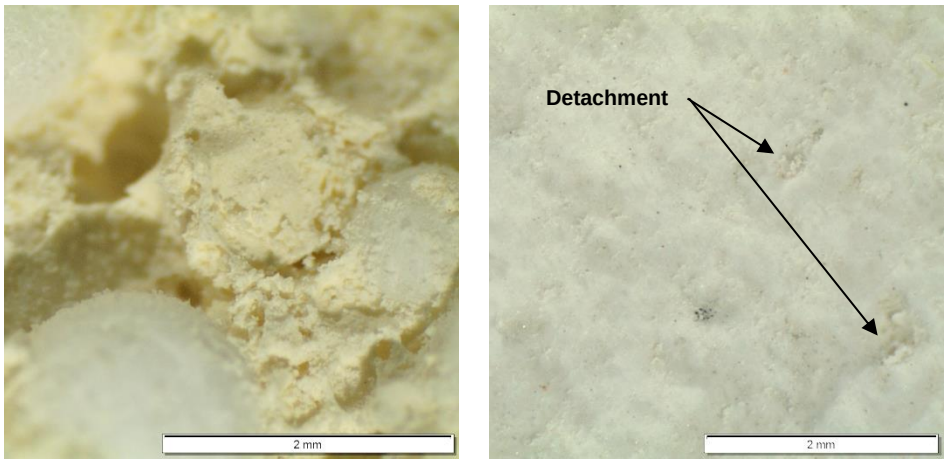

a) b)

Fig. 145 – Optical microscope images (2.5x) of S1-M after freeze-thaw ageing cycles: a) TR1; b) Mineral coating.

In the thermal render with the organic coating is possible to observe the several EPS granules, most of them little connected to the matrix, showing the segregation of the two materials (aggregate and binder), as seen in 5.2.3.2 and Fig. 143. Also, the finishing render shows significant cracks and embrittlement. Regarding the thermal render with mineral coating, the enlarged image shows the matrix embrittlement, supporting the higher presence of water seems with the mineral coating. An enlarged image of the mineral coating also shows the detachment of material (see Fig. 145-c)).

TR2 presents a similar aspect to the images shown in 5.2.2.4. The EPS granules are well involved by the matrix, as it can be seen in Fig. 146, resulting in more cohesive structures (corroborating the higher adhesive strength). Otherwise, the finishing coating presents several microcracks after ageing.

a) b) c)

Fig. 146 – Optical microscope images of S2 after freeze-thaw ageing cycles: a) TR2 (0.7x); b) TR2 (2.5x); c) Coating (7x).

5.2.4. SUMMARY

The experimental tests carried out to evaluate the durability of the thermal mortars and related systems allow to identify several problems and constraints with the testing operation itself:

- Regarding the liquid water permeability tests, the porous constitution and high absorption of the thermal renders do not allow reliable results, since they present a great amount of water diffusion by the surface;
- The Karsten tubes method consists of a quick and easy way of measuring the liquid water permeability under low pressure. The possibility of measurement in a vertical position allows the testing of wall specimens, where the cone method cannot be implemented;
- The execution of circular pre-cuts, to determine the adhesive strength, invalidated the test, since the circular frequency of the drilling machine pulls out the specimen. In that way, square pre-cuts were performed in order to enable the test. Studies on the effect of the type of pre-cut showed similar results for circular and square pre-cuts (Costa et al. 2007; Gonçalves 2004);
- Having a significant number of pull-offs is of great importance since the adhesion strength distribution is obtained with a good degree of confidence (Ramos et al. 2012);
- Observed damages in the coatings may be related to the handling of the specimens during the ageing in the different procedures (freezing and thawing), performed in different equipment;
- Observed cracks in the sealant, placed in the sides of the specimen, could be attributed to the temperature variations during the cycles, which also affect the sealant durability;
- The degradation of the thermal rendering systems may be distorted by these specific damages, resulting in overstated action.

In addition, the configuration of the specimen demonstrated a significant impact on the adhesive strength and on the impact resistance:

- The execution of the specimens considering a real application is of major importance in order to reproduce more reliable results;
- The application of 2 layers of thermal render and glass fibre mesh introduces an interface, where the fracture could occur (which was verified). In that way, the glass fibre mesh should be well embedded in the thermal render to minimize the interface effect;

- The lower thickness of the thermal render results in smaller depressions (less deep dents), which could be attributed to the substrate influence.

The accelerated ageing cycles envisaged in the existing procedures, gave a great amount of information that will help in the definition of the durability assessment methodology directly applicable to thermal rendering and plastering systems. The freeze-thaw cycles are more severe than the heating-freezing/humidification-freezing cycles, since, in general, a decrease in the mechanical resistance and an increase of the liquid water permeability are observed. The higher number of cycles and the severity of the freeze-thaw ageing cycles may reproduce the effect of colder climates (like the northern European countries). The heating-freezing/humidification-freezing cycles combine degradation mechanisms, which occur in several locations, mainly in south European countries, due to the high heating temperature.

After the different ageing procedures, the specimens generally presented an alteration of the matrix, an increase of the water permeability and a decrease of the mechanical strength. The mineral coating showed higher water absorption than the organic coating, highlighting the importance of assessing the durability taking into account the different components of the thermal rendering systems. The effect of water in gypsum-based materials promoted cracking and loss of the finishing plaster, due to the intrinsic properties of gypsum, which has high capillary absorption and dissolves in water. The finishing coatings also contributed to a more stable mechanical strength after ageing. The low mechanical strength of the thermal rendering and plastering systems highlighted the importance of carefully analyse the zones where these systems could be applied. The ageing cycles could produce an alteration on the matrix of the thermal renders. The water penetration and consequent freeze-thaw action promote the material expansion and contraction, breaking the several macropores.

In summary, a complete durability assessment methodology should take into account and reproduce the most relevant degradation mechanisms in thermal rendering and plastering systems, such as the freeze-thawing and/or temperature fluctuation. The ageing procedures in small-scale samples allow the implementation of specific procedures, which may complement the testing in large samples (walls).

5.3. DEVELOPMENT OF A NEW ACCELERATED AGEING HYGROTHERMAL CYCLE

5.3.1. FRAMEWORK

The development of accelerated ageing cycles adapted to thermal rendering systems, which replicate certain climate conditions, is the core task in the present study. The combination of the three methods presented by Daniotti, Spagnolo and Paolini (2008) in 2.5.2, was the base for the development of the heat-cold cycle, applied to thermal rendering systems:

- Climatic data: using existing climatic data files and “in situ” measurements;
- Existing standards: based on EN 1015-21 and ETAG 004, applied to mortars and ETICS, respectively;
- Preliminary degradation model: dynamic numerical simulation of the most representative degradation mechanisms.

The principle consists in combining the effect of temperature variation and water action in two distinct ways:

- High-temperature variation: heat-cold cycles;
- Thermal shock: abrupt decrease of a warm façade by cold rain.

The durability assessment of the thermal rendering systems was presented using an example, focused on the South European climate context. Hence the ageing cycles were developed taking into account a representative climate. In that way, a severe Portuguese climate was selected, since the current work was developed in the Portuguese context. The climate has to represent a high-temperature variation, such as cold winters (I3 climatic zone) and warm summers (V3 climatic zone). Therefore, the city of Bragança, located in the interior Northeast of Portugal, fitted the requirements, as it can be seen in Table *83* to Table 85.

5.3.2. DEVELOPMENT OF THE HEAT-COLD CYCLE

The heat-cold ageing cycle was developed through numerical simulation, using the hygrothermal simulation tool WUFI Pro (IBP 2016), already described in 4.2.1. The simulation model is the same presented in Fig. 57, excepting the substrate that was replaced by a 22 cm current ceramic brick masonry, which properties are defined in the WUFI Pro software database (650 kg/m^3 of density and 0.13 W/m.ºC of thermal conductivity) (IBP 2016). This is related to the general use of brick masonry walls in the southern European countries and to their widespread use to perform durability tests.

To maximize the temperature variation, the wall was modelled considering a high solar absorption coefficient (α=0.8) and the orientation with high solar radiation incidence (southwest orientation in the studied case), as shown in chapter 4.2. Although WUFI Pro does not consider the cooling of surfaces by the action of cold rain, the cooling effect by the subsequent evaporation of the imbibed water is correctly included (which is considerably higher in general) (IBP 2016). As such, to maximize the temperature variation, the rain incidence was not considered. The adopted methodology for the definition of the heat-cold cycle is presented in Fig. 147.

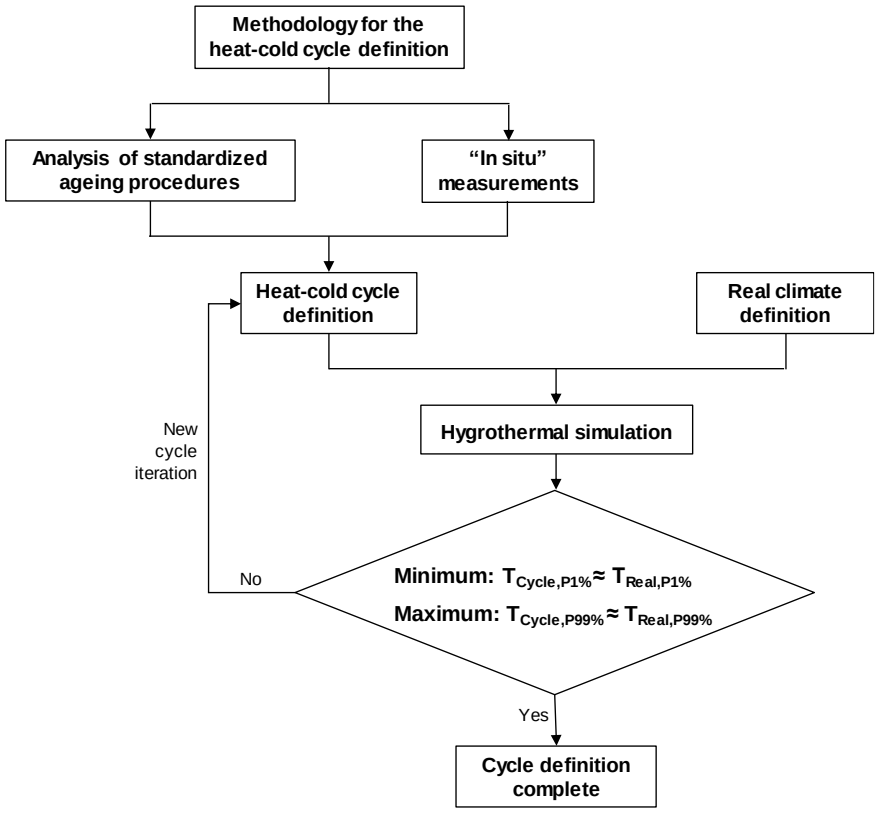

Fig. 147 – Adopted methodology for the definition of the heat-cold cycle.

After the definition of the required real climatic conditions, the cycles preconized in EN 1015-21 and in ETAG 004, as well as the "in situ" temperature measurements determined in Sá (2018), were analysed to define the first iteration of the heat-cold (HC) cycle.

The cycle is defined by the comparison of the obtained temperature, in the thermal render layer, in both the real climate and heat-cold cycle. Two temperature indicators were chosen: 1st percentile, which is a representative value of the cold period (winter season), and 99th percentile, which is a representative value of the warm period (summer season), as it can be seen in Fig. 148-a). When simultaneously the minimum temperature value of the 1st percentile and the maximum temperature value of the 99th percentile in the cycle and in the real climate are similar (see Fig. 148-a), the cycle is fixed. The heat-cold cycle resulting from the iteration process, until the achievement of the defined requirements, is presented in Fig. 148-b).

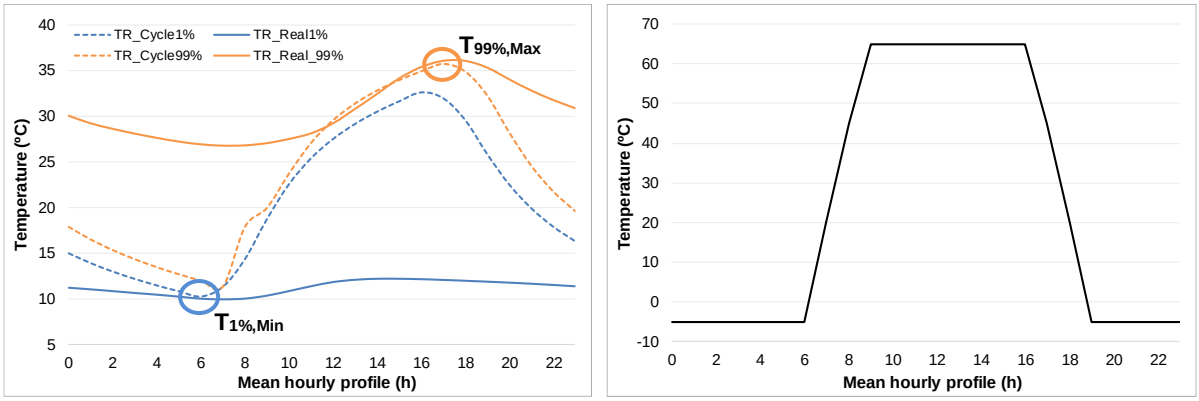

Fig. 148 – Heat-cold cycle definition: a) Comparison of the obtained temperatures in the thermal render layer, in the cycle and real climate; b) Defined heat-cold cycle.

The heat-cold cycle comprises a cold period (-5 ºC during 11h), a warm period (65 ºC during 7h) and the transitions between the 2 stages, resulting in a 24h cycle. The cycle is repeated 30 times, representing the duration of a month. This cycle, like the heat-cold cycle included in the ETAG 004, has a temperature amplitude of 70 ºC, similar to the one defined in EN 1015-21 (ΔT=75 ºC). The temperatures and respective duration were adjusted, by an iteration process, to fit the requirements for the definition of the heat-cold cycle.

5.3.3. DEVELOPMENT OF THE HEAT-RAIN CYCLE

The heat-rain (HR) ageing cycle was developed through the combination of the heat-rain cycle, included in ETAG 004, and the "in situ" temperature measurements, determined in Sá (2018). The maximum temperature was adapted taking into account the "in situ" measurements and the duration of each heat and rain periods, as well as the number of cycles, were defined based on the ETAG 004 heat-rain cycle.

As such, the heat-rain cycle comprises a warm period (70 ºC during 2h), a rain period (15 ºC and 1l/m^2.min. of water spraying, during 1h) and the transitions between the 2 stages, resulting in a 6h cycle, as it can be seen in Fig. 149. The cycle is repeated 80 times, comprising 20 days of ageing.

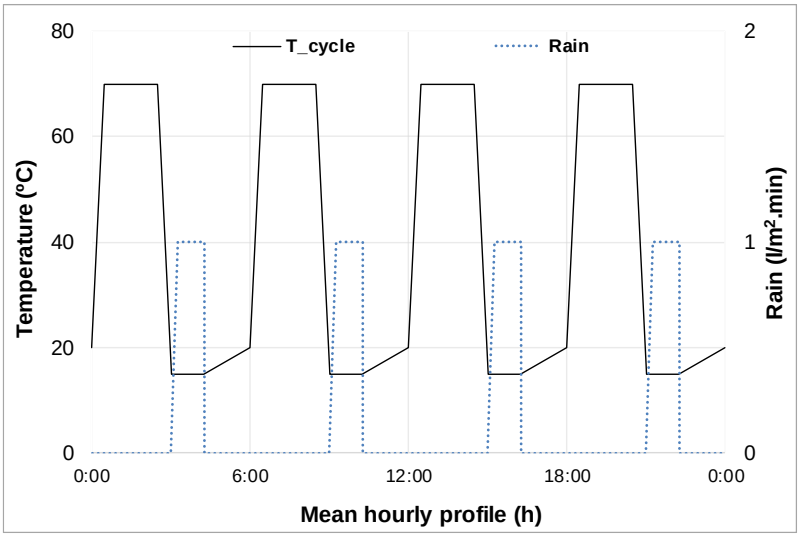

Fig. 149 – Defined heat-rain cycle.

5.4. IMPLEMENTATION OF THE DEVELOPED ACCELERATED AGEING HYGROTHERMAL CYCLE

5.4.1. SPECIMEN CONFIGURATION

The second part of the durability assessment consists of the implementation of the hygrothermal ageing cycle developed in 5.3 in an example case. The ageing cycles were implemented using a climatic chamber Aralab Climatest Fitoclima 700 EDTU, available in LNEC. The wall was built in a test rig with 3 x 2.5 m^2 of testing surface, where two rectangular openings (0.40 m wide by 0.60 m high), consisting of the absence of the thermal rendering system on the substrate at this area, is included at the superior corners of the rig, positioned at 0.40 m from the edges. The wall has the same constitution as the specimens (considering system S1) described in 5.2.1. Table 110 presents the scheduling of the different layers application, corresponding thicknesses and curing times, and the Fig. 150 to Fig. 158 all the stages of the wall preparation.

Table 110 – Wall specimen preparation – tasks and curing times.

Day	Task	Layer thickness (m)	Curing time (days)
1	- 1st layer of TR1 (Fig. 150-b)) - 1st layer of glass fibre mesh (Fig. 151-b)) - Mechanical fixation (Fig. 151-c))	0.04	1
2	- 2nd layer of TR1 (Fig. 152)	0.02	6
8	- Singular reinforcements (Fig. 154-a);b)) - Finishing renderC1 (Fig. 154-c)) - 2nd layer of glass fibre mesh (Fig. 155-a)) - Glass fibre mesh reinforcement: central zone (Fig. 155-b))	0.003	3
11	- Finishing coatings application: - S1-O: primer + organic coating (Fig. 156) - S1-M: mineral coating (Fig. 157)	0.002	28

Firstly, the substrate, consisting of a brick masonry wall (15 cm thickness) and the opening casts were prepared, as shown in Fig. 150-a). After the application of the first layer of thermal render (4 cm) (Fig. 150-b)), a glass fibre mesh (10 x 10 mm mesh and 110 g/m^2 of nominal mass) and the mechanical fixations (plastic nailed-in anchor (50 mm diameter) were applied (see Fig. 151-b)).

a) b)

Fig. 150 – Wall preparation – Day 1: a) Substrate preparation; b) Application of the 1st layer of TR1.

After 24 hours curing, the second layer of thermal mortar was applied (see Fig. 152). Before the application of the exterior layers, the thermal render was cured for 6 days (see Fig. 153).

a) b) c)

Fig. 151 – Wall preparation – Day 1: a); Regularization of TR1; b) 1st layer of glass fibre mesh application; c) Mechanical fixations application.

a) b)

Fig. 152 – Wall preparation – Day 2: a) Application of the 2nd layer of TR1; b) After TR1 application.

a) b)

Fig. 153 – Wall preparation – Day 8: a) After 3 days curing; b) Profile after 3 days curing.

The second part of the wall preparation consists in the application of the exterior layers: finishing render, reinforcement and coatings. Singular points, as the corners of the wall and the openings, were reinforced with glass fibre mesh (Fig. 154-a);b)) and subsequently the finishing render was applied (Fig. 154-c)). The next step consisted of applying the glass fibre mesh: a first mesh (10 x 10 mm mesh and 110 g/m^2 of nominal mass) covering the all area (Fig. 155-a)) and a central reinforcement of 1 m width with a stronger glass fibre mesh (6 x 6 mm mesh and 330 g/m2 of nominal mass) (Fig. 155-b)).

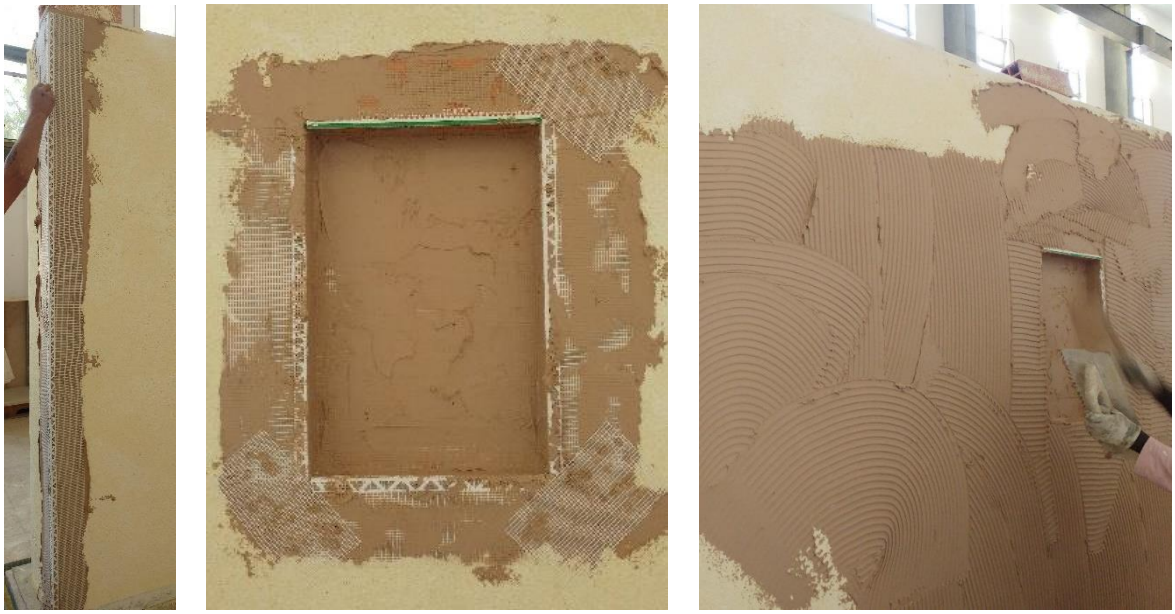

a) b) c)

Fig. 154 – Wall preparation – Day 8: a); Reinforcement of the corners; b) Reinforcement of the opening corners; c) Finishing render (C1) application.

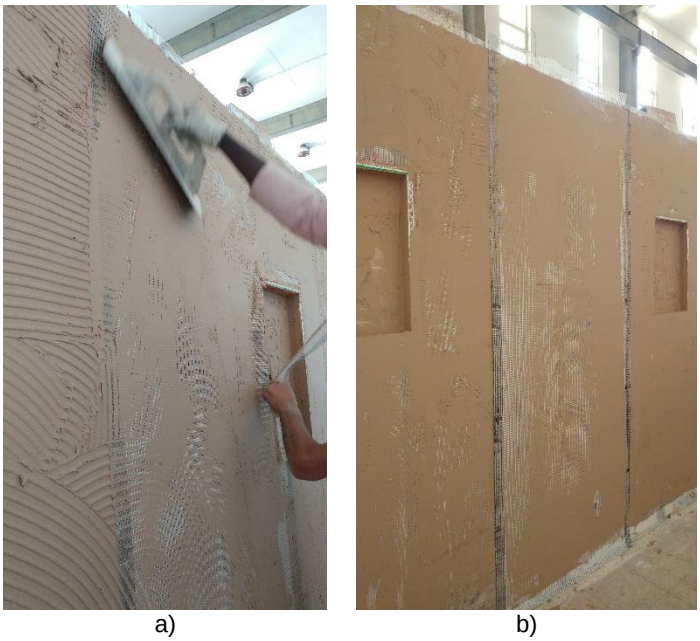

a) b)

Fig. 155 – Wall preparation – Day 8: Application of the: a) 2nd glass fibre mesh; b) Reinforcement mesh (central zone).

After a curing time of 3 days, the two coatings were applied. To evaluate the effect of the ageing in the finishing render, a lower strip of 50 cm height was left without coating application, as shown in Fig. 156-a) and Fig. 158-a). The organic coating was applied in the left half of the wall and the mineral coating on the right side. The organic coating requires the previous application of a key coat (Fig. 156-a)) and after that the organic coating itself.

a) b)

Fig. 156 – Wall preparation – Day 11: Application of S1-O: a) Primer; b) Organic coating.

The mineral coating is applied in a single layer, as demonstrated in Fig. 157-a), with a sand patch finishing aspect (see Fig. 157-b)).

a) b)

Fig. 157 – Wall preparation – Day 11: Application of S1-M: a) Mineral coating; b) Detailed view.

After the application of the two coatings, the wall was submitted to a curing period of 28 days, being the test configuration as demonstrated in Fig. 158.

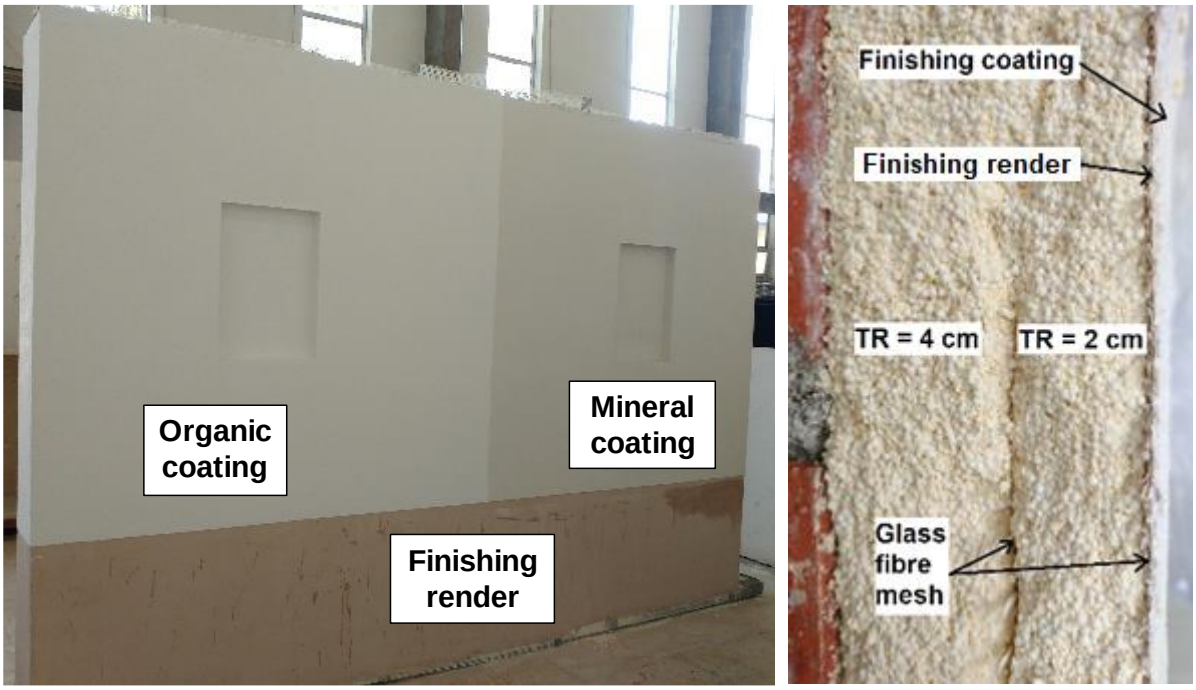

a) b)

Fig. 158 – Wall configuration after curing: a) Face view; b) Profile view.

5.4.2. EXPERIMENTAL RESULTS

Since the two ageing procedures were implemented in the same test wall, after the first procedure (heat-cold) only non-destructive tests could be performed, such as visual observation, liquid water permeability, surface temperature and ultrasonic pulse velocity. The destructive tests were performed after the second procedure (heat-rain).

The dynamic modulus and the flexural and compressive strength tests were only performed in the thermal render since the finishing render does not have the required dimensions to achieve reliable results.

All the experimental tests presented in 5.4.2 were carried out in LNEC, between 13/11/2017 and 16/01/2018.

5.4.2.1. Visual observation

Before any tests, a previous visual observation in order to detect existing damages, after each ageing cycle, was performed.

A general overview of the wall, after heat-cold ageing cycles, is presented in Fig. 159, where no significant deterioration is observed.

However, a closer observation allowed to identify cracks in the corners of the openings in both coatings, as it is demonstrated in Fig. 160 to Fig. 162. The organic coating also presented yellowing of the interior frame of the opening.

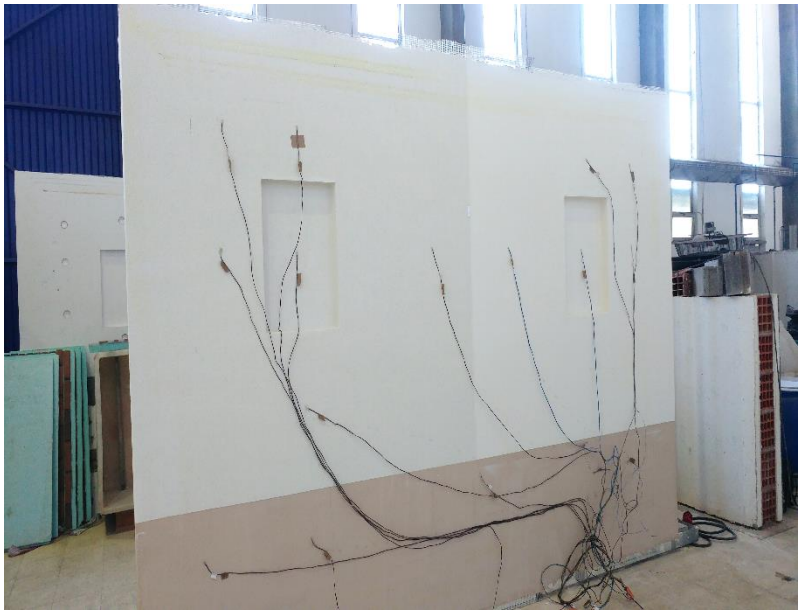

Fig. 159 – Overview of the wall surface, after heat-cold cycles.

a) b)

Fig. 160 – Cracks in the corners of the opening, using organic coating: a) Bottom left corner; b) Upper left corner.

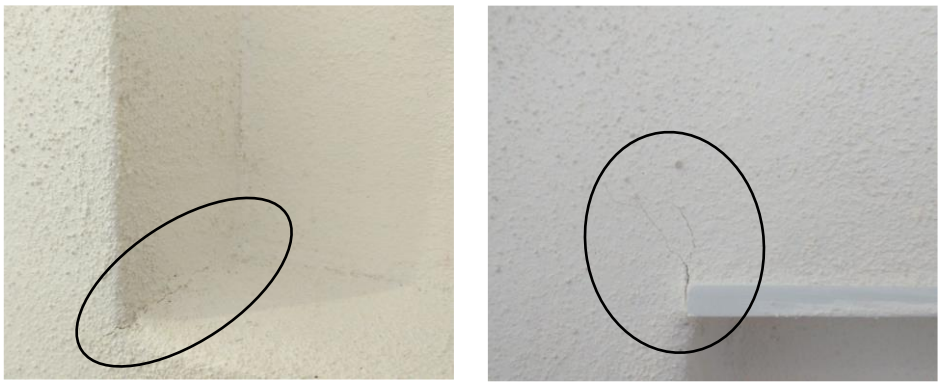

a) b)

Fig. 161 – Cracks in the corners of the opening, using mineral coating: a) Bottom left corner; b) Upper left corner.

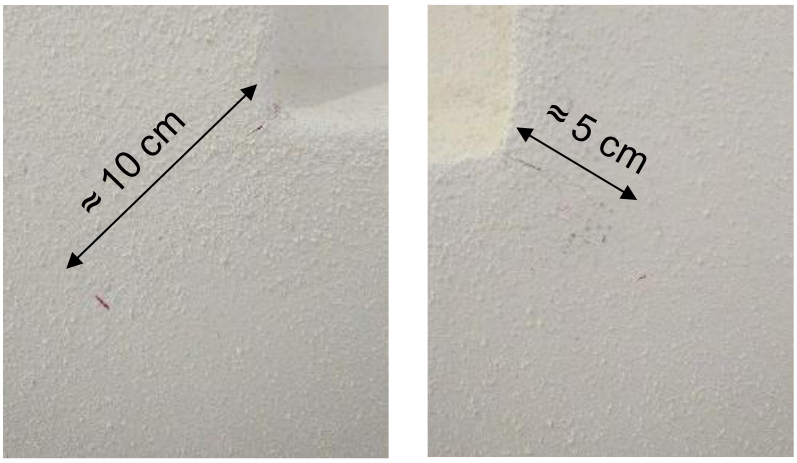

a) b)

Fig. 162 – Cracks in the corners of the opening, using mineral coating: a) Bottom left corner; b) Bottom right corner.

The cracks in the organic coating were shorter and thicker compared to the cracks in the mineral coating, which were, in general, longer and branched. In the mineral coating side, two specific cracks in the bottom corners of the opening were identified, having already 5 to 10 cm length.

After the heat-rain ageing cycles, the wall was completely wet, having the mineral coating a slightly darker colour (yellowing) comparing to the initial aspect (see Fig. 163). The finishing render also presented a darker colour, due to the presence of water.

Fig. 163 – Overview of the wall surface, after heat-rain cycles.

A closer observation, presented in Fig. 164, allowed to identify stains around the opening, in the mineral coating side. Generally, the mineral coating presented more visual degradation.

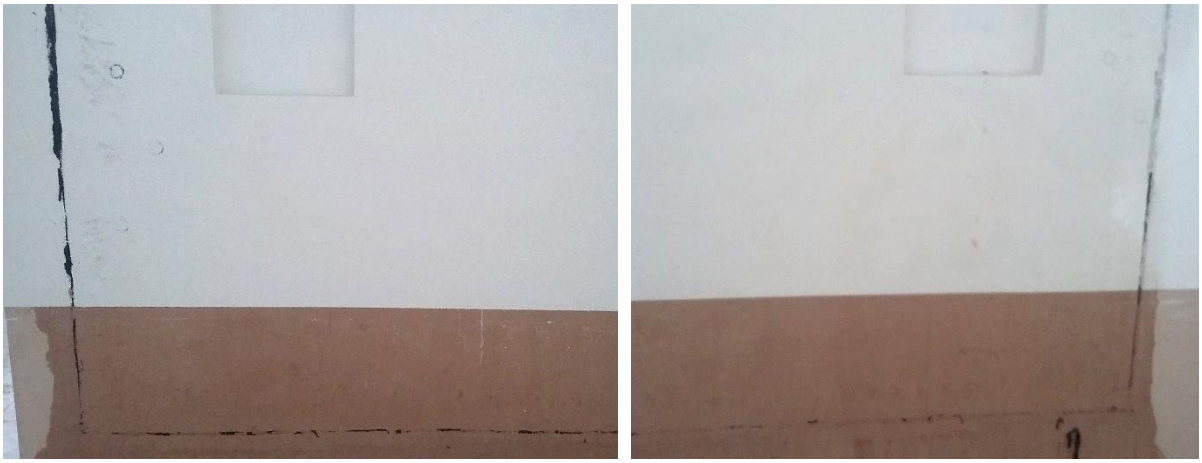

a) b)

Fig. 164 – Overview of the coatings surface, after heat-rain cycles: a) Organic; b) Mineral.

After one week of the end of the hygrothermal cycles, the water drainage allowed for a more realistic observation of the damages.

The organic coating presented less deterioration than the mineral coating since the colour and the previous detected stains and cracks remained constant. The finishing render presented vertical stains, due to the water slurry, while the mineral coating presented highlighted stains around the opening, with higher concentration in the bottom side, as shown in Fig. 165-a).

Regarding the mineral coating, the previously detected cracks became longer and highly dispersed. It was noted that the appearance of stains was related to the development of the microcracks (seeFig. 165-b)), since both stains and microcracks were in the same area.

a) b)

Fig. 165 – Overview of the wall surface, after one week of the end of the heat-rain cycles: a) Whole panel; b) Development of microcracks in the mineral coating side.

5.4.2.2. Liquid water permeability

The liquid water permeability was determined with the Karsten tubes method, as described in 5.2.1. The water permeability of the organic and the mineral coating was measured before and after each ageing procedure, in the current zone. The absorbed water volume was measured after 5, 10, 15, 20, 25, 30, 40, 60 and 120 min. Fig. 166 presents the absorbed water volume in the two coatings before and after the hygrothermal ageing cycles.

As it can be seen, the mineral coating presented, in every stage, a higher water volume and absorption rate than the organic coating. Comparing the two ageing procedures, after the heat-cold ageing the two coatings presented higher absorption than after the heat-rain cycle. The heat-cold cycles promoted high-temperature variation, which may have resulted in the rupture of the materials (such as, cracks in the coating and the capillary net expansion by rupture of air voids), enabling the water to easily penetrate in the system. The reduction of the water absorption after HC+HR, comparing to after HC, may be related to incomplete drying of the wall, which could be observed in 5.4.2.9. This fact could be attributed to the implementation of the tests in d and to the high dependence of the room conditions on the weather, which were cold and humid.

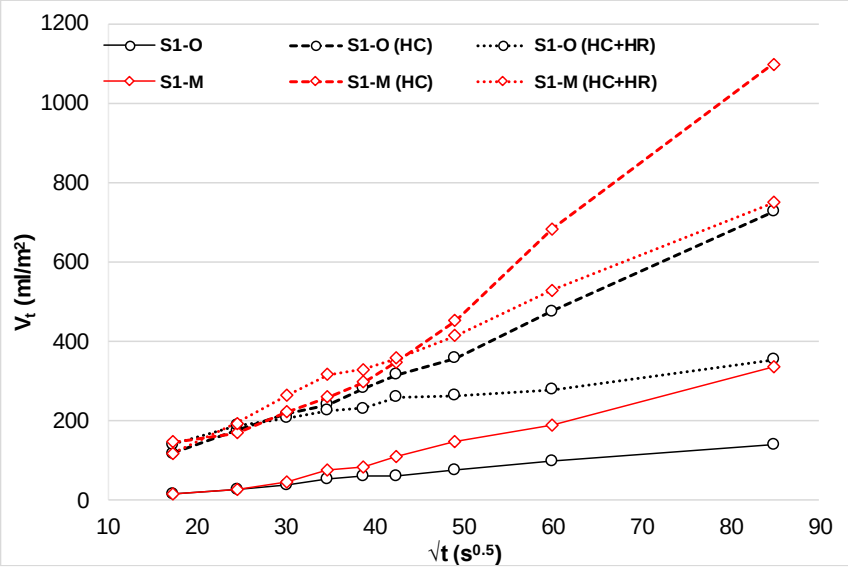

Fig. 166 – Water permeability test results, before and after the hygrothermal cycles (HC+HR), using the Karsten tubes method.

5.4.2.3. Porous structure

To evaluate the effect of the hygrothermal ageing cycles in the several materials, on a microscopic scale, optical microscope images are presented in Fig. 167 to Fig. 171. The images were obtained using the same optical microscope (Olympus SZH10) as previously referred in 3.1.3.2.

Regarding the microstructure of the thermal render in Fig. 167, alterations in the matrix after the hygrothermal ageing cycles were observed. This fact was especially verified when using the mineral coating, as also observed in 5.2.2.4 and 5.2.3.4. The higher water penetration, in the case of the mineral coating, leads to the loss of binder and consequent reduction of intrinsic pores.

When any coating is applied, the microstructure of the thermal render, presented in Fig. 168-a), is similar to the microstructure using the mineral coating, emphasizing the presence of water. Observing the

interface between the exterior thermal render layer and the finishing render, in Fig. 168-b), the two materials show interconnection, but also the absence of linking in some parts (highlighting the possible detachment of the two layers).

a) b) c)

Fig. 167 – Optical microscope images of TR1: a) Before ageing; b) After hygrothermal cycles, with organic coating; c) After hygrothermal cycles, with the mineral coating.

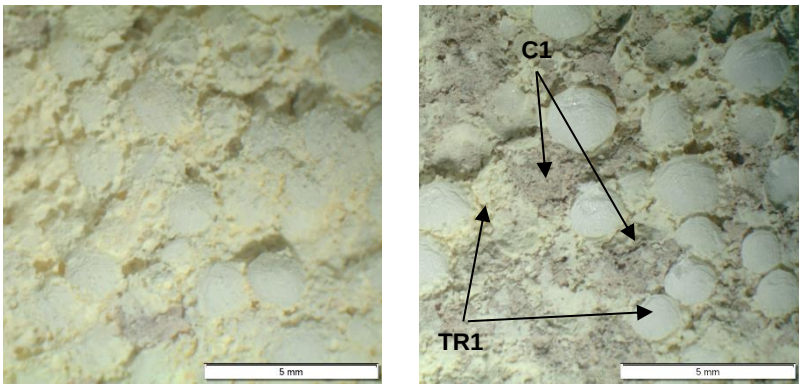

a) b)

Fig. 168 – Optical microscope images after hygrothermal cycles of: a) TR1, only with finishing render; b) Detailed view of the interconnection between TR1 (yellow) and C1 (pink).

Observing the finishing render layer, a colour degradation (discolouration) and a smoothing of the surface is evident. The higher exposition to the artificial "climate" actions, such as the presence of water, allowed by the absence of an exterior coating, explains the higher degradation compared to the initial conditions (see Fig. 169).

Fig. 170 and Fig. 171 present the effect of the hygrothermal ageing cycles in the two analysed coatings, organic and mineral, respectively. Regarding the organic coating, no significant alterations were found. The main observed difference is the increased granular aspect, after ageing, related to the higher action of the ageing procedures (temperature variation and water).

In the case of the mineral coating, the ageing has a more significant impact in the microstructure, also observed in 5.4.2.1. Initially, the mineral coating looks whiter and brighter, as it can be seen in Fig. 171-a). However, after the hygrothermal ageing cycles, the coating is yellowed and matt.

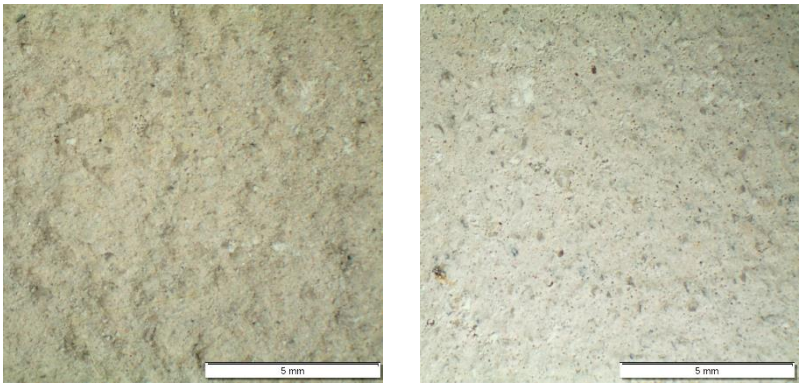

a) b)

Fig. 169 – Optical microscope images of C1: a) Before ageing; b) After hygrothermal cycles.

a) b)

Fig. 170 – Optical microscope images of the organic coating: a) Before ageing; b) After hygrothermal cycles.

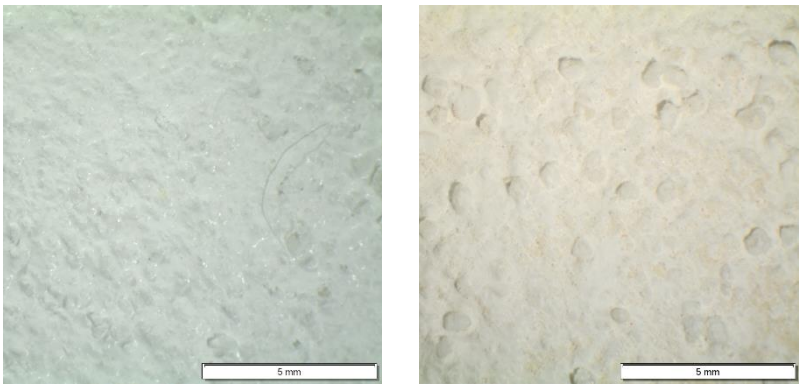

a) b)

Fig. 171 – Optical microscope images of the mineral coating: a) Before ageing; b) After hygrothermal cycles.

5.4.2.4. Surface temperature

The temperature distribution across the wall surface was monitored during the ageing procedures. Type T thermocouples were placed in the different zones of the wall, assessing possible distinct effects (see Fig. 172). The temperatures were recorded in a data logger – model Delta Logger Multi-channel from Delta-T Devices Burwell.

Fig. 172 – Distribution and numbering of the thermocouples.

The surface temperatures recorded during the heat-cold and the heat-rain ageing cycles are presented in Table 111. To an easier comparison of the obtained surface temperatures between the different configurations, the cumulative frequencies are presented in Fig. 173 and Fig. 174. The surface temperatures of each coating – organic (S1-O), mineral (S1-M) and finishing render (C1) –, the absence of thermal render (window/opening zone) and the two distinct reinforced zones – current zone (single mesh current zone) and reinforced central zone (double mesh) are analysed.

As expected, the surface temperature varies between the set-point temperatures of each ageing cycle. The constant temperature periods (heat and cold) represent a significant effect since in a large period of the time the temperature remained constant in each period (40% and 30% of the total time, in the cold and heat periods, respectively). Considering the different configurations and the significant statistic temperature differences, a particular comparison of each case should be performed. Fig. 173 shows the surface temperatures of each coating, in the current zone, considering the heat-cold (Fig. 173-a)) and the heat-rain (Fig. 173-b)) ageing procedures. The organic coating presents a higher temperature amplitude, reaching the lowest and highest temperatures. On the other hand, the mineral coating and the absence of coating (finishing render) resulted in a reduction of more than 4 ºC and 2ºC of the temperature amplitude, respectively. The higher temperature variation may be the origin of brittle fracture and larger cracks, observed in Fig. 160, in 5.4.2.1. The mineral coating may be a good alternative to the organic coating in climates or zones with low rain incidence. Both ageing procedures promote a similar behaviour of the different coatings, being noted approximated temperatures especially in the middle range – 10 to 30 ºC. The three coatings (S1-O, S1-M and C1) present higher variability considering the extreme temperature. That fact highlights that the exterior coating layer could have a significant impact on the durability of the wall systems, particularly in severe climates (high-temperature amplitude).

Table 111 – Surface temperatures during heat-cold ageing cycles.

Ageing		Heat-cold				Heat-rain			
	Description	Av.	Min.	Max	ΔT	Av.	Min.	Max	ΔT
2	S1-O (current)	24.2	-4.8	64.4	69.2	34.5	14.6	67.8	53.1
3		24.1	-4.7	64.1	68.8	34.3	14.8	67.0	52.2
4		24.1	-4.6	63.9	68.5	34.2	14.9	66.6	51.6
5	S1-O (window)	23.6	-3.3	61.1	64.4	32.8	15.8	61.1	45.4
6	C1 (current)	22.7	-4.0	60.4	64.4	31.4	15.3	63.4	48.1
7		23.9	-5.5	65.3	70.8	31.5	15.3	65.0	49.7
8	S1-O (double mesh)	24.0	-3.6	62.0	65.6	32.9	15.5	64.2	48.8
9	C1 (double mesh)	23.9	-4.5	64.3	68.8	31.3	15.2	64.3	49.1
10	S1-O (current)	24.0	-4.6	63.9	68.5	33.9	14.9	66.4	51.5
11	S1-M (current)	24.6	-2.4	61.8	64.3	32.8	15.5	64.3	48.8
12		25.5	-0.7	61.2	61.9	31.6	15.5	62.8	47.3
13	S1-M (double mesh)	23.9	-3.7	62.3	66.0	31.7	15.5	64.6	49.2
14	S1-M (window)	23.6	-2.8	59.7	62.5	30.9	16.0	58.2	42.2
15	S1-M (current)	25.0	-0.8	60.4	61.2	34.1	14.6	67.3	52.7
16		24.3	-5.5	65.3	70.8	32.0	15.4	64.4	49.0
17	C1 (current)	23.2	-3.9	61.9	65.8	31.2	15.2	63.5	48.3
Av.	S1-O (current)	24.1	-4.6	64.0	68.6	34.2	14.8	66.8	52.0
Av.	S1-M (current)	24.8	-2.2	62.0	64.2	32.6	15.4	64.4	49.0
Av.	C1 (current)	23.3	-4.1	62.2	66.2	31.4	15.3	64.0	48.7

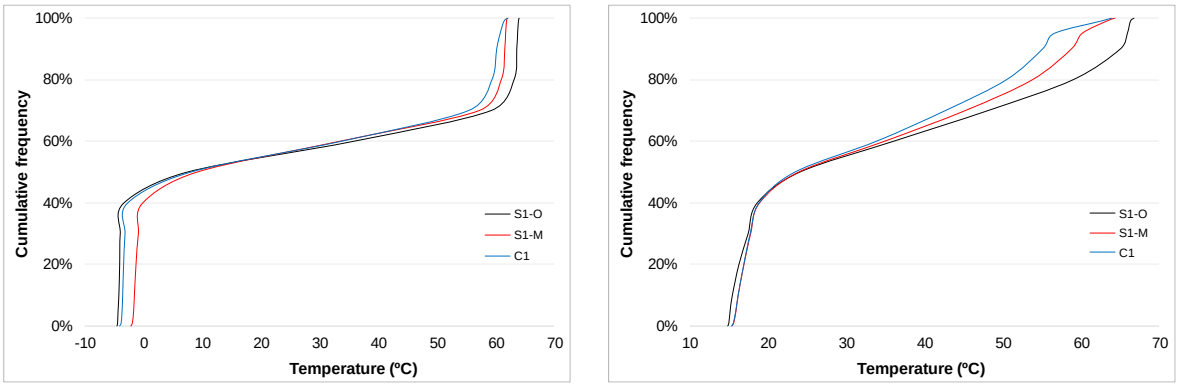

Fig. 173 – Surface temperature cumulative frequencies in the current zone during: a) Heat-cold cycles and b) Heat-rain cycles.

To analyse the effect of the absence of thermal render, the obtained temperatures in each coating are presented separately in Fig. 174.

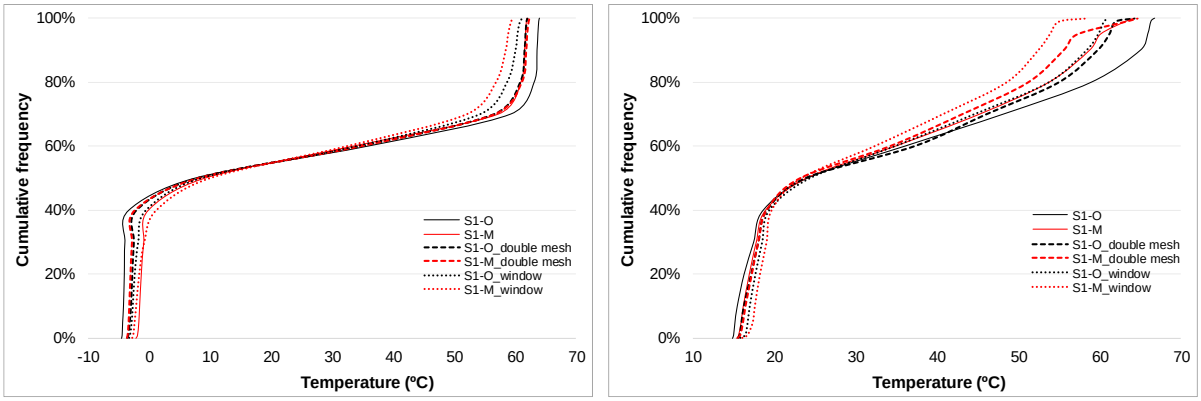

Fig. 174 – Surface temperature cumulative frequencies in the current zone, reinforced zone and openings during: a) Heat-cold cycles and b) Heat-rain cycles.

Regarding Fig. 174, both coatings in current zone presented higher amplitude than in the reinforced zone and the opening (without thermal render), which is explained by the higher thermal transmission (U), considering the steady state reached in each period (heat or cold). As explained by equation (32), considering the summer period (T_e>T_i), the higher the thermal transmission the lower the surface temperature (T_{se}).

$$T_{se} = T_e - U \cdot R_{se}(T_e - T_i) \tag{32}$$

Where R_{se} is the exterior surface resistance. As such, the temperature dissipation rate is different for each configuration, being visible the discontinuities introduced by the meshes and openings.

In every coating, the heat period (from both heat-cold and heat-rain cycles) promotes higher variability, considering the different configurations, than the cooling period (from both heat-cold and heat-rain cycles). In that way, the thermal shock effect may lead to an increase the differences among the analysed zones and consequently the thermal stresses.

In order to give a general overview of the temperatures on the entire surface, thermographic imaging was performed, right after the end of the heat-cold cycles. The images were taken with an infrared camera (640x480 pixels), model ThermaCAM P640 from FLIR Systems.

Fig. 175 presents an overview of the entire wall, after the heat-cold cycles, being visible the effect of the different configurations in the surface temperature. As verified before, the organic coating presents a higher temperature than the mineral coating. The double mesh zone and the openings are clearly distinguished by the lighter colours (yellow/orange), corroborating the previous conclusions on the thermal delay effect (greater in these particular areas with higher thermal transmission).

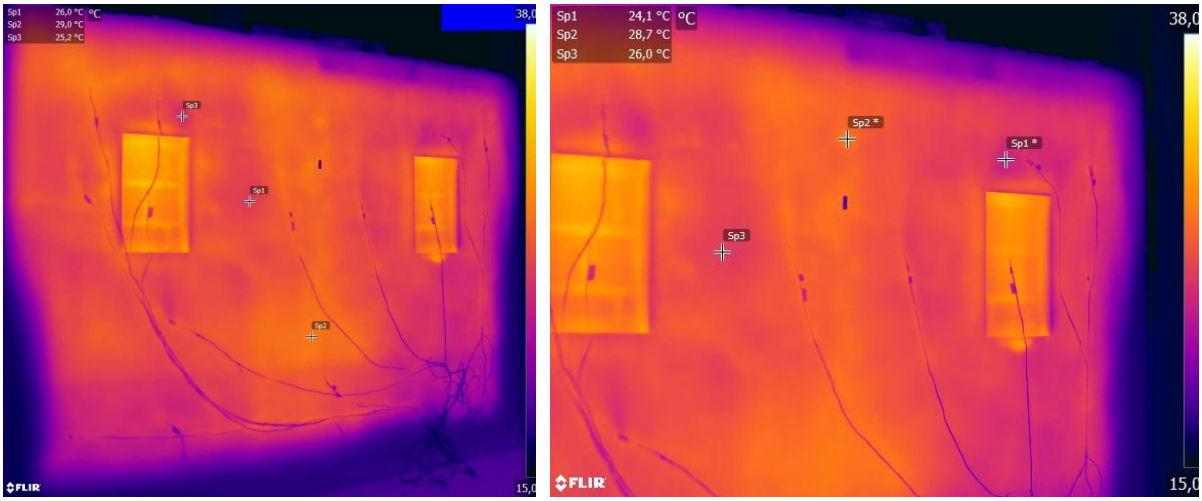

(a) (b)

Fig. 175 – Thermograms after heat-cold cycles: a) General overview; b) Expanded view.

Regarding Fig. 176, higher temperatures around the openings are observed. In the mineral coating, the bottom area of the opening presents higher temperature (more than 3 ºC) than the rest of the contour. It was also at the bottom of the window where the higher concentration of microcracks was observed (see Fig. 165).

The several observed discontinuities in terms of surface temperature may contribute to increase the stresses between them and consequently the cracking.

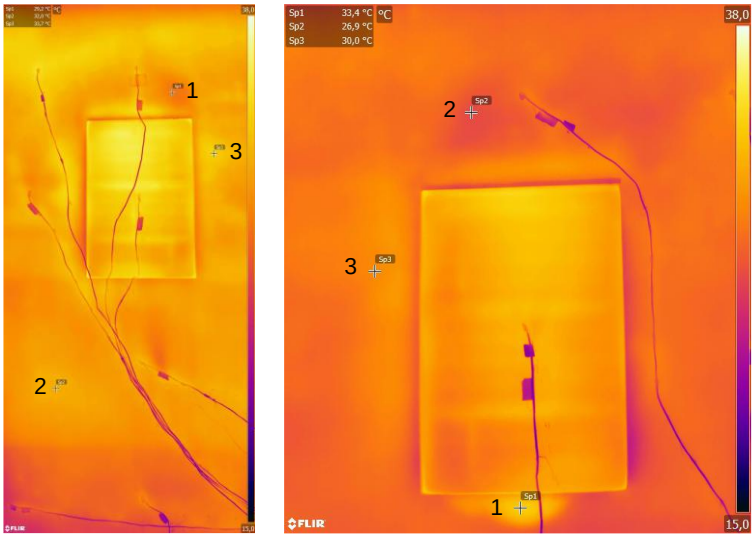

a) b)

Fig. 176 – Thermograms of the opening zone, after heat-cold cycles, with: a) Organic coating; b) Mineral coating.

5.4.2.5. Ultrasonic pulse velocity

The ultrasonic pulse velocity can be determined by a non-destructive test, carried out according to FE Pa 43 – "Mechanical characteristics assessment by ultrasound measurement" (LNEC 2010a). To determine the ultrasound propagation velocity, it is, therefore, necessary to determine the path crossed by the ultrasound wave and the time it took to perform it (between the transmitter and the receiver), being the velocity given by the ratio between the two parameters. As such, different types of wave transmission that depend on the position of the transducers may be used. In the present experimental procedure an indirect transmission was applied, using the Steinkamp Ultrasonic BP-7 Tester (see Fig. 177-a)), and two transducers placed on the opposite faces of the specimen, as demonstrated in Fig. 177-b).

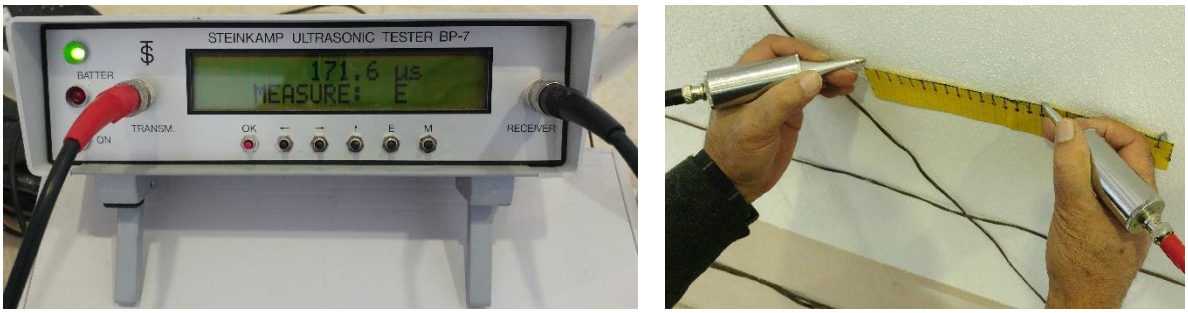

a) b)

Fig. 177 – Measurement of the ultrasonic pulse velocity: a) Tester; b) Transducers and scale.

The time that the ultrasound waves take to range the distance between the transducers is therefore plotted, being the ultrasonic pulse velocity given by the slope of the linear regression. Discontinuities in the linear plotting of the several measurements could mean microcracks or alterations in the microstructure. Fig. 178 to Fig. 180 present the distance between the transducers as a function of the time, obtained in the three coatings (S1-O, S1-M and C1) in the current and reinforced zone.

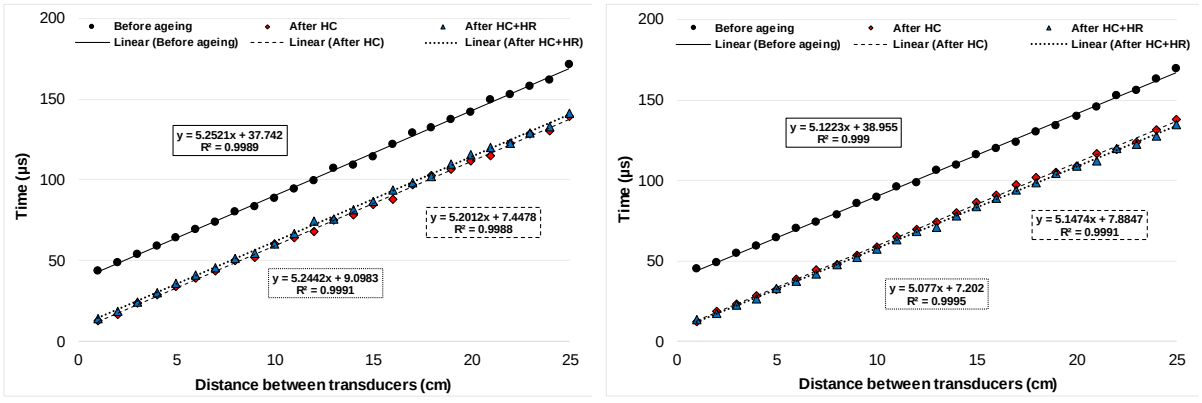

a) b)

Fig. 178 – Ultrasonic pulse velocity test: distance vs. time, obtained in the organic coating in: a) Current zone; b) Reinforced zone (double mesh).

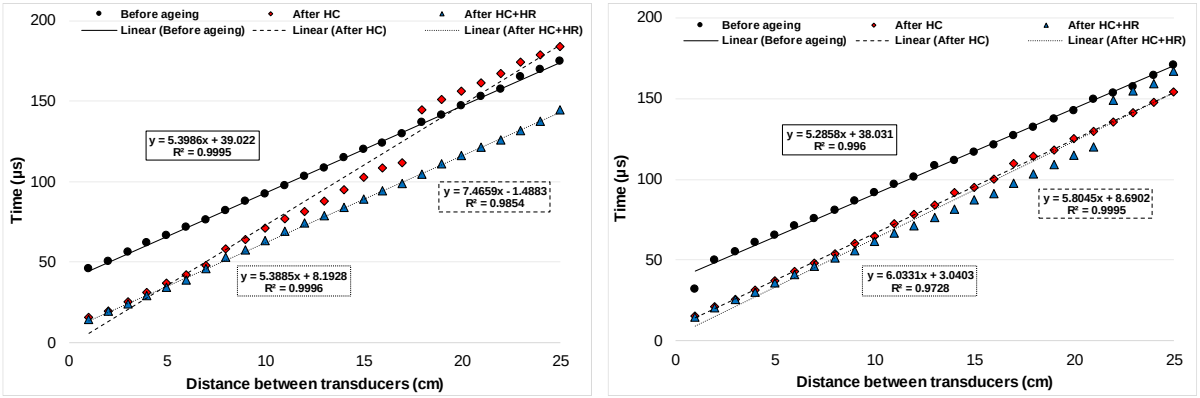

a) b)

Fig. 179 – Ultrasonic pulse velocity test: distance vs. time, obtained in the mineral coating in: a) Current zone; b) Reinforced zone (double mesh).

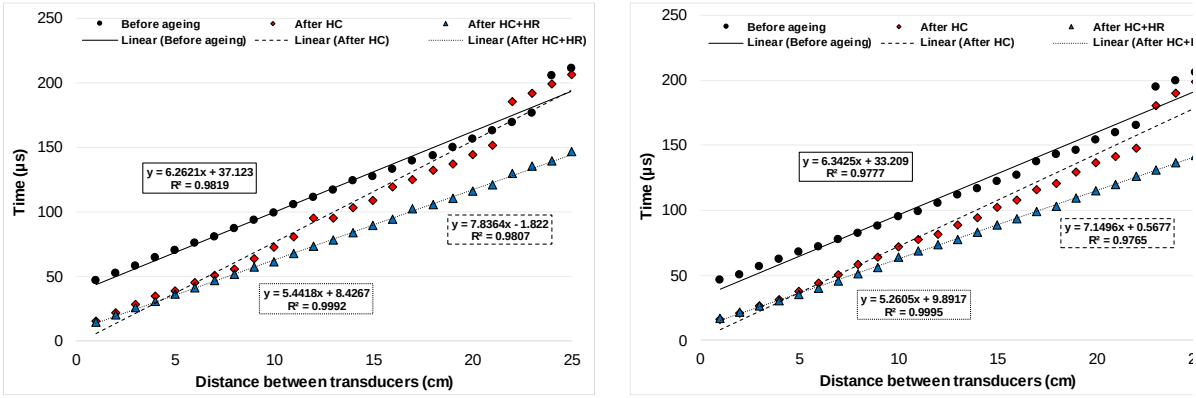

a) b)

Fig. 180 – Ultrasonic pulse velocity test: distance vs. time, obtained in the finishing render in: a) Current zone; b) Reinforced zone (double mesh).

The organic coating presented a similar behaviour regarding the current and the reinforced zone and no discontinuity was observed. Regarding the mineral coating and the finishing render, discontinuities after ageing were recorded. Those discontinuities result from a localised decrease of the propagation velocity, which could mean the existence of microcracks (in the coating) or air voids/areas with detachment between the layers. That fact corroborates the previous findings, which suggest that the organic coating presents more stability to the ageing procedures. On the contrary, the mineral coating and the absence of any coating (finishing render) allow the agents to promote higher degradation, such as generalized microcracking.

Fig. 181 presents the ultrasonic pulse velocity, obtained through the slope of the linear regressions, before and after heat-cold (HC) and heat-rain (HC+HR) ageing cycles.

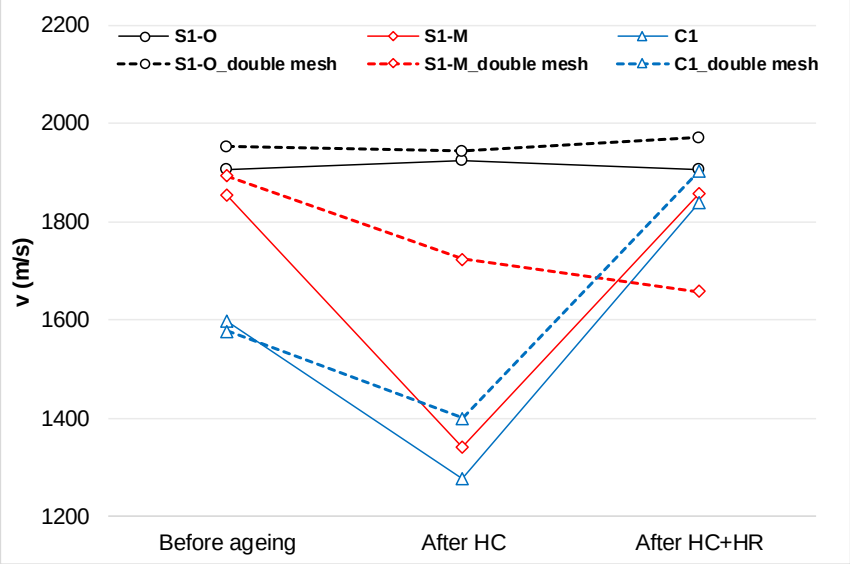

Fig. 181 – Ultrasonic pulse velocity before and after hygrothermal ageing cycles.

Similar velocity before and after ageing (HC+HR) using the mineral coating can be observed, as referred before. In general, the velocity in the reinforced zone is higher than in the current zone, which could be related to the increase of strength and compaction given by the double glass fibre mesh.

Regarding the mineral coating and finishing render, a trend can be observed, excepting S1-M in the reinforced zone. After heat-cold cycles, due to the high-temperature amplitude and the different thermo-mechanical properties of the materials, the formation of superficial microcracks and the rupture of the matrix microstructure are expected. This fact is in line with the reduction of the propagation velocity after heat-cold ageing cycles. On the other hand, after the heat-rain cycles, the water action contributes to the hydration of the binder (particles that were not hydrated), after the initial hardening, contributing to an increase of the mechanical strength (Zhang et al. 2018), resulting in greater propagation velocity. This effect seems to point out to some self-healing of the microcracks.

5.4.2.6. Dynamic modulus

To evaluate the effect of the hygrothermal ageing cycles in the elastic properties of the thermal render the dynamic modulus was determined. The measurements were carried out according to the fundamental resonance frequency test method described in 3.1.4.1. Fig. 182 presents the dynamic modulus before and after the hygrothermal ageing cycles.

In both coatings, the dynamic modulus increases after ageing, which means that the thermal render becomes more rigid, due to the strengthening and also to the late hydration of the binder. Following the previous statements, the dynamic modulus results present similar behaviour. After ageing, the thermal render with the mineral coating presents a dynamic modulus 62% higher than the thermal render with the organic coating, resulting from the higher water absorption due to higher microcracking rate. The lower the dynamic modulus the more elasticity and capacity of the material to absorb dimensional variations. Becoming the thermal render with mineral coating less flexible, the stresses increase and consequent cracking occurs.

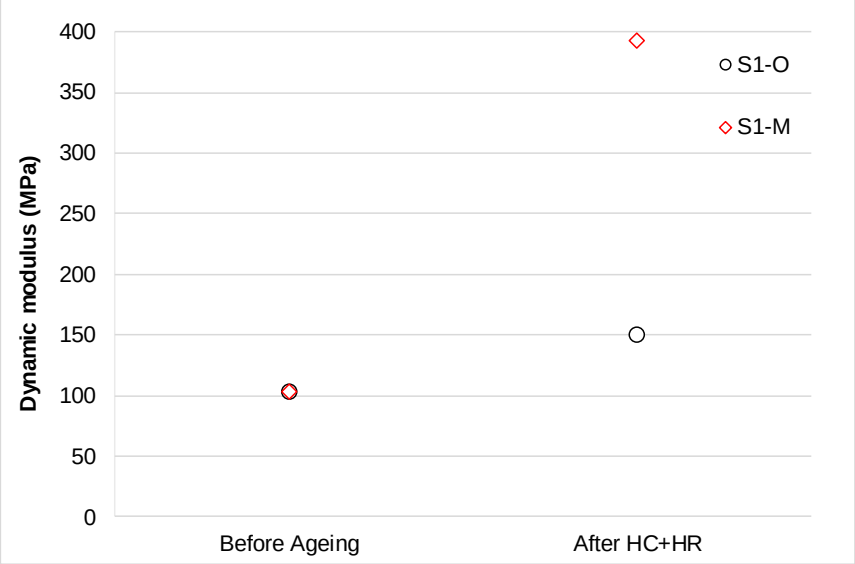

Fig. 182 – Dynamic modulus of TR1, with organic and mineral coatings, before and after hygrothermal ageing cycles.

Regarding Fig. 165, the mineral coating presents a higher occurrence of cracking than the organic coating. However, the lower elastic modulus presents greater advantages if the mechanical strength is not compromised. As such, the obtained results should be analysed as a whole in order to evaluate the effective mechanical strength.

5.4.2.7. Flexural and compressive strength

To evaluate the effect of the hygrothermal ageing cycles in mechanical strength of the thermal render the flexural and compressive strength were determined. Due to the deterioration of the thermal render with the mineral coating, it was only possible the collection of 2 samples. The measurements were carried out according to the test method described in 3.1.4.2. Table 112 presents the flexural and compressive strength after the hygrothermal ageing cycles (HC+HR) and Fig. 183 the results before and after ageing.

Table 112 – Flexural and compressive strength results.

Coating	R_{flex}* (MPa)		R_{comp}*(MPa)	
Property	Organic	Mineral	Organic	Mineral
TR1	0.12±0.072	0.11±0.044	0.20±0.042	0.29±0.085

* Results presented as (average ± standard deviation)

As expected, the flexural strength is similar using the two coatings. However, the compressive strength is around 45% higher using the mineral coating, which is in accordance with the previous findings, due to the strengthening of the thermal render, resulting from the additional hydration enabled by microcracking of the mineral coating.

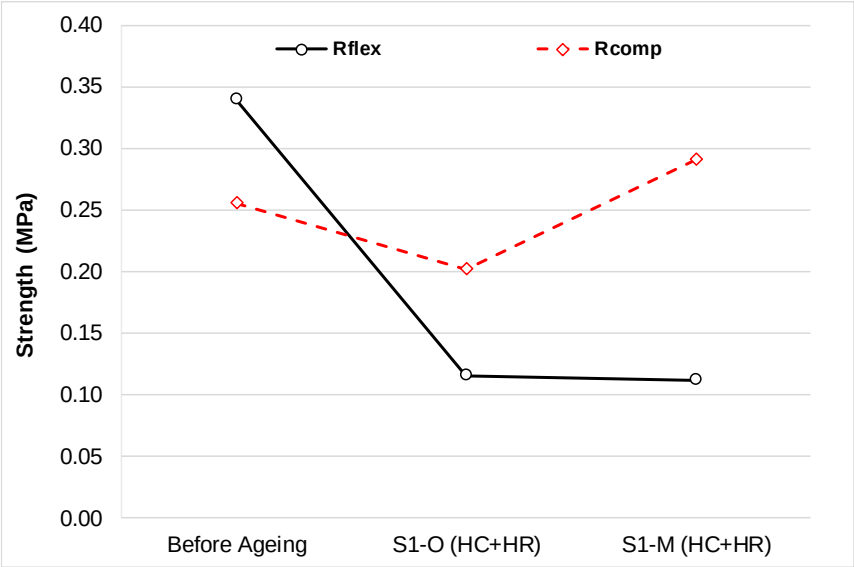

Fig. 183 – Flexural and compressive strength in TR1, with organic and mineral coatings, before and after hygrothermal ageing cycles.

Regarding the results before ageing, the flexural strength presents a higher decrease after ageing – around 66% and 67% using organic and mineral coating, respectively. The embrittlement of the matrix and loss of cohesive connection between the materials contribute to that significant reduction. On the other hand, the compressive strength presents an opposite trend in both coatings. Since the organic coating is less permeable than the mineral coating, the water action has a significant impact in the previous one, resulting in the increase of the compressive strength (due to the later hydration of the binder and the strengthening of the matrix). The thermal render with the organic coating keeps its porous structure more stable after ageing, which allows lower compressive strength.

Despite the increase of the compressive strength using the mineral coating, the results still do not fit the EN 998-1 requirements.

5.4.2.8. Adhesive strength

In order to have an extensive analysis of the mechanical strength after the implementation of hygrothermal ageing cycles, the adhesive strength of the thermal rendering systems was determined. The measurements were carried out according to the test method described in 3.1.4.3. Five circular pre-cuts were performed, using a core drilling machine (see Fig. 184-a)), in each coating (S1-O, S1-M and C1) considering the current and reinforced zone. The testing machine is a dynamometer CONTROLS C 215/D with manometer with a scale 0 to 5 kN with resolution 50 N, as shown in Fig. 184-b).

Due to the constraints related to the samples pre-cutting (rupture of the samples when performing pre-cuts to the substrate), the adhesive strength will be analysed only between the thermal render and exterior layers (pre-cut to the thermal render) (see Fig. 185). Studies on the effect of the type of pre-cut showed similar results for circular and square pre-cuts (Costa et al. 2007; Gonçalves 2004).

Table 113 to Table 115 present the adhesive strength and failure pattern after the hygrothermal ageing cycles.

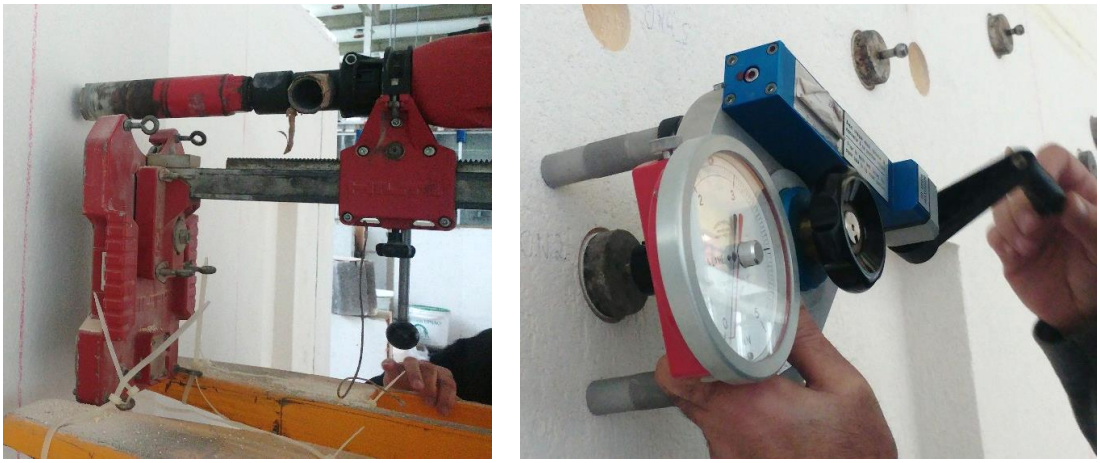

a) b)

Fig. 184 – Adhesive strength test apparatus: a) Core drilling machine; b) Testing machine.

a) b)

Fig. 185 – Pre-cut into the substrate: a) Cutting zone; b) Resulting specimen.

Generally, the ruptures were cohesive inside the thermal render, with the exception of one specimen using the mineral coating, where a deficient curing of the glue was observed.

Regarding the ETAG 004 requirements, the thermal render fits the adhesion requirements. Despite de lower values (≤ 0.08 MPa in most of the cases), the test results are considered admissible, due to the cohesive rupture inside the thermal render.

For an easier analysis, Fig. 186 presents the single and average adhesive strength values.

Table 113 – Adhesive strength and fracture patterns obtained in S1-O, after the hygrothermal ageing cycles.

Zone	Current		Reinforced	
Measurement	Adhesive strength (MPa)	Fracture pattern	Adhesive strength (MPa)	Fracture pattern
1	0.126		0.076	
2	0.076		0.076	
3	0.126		0.088	
4	0.000*		0.025	
5	0.126		0.050	
Average	0.091	100% cohesion in the TR itself	0.063	100% cohesion in the TR itself

*Rupture by attachment of the test machine

Table 114 – Adhesive strength and fracture patterns obtained in S1-M, after the hygrothermal ageing cycles.

Zone	Current		Reinforced	
Measurement	Adhesive strength (MPa)	Fracture pattern	Adhesive strength (MPa)	Fracture pattern
1	0.050		0.000*	
2	0.000*		0.076	
3	0.050		0.000	
4	0.050		0.050	
5	0.000*		0.076	
Average	0.030	100% cohesion in the TR itself	0.040	1 to 4: 100% cohesion in the TR itself; 5: 50% cohesive in the coating and 50% adhesive in the glue-coating interface

*Rupture by attachment of the test machine

Table 115 – Adhesive strength and fracture patterns obtained in C1, after the hygrothermal ageing cycles.

Zone	Current		Reinforced	
Measurement	Adhesive strength (MPa)	Fracture pattern	Adhesive strength (MPa)	Fracture pattern
1	0.076		0.000*	
2	0.126		0.000*	
3	0.050		0.126	
4	0.076		0.050	
5	0.101		0.076	
Average	0.086	100% cohesion in the TR itself	0.051	100% cohesion in the TR itself

*Rupture by attachment of the test machine

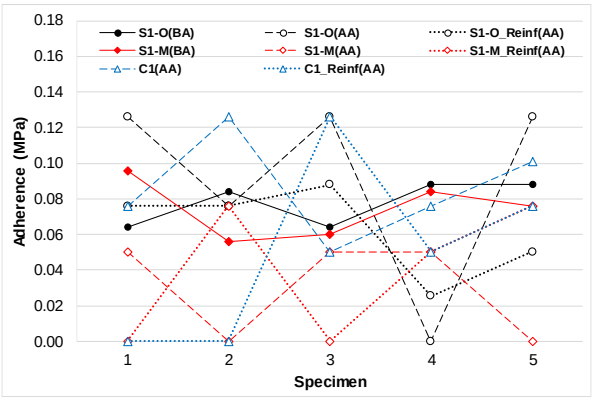

a)

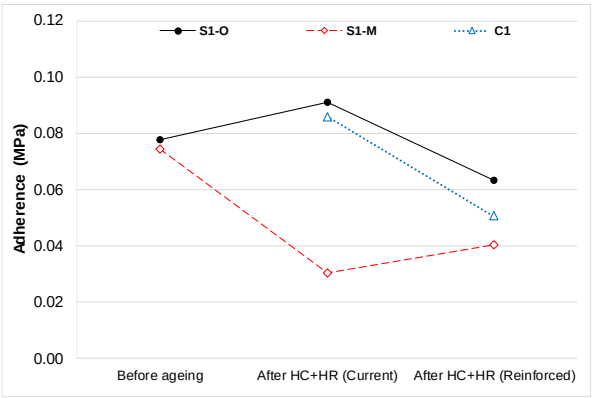

b)

Fig. 186 –Adhesive strength of thermal rendering systems before (BA) and after ageing: a) Single values; b) Average values.

The embrittlement of the thermal render in the mineral coating system, contributes to the considerable reduction of the adhesive strength, due to the rupture of some specimens during the attachment of the test machine. In contrast, the organic coating allows a lower variation of the adhesive strength, which may indicate that the materials keep their properties during more time. The difference between the current and the reinforced zone may be related to the heterogeneity of the thermal render.

The finishing render presents higher values than the observed with the mineral coating. This could be a consequence of the later hydration of the binder in the test area.

As expected, the glass fibre mesh did not directly contribute to the increase of the adhesive strength.

5.4.2.9. Water content

After performing the destructive tests, the thermal render with mineral coating presents a darker colour and embrittlement, referring to the presence of water, as shown in Fig. 187.

a) b)

Fig. 187 – Aspect of the thermal render after the hygrothermal ageing with: a) Organic coating and b) Mineral coating.

In that way, samples were collected in order to analyse the water content in the thermal render at that time (about a week after the ageing cycles completion). To determine the water content, the samples were placed in an oven, at 70ºC, until complete drying. Table 116 presents the water content variation after 24h, 48h, 72h and 96h and the total water content in each material, at that time.

Table 116 – Water content variation after one week of the end of the hygrothermal ageing cycles.

Time	Organic coating			Mineral coating		
(h)	TR1	C1	S1	TR1	C1	S1
24	6.08%	1.13%	3.73%	10.01%	1.55%	8.18%
48	0.07%	0.05%	0.00%	0.15%	0.13%	0.07%
72	0.00%	0.00%	0.00%	0.00%	0.05%	0.04%
96	0.00%	0.01%	0.00%	0.00%	0.00%	0.00%
w (kg/kg-%)	6.2	1.2	3.7	10.1	1.7	8.3
w (kg/m^3)	12.0	14.3	—	19.8	20.7	—

As expected, the mineral coating samples present higher water content in all the materials and in the whole analysed system (S1). That fact is in accordance with the previous conclusions.

5.4.2.10. Impact resistance

In order to evaluate the effect of the reinforcement, after the implementation of hygrothermal ageing cycles, the impact resistance was analysed. The measurements were carried out according to the test method presented in EN 13497 (CEN 2002b), using the *Martinet Baronnie* apparatus, considering 3 and 10 J impact energies (see Fig. 188).

a) b)

Fig. 188 – Martinet-Baronie apparatus, with impact energy of: a) 3 Joules; b) 10 Joules.

Table 117 and Fig. 189 present the average dent diameter in each coating (S1-O, S1-M and C1) considering the current and reinforced zones, after the hygrothermal ageing.

Table 117 – Average dent diameter of the hard body impact, after hygrothermal ageing cycles.

Impact energy	3J* (mm)		10J* (mm)	
Zone	Current	Reinforced	Current	Reinforced
S1-O	20.6±0.89	17.8±1.30	39.6±2.30	39.0±2.45
S1-M	24.0±2.24	19.6±1.67	42.60±2.70	37.6±2.07
C1	22.0±0.71	20.0±1.22	47.4±2.30	40.2±7.29

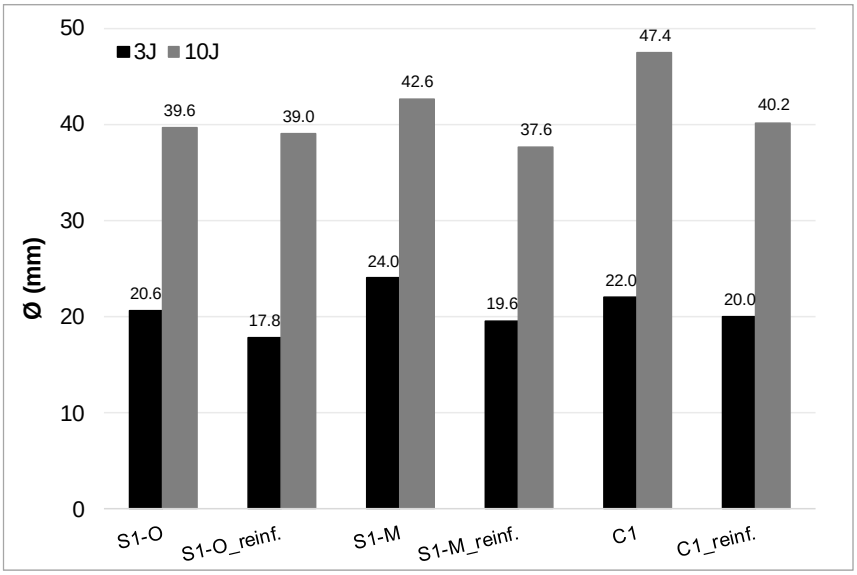

Fig. 189 – Average dent diameter after hygrothermal ageing cycles.

The dent diameter is significantly reduced regarding the reinforced zone, which was expected. Beyond the quantitative analysis, by the dent diameter measurement, a qualitative analysis by means of any observed damages is performed. In that way, Table 118 to Table 120 present the observed damages in the different systems, before and after the ageing procedures.

In general, the thermal rendering systems present more damages, like cracking and detachment, in the current zone. Also, a significant reduction in the depth of the depression is verified in the reinforced zone. The organic coating results in larger cracks and complete perforation (being the finishing render visible), especially with 10J energy impact. While the mineral coating does not allow perforation, resulting in microcracks. However, higher depressions, detachment and loss of material, with the mineral coating, is observed. The large cracking and damages in the finishing render reinforce the importance of the application of exterior coatings, conferring greater impact resistance of the whole system.

Table 118 – Visual observation of the dent obtained by hard body impact in S1-O, after hygrothermal ageing cycles.

Zone	Current		Reinforced	
Impact energy	3J	10J	3J	10J
1				
2				
3				
4				
5				
Visual observation	Circular cracking, without total rupture of the coating	Circular cracking, with a total rupture of the coating	Circular cracking, without total rupture of the coating	Circular cracking, without total rupture of the coating

Table 119 – Visual observation of the dent obtained by hard body impact in S1-M, after hygrothermal ageing cycles.

Zone	Current		Reinforced	
Impact energy	3J	10J	3J	10J
1				
2				
3				
4				
5				
Visual observation	Circular cracking, without total rupture of the coating (expecting 5)	Circular cracking, with a total rupture of the coating; detachment; large depression	Circular cracking, without total rupture of the coating	Circular cracking, with a total rupture of the coating; detachment; slight depression

Table 120 – Visual observation of the dent obtained by hard body impact in C1, after hygrothermal ageing cycles.

Zone	Current		Reinforced	
Impact energy	3J	10J	3J	10J
1				
2				
3				
4				
5				
Visual observation	Circular cracking, with total rupture	Significant circular cracking, with a total rupture of the coating; detachment; large depression	Circular cracking, with a total rupture of the coating	Circular cracking, with a total rupture of the coating; detachment; slight depression

Regarding the ETAG 004 classification (EOTA 2013), an adaptation to the thermal rendering systems is presented in Table 121.

Table 121 – Thermal rendering systems classification according to hard body impact, based on the ETAG 004 requirements.

Procedure	Before ageing		After hygrothermal ageing cycles		Category
Impact energy	3J	10J	3J	10J	
S1-O	Rendering not penetrated	Rendering perforation	Rendering not penetrated	Rendering perforation	III
S1-M	Rendering not penetrated	Rendering perforation; delamination	Rendering not penetrated	Rendering perforation; delamination	III
C1	Rendering perforation				—

The application of the exterior coatings, both mineral and organic, allow the increase of impact resistance. Nevertheless, the performance is still limited, corresponding to category III defined in ETAG for ETICS.

5.5. ANALYSIS OF THE IMPLEMENTED DURABILITY ASSESSMENT METHODOLOGIES

5.5.1. EXPERIMENTAL METHODOLOGIES FOR THE DURABILITY ASSESSMENT

In the previous chapters, different accelerated ageing procedures and their applicability to thermal rendering systems were evaluated.

Regarding the configuration of the specimens, the different ageing procedures – both the existing and the developed hygrothermal cycle – present some problems and constraints, which affect the obtained results. The execution of the specimens as the systems are applied on-site was considered of major importance since different configurations of the same systems led to different results. This fact was also verified by Torres, Veiga and Freitas (2018), highlighting the influence of the substrate characteristics (such as the porosity and the water absorption) on the properties of the mortars. The application of two layers of thermal render and glass fibre mesh introduced an interface, where the fracture occurred when analysing the adhesive strength. Beyond the configuration of the different layers, also consistent thicknesses should be guaranteed, in order to produce results more reliable.

Despite the easier production of the small-size samples, such as the used in the existing methodologies, they introduced more variables that may distort the results. On one hand, the need of sealing the sides of the specimens and their handling during the different ageing procedures (such as the freezing-thawing) increase the risk of damages in the thermal rendering system layers. That fact may distort the results, overstating the damages. On the other hand, the small-scale samples allow a quicker activation of the degradation mechanisms, such as the freeze-thawing, since the materials are directly and constantly submitted to the water action, which does not happen in the real-scale specimens (wall). However, a faster ageing by intensifying the degradation agents may activate other degradation mechanisms, distorting the expectable degradation.

Regarding the different performed ageing procedures and experimental tests, significant conclusions of the thermal rendering systems durability were drawn.

The durability evaluation of the gypsum-based materials, suitable for the interior application, was little explored. However, considering the envisaged ageing procedures (heat-freezing+humidification-freezing), a quite significant decrease in durability was observed, despite the short ageing period. This states the importance of an accurate analysis of the durability in every system, even in less severe environments (indoor application), without liquid water action (humidification procedure). However, future developments concerning this application should be performed, since the heat-freezing cycles described in EN 1015-21 and implemented in the thermal plastering system do not represent usual interior conditions.

Since the thermal renders generally present higher water absorption compared with insulations, such as EPS (almost impermeable), the exterior layers (finishing coating+finishing render) proved to have a relevant impact in the durability of the inner layers, acting as a barrier. In that way, the durability assessment should take into account the entire system and the more relevant properties of the materials to each ageing procedure that they are subjected to. Fig. 190 to Fig. 192 present the effect of the different ageing procedures (before ageing (BA), heat-freezing+humidification-freezing (HF+HumF), freeze-thawing (FT), heat-cold (HC) and heat-rain (HC+HR) cycles) in the two coatings (organic and mineral), regarding the water permeability, adhesive strength and impact resistance, respectively.

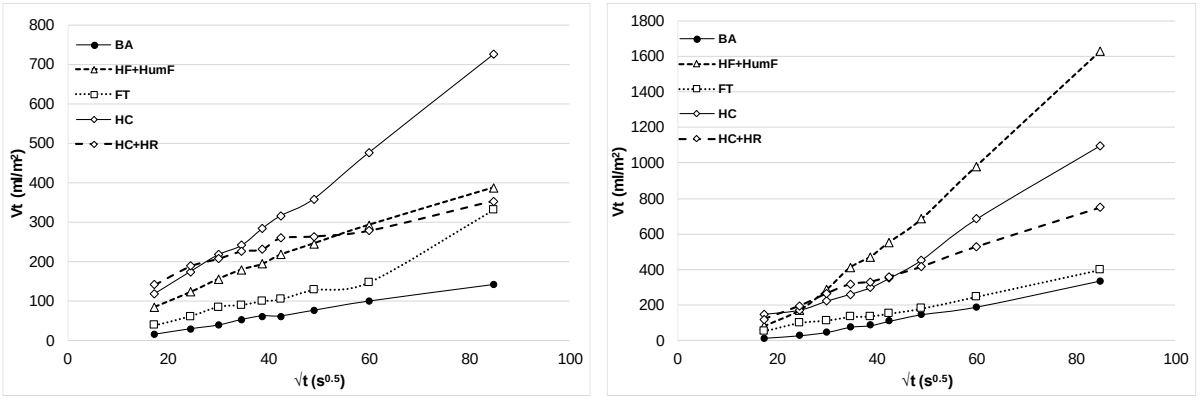

(a) (b)

Fig. 190 – Water permeability, determined with Karsten tubes method, after ageing procedures with: a) Organic coating and b) Mineral coating.

As shown in Fig. 190, the two coatings present a completely different behaviour; the water absorbed by the mineral coating more than doubles the amount absorbed by the organic coating. Furthermore, the ageing procedures produce distinct degradation levels on both coatings.

The heat-rain cycles, applied after the heat-cold cycles, result in a higher amount of absorbed water comparing to after the heat-cold cycles. The water action contributes to the compaction of the matrix of the materials reducing the water absorption capacity, while the high-temperature variation in the heat cold cycles, promotes cracking in the coating, enabling the water to easily penetrate in the system. As such, the liquid water permeability should be analysed in combination with other durability tests, since lower values may distort the degradation level. The procedures applied in the small-size specimens (HF+HumF and FT) showed that the severity of the freeze-thawing contributes to the matrix consolidation and consequent reduction of absorbed water but it also produced some cracking of the interface between materials and light aggregates. In addition, the tests were performed after a conditioning period (at least one week), at room conditions. However, the materials may not be completely dried, as it was demonstrated in 5.4.2.9, which reduces the absorbed volume.

Fig. 191 shows the influence of the different ageing procedures in the adhesive strength of the two coatings.

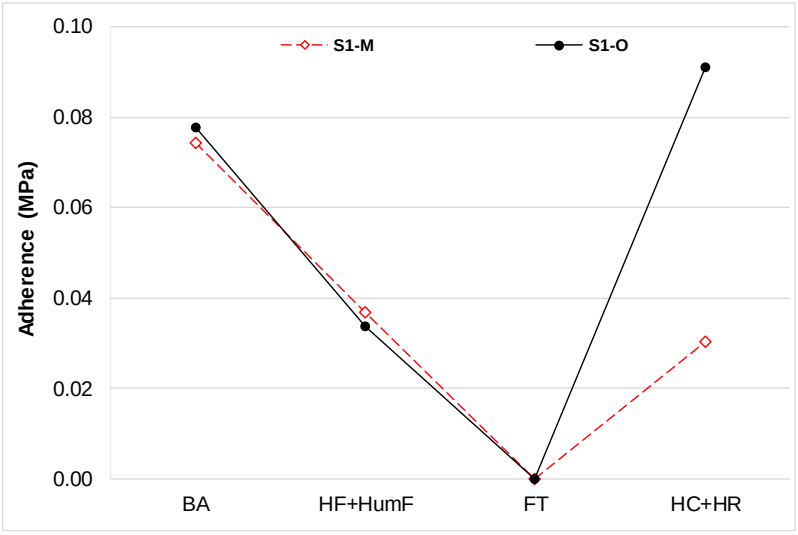

Fig. 191 – Adhesive strength of thermal rendering systems, after the ageing procedures.

Regarding the small size samples, the two coatings present similar adhesive strength. However, as long as the pre-cuts are different as well (until de substrate or into the TR), the hygrothermal cycles (HC+HR) result in different adhesive strength in both coatings. As already referred in 5.2.4, circular and square pre-cuts showed similar results (Gonçalves 2004; Costa et al. 2007), highlighting a small influence of the geometry of the pre-cut. The damages observed in the sealant and coating of the small samples contribute to reduce the adhesive strength and lead to adhesive ruptures in the more fragile interfaces (glass fibre mesh between the thermal render layers and between the base coat and thermal render), especially in the longer freeze-thawing (FT) cycles. The square pre-cuts showed to be the best option to perform adhesive tests in thermal rendering and plastering systems since these pre-cuts have less interference in the material deterioration comparing to the circular pre-cuts. The increase of the adhesive strength after ageing may be a consequence of the later hydration of the binder, which indicates that the results should be carefully analysed on the tests set. Fig. 192 shows the influence of the different ageing procedures in the hard body impact of the two coatings.

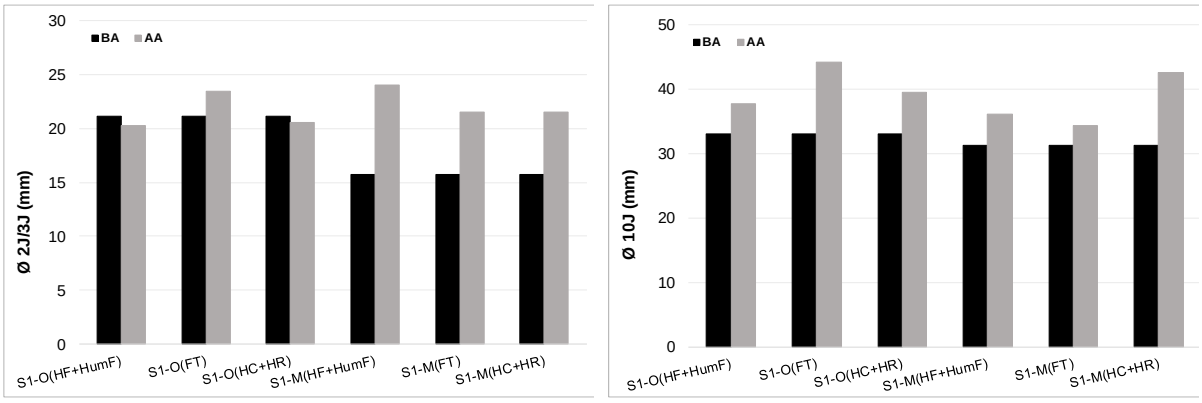

a) b)

Fig. 192 – Average dent diameter with hard body impact, after ageing procedures considering: a) 2/3J impact energy; b) 10J impact energy.

In terms of dent diameter, the results did not differ much between the different ageing procedures, highlighting the importance of the qualitative analysis. The HF+HumF and the FT ageing procedures result in higher degradation of the impact resistance comparing to the hygrothermal cycles (HC+HR) since perforation is observed. However, after the hygrothermal cycles (HC+HR) the organic and mineral coatings only present perforation for higher impact energy (and delamination), fitting the ETAG 004 requirements to the classification as Category III. This is in accordance with the higher deterioration of the small samples. To achieve more reliable results, high resistant sealants (high resistance to water action and temperature variation) should be used. Otherwise, several tests results could be distorted.

In general, the studied organic coating led to lower degradation of the thermal render comparing to the mineral coating. However, the organic particles present higher degradation due to solar action, particularly to UV radiation (Ochs, Vogelsang and Meyer 2003; Johnson and McIntyre 1996). As such, the performed "heat" procedure, without UV radiation, did not imply a severe degradation of the organic particles. The application of the referred coatings in warm climates, especially in Zone C climates (described in Table 81), requires the durability evaluation to UV radiation.

All the tested ageing procedures produced degradation in the thermal rendering systems, which states that degradation mechanisms (freeze-thaw, shrinkage and temperature fluctuations, as indicated in Table 33 in the sub-chapter 2.6) related to the implemented actions were activated.

The higher number of cycles and the severity of the freeze-thawing (FT) can reproduce the effect of colder climates, such as the northern European countries. The heating-freezing/humidification-freezing (HF+HumF) cycles combine distinct degradation mechanisms that occur in several locations, mainly in south European countries, due to the high heating temperature. However, the low number of cycles and the combination of such different degradation mechanisms (thermal shock by IR radiation and freezing or humidification) requires further investigation.

The freeze-thawing ageing is adequate to evaluate the degradation in colder climates. Considering that in warmer climates the absorbed water evaporates, the freeze-thawing degradation is not expectable to occur. However, in moderate climates that evaporation does not occur as fast as in warm climates. As such, since the thermal render has higher water absorption than a common insulation (such as EPS), the freezing may occur. In that way, it is a fact to take into consideration in the durability assessment.

The thermal shock obtained by an abrupt decrease of temperature, such as the cold rain incidence in a warm façade, is suitable to be analysed in warmer climates, where high solar radiation is registered. The reproduction of the heating should be replicated as close as possible to the solar radiation. As such, the heating procedure is more reliable when the UV radiation is implemented. However, artificial UV radiation is obtained with special UV lamps, which are very expensive and present limited duration. As such, the UV radiation should be used to reproduce reliable degradation when relevant, as is the case of synthetic coatings.

The effect of temperature is transversal to different climates but more significant in climates with higher temperature amplitude. The hygrothermal cycle developed in 5.3 allows evaluating the durability of thermal rendering systems in the Portuguese climatic context since it covers the variability of Portuguese climates. As well, other southern European countries that present similar climates could be well represented by the developed ageing cycles. Moreover, as the cycle was developed taking into account the Portuguese climatic context, the temperatures could be adapted to other climates in order to reproduce a more reliable durability assessment.

In summary, the distinct ageing procedures are suitable to analyse several degradation mechanisms in a wide range of climates. The implementation of the standard procedures to different thermal rendering

and plastering systems allowed understanding the deterioration caused by each degradation mechanism. The acquired knowledge contributed to the development of the hygrothermal ageing cycles since the relevant gaps were identified and bridged. The several experimental tests, performed before and after the different ageing procedures, deepened the knowledge of thermal renders/plasters and the respective systems, giving significant information about their properties and performance. This knowledge is fundamental to develop the durability assessment methodology, applicable to thermal rendering and plastering systems, together with the developed hygrothermal cycle.

5.5.2. DEVELOPED HYGROTHERMAL AGEING CYCLE – EXPERIMENTAL RESULTS VS. NUMERICAL SIMULATION

In the present sub-chapter, some parameters that were measured during the implementation of the hygrothermal cycles were compared to the results obtained by numerical simulation, in order to validate the simulation model.

Fig. 193 presents the exterior surface temperature obtained during the heat-cold ageing cycles by hygrothermal simulation and during the implementation of the cycles (as presented in 5.4.2.4).

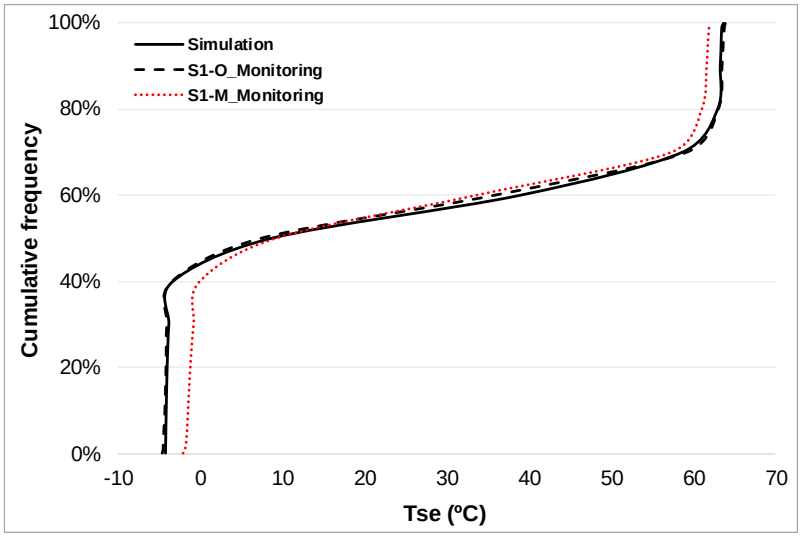

Fig. 193 – Exterior surface temperature obtained during the heat-cold cycle: simulation vs. implementation.

As it can be seen, the simulated temperature matches the monitored temperatures in the organic coating, while the mineral coating presented a variation of the higher and lower temperatures. This fact was expectable since the simulation was performed considering the organic coating. Nevertheless, the mineral coating presented a variation of 0.9% between the simulated and the measured average temperatures, the same variation as observed in the organic coating. The main difference is in the amplitude – 1.2% for the organic and 5.4% for the mineral coating.

Regarding the water content in the thermal render, considering the organic coating, the maximum obtained value in the simulation is of 11.3 kg/m^3 and the measured after ageing is of 12.0 kg/m^3, which corresponds to a variation of 6.3%. Since the liquid water transport is more difficult to simulate, comparing to the surface temperatures, the obtained variation is acceptable.

As such, regarding both measured and simulated surface temperature and water content, the hygrothermal simulation model is validated. To evaluate the obtained thermo-mechanical degradation, such as cracking, the wall specimen was numerically modelled and analysed by a temperature-

displacement method, using the Abaqus software, as performed in 4.3. Fig. 194 presents the 3D model that was modelled, representing the wall specimen used in the implementation of the hygrothermal ageing cycles.

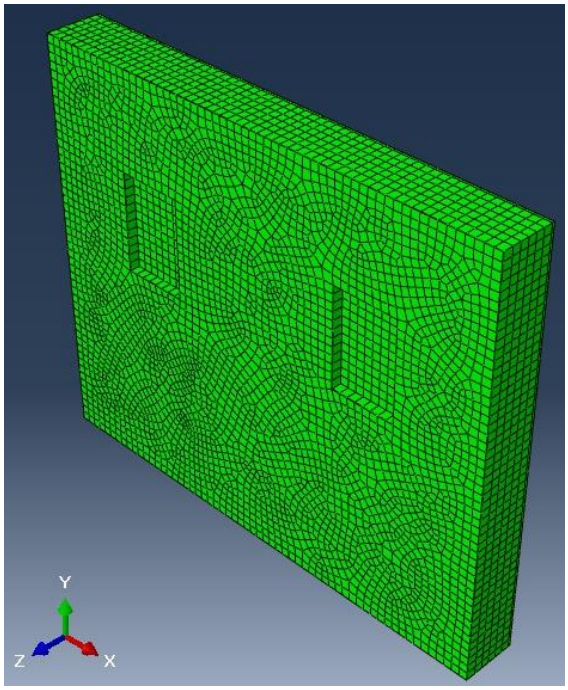

Fig. 194 – Schematic representation of the wall specimen.

Since the wall is blocked in the base, a first simulation considering only the fixed support of the base nodes as boundary constraint was performed. As such, higher tensile stresses after the heating period and compressive stresses after the cold period were observed (see Fig. 195 and Fig. 196, respectively).

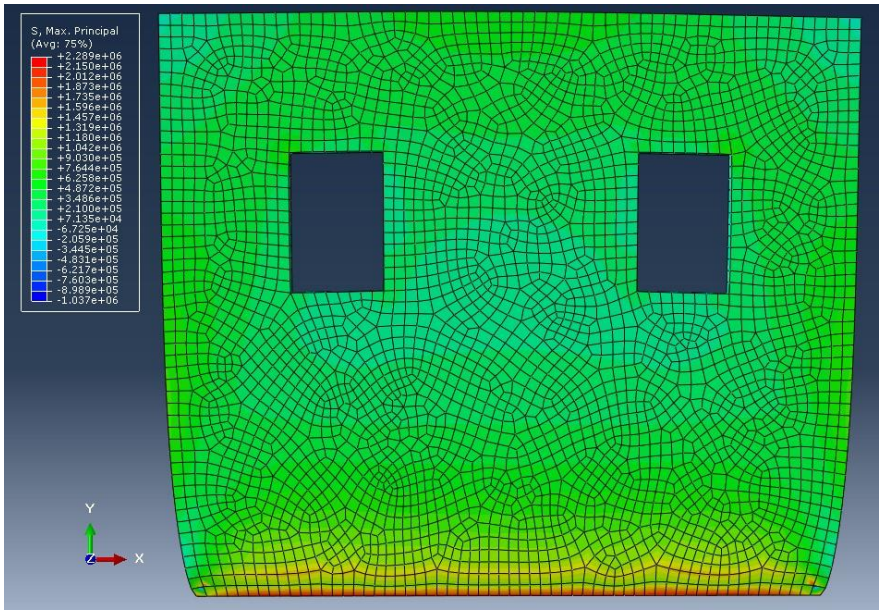

Fig. 195 – Maximum principal stresses, after heating period.

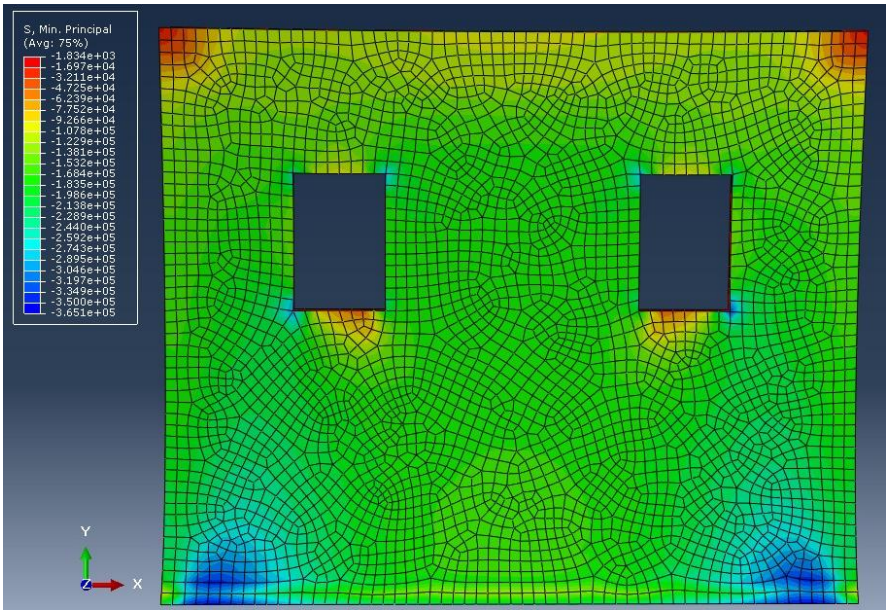

Fig. 196 – Minimum principal stresses, after cooling period.

As it can be observed, by the stresses distribution excluding the surrounding area of the wall base, the heating promotes higher stresses in the top of the wall (of the openings) and the cooling higher compressive stresses especially in the corners and bottom of the openings. This is in line with the obtained thermograms after performing the heat-cold ageing cycles, as presented in Fig. 175 and Fig. 176, in sub-chapter 5.4.2.4. Fig. 197 presents the deformed shapes and displacements.

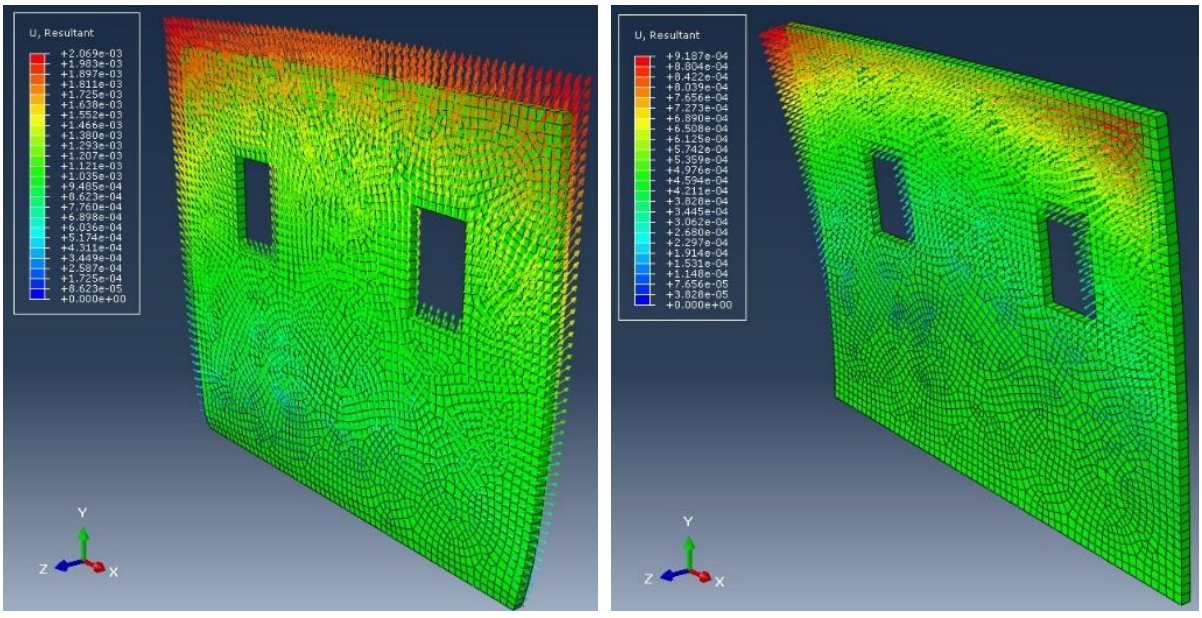

a) b)

Fig. 197 – Deformed shape and displacements after simulation of the: a) Heating period; b) Cooling period.

Considering a central node of the wall, after the heating, tensile stress of 0.176 MPa was obtained, while after the cooling compressive stress of 0.178 MPa was observed. Also, in the contour of the openings, tensile stresses of around 0.33 MPa and compressive stresses of 0.12 MPa were obtained. Regarding the flexural and compressive strength, determined after the hygrothermal ageing, the tensile stress exceeds the measured strength, which could explain the cracks after the heat-cold procedure.

Since the brick masonry support may introduce more restrict constraints, the model was simulated considering:

- Fixed support: base of the wall;
- Displacements in *z* axis blocked: exterior and interior surfaces;
- Displacements in xz axis blocked: top of the wall.

Since the displacements are highly restricted, the thermal render presents higher compressive stresses than in the previous simulations, even during the heating period, as it can be seen in Fig. 198. The obtained values are above the determined compressive strength, which results in the rupture of the material.

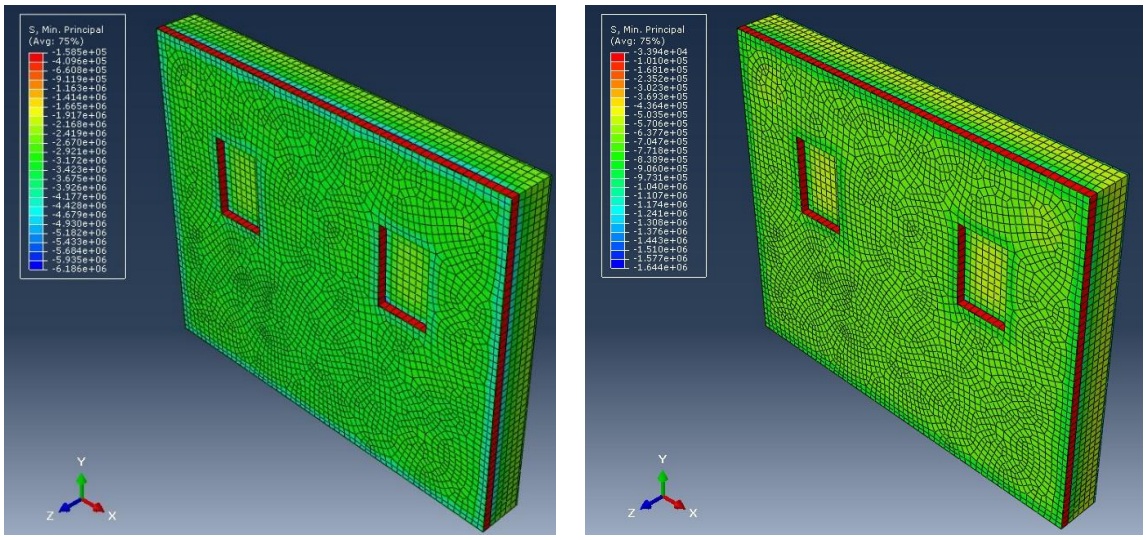

a) b)

Fig. 198 – Minimum principal stresses after: a) Heating period; b) Cooling rain period.

In addition, the restriction of the surfaces promotes higher stresses in the contour of the openings, with alternation of the directions, as shown in Fig. 199. The obtained failure lines are in accordance with the cracks showed in Fig. 160 to Fig. 165, in sub-chapter 5.4.2.1, which mainly occurred in the corners of the openings, with a radial distribution. Regarding also the stresses distribution in the surface of the façade, presented in Fig. 200, higher stresses are observed in the openings, in both heating and cooling periods, corroborating the higher cracking in the corners.

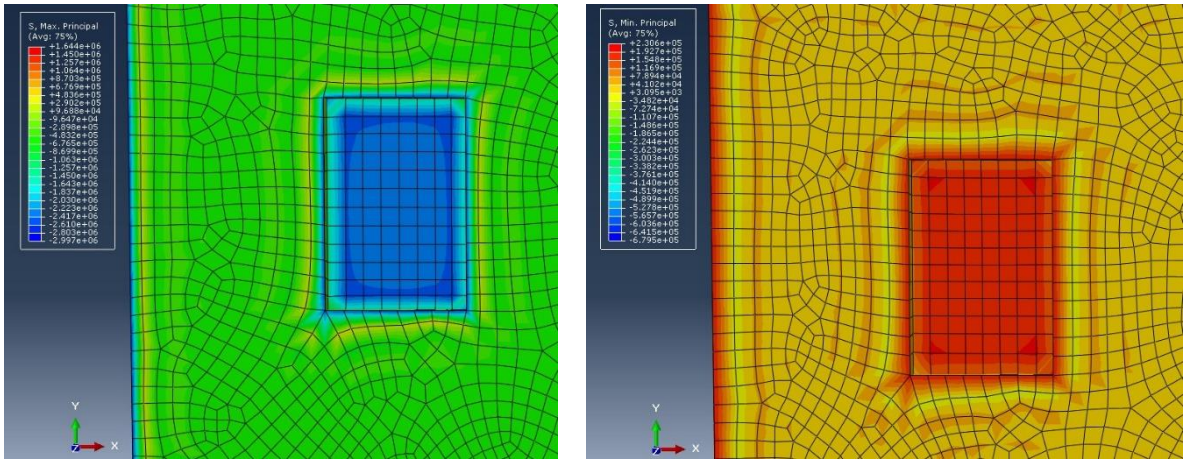

a) b)

Fig. 199 – a) Maximum principal stresses after the heating period; b) Minimum principal stresses after the cooling period.

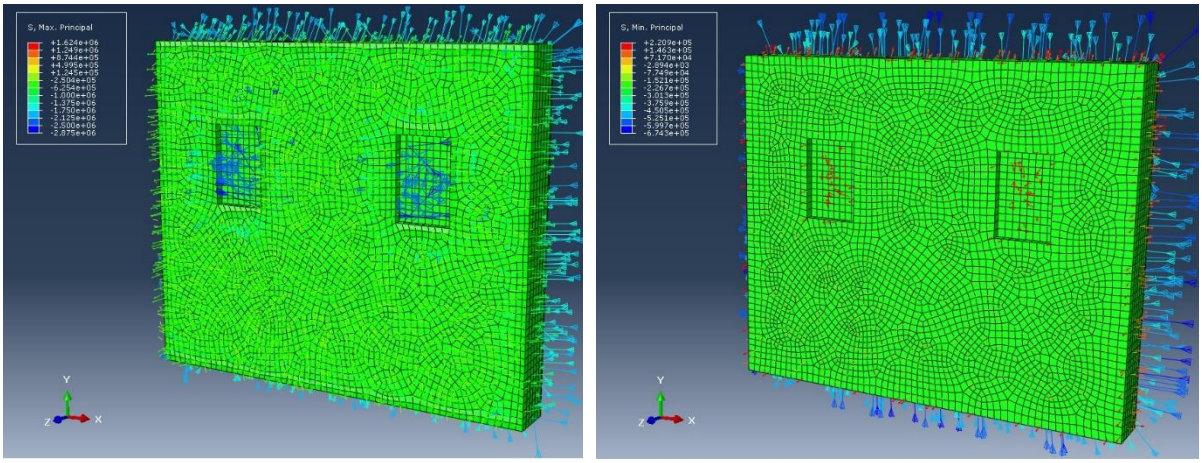

a) b)

Fig. 200 – Vectorial representation of the: a) Maximum principal stresses after the heating period; b) Minimum principal stresses after the cooling period.

Fig. 201 presents the stresses in the perpendicular planes to the thermal render interface, after the heating period. The wall is presented in the longitudinal plane (*xx* axis cut). The stresses in the *xx* axis (S11) in the thermal render interface with the finishing render present different directions, which contribute to the cracking of the adjacent layers. In addition, the stresses in the *zz* axis (S33) showed, in the interface, negative values. Being the displacements of the finishing render blocked in *zz* axis, the negative tensions may contribute to the detachment of the thermal render and finishing render layers.

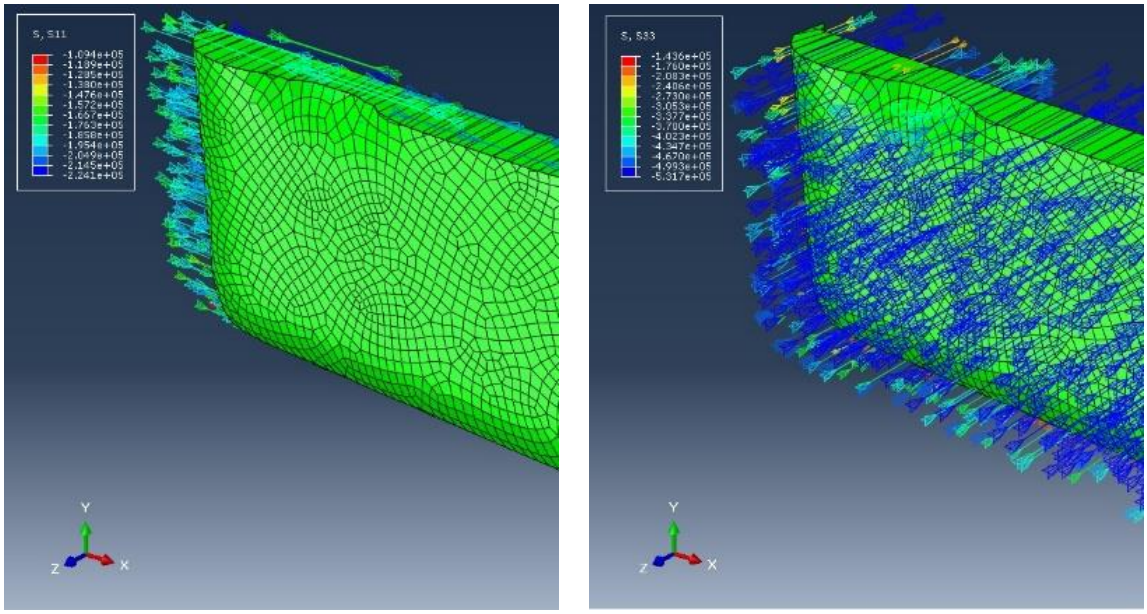

a) b)

Fig. 201 – Vectorial representation of the stresses after the heating period in the perpendicular planes to the TR interfaces: a) *xx* axis (S11); b) *zz* axis (S33).

5.6. DURABILITY ASSESSMENT METHODOLOGIES

5.6.1. METHODOLOGIES APPLICABLE TO THERMAL RENDERING AND PLASTERING SYSTEMS

In this section, a summary of all the acquired knowledge regarding the durability assessment of thermal rendering and plastering systems is presented. The development of methodologies that reproduce the most relevant degradation mechanisms in thermal rendering and plastering systems were performed.

According to the requirements applicable to thermal renders and considering the materials properties, a methodology regarding the application of the thermal rendering system is presented in Fig. 206.

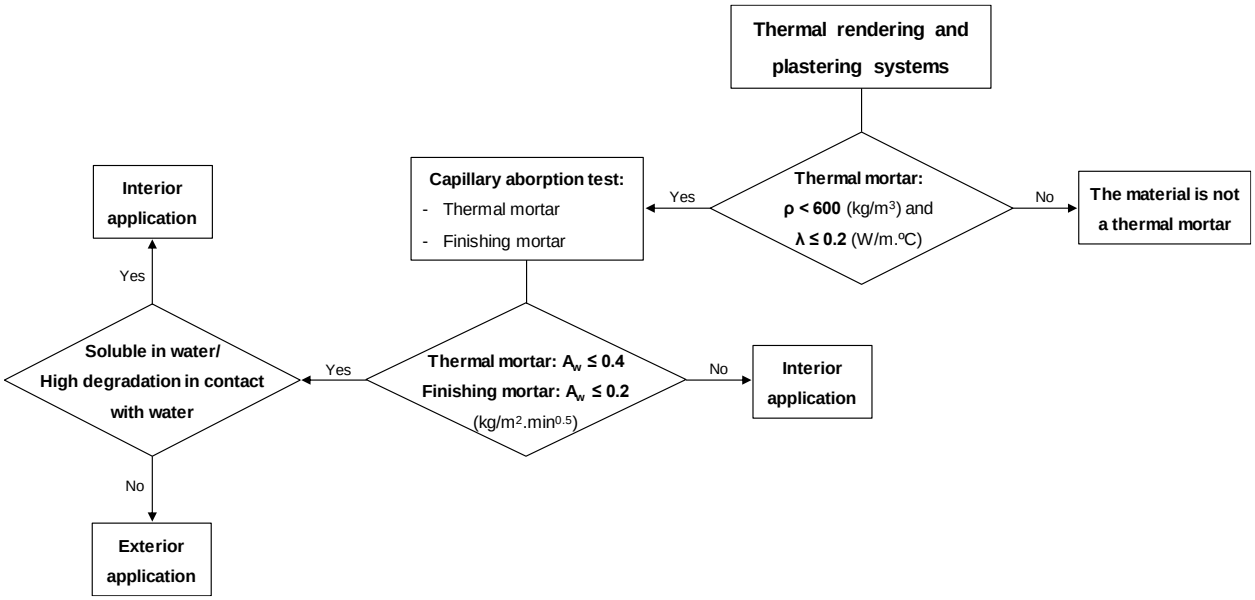

Fig. 202 – Methodology of application of thermal rendering and plastering systems.

In summary, a thermal rendering or plastering system can only be designated as that if the thermal render presents specific characteristics, namely low density and low thermal conductivity, according to (Veiga 2011) and (CEN 2010), respectively. For exterior application, one of the most relevant properties is the capillary absorption, since the water action is one of the main causes of degradation. As such, the outer layers should present lower capillary absorption than the thermal render. The capillary absorption coefficients were fixed regarding the EN 998-1 (CEN 2010) requirements and the obtained values in the experimental campaign. The test methods should be carried out according to the the procedures defined in EN 998-1 (CEN 2010). Another relevant fact is the solubility and the high degradation in the presence of water of some materials. That condition disables their exterior application. Gypsum-based materials are an example of materials that are not suitable for the exterior application, due to its intrinsic properties (dissolution in water).

Despite the little development of the durability assessment of thermal plastering systems, the implemented ageing cycles allow observing the degradation of the system performance. As such, a preliminary proposal of a durability assessment methodology applicable to thermal plastering systems, regarding the interior application, is presented in Fig. 203. The capillary absorption requirement is supported by the capillary classes defined in EN 998-1 (CEN 2010). The heating (60 ºC)-freezing (-15 ºC) procedure (defined according to EN 1015-21 (CEN 2002a)), allows analysing the effect of the temperature fluctuation, regarding high-temperature variations. However, the effect of humid environments, at high or low temperatures, was not evaluated and is a crucial aspect concerning the durability of plasters. In addition, future developments concerning this application should be performed, since the heat-freezing cycles described in EN 1015-21 do not represent usual interior conditions, due to the freezing temperatures. In short, the application of thermal plastering systems requires an accurate analysis, regarding the environmental conditions where the system is intended to be applied, and the definition of the related ageing cycles (that should represent the environment as accurately as possible).

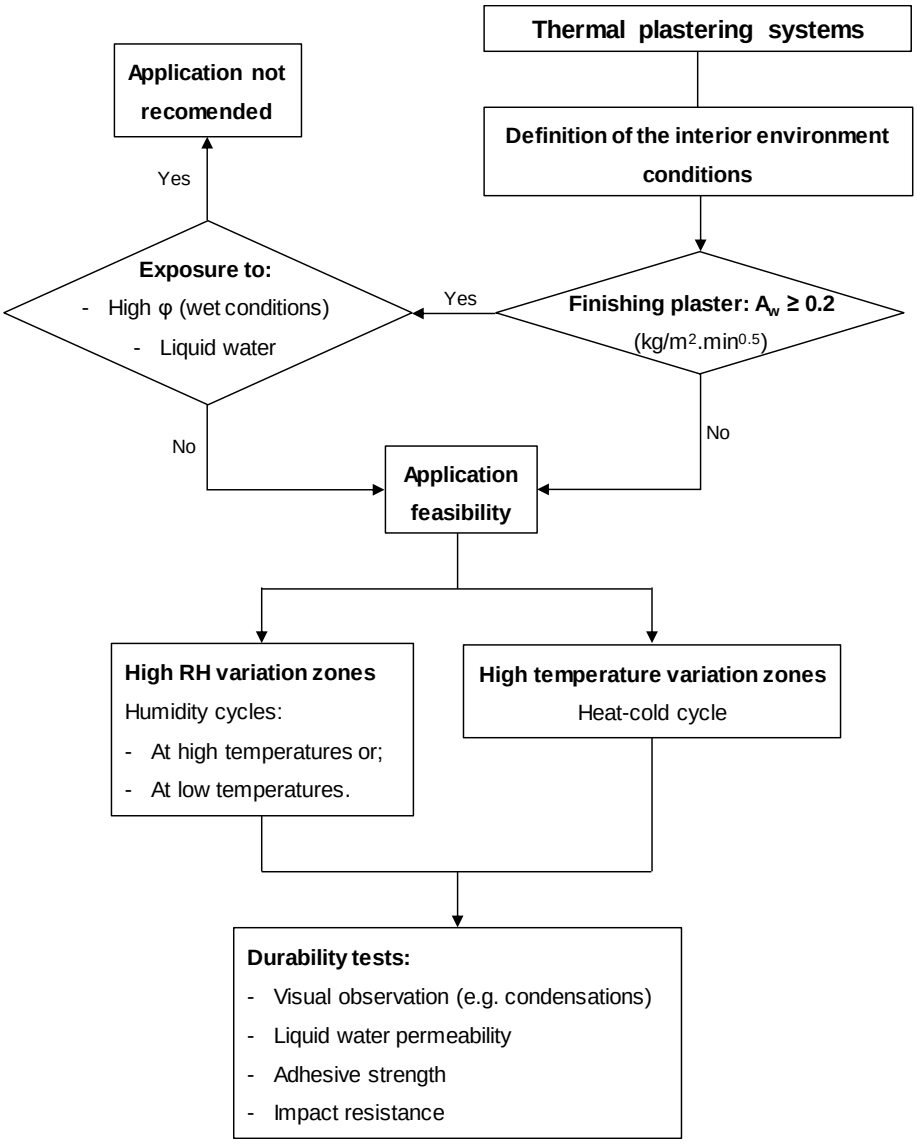

Fig. 203 – Preliminary durability assessment methodology applicable to thermal plastering systems.

The characteristics and durability of thermal rendering systems, suitable for the exterior application, were highly explored in the present work. In that way and regarding the main goal of the current thesis – the development and implementation of a durability assessment methodology applied to thermal rendering systems – the paths to evaluate that type of systems are schematically presented in Fig. 204.

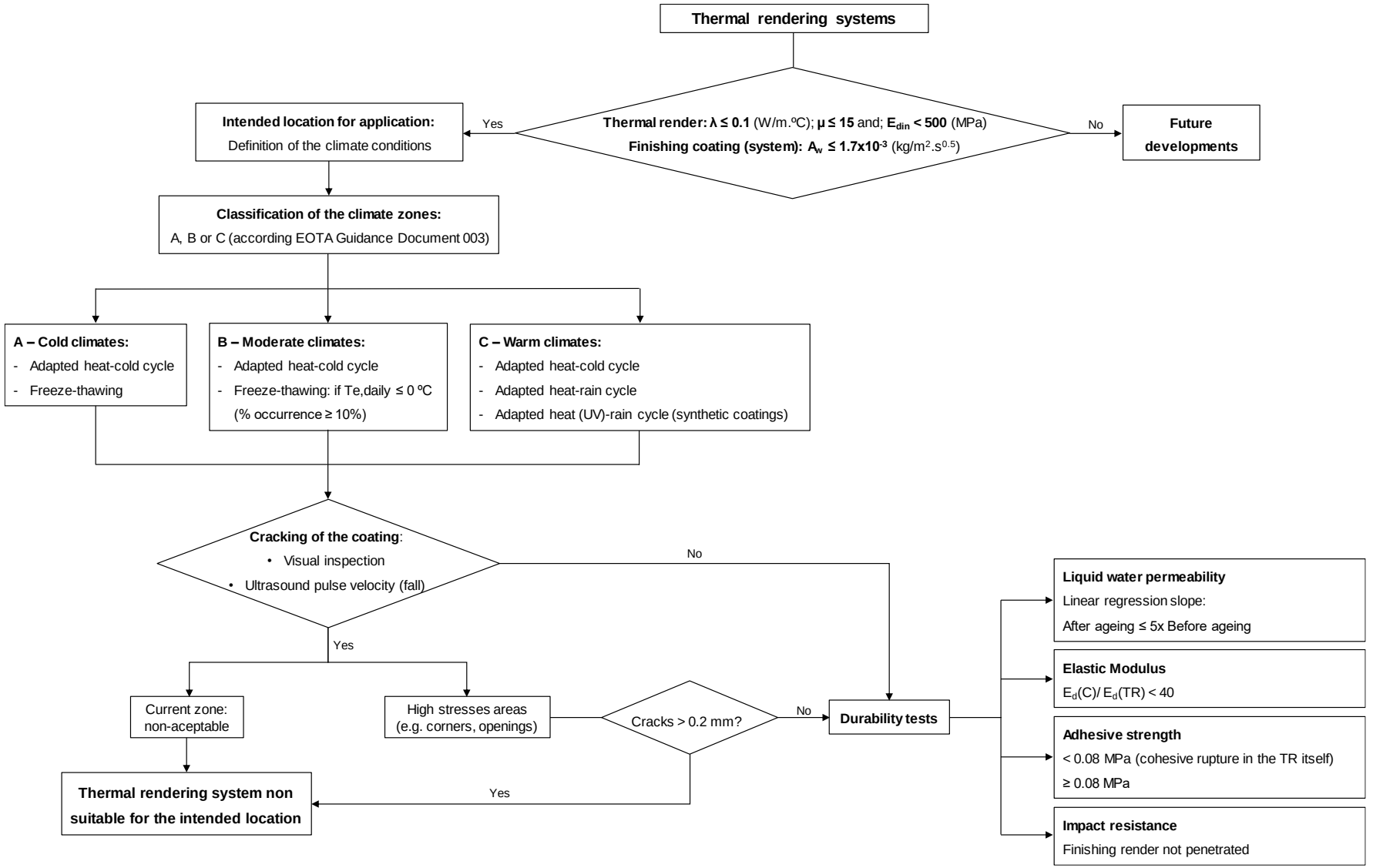

Fig. 204 – Durability assessment methodology applicable to thermal rendering systems for exterior application.

The methodology was developed taking into account the existing requirements presented in standards or guides, such as EN 998-1 and ETAG 004, and also in the experimental and simulation results, obtained in Chapters 3, 4 and 5. First of all, specific criteria regarding the material properties were defined in order to enhance the performance of the thermal rendering system.

As the trend on the development of new materials is in the lowering of the thermal conductivity of the thermal renders, the methodology is applicable to thermal renders with low thermal conductivity (less than or equal to 0.1 W/m.ºC – T1 classification) (CEN 2010). Beyond the thermal conductivity, the water vapour permeability resistance factor should be less than 15 (CEN 2010) and the dynamic modulus less than 500 MPa, which were obtained in the experimental campaign in the two lightweight thermal renders (with EPS addition). Being the easier application in irregular surfaces one of the great advantages of the thermal renders, the high water vapour permeability allows better compatibility to ancient materials, comparing to ETICS, without compromising the thermal performance. The lower dynamic modulus also allows the absorption of higher displacements resulting in better compatibility with rigid substrates. Beyond the thermal render requirements, the establishing of finishing renders with low capillary absorption is of great importance, since the durability assessment is performed to the system as a whole that has to present an acceptable behaviour to the exterior application. The fixed requirement is based on the experimental tests carried out on the present work. To extrapolate the developed methodology to systems with other characteristics further developments are required.

One of the most important steps is the definition of climate conditions where the system is intended to be applied. Since the same thermal rendering system presents different deterioration to different degradation mechanisms, a material suitable for the application in a specific climate zone may not be applied in a different location. The climate zones were divided according to the classification of EOTA Guidance Document 003 (EOTA 1999). In that way, to optimize the durability assessment, different ageing procedures were associated to each climatic zone, regarding the collected knowledge of the durability assessment performed in Chapter 5, combining the existing procedures with the developed hygrothermal cycles.

Since the freeze-thawing showed a high deterioration of the system, despite the low water absorption of the coating, its evaluation in cold climates is of great importance. In addition, due to the ability of the thermal render to retain water, even in moderate climates, where the evaporation process is faster than in cold climates, the water may remain longer and be subjected to freezing conditions. The ageing procedures (freezing and thawing temperature, duration and number of cycles) should be the same as the described in the ETAG 004 (EOTA 2013), for small-size samples.

Regarding the heat-cold cycles, each heat and cold temperatures can be adapted to the climate conditions where the systems are intended to be applied. For example, the developed heat-cold cycle can represent the effect of the temperature variation in the Portuguese climatic conditions, since the most severe conditions were chosen. In the same way, regarding the logic of development of the heat-cold cycle presented in 5.3.2, the heat-cold cycle can be defined specifically to different European climates, as it is shown in 5.6.2.

The heat-rain cycle is intended to be applied after the heat-cold cycle in the same specimen. The specimen may have the same configuration as the rig preconized in the ETAG 004. The heating temperature should also be adapted to the maximum reached temperatures, considering a worst-case scenario (high solar radiation incidence, high solar absorption of the coating), obtained by hygrothermal simulation or "in-situ" measurements. Being the heat-rain cycle developed taking into account the Portuguese climatic conditions, the heating temperature may represent a wide range of European climates. Considering warm climates, an accurate definition of the heating temperature is of great

importance, since the thermal shock could increase and present higher detrimental consequences in the systems than in colder climates. The ETAG 004 (EOTA 2013) refers that, in general, the maximum considered surface temperature is 80 ºC, which is 10 ºC higher than the tested one. This highlights the importance of determining the maximum surface temperatures reached in warm climates, which are essential to adapt the heat-rain cycle temperature. When the durability assessment methodology were applied to synthetic coatings, the heat-rain cycles should be performed using UV radiation during the heating procedure, considering Zone C (warm climates). This is due to the higher degradation of these specific coatings to solar radiation action, which is particularly severe in warm climates emphasized by thermal shock due to rain action. The application of the referred coatings in warm climates, especially in Zone C climates requires the durability evaluation to UV radiation. However, the study of the UV radiation action in thermal rendering systems requires further developments.

Regarding the experimental tests to evaluate the durability, a visual inspection and the determination of the ultrasonic pulse velocity (in different areas of the specimen) for the detection of cracks in the coating is required. The ultrasonic pulse velocity should be determined according to the procedure described in 5.4.2.5, which measures the path crossed by the ultrasound wave and the time it took to perform it. A fall of the ultrasonic pulse velocity reveals possible cracks. Cracking of the coating in the current zone is not admissible, since it demonstrates the weakness of the system in areas without higher concentration of stresses, allowing the water penetration in the entire system. In this case, the system should be classified as non-admissible for the tested climate zone. If no cracks are detected or if they occurred in areas with higher concentration of stresses and have less or equal to 0.2 mm thickness, the durability evaluation should continue and the water permeability, elastic modulus, adhesive strength and impact resistance are determined.

The liquid water permeability should be performed using the Karsten tubes method, already described in 5.2.1. This test allows the comparison of the absorbed water volume by the system in a vertical position (between the wall and the small-size samples). In addition, a simple setup is required, allowing quicker results. This method approximately describes some natural actions, such as the incidence of rain due to strong winds. Three different tubes should be placed in different current areas, without cracks. The average values should be plotted and the slope of the resulting linear regression evaluated. Regarding the obtained results in 5.4.2.2, a slope bigger than five times of the initial slope (before ageing) is considered as potentially harmful, since it reveals that the water absorption rate increases very fast.

As demonstrated by thermo-mechanical simulation, the elastic modulus compatibility between the thermal and finishing render is of major importance, since high E_d (C)/E_d (TR) ratio results in higher stresses. As such, samples should be collected and the dynamic elastic modulus determined by the fundamental resonance frequency method as in 3.1.4.1. The E_d(C)/E_d(TR) ratio is also recommended to be lower than 40.

The adhesive strength should be determined according to the procedures defined in 3.1.4.3, using square pull-heads. In order to evaluate the adherence of the thermal render to the substrate and to the finishing render two different pre-cuts should be performed. The determination of the adhesive strength between the thermal render and the substrate implies five quadrangular pre-cuts until the substrate and between the thermal render and finishing render five quadrangular pre-cuts into the thermal render. The average value of each analysis should be registered. Since the thermal renders present in general a lower adhesive strength than current renders, low values are admissible if the ruptures are cohesive in the thermal render itself, since it means that the adhesive strength is greater than the test value.

The impact resistance should be tested according to the procedures defined in 3.1.4.4, using the Martinet-Baronie apparatus, since it allows the test in a vertical position. The 3J and 10J impact energies should be tested and the results are admissible if the finishing render is not penetrated by either of impact energies.

The referred experimental tests are required both before and after the ageing action. These properties should not present high variation before and after ageing, in order to have a stable performance. The calculation of the liquid water permeability requirement needs both before and after results. The $E_d(C)/E_d(TR)$ ratio is also recommended to be lower than 40, the adhesive strength bigger than 0.08 MPa and the finishing render not penetrated, even before ageing.

The developed durability assessment methodologies may not be applicable to all the thermal rendering and plastering systems, but cover a wide range of solutions and can be extrapolated to other systems with further developments.

5.6.2. THEORETICAL METHODOLOGY FOR THE DEFINITION OF HEAT-COLD CYCLES IN EUROPE

Each heat-cold cycle could be obtained knowing two exterior air temperature indicators: 1st percentile, of the winter period (December to February), and 99th percentile, of the summer period (June to August) since they are more representative of extreme temperatures that occur more often. Each period has a theoretical linear regression which gives the cold and heat cycle temperatures, respectively.

To obtain the theoretical linear regressions that represent the European climatic variability, 22 different European climates (referred as Group A) were chosen (see Fig. 205). The choice of the 22 different climates is related to a wide representation of the main European climate conditions. In addition, the climatic data were all in the database of the WUFI Pro software.

Fig. 205 – European climates distribution used in the definition of the theoretical linear regressions for the heat-cold cycles determination – Group A.

The WUFI Pro software was used to simulate the effect of one year of ageing, on the thermal render layer, in each of the 22 climates. The same temperature indicators – 1st percentile, of the winter period (December to February), and 99th percentile, of the summer period (June to August) – were determined for the thermal render layer considering each climate and then compared to the obtained with the heat-cold cycle. The stop criterion is the same as the used in the previous sub-chapter 5.3.2, presented in Fig. 147: the similarity of the temperature in the thermal render between the climate and the cycle simulations. The cycle configuration, such as the duration of the heat and the cold periods and the ramp time, is the same as the defined in 5.3.2. To obtain a robust theoretical regression the similarity was defined as less than 5% of the variation between the obtained temperature with each of the 22 climates and the respective cycle. Fig. 206 presents a schematic representation of the methodology used to develop the theoretical regressions.

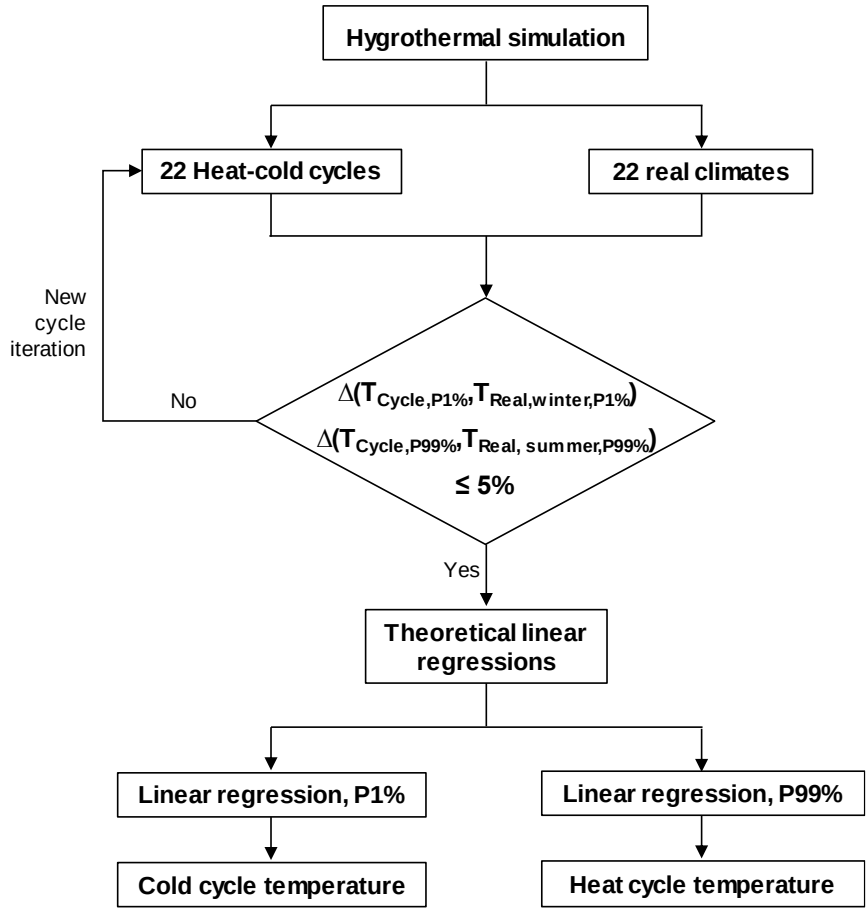

Fig. 206 – Methodology for the definition of the theoretical algorithm for the heat and cold cycles temperatures determination.

Table 122 presents the temperature indicators of the 22 real climates used to define the heat and cold cycle temperatures, by an iteration process through the minimum differences between the thermal render temperatures (1st and 99th percentiles). The temperatures variation in the thermal render considering the real climate and the heat-cycle are lower or equal to 5%, which were considered as a very good approximation, due to the temperature differences. Only in Tromsoe, a variation of 28% was verified. However, a temperature difference of only 0.07 ºC is obtained, which was considered as admissible.

Table 122 – Temperature indicators used in the definition of the theoretical algorithm for the heat-cold cycles – Group A.

Climate	Real climate (ºC)				Cycle (ºC)				$\Delta T_{TR,P1\%}$	$\Delta T_{TR,P99\%}$
	$T_{e,P1\%}$	$T_{e,P99\%}$	$T_{TR,P1\%}$	$T_{TR,P99\%}$	$T_{e,P1\%}$	$T_{e,P99\%}$	$T_{TR,P1\%}$	$T_{TR,P99\%}$	(%)	(%)
Lisboa	3.5	33.2	12.0	35.0	-5.0	65.0	11.9	35.2	0.7	0.7
Madrid	-0.3	34.4	10.2	35.8	-8.0	68.0	10.7	36.1	4.9	0.7
Malaga	2.9	37.2	13.1	36.9	-5.5	71.0	12.5	38.2	4.9	3.5
Barcelona	0.1	30.1	10.7	34.8	-7.5	63.5	10.5	34.1	2.1	1.8
Paris	-5.0	33.1	6.3	34.4	-16.0	65.0	6.2	33.1	0.6	3.7
Brest	-2.8	23.8	7.0	30.9	-11.0	57.0	7.3	29.6	3.8	4.3
Marseille	-3.4	31.8	9.3	35.7	-11.0	64.5	8.8	34.0	5.0	4.8
Modena	-0.7	33.2	8.4	34.4	-8.5	65.0	8.7	34.1	4.1	0.8
Milan	-1.1	32.0	8.9	35.8	-10.0	64.5	9.3	34.1	4.9	4.8
Brussels	-5.5	30.0	6.1	32.0	-16.0	63.5	6.3	32.7	3.6	2.1
Potsdam	-13.0	28.1	2.8	31.7	-23.0	63.0	2.8	31.2	1.8	1.5
Augsburg	-14.2	27.9	1.7	32.7	-26.5	63.0	1.7	31.3	0.2	4.2
Palma	-1.7	33.5	10.0	35.9	-10.0	66.5	9.6	35.2	4.3	2.2
Vienna	-9.2	30.5	3.9	33.5	-20.5	64.0	4.1	32.0	3.9	4.4
Hradec Králové	-11.4	31.7	3.8	34.6	-22.5	64.5	3.9	32.9	3.9	4.8
Warsaw	-13.7	28.8	1.1	32.2	-26.0	63.0	1.1	30.6	5.0	5.0
Trieste	0.8	30.3	10.5	35.0	-7.0	63.5	10.6	34.1	0.6	2.7
Graz	-8.2	29.6	5.0	33.4	-18.5	63.5	5.2	32.4	3.4	2.9
München	-15.2	27.7	0.7	32.2	-28.0	63.0	0.7	30.8	0.6	4.3
Oostende	-3.6	25.4	7.0	30.2	-12.5	59.0	7.3	30.9	4.2	2.2
Tromsoe	-13.5	20.7	-0.3	28.4	-27.5	55.5	-0.2	27.1	28.2*	4.7
Lund	-5.7	26.8	5.7	32.6	-16.5	60.0	5.9	31.2	2.0	4.5

*The % was admissible since it represents a difference of 0.07 ºC.

Plotting the 1st and 99th percentiles of the exterior temperatures – real climate as a function of the cycle – two linear regressions for each cold (1st percentile) and heat (99th percentile) periods are determined, as shown in Fig. 207.

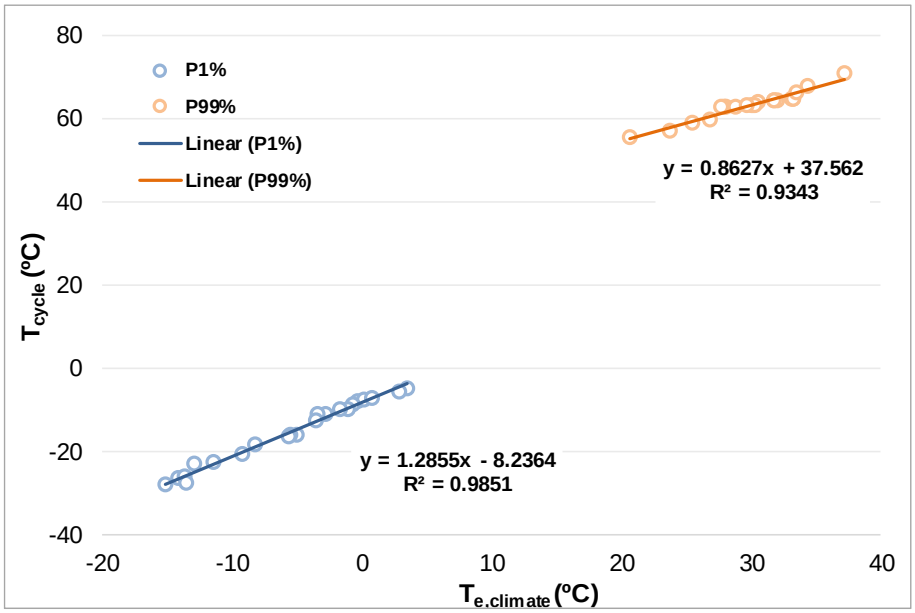

Fig. 207 – Theoretical linear regressions for the heat-cold cycles determination.

Therefore, to define each temperature for the cold and heat periods, the equations (50) and (51) are used.

$$T_{cycle}(cold) = 1.2855 \times T_{e,P1\%} - 8.2364 \quad (33)$$

$$T_{cycle}(heat) = 0.8627 \times T_{e,P99\%} + 37.562 \quad (34)$$

This allows determining any heat-cold cycle from the knowledge of the two temperature indicators $T_{e,P1\%}$ and $T_{e,P99\%}$ of a real climate.

To validate the developed methodology, other 20 European climates (referred as Group B) were chosen to implement the theoretical regressions, as shown in Fig. 208. The choice of the 22 climates is linked to the available data files in WUFI Pro.

Fig. 208 – European climates distribution used in the validation of the theoretical linear regressions for the heat-cold cycles determination – Group B.

As such, the 1st percentile temperature, of the winter period (December to February), and 99th percentile temperature, of the summer period (June to August) of each climate of the Group B were determined and placed in each theoretical regression, resulting in the heat and cold cycle temperatures, respectively. The validation was performed using the inverse methodology used in the definition process, described in Fig. 206. Each theoretical heat-cold cycle was simulated and the thermal render temperature compared to the obtained with the real climate. If the temperature differences between the real climate and theoretical cycle were less than 10% the methodology is validated. The percentages were defined regarding the observed residual temperature differences.

Table 123 presents the temperature indicators of the 20 real climates used to validate the heat and cold cycle temperatures, determined by equations (50) and (51), using the theoretical linear regressions. The temperatures variation in the thermal render considering the real climate and the heat-cycle are lower or equal to 10%, which were considered as a very good approximation, due to the temperature differences. The higher differences are observed in the colder climates, which represent a large part of the sample. This is due to the higher concentration of climatic data files, existing in the WUFI Pro database, in the central and northern Europe. Despite that, an average temperature variation of 6% and 4% in the cold and heat periods were obtained, respectively, which corresponds to 0.2 ºC and 1.3 ºC.

Table 123 – Temperature indicators used in the validation of the theoretical algorithm for the heat-cold cycles – Group B.

Climate	Real climate (ºC)				Cycle (ºC)				$\Delta T_{TR,P1\%}$	$\Delta T_{TR,P99\%}$
	$T_{e,P1\%}$	$T_{e,P99\%}$	$T_{TR,P1\%}$	$T_{TR,P99\%}$	$T_{e,P1\%}$	$T_{e,P99\%}$	$T_{TR,P1\%}$	$T_{TR,P99\%}$	(%)	(%)
Bilbao	-0.5	31.0	9.6	33.7	-8.9	64.3	9.8	34.2	2.5	1.5
Bordeaux	-1.2	30.6	8.2	33.3	-9.8	64.0	8.9	33.4	8.5	0.2
Torino	-3.2	32.2	8.1	34.5	-12.4	65.3	8.2	34.0	1.1	1.3
Udine	-4.1	31.6	7.9	34.6	-13.5	64.8	7.6	33.6	4.0	2.7
Bolzano	-6.6	32.6	7.1	34.7	-16.7	65.7	6.6	34.0	7.0	2.1
Freiburg	-7.7	29.7	4.9	34.5	-18.1	63.2	5.2	32.1	5.5	6.8
Saint Hubert	-9.7	23.5	3.1	29.3	-20.7	57.8	3.2	29.1	2.2	0.7
Krakow	-16.1	28.1	0.6	32.4	-29.0	61.8	0.6	30.7	5.4	5.1
Trier	-8.5	30.6	4.0	33.4	-19.2	64.0	4.3	31.8	7.6	5.0
Mannheim	-11.7	30.4	4.0	33.2	-23.3	63.8	3.6	32.5	10.0	2.0
Wurzburg	-12.8	30.3	2.1	33.8	-24.7	63.7	2.0	31.2	8.1	7.6
Frankfurt	-11.5	30.2	2.9	33.2	-23.0	63.6	2.7	31.4	4.3	5.6
Essen	-6.4	27.9	4.6	32.1	-16.5	61.6	4.9	30.7	7.0	4.2
Chemnitz	-12.4	28.0	2.0	31.5	-24.2	61.7	2.0	30.4	1.4	3.6
Hof	-14.1	26.6	1.1	31.7	-26.4	60.5	1.2	29.9	9.4	5.6
Enemonzo	-8.2	28.3	5.8	31.7	-18.8	62.0	5.5	32.3	6.4	1.8
Innsbruck	-8.9	29.5	4.0	32.5	-19.7	63.0	4.2	31.6	3.9	3.0
Oslo	-12.8	27.3	1.6	32.8	-24.7	61.1	1.7	30.1	8.0	8.3
Hamburg	-9.2	24.9	4.7	29.4	-20.1	59.0	4.3	30.5	8.5	3.6
Stockholm	-17.1	27.8	-0.2	33.6	-30.2	61.5	-0.1	30.3	9.8	9.9
Average									6.0±2.7	4.0±2.6
ΔT_{TR} (ºC)									0.2±0.17	1.3±0.88

In summary, the developed methodology contributes to increment the knowledge on the thermal rendering systems, especially regarding their durability performance. In addition, the obtained results

may contribute to the development of durability assessment methodologies applicable to thermal rendering systems, enhanced by the possibility of adaption of the analysis to each climatic zone.

6. CONCLUSIONS

6.1. FINAL CONCLUSIONS

The work developed in this Thesis contributes to cover some identified gaps in the knowledge about thermal rendering and plastering systems, with focus on the durability assessment. In addition, the developed work gives the necessary tools to continue exploring and complementing the research in the durability assessment of thermal rendering and plastering systems area.

The established main goal was accomplished by the development and implementation of a durability assessment methodology applicable to thermal rendering systems, regarding the material properties, the system as a whole and the intended application requirements. The sub-goals defined in the sub-chapter 1.2 were successfully accomplished, enabling the statement of the main conclusions of this Thesis.

The compilation of the state of the art in the different subjects related to the durability of thermal rendering and plastering systems allowed concluding the following:

- Renders and plasters are mortars, applied in the exterior and in the interior of walls, respectively, which are constituted by a mixture of binder(s) and aggregate(s). To achieve certain characteristics special additives may be introduced into the mixture or specific aggregates, that confer special properties, replacing a percentage of the current aggregate (usually mineral aggregates);
- Thermal mortars are defined and classified in the EN 998-1 (CEN 2010), taking into account the thermal conductivity of the material, which should be less than 0.2 W/m.ºC. To increase their thermal performance, the thermal mortars mainly have to present low density, which is usually achieved by replacing the heavy aggregates by lightweight and porous aggregates;
- The application by mechanical spraying promotes an easier and continuous application and greater adaptability to irregular and curved surfaces, which is a benefit comparing to ETICS;
- The majority of the thermal mortars present cement, lime or gypsum, as binder matrices, and a high diversity of aggregates. Cork, EPS, vermiculite and industrial wastes have been widely used. The low thermal conductivity and low density of the aggregates are highly explored. The origin of the aggregates is assumed as a key aspect, in order to develop more sustainable materials from an environmental and energy point of view. Thus, raw materials, such as cork and mineral additions, and wastes, such as EPS and artificial fibres were intensively used in several research studies;
- Despite the enhanced thermal performance, thermal mortars present low mechanical strength, resulting from the lower density and increase of the porosity. To fill this gap, the

incorporation of materials with high mechanical performance, such as synthetic fibres, industrial or natural wastes, are incorporated into the mixture;

- Although the increasing interest in the development of new façade systems with thermal enhanced properties, such as the thermal rendering systems, ETICS are still widely used in construction. In that way, since both are exterior thermal insulation solutions, applied in a multilayer system, the requirements, performance and testing procedures of ETICS were often used as a reference for the analysis of thermal rendering and plastering systems throughout this work;
- The durability of the materials and systems and the increase of their service life, directly contribute to lowering the production and accumulation of waste, directly contributing to achieving more sustainable materials;
- The identification of the degradation mechanisms allows a correct evaluation of the durability of materials and systems. The most common degradation mechanism in renders are the freeze-thaw, the alkali-aggregate reaction, the leaching of lime, the biological attack, the shrinkage and the temperature fluctuation;
- The porous structure proved to have a great impact on the hygrothermal performance of mortars since permeability depends on the porous network, its connection, size, shape and distribution of the pores;
- The existing standardization for the durability assessment of hardened mortars does not allow a consistent evaluation considering non-traditional mortars in general, and thermal mortars in particular;
- The lack of requirements in EN 998-1 (CEN 2010) and the test methodology for one-coat mortars, envisaged in EN 1015-21 (CEN 2002a), do not allow to classify and to show the added value of the thermal rendering systems, since the evaluation of the system as a whole is not considered;
- The durability assessment methodologies preconized in the ETAG 004 (EOTA 2013), are directly applied to multilayer systems (ETICS), from which it is possible to move forward in the development of methodologies directly applicable to thermal rendering systems;
- Accelerated ageing tests carried out in thermal mortars by several authors do not follow a methodology directly related to actual performance. Hence, they may not be the most appropriate way of evaluating the material/system. A trend regarding temperatures is observed in most tests, being the temperature in the freezing period approximately -20°C and in the thawing period carried out at room temperature;
- The calculation of acceleration factors requires a wide previous knowledge on the quantification of the periods and rates that originate the failure. As such, a large database containing those parameters is necessary. Since the thermal rendering systems gained importance in the market mainly in the last decade and the existing solutions are quite different between them, the required parameters are difficult to obtain;
- The combination of the methods used to pre-design ageing cycles, described by Daniotti, Spagnolo and Paolini (2008), regarding the existing standards, the climatic data analysis and the development of preliminary degradation model, based on simulation, shows to be the most adequate and reliable path to develop the durability assessment methodology applicable to thermal rendering and plastering systems;
- Directing the durability evaluation to the desired performance will guarantee solutions that are more durable, raising the adequacy of this type of systems to the climate where they will be applied.

The determination of the most relevant properties, such as physical, hygrothermal and mechanical properties, of the four examples of thermal rendering and plastering systems, supplied by industrial partners, led to the following results:

- The inclusion of lightweight aggregates, such as EPS and cork, contributes to the reduction of the density and the thermal conductivity of thermal renderings, comparing to current renders. This allowed the classification of the designated thermal renders as T1 and T2, according to EN 998-1 (CEN 2010) except the material TR4, which was discarded;
- The bulk density is lower than 600 kg/m^3, which is within the recommended range (Veiga 2010);
- The thermal conductivity linearly increased as a function of the water content, presenting the gypsum-based thermal render (TR3), and as expected, a higher rate of increasing the thermal conductivity in presence of water;
- The high rate of mesopores results in higher water absorption coefficients, due to their capillary network, contributing to relevant moisture content during the lifetime of the building and therefore to an increase in the thermal conductivity;
- The lowering of the density is not directly correlated with the increase of the measured porosity (open porosity). The thermal renders with EPS addition (TR1 and TR2) have high enclosed porosity (due to the EPS particles), but present lower open porosity than the gypsum-based thermal render (TR3);
- The studied thermal renders presented lower liquid transport coefficient for suction comparing to a current cement-lime and gypsum mortars, which is an added value in terms of capillary water uptake;
- The thermal renders presented low water vapour resistance comparing to EPS, allowing higher water vapour exchanges. That fact contributes to the regulation of the moisture content of the materials and to higher compatibility with ancient materials;
- The thermal renders presented low mechanical resistance comparing to traditional cement and lime-based mortars. However, they are more flexible, since the dynamic modulus is lower, contributing to the absorption of significant dimensional variation;
- Despite the low adhesive strength of the thermal rendering and plastering systems, the fractures are cohesive.;
- To achieve better thermal performance, the thermal renders compromise their mechanical strength, not meeting, in a large part, the requirements of EN 998-1 (CEN 2010). This fact points out the importance to adequate the requirements to the system as a whole;
- The determination of the different material properties allows deepening the knowledge of thermal renders, plasters and the whole system, contributing to develop more reliable simulations and to understand the effect of the degradation mechanisms.

The hygrothermal simulation of the most relevant degradation mechanisms in the studied thermal rendering systems and ETICS evidenced the following points:

- The simulation of the different systems highlights the great impact of the finishing coatings since a thermal render with higher water absorption capacity could present lower water content due to the lower absorption of the finishing coating system, even if the water vapour resistance increases;
- The determination of the thermal conductivity as a function of the moisture content allows a more reliable assessment of the hygrothermal risk. The higher water content in the thermal render layer increases the ratio between the average and the reference U-values, raising the

hygrothermal risk and, consequently, compromising the durability of the whole façade system;

- The hygrothermal impact depends on the material properties, but also on the climatic conditions and application, such as the wall orientation. At lower latitudes, where the solar radiation has a higher impact, the north façade presents a higher hygrothermal risk, with higher Uav/Uref and condensation potential. However, in central and northern Europe climates a lower variation considering the 4 orientations is observed. This is due to the lower solar radiation and rain comparing with some southern European climates;
- The lower the solar radiation and total rain, the lower the variation of the hygrothermal indicators considering the 4 orientations and the 4 studied systems;
- The simulated ETICS showed good performance, in general, but especially in colder climates, resulting from the low thermal transmission and low water absorption. In warmer and more humid climates, the enhanced hygrothermal properties of the thermal renders, such as the higher water vapour permeability and thermal effusivity, contribute to the regulation of the humidity and to better compatibility with the masonry substrate (which is typical in southern Europe). In contrast, in these climates, the analysed ETICS showed higher condensation potential, compared to the thermal rendering systems;
- The solar absorption coefficient of the finishing coating has a significant impact on the hygrothermal behaviour because it contributes to the reduction of the hygrothermal risk, by increasing the drying process. However, it promotes an increase of the surface temperature and consequently of the thermal stresses, especially in warmer climates with high solar radiation. In contrast, for climates with low solar radiation, a high solar absorption coefficient constitutes a good way to increase hygrothermal performance;
- The thermal plastering system (interior application) presents better performance when applied in mild climates, because it results in lower thermal stresses, as a consequence of the low surface temperature differences, and also in a reduction of the condensation potential, which is significant in such climates. However, the internal insulation systems do not contribute to thermal inertia and hence they are not favourable for summer comfort in warm climates;
- The observed behavioural dependence of thermal rendering systems on climate conditions and the effect of the different material properties contribute to enhance the development of the durability assessment methodology.

The thermo-mechanical simulation of the temperature effect in the studied thermal rendering systems and ETICS, showed the following points:

- The higher the temperature variation the higher the induced stresses. Consequently, high solar absorption coefficients produced high tensile stresses and displacements. This fact is highlighted in warmer climates, where the solar radiation is bigger;
- Lower rigidity of the thermal render did not directly contribute to the decrease of the tensile stresses regarding the finishing render-thermal render interface, which is due to high rigidity of the finishing render. However, allowed a better compatibility with the substrate, since the tensile stresses are lower considering thermal renders with lower elastic modulus;
- In colder climates, considering extreme conditions, the exterior temperature is considerably lower than the interior temperature, resulting in a significant contraction of the thermal insulation systems and consequently the compressive stresses are dominant. The high porosity and the low density promoted higher compressive stresses, contributing to the deterioration of the porous structure;

- The thermal shock results in a quick change in the stress state (tensile to compressive), which promotes cracking in the coating, allowing the climate agents to activate other failure mechanisms in the thermal render;
- Higher elastic modulus of the finishing renders contributed to increase the stresses, since the dimensional variation is restricted, resulting in lower displacements;
- The higher the difference of rigidity between the thermal and finishing renders the higher the stresses, highlighting the importance of compatibility of adjacent layers;
- ETICS promoted higher tensile stresses than the thermal renders, even considering the same finishing render, due to the much higher thermal expansion coefficient of EPS than the thermal renders;
- Less rigid substrates promoted lower tensile stresses in the thermal renders.

The numerical simulation allowed evaluating the most significant degradation mechanisms and the related failure of the thermal rendering and plastering systems, which contributed to adequate the durability assessment methodology to these systems in particular.

The proposed durability assessment methodologies were based on the following principles:

- Regarding the intrinsic properties of the thermal rendering and plastering systems, it is possible to define where the system is suitable to apply – interior and exterior application;
- Beyond the specific characteristics of the materials, the definition of requirements is a very important stage, since the application is adjusted to them;
- A thermal rendering system presents different deterioration levels when facing different degradation mechanisms. As such, a material suitable for the application in a specific climate zone may not be adequate for a different location;
- The identification of the main degradation mechanisms allowed to define representative ageing procedures.

The existing durability methodologies applicable to renders and thermal multilayer systems (ETICS) are suitable to be adapted to thermal rendering and plastering systems since they present some similar characteristics. This adaptation allowed collecting reliable data and inputs to the development of durability assessment methodologies directly applicable to thermal rendering and plastering systems. The analysis consisted of testing small-scale samples to heating-freezing + humidification-freezing and freeze-thawing ageing procedures and allowed the following conclusions:

- Both methods allowed the activation of the most relevant degradation mechanisms in thermal rendering and plastering systems, such as the freeze-thawing and temperature fluctuation;
- The higher number of cycles and the severity of the freeze-thaw ageing cycles, according to ETAG 004, may reproduce the effect of the northern European climates;
- The heating-freezing/humidification-freezing cycles, described in EN 1015-21, combine degradation mechanisms that occur in central and southern European climates;
- After the different ageing procedures, the specimens generally presented an increase of the water permeability and a decrease of the mechanical properties – adhesive strength and impact resistance;
- The systems with mineral coating showed higher water absorption than those with the organic coating, highlighting the importance of assessing the durability taking into account the different components of the thermal rendering systems;
- The experimental tests carried out to evaluate the durability allowed identifying several constraints regarding the testing operation itself;

- The liquid water permeability test was not feasible to implement in high porosity materials, such as the thermal renders since they presented high water dispersion at the surface, showing higher capillary absorption than water permeability under pressure.;
- The pre-cuts to perform the adhesive strength test should be square, due to the low adhesive strength of the thermal renders, which are pulled out using the circular drilling machine;
- The specific constraints of using small-scale samples also introduced unexpected conditions, such as the damage of the coating, due to the handling of the specimens between the ageing procedures, and the cracks in the sealant, due to the temperature variation during the ageing cycles. These allowed a quicker degradation of the thermal rendering systems since the degradation agents could easier penetrate in the inner layers;
- The accelerated ageing cycles envisaged in the standardized procedures provided a great amount of information to the development of the definition of the durability assessment methodology directly applicable to thermal rendering systems.

The obtained knowledge with the existing methodologies contributed to the development and implementation of a new accelerated ageing hygrothermal cycle applicable to thermal rendering systems showed that:

- Real-scale samples contribute to more reliable results since several configurations and experimental tests could be performed. However, the execution and the configuration of the specimens should be well performed in order to guarantee a greater approximation to "in situ" conditions;
- The hygrothermal simulation allowed optimizing the heat-cold ageing cycles, to specific thermal rendering systems;
- The hygrothermal model was validated since very low differences between the measured and the simulated surface temperatures (average variation of 0.9% and 1.2% of amplitude) were observed. Since the liquid water transport is more difficult to simulate, comparing to the surface temperatures, the water content variation in the thermal render, considering the simulated and the measured results, was also acceptable (6.3%);
- The thermo-mechanical model showed the areas with higher concentration of thermal induced stresses, which were in accordance with the resulting cracking after the hygrothermal ageing cycles;
- The developed hygrothermal cycle allowed to evaluate the durability of thermal rendering systems in the Portuguese climatic context since it covers the variability of climates. As well, other southern European countries that present similar climates could be well represented by the developed ageing cycles;
- The heat-cold and heat rain cycles allowed the activation of the temperature fluctuation degradation mechanism and consequent cracking. In addition, the alteration of the porous structure of the matrix, by the water action, showed to be another relevant degradation mechanism, which was not previously defined.

The hygrothermal cycle development and implementation enabled developing and optimizing specific heat-cold and hear-rain cycles to different European climates. The development of a theoretical algorithm regarding the heating and the cooling periods allowed the direct determination of the heat and cold cycle temperatures, based on the exterior air temperature of each climate.

In summary, the prior knowledge in the durability assessment of thermal rendering and plastering systems showed to be inadequate and incomplete. As such, a reliable durability assessment, based on measured properties, regarding the thermal renders and also the system as a whole was performed. The numerical simulation proved to be a very useful and strong tool in the analysis of the most relevant

degradation mechanisms, by detecting, in a first stage, the properties and configuration of the systems, which have a higher influence in the durability performance. Furthermore, allowed the development of the durability methodology adapted to different European climates. The different tested ageing procedures allowed the evaluation of the most relevant degradation mechanisms, considering the thermal rendering and plastering systems, understanding their feasibility and adequability to the development of a durability assessment methodology applicable to the studied systems. The combination of all the referred aspects, during this Thesis, allowed developing new durability assessment methodologies that contribute to increase the knowledge on the thermal rendering and plastering systems, especially regarding their durability performance, enhanced by the possibility of adaption of the analysis to each climatic zone.

6.2. FUTURE DEVELOPMENTS

The results obtained in the current Thesis allowed establishing the paths to continue the developed work:

- Evaluate the water absorption coefficient threshold, of the exterior coating, which does not cause significant damages in the thermal render, after the hygrothermal ageing cycles. That analysis assumes a good compromise between the liquid water absorption and the vapour permeability properties;
- Evaluate the application of thermal rendering systems in ancient buildings, in terms of hygrothermal impact and salts crystallization action;
- Evaluate the UV radiation action of thermal rendering systems with synthetic coatings;
- Develop a durability assessment methodology applicable to thermal plastering systems, regarding the interior environment and specific requirements;
- Evaluate the adapted heat-cold cycles methodology considering other climatic data files and comparing to the currently developed methodology;
- Compare and optimize the durability assessment methodology considering natural ageing and “in situ” data;
- Implement the developed durability assessment methodology to thermal rendering systems with high reflectance coatings;
- Evaluate the urban heat island effect of thermal wall systems with high reflectance coatings in comparison with similar coatings, without reflective particles, with low solar absorption coefficient.

REFERENCES

A Silva, D., L. M F Roman, Márcio Fredel and H. R. Roman. 1999. *Theoretical Analysis on the Thermal Stress of Ceramic Tile Coating Systems*. Vol. 8.

ABCB. 2006. *Durability in Buildings. Handbook*. Edited by Australian Building Codes Board. Guideline Document.

Abidi, S., B. Nait-Ali, Y. Joliff and C. Favotto. 2015. "Impact of perlite, vermiculite and cement on the thermal conductivity of a plaster composite material: Experimental and numerical approaches". *Composites Part B: Engineering* no. 68:392-400. https://www.sciencedirect.com/science/article/pii/S1359836814003102.

ACEPE. 2014. "EPS - Expanded polystyrene". Paper presented at Energy Efficient Façades Seminar in Lisboa. 8 May 2014. (*in Portuguese*)

Actu-Environment. 2008. "Principe de base de l'éco-construction". Accessed 28 Janeiro. http://www.actu-environnement.com/ae/dossiers/energiebat/principes_energie_batiment.php4. (*in French*)

Addleson, Lyall. 1992. *Buildings Failures: A Guide to Diagnosis, Remedy and Prevention*. 3rd ed. Oxford, England: Butterworth Architecture.

Aguiar, José, A. Cabrita and J. Appleton. 2002. *Support guide for the rehabilitation of residential buildings*. Edited by LNEC. Vol. 1 and 2. Lisboa. (*in Portuguese*)

Ahmadi, Zahra, Jamshid Esmaeili, Jamil Kasaei and Robab Hajialioghli. 2018. "Properties of sustainable cement mortars containing high volume of raw diatomite". *Sustainable Materials and Technologies* no. 16:47-53. http://www.sciencedirect.com/science/article/pii/S221499371730057X.

Alaimo, Giuseppe, D. Enea, G. L. Guerrini and L. Bottalico. 2012. "Experimental evaluation of the durability of innovative cementitious coatings: Photocatalytic activity and colour". Paper presented at Proceedings of SPIE - The International Society for Optical Engineering.

Allen, Robert. 1980. *How to Save the World: Strategy for World Conservation*. Toronto, Canada: Prentice-Hall.

Alvarez, José, Cristina Sequeira and Marta Costa. 2005. "Teachings to be taken from the Historic Past of Mortars". Paper presented at I Portuguese Congress in Construction Mortars in Lisbon. (*in Portuguese*)

Amaral, C., R. Vicente, P. A. A. P. Marques and A. Barros-Timmons. 2017. "Phase change materials and carbon nanostructures for thermal energy storage: A literature review". *Renewable and Sustainable Energy Reviews* no. 79:1212-1228. http://www.sciencedirect.com/science/article/pii/S1364032117307293.

Ang, C. N. and Y. C. Wang. 2004. "The effect of water movement on specific heat of gypsum plasterboard in heat transfer analysis under natural fire exposure". *Construction and Building Materials* no. 18 (7):505-515. http://www.sciencedirect.com/science/article/pii/S0950061804000480.

APFAC. 2015a. "Construction mortars: factory-produced or prepared on-site?". *APFAC Informa*, February 2015. (*in Portuguese*)

APFAC. 2015b. "Portuguese Association of Construction Mortars Manufacturers ". Accessed 26 January. http://www.apfac.pt/. (*in Portuguese*)

ASHRAE. 2009. 160. In *Criteria for Moisture-Control Design Analysis in Buildings*: ANSI.

ASTM. 2008a. C 666/C 666M – 03. In *Standard Test Method for Resistance of Concrete to Rapid Freezing and Thawing*. United States of America: ASTM International.

ASTM. 2008b. C 1260 – 07. In *Standard Test Method for Potential Alkali Reactivity of Aggregates (Mortar-Bar Method)*. United States of America: ASTM International.

ASTM. 2010. C 1371-04a. In *Standard Test Method for Determination of Emittance of Materials Near Room Temperature Using Portable Emissometers*. United States of America: ASTM International.

Athena Institute. 2006. Service life considerations in relation to green building rating systems.: an exploration study. edited by Athena Sustainable Materials Institute. Canada.

Barbero Barrera, María del Mar. 2011. "Improvement of thermal behaviour of additived lime mortars and their use in rehabilitation of buildings", Departamento de Construcción y Tecnología Arquitectónicas, Universidad Politécnica de Madrid - Escule Técnica Superior de Arquitectura.

Barclay, M., N. Holcroft and A. D. Shea. 2014. "Methods to determine whole building hygrothermal performance of hemp–lime buildings". *Building and Environment* no. 80:204-212. http://www.sciencedirect.com/science/article/pii/S0360132314001899.

Barreira, E., J. M. P. Q. Delgado, N. M. M. Ramos and V. P. de Freitas. 2013. "Exterior condensations on façades: numerical simulation of the undercooling phenomenon". *Journal of Building Performance Simulation* no. 6 (5):337-345. https://doi.org/10.1080/19401493.2011.560685.

Barreira, Eva. 2010. "Biological degradation of facades with external thermal insulation systems due to the hygrothermal performance", Civil Engineering, Faculty of Engineering of University of Porto. http://hdl.handle.net/10216/59228.

Barreira, Eva, Elton Bauer, N. Mustelier and V. Freitas. 2015. *Measurement of materials emissivity – Influence of the procedure*.

Barreira, Eva and Vasco P. de Freitas. 2013. "Experimental study of the hygrothermal behaviour of External Thermal Insulation Composite Systems (ETICS)". *Building and Environment* no. 63:31-39. http://www.sciencedirect.com/science/article/pii/S0360132313000504.

Batchelor, Andrew W, Nee Lam Loh and Margam Chandrasekaran. 2011. *Materials Degradation and its Control by Surface Engineering*. 3rd ed. London: Imperial College Press. https://books.google.com/books?id=In9Ygl5yKt8C&lpg=PP1&hl=pt-PT&pg=PP1#v=onepage&q&f=false.

Bedon, Chiara, Carlos Pascual Agullo, Alessandra Luna-Navarro, Mauro Overend and Fabio Favoino. 2018. "Thermo-mechanical Investigation of Novel GFRP-glass Sandwich Facade Components". *Challenging Glass Conference Proceedings*:501-512%V 6. https://journals.open.tudelft.nl/index.php/cgc/article/view/2172.

Benmansour, Nadia, Boudjemaa Agoudjil, Abdelkader Gherabli, Abdelhak Kareche and Aberrahim Boudenne. 2014. "Thermal and mechanical performance of natural mortar reinforced with date palm fibers for use as insulating materials in building". *Energy and Buildings* no. 81:98-104. http://www.sciencedirect.com/science/article/pii/S0378778814004368.

Berardi, Umberto and Roya Hamideh Nosrati. 2018. "Long-term thermal conductivity of aerogel-enhanced insulating materials under different laboratory aging conditions". *Energy* no. 147:1188-1202. http://www.sciencedirect.com/science/article/pii/S0360544218300641.

Bocca, P. and A. Grazzini. 2012. "Mechanical Properties and Freeze-Thaw Durability of Strengthening Mortars". *Journal of Materials in Civil Engineering* no. 25 (2):274-280. Accessed 2016/02/16. http://dx.doi.org/10.1061/(ASCE)MT.1943-5533.0000597.

Borges, A., I. Flores-Colen and J. de Brito. 2018. "Physical and mechanical performance of cement-based renders with different contents of fly ash, expanded cork granules and expanded clay". *Construction and Building Materials* no. 191:535-543. https://www.sciencedirect.com/science/article/pii/S0950061818324425.

Borges, C., A. Santos Silva and R. Veiga. 2014. "Durability of ancient lime mortars in humid environment". *Construction and Building Materials* no. 66:606-620. http://www.sciencedirect.com/science/article/pii/S0950061814004917.

Bourdeau, Luc. 1998. "Sustainable Development and the future of construction in France - Report 3". Paper presented at Sustainable Development and the Future of Construction: A Comparison of Visions from Varous Countries, in Rotterdam.

Bourdeau, Luc. 1999. "Sustainable development and the future of construction: a comparison of visions from various countries". *Building Research & Information* no. 27 (6):354-366. https://doi.org/10.1080/096132199369183.

Braga, Mariana, Jorge de Brito and Rosário Veiga. 2012. "Incorporation of fine concrete aggregates in mortars". *Construction and Building Materials* no. 36:960-968. http://www.sciencedirect.com/science/article/pii/S0950061812004230.

Brás, Ana and Paulina Faria. 2017. "Effectiveness of mortars composition on the embodied carbon long-term impact". *Energy and Buildings* no. 154:523-528. http://www.sciencedirect.com/science/article/pii/S037877881730395X.

Brás, Ana, Márcio Leal and Paulina Faria. 2013. "Cement-cork mortars for thermal bridges correction. Comparison with cement-EPS mortars performance". *Construction and Building Materials* no. 49:315-327. http://www.sciencedirect.com/science/article/pii/S0950061813007368.

BRE. 2008. *Sustainable Construction: Simple ways to make it happen*. Edited by Building Research Establishment. United Kingdom: IHS BRE Press.

Brites, Joana, Dina Frade and Ana Santos. 2014. "Thermal mortars: the use of different types of aggregates and binders". Paper presented at Argamassas 2014 - I Symposium on Mortars and Thermal Coating Solutions, in Coimbra, Portugal. 5 and 6 June 2014. (*in Portuguese*)

Brundtland, Gro Harmen. 1987. *Our Common Future. Report of the World Commission on Environment and Development.*: United Nations.

Bruno Daniotti and Fulvio Re Cecconi. 2010. *State of the Art Report on Accelerated Laboratory Test Procedure and Correlation between Laboratory Tests and Service Life Data*. Edited by CIB. Vol. Publication 331, W080: Test Methods for Service life Prediction: Politecnico di Milano.

BSI. 2003. BS 7543: Guide to durability of buildings and building elements, products and components. United Kingdom: BSI.

Buratti, Cinzia, Elisa Moretti, Elisa Belloni and Fabrizio Agosti. 2014. "Development of Innovative Aerogel Based Plasters: Preliminary Thermal and Acoustic Performance Evaluation". *Sustainability* no. 6:5839-5852.

Cascione, Valeria, Eleonora Marra, Daniel Zirkelbach, Stefania Liuzzi and Pietro Stefanizzi. 2017. "Hygrothermal analysis of technical solutions for insulating the opaque building envelope". *Energy Procedia* no. 126:203-210. http://www.sciencedirect.com/science/article/pii/S1876610217336275.

Çavdar, A. 2012. "A study on the effects of high temperature on mechanical properties of fiber reinforced cementitious composites". *Composites Part B: Engineering* no. 43 (5):2452-2463. https://www.sciencedirect.com/science/article/pii/S1359836811004525.

CEB. 1992. Durable Concrete Structures. In *Design Guide*, edited by Comite Euro-International du Beton. Thomas Telford.

CEN. 1999. EN 1015 Methods of test for mortar for masonry. In *Part 11: Determination of flexural and compressive strength of hardened mortar*. Brussels: European Committee for Standardization.

CEN. 2000a. EN 197 Cement. In *Part 1: Composition, specifications and conformity criteria for common cements*. Brussels: European Commitee for Standardization.

CEN. 2000b. EN 1015 Methods of test for mortar for masonry. In *Part 12: Determination of adhesive strength of hardened rendering and plastering mortars on substrates*. Brussels: European Commitee for Standardization.

CEN. 2001. EN 12667 Thermal performance of building materials and products. . In *Determination of thermal resistance by means of guarded hot plate and heat flow meter methods. Dry and moist products of high and medium thermal resistance* Brussels: European Commitee for Standardization.

CEN. 2002a. EN 1015 Methods of test for mortar for masonry. Versão portuguesa da EN 998-1:2010, In *Part 21: Determination of the compatibility of one-coat rendering mortars with substrates*. Brussels: European Commitee for Standardization.

CEN. 2002b. EN 13497 Thermal insulation products for building applications In *Determination of the resistance to impact of external termal insulation composite systems (ETICS)*. Brussels: European Commitee for Standardization.

CEN. 2004a. EN 12504 Testing concrete in structures. In *Part 4: Determination os ultrasonic pulse velocity*. Brussels: European Commitee for Standardization.

CEN. 2004b. EN 13278 Gypsum binders and gypsum plasters. In *Part 2: Test Methods*. Brussels: European Commitee for Standardization.

CEN. 2007. EN 15026 Hygrothermal performance of building components and elements. In *Assessment of moisture transfer by numerical simulation*. Brussels: European Commitee for Standardization.

CEN. 2008. EN 13278 Gypsum binders and gypsum plasters. Versão portuguesa da EN 998-1:2010, In *Part 1: Definitions and requirements*. Brussels: European Commitee for Standardization.

CEN. 2010. EN 998 Specification for mortar for masonry. In *Part 1: Rendering and plastering mortar*. Brussels: European Commitee for Standardization.

CEN. 2017. EN 15824 Specifications for external renders and internal plasters based on organic binders. Brussels: European Commitee for Standardization.

CETEM. 2005. *Rochas e Minerais Industriais: Usos e Especificações*. Edited by A. B. da Luz and F. F. Lins. Rio de Janeiro: CETEM-MCT: Centro de Tecnologia Mineral, Ministério da Ciência e Tecnologia.

Cherki, A. B., B. Remy, A. Khabbazi, Y. Jannot and D. Baillis. 2014a. "Experimental thermal properties characterization of insulating cork-gypsum composite". *Construction and Building Materials* no. 54:202-209. https://www.sciencedirect.com/science/article/pii/S0950061813012336.

Cherki, Abou-bakr, Abdelhamid Khabbaz, Soumia Mounir and Youssef Maaloufa. 2014b. "Thermal properties of a new ecological building material / Granular cork embedded in white cement". Paper presented at International Congress on Materials & Structural Stability.

Chong, Choong Fee. 2015. "Increased Efficiency by Sustainable Mortars: Optiroc-Eco Line". Accessed 29 Janeiro. http://www.sika.com/en/group/sustainability/sustainability_news/sustainable-mortars.html.

Concrete Society. 1987. *Permeability Testing of Site Concrete. A review of methods and experience*.

Coomer, James C. 1979. *Quest for a sustainable society* Woodlands Conference on Growth Policy: Pergamon Policy Studies. https://books.google.com/books?hl=pt-PT&lr=&id=xt1sBQAAQBAJ&oi=fnd&pg=PP1&dq=the+nature+of+the+quest+for+a+sustainable+society&ots=W_csph-u8M&sig=6RkBoCIpfEA6QGAQQp1Vgow9DKo#v=onepage&q=the%20nature%20of%20the%20quest%20for%20a%20sustainable%20society&f=false.

Costa, Cristiana, Ana Velosa, Ângela Cerqueira, Paulo Caetano and Fernando Rocha. 2018. *Characterization of Portuguese diatomites in order to assess potential applications*. Vol. 15.

Costa, E., H. Carasek, O. Cascudo and S. Almeida. 2007. "Evaluation of brasilian test method for the adhesive strength determination of renders ". Paper presented at II National Congress on Construction Mortars, in Lisbon. 22-23 November. (*in Portuguese*)

Costigan, A. and S. Pavía. 2018. *Mechanical properties of clay brick masonry bound with hydraulic limes and hydrated calcium lime*.

Coutinho, A. Sousa. 1988. *Concrete Manufacturing and Properties*. Vol. 1: National Laboratory of Civil Engineering. (*in Portuguese*)

Coutinho, Joana de Sousa. 2002. Lime and hydraulic lime. In *Science os Materials – 1st Part*. Porto: FEUP. (*in Portuguese*)

Coutinho, Maria Joana Álvares Ribeiro de Sousa. 1998. "Improvement of the Durability of Concrete by Formwork Treatment", Civil Engineering, University of Porto. (*in Portuguese*)

Crowe, dana and Alec Feinberg. 2001. *"Concepts in Accelerated Testint" in Design for Reliability*. Edited by Jerry C. Whitaker. Electronics Handbook Series. Boca Raton, USA.

CSA. 2007. CSA S478-95 (R2007): Guideline on Durability in Buildings. Canada: CSA.
ČSN. 1968. ČSN 72 2452 - Testing of frost resistance of mortar. . Czech standard.
CSTB. 1993. Cahier 2669-4: Certification CSTB des enduits monocouches d'imperméabilisation. In *Modalités d'essais*. Paris: Center Scientifique et Technique du Bâtiment. (*in French*)
CSTB. 2016. "Avis Technique ou ATec". Accessed 5 Fevereiro. http://evaluation.cstb.fr/avis-technique/. (*in French*)
Cui, H. 2005. "Accelerated temperature cycle test and Coffin-Manson model for electronic packaging". Paper presented at Annual Reliability and Maintainability Symposium, 2005. Proceedings. 24-27 Jan. 2005.
D&S. 2011. D&S Technical Note 11-2. In *Model AE1 Emmitance Measurements using a Port Adapter, Model AE-ADP*, edited by Devices and Services Company. Dallas, Texas, USA.
D'Orazio, M. and A. Stazi. 2006. "Dynamic of moisture transfer in ancient plasters". *Journal of Cultural Heritage* no. 7 (2):116-122. Accessed 2006/6//. http://www.sciencedirect.com/science/article/pii/S1296207406000069.
Daniotti, Bruno, Fulvio Re Cecconi, Riccardo Paolini and Rosanna Galliano. 2013. "Durability Evaluation of External Thermal Insulation Composite Systems: Frequency Assessment of Thermal Shocks". Paper presented at CIB World Building Congress 2013, in Queensland. Maio 2013.
Daniotti, Bruno, Fulvio Re Cecconi, Riccardo Paolini, Rosanna Galliano, Jesica Ferrer and Luca Battaglia. 2012. "Durability evaluation of ETICS: analysis of failures case studies and heat and moisture transfer simulations to assess the frequency of critical events". Paper presented at IV Portuguese Congress in Construction Mortars and ETICS, in Coimbra.
Daniotti, Bruno, Sonia Lupica Spagnolo and Riccardo Paolini. 2008. "Climatic Data Analysis to Define Accelerated Ageing for Reference Service Life Evaluation". Paper presented at 11DBMC: 11th International Conference : Durability of Building Materials and Components, in Istanbul, Turkey. 11-14 May.
Dassault Systemes. 2015a. "Abaqus Analysis User's Guide". http://abaqus.software.polimi.it/v6.14/books/usb/default.htm.
Dassault Systemes. 2015b. "Introduction to Abaqus". http://academy.3ds.com/learning-materials/.
de Oliveira, M. P., N. P. Barbosa, S. M. Torres, A. F. Leal and C. G. Silva. 2012. "Gypsum-based composites with EVA waste and vermiculite". *Brazilian Journal of Agricultural and Environmental Engineering* no. 16 (6):684-689. https://www.researchgate.net/publication/262615493_Gypsum-based_composites_with_EVA_waste_and_vermiculite.
Degirmenci, N. and A. Yilmaz. 2009. "Use of diatomite as partial replacement for Portland cement in cement mortars". *Construction and Building Materials* no. 23 (1):284-288. https://www.sciencedirect.com/science/article/pii/S0950061807003236.
del Coz Díaz, J. J., P. J. García Nieto, C. Betegón Biempica and M. B. Prendes Gero. 2007. "Analysis and optimization of the heat-insulating light concrete hollow brick walls design by the finite element method". *Applied Thermal Engineering* no. 27 (8):1445-1456. http://www.sciencedirect.com/science/article/pii/S1359431106003450.
Delgado, J. M. P. Q., N. M. M. Ramos, E. Barreira and V. P. De Freitas. 2010. "A critical review of hygrothermal models used in porous building materials". *Journal of Porous Media* no. 13 (3):221-234. https://www.researchgate.net/publication/245407050_A_critical_review_of_hygrothermal_models_used_in_porous_building_materials.
Di Bella, G., V. Fiore, G. Galtieri, C. Borsellino and A. Valenza. 2014. "Effects of natural fibres reinforcement in lime plasters (kenaf and sisal vs. Polypropylene)". *Construction and Building Materials* no. 58:159-165. http://www.sciencedirect.com/science/article/pii/S0950061814001810.
do Rosário Veiga, M., Ana Fragata, Ana Luisa Velosa, Ana Cristian Magalhães and Goreti Margalha. 2010. "Lime-Based Mortars: Viability for Use as Substitution Renders in Historical Buildings".

International Journal of Architectural Heritage no. 4 (2):177-195. https://doi.org/10.1080/15583050902914678.

Doleželová, M., J. Krejsová and A. Vimmrová. 2018. "Influence of fine aggregate on some properties of gypsum mortars". *IOP Conference Series: Materials Science and Engineering* no. 379 (1):012005. http://stacks.iop.org/1757-899X/379/i=1/a=012005.

Donatelli, Antonio, Daniela Cuna, Maria ANtonia Tagliente, Maria Lucia Protopapa, Anna Mevoli, Patrizia Aversa, Caterina Blasi, Laura Capodieci and Vincenza Anna Maria Luprano. 2017. "Durability and resistance to degradation of hemp fibres-based insulationg envelopes". Paper presented at XIVDBMC: 14th International Conference on Durability of Building Materials and Components, in Ghent, Belgium. 29-31 May.

Duarte, Carlos. 2015. "Mortars and Thermal Insulation". *Expresso Special Dossier*, 17/10/2015. (*in Portuguese*)

Dylewski, R. and J. Adamczyk. 2014. "The comparison of thermal insulation types of plaster with cement plaster". *Journal of Cleaner Production* no. 83:256-262. https://www.sciencedirect.com/science/article/pii/S0959652614007598.

Dylewski, Robert and Janusz Adamczyk. 2011. "Economic and environmental benefits of thermal insulation of building external walls". *Building and Environment* no. 46 (12):2615-2623. http://www.sciencedirect.com/science/article/pii/S0360132311002034.

EAE. 2015. *Supporting the Development of Sustainable Buildings*. Baden-Baden.

EC. 2012. "Eco-Innovation: When Business Meets the Environment". Accessed 3 Fevereiro. https://ec.europa.eu/environment/eco-innovation/projects/en/projects/eamt.

ECEEE. 2018. Amending Directive 2010/31/EU on the energy performance of buildings and Directive 2012/27/EU on energy efficiency. edited by Directive 2018/844/EU. Official Journal of the European Union: European Comission.

EMO. 2013. "Goal 6". Accessed 29 Janeiro. http://www.euromortar.com/7-goals/6-creating-awareness-for-sustainability/.

EOTA. 1999. Assessment of working life of products. In *Guidance Document 003*. Brussels: European Organisation for Technical Approvals.

EOTA. 2004. *Exposure procedure for artificial weathering*. Brussels.

EOTA. 2013. ETAG 004. In *Guideline for European Technical Approval of External Thermal Insulation Composite Systems with Rendering*. Brussels: European Organisation for Technical Approvals.

Erhorn, Hans, Jens Ole Hansen, Henk Kaan and Mike Barker. 2007. *What are Eco-Buildings and are they needed in the Seventh Framework Programme (FP7)?*: BRITA in PUBs.

Escobar, Luis A. and William Q. Meeker. 2006. "A Review of Accelerated Test Models". *Statist. Sci.* no. 21 (4):552-577. https://projecteuclid.org:443/euclid.ss/1177334529.

ESCSI. 2007. *ENGINEERING PROPERTIES OF STRUCTURAL LIGHTWEIGHT CONCRETE*. Edited by Clay & Slate Institute Expandad Shale. Chapter 7.

Faria, Paulina, Vitor Silva and Inês Flores-Colen. 2012. "Hydraulic lime mortars and artificial pozzolans: laboratorial evaluation ". Paper presented at IV Portuguese Congress in Construction Mortars and ETICS, in Coimbra. (*in Portuguese*)

Farooqi, J. K. and M. A. Sheikh. 2005. "Finite Element Modeling of Thermal Transport in Composite Unit Cell using ABAQUS/CAE". Paper presented at ABAQUS Users' Conference, in Stockholm, Sweden. May 18-20, 2005

Fassa Bortolo. 2017. Cement-based thermal render. Techical information. http://sistemaintegrado.fassabortolo.pt/fichas-tecnicas/MI%20216_FT.pdf.

Ferrándiz-Mas, V., T. Bond, E. García-Alcocel and C. R. Cheeseman. 2014. "Lightweight mortars containing expanded polystyrene and paper sludge ash". *Construction and Building Materials* no. 61:285-292. http://www.sciencedirect.com/science/article/pii/S0950061814002827.

Ferrándiz-Mas, V. and E. García-Alcocel. 2013. "Durability of expanded polystyrene mortars". *Construction and Building Materials* no. 46:175-182. https://www.sciencedirect.com/science/article/pii/S0950061813003528.

Figueiredo, António, Romeu Vicente, José Lapa, Claudino Cardoso, Fernanda Rodrigues and Jérôme Kämpf. 2017. "Indoor thermal comfort assessment using different constructive solutions incorporating PCM". *Applied Energy* no. 208:1208-1221. http://www.sciencedirect.com/science/article/pii/S0306261917313156.

Fish, Jacob and Ted Belytschko. 2007. *A First Course in Finite Elements*. England: John Wiley & Sons, ltd.

Flores-Colen, I, J de Brito, VP Freitas, H Corvacho, A Sá and MA Quintela. 2010. "Performance assessment of external renders on facades". *A state of the art report on accelerated laboratory test procedures and correlation laboratory tests and service life data, CIB W80: Test methods for service life prediction*.

Flores-Colen, Inês, J de Brito and VP Freitas. 2005. "Diagnostic and maintenance techniques for removing stains on rendered walls". Paper presented at I Portuguese Congress in Construction Mortars, in Lisbon. (*in Portuguese*)

Flores-Colen, Inês dos Santos 2009. "Methodology for the In Service Performance Evaluation of Rendered Façades in the Perspective of Predictive Maintenance", Civil Engineering, Instituto Superior Técnico. (*in Portuguese*)

Fradical. 2016. "Design and Environment". Accessed 3 February. http://www.fradical.pt/empresa3.php. (*in Portuguese*)

Fragata, Ana, M. Rosário Veiga and Ana Velosa. 2016. "Substitution ventilated render systems for historic masonry: Salt crystallization tests evaluation". *Construction and Building Materials* no. 102:592-600. http://www.sciencedirect.com/science/article/pii/S0950061815305559.

Freitas, Vasco and Andreia Miranda. 2014. *Pathologies of external thermal insulation systems of ETICS type*. (*in Portuguese*)

Futureng. 2016. "EPS - Expanded Polystyrene". Accessed 15 March. http://www.futureng.pt/eps. (*in Portuguese*)

Gakkai, Nihon Kenchiku. 1993. *The English Edition of Principal Guide for Service Life Planning of Buildings*. Architectural Institute of Japan.

Gaspar, Pedro L. and Jorge De Brito. 2008. "Service life estimation of cement-rendered facades". *Building Research & Information* no. 36 (1):44-55. http://dx.doi.org/10.1080/09613210701434164.

Gomes, Augusto, Ana Paula Ferreira Pinto and João Bessa Pinto. 2013a. Gypsum and Lime for Construction. In *Construction Materials*. Lisbon: Instituto Superior Técnico. (*in Portuguese*)

Gomes, Augusto, Ana Paula Ferreira Pinto and João Bessa Pinto. 2013b. Portland Cement and Additions. In *Construction Materials*. Lisbon: Instituto Superior Técnico. (*in Portuguese*)

Gomes, M. Glória, I. Flores-Colen, F. da Silva and M. Pedroso. 2018. "Thermal conductivity measurement of thermal insulating mortars with EPS and silica aerogel by steady-state and transient methods". *Construction and Building Materials* no. 172:696-705. http://www.sciencedirect.com/science/article/pii/S0950061818306615.

Gomes, M. Glória, I. Flores-Colen, L. M. Manga, A. Soares and J. de Brito. 2017. "The influence of moisture content on the thermal conductivity of external thermal mortars". *Construction and Building Materials* no. 135:279-286. http://www.sciencedirect.com/science/article/pii/S0950061816320876.

Gonçalves da Silva, M. 2004. "Influence of Environmental Aging on Properties of Polymeric Mortars". *Journal of Materials in Civil Engineering* no. 16 (5):461-468. Accessed 2016/02/16. http://dx.doi.org/10.1061/(ASCE)0899-1561(2004)16:5(461).

Gonçalves de Carvalho, Carmo, Inês Flores-Colen and Paulina Faria. 2015. "Rehabilitation of renders of old buildings in Portugal: Survey, supporting methodology proposal and case study". *Structural Survey* no. 33 (4/5):337-353. https://www.emeraldinsight.com/doi/abs/10.1108/SS-04-2015-0024.

Gonçalves, S. 2004. "Variability and dispersion factor of adhesive strength of renders - Case study", Technology Faculty - Civil and Environment Engineering Department, University of Brasília. (*in Portuguese*)

Government of Portugal. 2013. Energy Regulation of Residential Buildings (REH). Decreto-Lei, In *1ª série - nº159*. Diário da República.

Grunewald, J. 2000. "DELPHIN 4.1–Documentation, theoretical fundamentals". *TU Dresden*.

Gutiérrez-González, S., J. Gadea, A. Rodríguez, M. T. Blanco-Varela and V. Calderón. 2012a. "Compatibility between gypsum and polyamide powder waste to produce lightweight plaster with enhanced thermal properties". *Construction and Building Materials* no. 34:179-185. Accessed 29 March 2012. https://www.sciencedirect.com/science/article/pii/S0950061812001389.

Gutiérrez-González, S., J. Gadea, A. Rodríguez, C. Junco and V. Calderón. 2012b. "Lightweight plaster materials with enhanced thermal properties made with polyurethane foam wastes". *Construction and Building Materials* no. 28 (1):653-658. Accessed 29 November 2011. https://www.sciencedirect.com/science/article/pii/S0950061811006040.

Hagentoft, C.E. 2001. *Introduction to Building Physics*. Ligthning Source.

Haillant, Olivier. 2011. "Accelerated weathering testing principles to estimate the service life of organic PV modules". *Solar Energy Materials and Solar Cells* no. 95 (5):1284-1292. http://www.sciencedirect.com/science/article/pii/S0927024810005180.

Hannawi, Kinda and William Prince-Agbodjan. 2015. "Transfer behaviour and durability of cementitious mortars containing polycarbonate plastic wastes". *European Journal of Environmental and Civil Engineering* no. 19 (4):467-481. http://dx.doi.org/10.1080/19648189.2014.960100.

Hens, H. and J. Carmeliet. 2001. "Performance prediction for masonry walls with EIFS using calculation procedures and laboratory testing". *Journal of Thermal Envelope and Building Science* no. 25 (3):167-188. https://journals.sagepub.com/doi/abs/10.1177/007542420202500314l?journalCode=jenc.

Hernández-Olivares, F., M. R. Bollati, M. Del Rio and B. Parga-Landa. 1999. "Development of cork-gypsum composites for building applications". *Construction and Building Materials* no. 13 (4):179-186. https://www.sciencedirect.com/science/article/pii/S0950061899000215.

Hong, Dongdong, Ming Fan, Lingjie Yu and Jian Cao. 2018. "An experimental study simulating the dissolution of gypsum rock". *Energy Exploration & Exploitation* no. 36 (4):942-954. https://journals.sagepub.com/doi/abs/10.1177/0144598717751927.

Huebner, Kenneth H., Donald L. Dewhirst, Douglas E. Smith and Ted G. Byrom. 2001. *The Finite Element Method for Engineers*. 4th ed.: Jonh Wiley & Sons, Inc.

WUFI Pro Germany.

IBP. 2016. WUFI Pro. In *WUFI Pro Manual*, edited by Fraunhofer Institut Bauphysik.

IETcc. 2016. http://www.ietcc.csic.es/index.php/en/technical-support/innoproductdit.

INE. 2015. "National Institute of Statistics". Accessed 1 February. https://www.ine.pt/xportal/xmain?xpid=INE&xpgid=ine_indicadores&indOcorrCod=0000085&contexto=bd&selTab=tab2. (*in Portuguese*)

ISO. 2000a. ISO 12571 Hygrothermal performance of building materials and products. In *Determination of higroscopic sorption properties*: International Standard.

ISO. 2000b. ISO 12572 Hygrothermal performance of building materials and products. In *Determination of water vapour transmission properties*: International Standard.

ISO. 2000c. ISO 15686 Buildings and constructed assets - Service life planning. In *Part 1: General principles*.

ISO. 2002. ISO 15148 Hygrothermal performance of building materials and products. In *Determination of water absorption coefficient by partial immersion*: International Standard.

ISO. 2006. ISO 9227: Corrosion tests in artificial atmospheres - Salt spray tests. International Standard.

ISO. 2007. ISO 8894 Refractory materials - Determination of thermal conductivity. In *Part 2: Hot-wire method (parallel)*: International Standard.

ISO. 2011. ISO 15686 Buildings and constructed assets - Service life planning. In *Part 1: General principles and framework*.

ISO. 2012. ISO 15686 Buildings and constructed assets - Service life planning. In *Part 2: Service life prediction procedures*.

ISORENEL. 2015. "Sprayed Cellulose". Accessed 18 December. http://www.isorenel.pt/1/celulose_projectada_898415.html. (*in Portuguese*)

IUCN. 1980. *The World Conservation Strategy: Living Resource Conservation for Sustainable Development*. Edited by United Nations Environmet Programme UNEP and World Wildlife Fund WWF. Gland, Switzerland: International Union for Conservation of Nature and Natural Resources.

Jelle, Bjørn Petter. 2012. "Accelerated climate ageing of building materials, components and structures in the laboratory". *Journal of Materials Science* no. 47 (18):6475-6496. https://doi.org/10.1007/s10853-012-6349-7.

Jelle, Bjørn Petter and Tom-Nils Nilsen. 2011. "Comparison of accelerated climate ageing methods of polymer building materials by attenuated total reflectance Fourier transform infrared radiation spectroscopy". *Construction and Building Materials* no. 25 (4):2122-2132. http://www.sciencedirect.com/science/article/pii/S0950061810005489.

Johnson, B. W. and R. McIntyre. 1996. "Analysis of test methods for UV durability predictions of polymer coatings". *Progress in Organic Coatings* no. 27 (1):95-106. http://www.sciencedirect.com/science/article/pii/0300944094005257.

Joseph, B. 2016. "Quality, Efficiency, Sustainability and Available Standards of Dry Mix Mortars ". *Techline 8 for the Construction Industry*.

Júlio, Maria de Fátima, António Soares, Laura M. Ilharco, Inês Flores-Colen and Jorge de Brito. 2016a. "Aerogel-based renders with lightweight aggregates: Correlation between molecular/pore structure and performance". *Construction and Building Materials* no. 124:485-495. http://www.sciencedirect.com/science/article/pii/S0950061816312041.

Júlio, Maria de Fátima, António Soares, Laura M. Ilharco, Inês Flores-Colen and Jorge de Brito. 2016b. "Silica-based aerogels as aggregates for cement-based thermal renders". *Cement and Concrete Composites* no. 72:309-318. http://www.sciencedirect.com/science/article/pii/S0958946516302815.

Kabeer, K. I. Syed Ahmed and Ashok Kumar Vyas. 2018. "Utilization of marble powder as fine aggregate in mortar mixes". *Construction and Building Materials* no. 165:321-332. http://www.sciencedirect.com/science/article/pii/S0950061818300631.

Klimchouk, Alexander. 2000. *Dissolution and conversions of gypsum and anhydrite*.

Kottek, Markus, Jürgen Grieser, Christoph Beck, Bruno Rudolf and Franz Rubel. 2006. "World Map of the Köppen-Geiger climate classification updated". *Meteorologische Zeitschrift* no. 15 (No.3):259-263.

Krus, M. 1996. *Moisture transport and storage coefficients of porous mineral building materials: Theoretical principles and new test methods*.

Krus, M., T. S. Nouidui and K. Sedlbauer. 2009. "Application of software tools for moisture protection of buildings in different climate zones. Special Example: Control of air humidifier in a cold climate for high comfort and no risk of mould growth in building room ". Paper presented at 6th International Conference on Cold Climate, Heating, Ventilating and Air-Conditioning, in Sisimiut, Greenland. 16-19 March 2009.

Künzel, H. M., Th Schmidt and A. Holm. 2002. *Exterior Surface Temperature of Different Wall Constructions Comparison of Numerical Simulation and Experiment*. Vol. 11.

Künzel, Hartwig M. 1995. "Simultaneous Heat and Moisture Transport in Building Components. One- and two-dimensional calculation using simple parameters.".

Künzel, Hartwig M. and Kurt Kiessl. 1996. *Calculation of heat and moisture transfer in exposed building cmponents*. Vol. 40.

Kus, Hülya and G. Kalmar. 2002. "Long-term performance of external renderings on Autoclaved Aerated Concrete walls". Paper presented at 9DBMC: 9th International Conference : Durability of Building Materials and Components.

Lalic, Milan. 2017. "Mechanical Behavior of thermal mortars with expanded polystyrene aggregates".

Leitão, Luiz Augusto. 1896. *Engineering Department: elementary course of constructions:*. Edited by Central School programme of Engineering Department. Lisbon: National Press. (*in Portuguese*)

Lertsutthiwong, Pranee, Srichalai Khunthon, Krisana Siralertmukul, Khanittha Noomun and Suwalee Chandrkrachang. 2008. "New insulating particleboards prepared from mixture of solid wastes from tissue paper manufacturing and corn peel". *Bioresource Technology* no. 99 (11):4841-4845. http://www.sciencedirect.com/science/article/pii/S0960852407007961.

Lewry, A. and L. F. E. Crewdson. 1994. *Approaches to testing the durability of materials used in the construction and maintenance of buildings*. Vol. 8.

Liu, G. R. and S. S. Quek. 2003. *The Finite Element Method. A practical course.* Edited by Elsevier Science. Butterworth-Heinemann.

LNEC. 2002. FE Pa 39 - Test Report of Wall Coatings. In *Determination of water absorption under low pressure*. Lisbon.

LNEC. 2010a. FE Pa 43 - Test Report of Wall Coatings. In *Mechanical characteristics assessment by ultrassounds measurement.* Lisboa.

LNEC. 2010b. *Rules for the elaboration of a European Technical Approval (ETA) for external thermal insulationcomposite systems (ETICS)*. Lisbon. (*in Portuguese*)

LNEC. 2015a. FE Pa 44 - Test Report of Wall Coatings. In *Determination of open porosity and bulk and real densities*. Lisbon.

LNEC. 2015b. *FE Pa 44 - Test Report of Wall Coatings, in Determination of open porosity and bulk and real densities*. Lisbon.

LNEC. 2016a. "Agreement of Construction Products and Systems". Accessed 5 February. http://www.lnec.pt/pt/servicos/apreciacao-de-produtos-e-sistemas-de-construcao/documentos-de-homologacao-dh/.

LNEC. 2016b. "Evaluation/European Technical Approval (ETA)". Accessed 5 February. http://www.lnec.pt/pt/servicos/apreciacao-de-produtos-e-sistemas-de-construcao/avaliacoes-aprovacoes-tecnicas-europeias-eta/. (*in Portuguese*)

LNEC. 2018. ETA Weber.therm classic system. Eupean Technical Assessment. https://www.weber.com.pt/uploads/media/ETA_18_0150_en_weber.therm_classic_2018.pdf.

López, O., I. Torres, A. S. Guimarães, J. M. P. Q. Delgado and V. P. de Freitas. 2017. "Inter-laboratory variability results of porous building materials hygrothermal properties". *Construction and Building Materials* no. 156:412-423. http://www.sciencedirect.com/science/article/pii/S0950061817317476.

Madrigal, Leticia Ortega, Begoña Serrano Lanzarote and José M Fran Bretones. 2015. "Proposed method of estimating the service life of building envelopes". *Revista de la construcción* no. 14:60-68. http://www.scielo.cl/scielo.php?script=sci_arttext&pid=S0718-915X2015000100008&nrm=iso.

Maia, J., N. M. M. Ramos, V. P. De Freitas and Â Sousa. 2015. "Laboratory tests and potential of thermal insulation plasters". Paper presented at Energy Procedia.

Maia, J., N. M. M. Ramos and R. Veiga. 2016. "Properties of thermal mortars: their relevance to the product assessment, based on hygrothermal simulation". Paper presented at Argamassas 2016 - Symposium on Mortars and Thermal Coating Solutions, in Coimbra, Portugal. 16-17 June.

Maia, J., N. M. M. Ramos and R. Veiga. 2017. "Durability of thermal renders: material properties and system performance". Paper presented at XIV DBMC – 14th International Conference on Durability of Building Materials and Components, in Ghent University, Belgium. 29-31 May 2017.

Maia, J., N. M. M. Ramos and R. Veiga. 2018a. "Hygrothermal performance of thermal plastering systems to the rehabilitation of walls". Paper presented at Patorreb 2018 – XI Conference on Pathology and Building Rehabilitation, in Rio de Janeiro, Brazil. 4-6 April 2018. (*in Portuguese*)

Maia, J., Nuno M. M. Ramos and R. Veiga. 2018b. "Evaluation of the hygrothermal properties of thermal rendering systems". *Building and Environment* no. 144:437-449. http://www.sciencedirect.com/science/article/pii/S0360132318305298.

Malanho, Sofia and Maria do Rosário Veiga. 2014. "Adapted techniques and requirements for ETICS not covered by ETAG 004". Paper presented at Argamassas 2014 - I Symposium on Mortars and Thermal Coating Solutions, in Coimbra, Portugal. 5 and 6 June 2014. (*in Portuguese*)

Martias, C., Y. Joliff and C. Favotto. 2014. "Effects of the addition of glass fibers, mica and vermiculite on the mechanical properties of a gypsum-based composite at room temperature and during a fire test". *Composites Part B: Engineering* no. 62:37-53. https://www.sciencedirect.com/science/article/pii/S1359836814000961.

Martias, C., Y. Joliff, B. Nait-Alib, J. Rogezc and C. Favottoc. 2013. "A new composite based on gypsum matrix and mineral additives: Hydration process of the matrix and thermal properties at room temperature". *Thermochimica Acta* no. 567:15-26. https://www.sciencedirect.com/science/article/pii/S0040603113001184.

Matias, Gina, Paulina Faria and Isabel Torres. 2014. "Lime mortars with ceramic wastes: Characterization of components and their influence on the mechanical behaviour". *Construction and Building Materials* no. 73:523-534. http://www.sciencedirect.com/science/article/pii/S0950061814011246.

Matias, Gina, Saúl Martins, Ana Isabel Neves, Nuno Simões, Paulo Amado Mendes and Hugo Borrego. 2014. "Characterization of sprayed cork in emulsion". Paper presented at Argamassas 2014 - I Symposium on Mortars and Thermal Coating Solutions, in Coimbra, Portugal. 5 and 6 June 2014. (*in Portuguese*)

Mazhoud, Brahim, Florence Collet, Sylvie Pretot and Julien Chamoin. 2016. "Hygric and thermal properties of hemp-lime plasters". *Building and Environment* no. 96:206-216. http://www.sciencedirect.com/science/article/pii/S0360132315301761.

McCarthy, Kathryn A. 2018. "Thermal conduction in solids". Accessed 2018/9/28/. https://www.accessscience.com:443/content/thermal-conduction-in-solids/689300.

Melo, M. O. B. C., L. B. Da Silva, A. S. Coutinho, V. Sousa and N. Perazzo. 2012. "Energy efficiency in building installations using thermal insulating materials in northeast Brazil". *Energy and Buildings* no. 47:35-43. https://www.sciencedirect.com/science/article/pii/S0378778811005676.

Memon, Shazim Ali. 2014. "Phase change materials integrated in building walls: A state of the art review". *Renewable and Sustainable Energy Reviews* no. 31:870-906. http://www.sciencedirect.com/science/article/pii/S1364032113008563.

Millar, William and George Bankart. 2009. *Plastering Plain & Decorative*. ed Taylor &Francis. Fourth ed: Routledge. https://books.google.com/books?id=PyLICQAAQBAJ&lpg=PP4&ots=FCSSEejwdi&dq=Plastering%20Plain%20%26%20Decorative%2C%20ed.%20William%20Millar%20%20and%20George%20Bankart&hl=pt-PT&pg=PP4#v=onepage&q=Plastering%20Plain%20&%20Decorative,%20ed.%20William%20Millar%20%20and%20George%20Bankart&f=false.

Ministère de l'Égalité des Territoires et du Logement. 2012. RT 2012 - Réglementation Thermique. In *Décret nº. 2012-1530 du 28 décembre 2012 relatif aux caractéristiques thermiques et à la performance énergétique des constructions de bâtiments*. Journal Officiel de la République Française

Ministry of Local Government and Modernisation. 2017. TEK17 - Regulations on technical requirements for building works.

Mňahončáková, E., M. Jiřičková, Z. Pavlík, L. Fiala, P. Rovnaníková, P. Bayer and R. Černý. 2006. "Effect of Moisture on the Thermal Conductivity of a Cementitious Composite". *International Journal of Thermophysics* no. 27 (4):1228-1240. https://doi.org/10.1007/s10765-006-0073-y.

Nilica, R. and H. Harmuth. 2005. "Mechanical and fracture mechanical characterization of building materials used for external thermal insulation composite systems". *Cement and Concrete Research* no. 35 (8):1641-1645. https://www.mdpi.com/2071-1050/9/3/373/pdf.

Norvaišiene, R., G. Griciute, R. Bliudžius and J. Ramanauskas. 2013. "The changes of moisture absorption properties during the service life of external thermal insulation composite system". *Medziagotyra* no. 19 (1):103-107. http://www.matsc.ktu.lt/index.php/MatSc/article/viewFile/3834/2397.

Nosrati, R. H. and U. Berardi. 2018. "Hygrothermal characteristics of aerogel-enhanced insulating materials under different humidity and temperature conditions". *Energy and Buildings* no. 158:698-711. https://www.sciencedirect.com/science/article/pii/S0378778817318091.

Ochs, Hartmut, Jörg Vogelsang and Gabriela Meyer. 2003. "Enhanced surface roughness of organic coatings due to UV-degradation: an unknown source of EIS-artifacts". *Progress in Organic Coatings* no. 46 (3):182-190. http://www.sciencedirect.com/science/article/pii/S0300944003000043.

Oliveira, R., J. de Brito and R. Veiga. 2013. "Incorporation of fine glass aggregates in renderings". *Construction and Building Materials* no. 44:329-341. http://www.sciencedirect.com/science/article/pii/S0950061813002523.

Oliveira, Renata, Jorge de Brito and Rosário Veiga. 2015. "Reduction of the cement content in rendering mortars with fine glass aggregates". *Journal of Cleaner Production* no. 95:75-88. http://www.sciencedirect.com/science/article/pii/S0959652615001626.

Ou, Danny, Roxana Trifu and Gregory Caggiano. 2013. "Sprayable Aerogel Bead Compositions With High Shear Flow Resistance and High Thermal Insulation Value ". Accessed 18 Dezembro. http://www.techbriefs.com/component/content/article/ntb/tech-briefs/materials/16129.

Paiva, Anabela, Sandra Pereira, Ana Sá, Daniel Cruz, Humberto Varum and Jorge Pinto. 2012. "A contribution to the thermal insulation performance characterization of corn cob particleboards". *Energy and Buildings* no. 45:274-279. http://www.sciencedirect.com/science/article/pii/S0378778811005652.

Palomo, A., M.T. Blanco-Varela, S. Martinez-Ramirez, F. Puertas and C. Fortes. 2000. " Historic Mortars: Characterization and Durability. New Tendencies for Research ". Paper presented at Proceedings 9th International Congress on Deterioration and Conservation of Stone, in Venice. 19-24 June 2000.

Pan, Zhongxiang, Bohong Gu and Baozhong Sun. 2015. "Numerical analyses of thermo-mechanical behaviors of 3-D rectangular braided composite under different temperatures". *The Journal of The Textile Institute* no. 106 (2):173-186. https://doi.org/10.1080/00405000.2014.906941.

Panesar, D. K. and B. Shindman. 2012. "The mechanical, transport and thermal properties of mortar and concrete containing waste cork". *Cement and Concrete Composites* no. 34 (9):982-992. https://www.sciencedirect.com/science/article/pii/S0958946512001205.

Papanyianni, I. and M. Stefanidou. 2001. "The Evolution of Porosity in Lime Based Mortars". Paper presented at 8th Euroseminar on Microscopy Applied to Building Materials, in Athens, Greece.

Pedro Júlio, João, Anabela Paiva and Caroline Dominguez. 2013. *Aspects for the evaluation of Portuguese dwellings' quality and sustainability*. Vol. 5.

Pereira, F. 2008. "Influence of Temperature Variations on Performance of Masonry Façades", Civil Engineering, University of Porto. (*in Portuguese*)

Pereira, H. 1979. "Chemical composition of cork. Present state of knowledge". *Cortiça* no. 483:259-264.

Pereira, Helena. 2007. *Cork: Biology, Production and Uses*.

Pérez-Lombard, Luis, José Ortiz and Christine Pout. 2008. "A review on buildings energy consumption information". *Energy and Buildings* no. 40 (3):394-398. http://www.sciencedirect.com/science/article/pii/S0378778807001016.

Perman, Roger, Yue Ma, James McGilvray and Michael Common. 2003. *Natural Resource and Environmental Economics*. 3rd ed. Edinburgh Gate, Harlow, Essex CM20 2JE: Pearson Education Limited

Pinheiro, Manuel Duarte. 2006. *Environment and Sustainable Construction*. Edited by IST/DECivil. Amadora. (*in Portuguese*)

Pipilikaki, P. and M. Beazi-Katsioti. 2009. "The assessment of porosity and pore size distribution of limestone Portland cement pastes". *Construction and Building Materials* no. 23 (5):1966-1970. http://www.sciencedirect.com/science/article/pii/S0950061808002638.

Polirigido. 2015. "Products - Rock wool". Accessed 18 December. http://www.polirigido.com/pt/produtos/isolamentos-termicos/la-de-rocha-projetada/la-de-rocha. (*in Portuguese*)

Puertas, F., T. Amat, A. Fernández-Jiménez and T. Vázquez. 2003. "Mechanical and durable behaviour of alkaline cement mortars reinforced with polypropylene fibres". *Cement and Concrete Research* no. 33 (12):2031-2036. http://www.sciencedirect.com/science/article/pii/S0008884603002229.

Ramos, N. M. M., J. M. P. Q. Delgado and V. P. de Freitas. 2010. "Influence of finishing coatings on hygroscopic moisture buffering in building elements". *Construction and Building Materials* no. 24 (12):2590-2597. http://www.sciencedirect.com/science/article/pii/S0950061810002333.

Ramos, N. M. M., M. L. Simões, J. M. P. Q. Delgado and V. P. de Freitas. 2012. "Reliability of the pull-off test for in situ evaluation of adhesion strength". *Construction and Building Materials* no. 31:86-93. http://www.sciencedirect.com/science/article/pii/S0950061811007872.

Ramos, Nuno, Eva Barreira, Maria Simões and João Delgado. 2014. *Probabilistic Risk Assessment Methodology of Exterior Surfaces Defacement Caused by Algae Growth*. Vol. 140.

Ramos, Nuno Monteiro, João Quesado Delgado, Eva Barreira and Vasco Peixoto de Freitas. 2009. "Hygrothermal properties applied in numerical simulation: Interstitial condensation analysis". *Journal of Building Appraisal* no. 5 (2):161-170. https://doi.org/10.1057/jba.2009.27.

Reichenauer, G., U. Heinemann and H. P. Ebert. 2007. "Relationship between pore size and the gas pressure dependence of the gaseous thermal conductivity". *Colloids and Surfaces A: Physicochemical and Engineering Aspects* no. 300 (1):204-210. http://www.sciencedirect.com/science/article/pii/S0927775707000453.

RILEM. 1998. RILEM-MS-A4: Determination of the durability of hardened mortar. Materials and structures.

Rouquerol, J., D. Avnir, C. W. Fairbridge, D. H. Everett, J. M. Haynes, N. Pernicone, J. D. F. Ramsay, K. S. W. Sing and K. K. Unger. 1994. Recommendations for the characterization of porous solids (Technical Report). In *Pure and Applied Chemistry*. https://www.degruyter.com/view/j/pac.1994.66.issue-8/pac199466081739/pac199466081739.xml.

Sá, João. 2018. "Durability of ETICS with high solar absorption ", Civil, Faculty of Engineering of University of Porto. (*in Portuguese*)

Saint-Gobain Weber. 2016. Weber.therm mechanic system. Techical information. https://www.weber.com.pt/uploads/media/Ficha_Tecnica_Sistema_weber.therm_mechanic_obra_nova_2015.pdf.

Salavessa, Eunice, S. Jalali, L. M. O. Sousa, L. Fernandes and A. M. Duarte. 2013. "Historical plasterwork techniques inspire new formulations". *Construction and Building Materials* no. 48:858-867. https://www.sciencedirect.com/science/article/pii/S0950061813006788.

Sariisik, Ali and Gencay Sariisik. 2012. "New production process for insulation blocks composed of EPS and lightweight concrete containing pumice aggregate". *Materials and Structures* no. 45 (9):1345-1357. https://doi.org/10.1617/s11527-012-9836-z.

Secil Argamassas. 2017. Isodur - Sprayed thermal render. Techical information. https://secilpro.com/upload/documents/5970d8aa95bf1.pdf.

Sehizadeh, Ali and Hua Ge. 2016. "Impact of future climates on the durability of typical residential wall assemblies retrofitted to the PassiveHaus for the Eastern Canada region". *Building and Environment* no. 97:111-125. http://www.sciencedirect.com/science/article/pii/S0360132315301943.

Šeputyte-Jucike, J., G. A. Sezeman, M. Sinica, M. Kligys and S. Vaitkus. 2014. "Impact of granules from crushed expanded polystyrene package on properties of thermo-insulating plaster". *Journal of Civil Engineering and Management* no. 20 (4):581-589. http://journals.vgtu.lt/index.php/JCEM/article/download/3153/2616.

Sequeira, P., N. Vieira, L. Silva, I. Flores-Colen and A. Soares. 2016. "Behaviour of a predosed thermal insulation mortar for walls coating as a function of mixing and preparation conditions". Paper presented at Argamassas 2016 - Symposium on Mortars and Thermal Coating Solutions, in Coimbra, Portugal. (*in Portuguese*)

Silva, A. 2015. "Statistical Modeling of Service Life Prediction of Façade Coatings", Civil Engineering, Instituto Superior Técnico. (*in Portuguese*)

Silva, A., J. de Brito and P. L. Gaspar. 2011. "Service life prediction model applied to natural stone wall claddings (directly adhered to the substrate)". *Construction and Building Materials* no. 25 (9):3674-3684. http://www.sciencedirect.com/science/article/pii/S0950061811001280.

Silva, A., J. de Brito and P. L. Gaspar. 2012. "Application of the factor method to maintenance decision support for stone cladding". *Automation in Construction* no. 22:165-174. http://www.sciencedirect.com/science/article/pii/S0926580511001269.

Silva, António Santos. 2013. "The importance of characterising old mortars for conservation and rehabilitation of buildings". Paper presented at Seminar on Renderings of Old Buildings, in Ponta Delgada, Açores. (*in Portuguese*)

Silva, N., José Luís Aguiar, Luís Bragança, M. T. Freire and Julissa Avellaneda. 2018. *Interior comfort regulation with gypsum plasters*.

Silva, S. P., M. A. Sabino, E. M. Fernandes, V. M. Correlo, L. F. Boesel and R. L. Reis. 2005. "Cork: properties, capabilities and applications". *International Materials Reviews* no. 50 (6):345-365. https://doi.org/10.1179/174328005X41168.

Sival - Gessos Especiais. 2017. Project Thermo C. Techical information. https://sival.pt/img/cms/pdfs/fichas_tecnicas_pt/PROJECT%20THERMO%20C.pdf.

Skoczylas, Katarzyna and Teresa Rucińska. 2018. "The effects of waste glass cullets and nanosilica on the long-term properties of cement mortars". *E3S Web Conf.* no. 49:00102. https://doi.org/10.1051/e3sconf/20184900102.

Soares, A., M. de Fátima Júlio, I. Flores-Colen, L. M. Ilharco and J. D. Brito. 2018. "EN 998-1 performance requirements for thermal aerogel-based renders". *Construction and Building Materials* no. 179:453-460. https://www.sciencedirect.com/science/article/pii/S0950061818312832.

Soares, António, Inês Flores-Colen and Jorge de Brito. 2017. "Experimental Study of the Compressive Strength of Multi-Coat Renders". *Materials Research* no. 20:1254-1265. https://www.researchgate.net/publication/271677601_Influence_of_slenderness_on_the_compressive_strength_evaluation_of_cores_of_renders.

Soares, António, Maria Júlio, Inês Flores-Colen, Laura Ilharco, Jorge Brito and José Martinho. 2014. *Water-Resistance of Mortars with Lightweight Aggregates*. Vol. 634.

Sousa, Luísa C., Catarina F. Castro, Carlos C. António and Hipólito Sousa. 2011. "Topology optimisation of masonry units from the thermal point of view using a genetic algorithm". *Construction and Building Materials* no. 25 (5):2254-2262. http://www.sciencedirect.com/science/article/pii/S0950061810005222.

Sousa, R. 2009. "Caracterização Experimental Mecânica e Análise Numérica de Elementos para Alvenaria com Isolamento Térmico Distribuído", Civil Engineering, University of Porto.

Sousa, Rita, Dina Frade and Ana Santos. 2014. "Development, characterization and execution of thermal solutions with cork". Paper presented at Argamassas 2014 - I Symposium on Mortars and Thermal Coating Solutions, in Coimbra, Portugal. 5 and 6 June 2014. (*in Portuguese*)

Sousa, Vitor, Fernando Dias Pereira and Jorge de Brito. 2005. "Traditional Mortars: Main Causes of Degradation". *Engenharia Civil* no. 23 5-18.

Stahl, Th, S. Brunner, M. Zimmermann and K. Ghazi Wakili. 2012. "Thermo-hygric properties of a newly developed aerogel based insulation rendering for both exterior and interior applications". *Energy and Buildings* no. 44 (1):114-117. https://www.scopus.com/inward/record.uri?eid=2-s2.0-81855218661&doi=10.1016%2fj.enbuild.2011.09.041&partnerID=40&md5=273199aa88c0c9af1b6b3ed82c4e7037.

Swimm, K., G. Reichenauer, S. Vidi and H.-P. Ebert. 2009. "Gas Pressure Dependence of the Heat Transport in Porous Solids with Pores Smaller than 10 μm". *International Journal of Thermophysics* no. 30 (4):1329-1342. https://doi.org/10.1007/s10765-009-0617-z.

Tavares, A., A. Costa, F. Rocha and A. Velosa. 2016. "Absorbent materials in waterproofing barriers, analysis of the role of diatomaceous earth". *Construction and Building Materials* no. 102:125-132. http://www.sciencedirect.com/science/article/pii/S0950061815305900.

The World Bank. 2014. "CO2 emissions from manufacturing industries and construction (% of total fuel combustion) ". Accessed 29 Janeiro. http://data.worldbank.org/indicator/EN.CO2.MANF.ZS/countries/EU-1W-PT?display=graph.

Tittarelli, F. 2013. "Effect of low dosages of waste GRP dust on fresh and hardened properties of mortars: Part 2". *Construction and Building Materials* no. 47:1539-1543. https://www.sciencedirect.com/science/article/pii/S0950061813006041.

Toman, J and R Černý. 2001. "Thermal conductivity of high performance concrete in wide temperature and moisture ranges". *Acta Polytechnica* no. 41 (1).

Torres, I. and G. Matias. 2016. "Waste recovery to integration in renders". Paper presented at Argamassas 2016 - Symposium on Mortars and Thermal Coating Solutions, in Coimbra, Portugal. 16-17 June. (*in Portuguese*)

Torres, Isabel, Rosário Veiga and Vasco Freitas. 2018. "Influence of Substrate Characteristics on Behavior of Applied Mortar". *Journal of Materials in Civil Engineering* no. 30 (10):04018254. https://ascelibrary.org/doi/abs/10.1061/%28ASCE%29MT.1943-5533.0002339.

Ünal, Osman, Tayfun Uygunoğlu and Ahmet Yildiz. 2007. "Investigation of properties of low-strength lightweight concrete for thermal insulation". *Building and Environment* no. 42 (2):584-590. http://www.sciencedirect.com/science/article/pii/S0360132305004294.

UNEP. 2004. "Eco-Design". In *Resource Kit on Sustainable Consumption and Production*, edited by United Nations Environment Programme. UNEP.

Vale, Henrique, Humberto Melo, António Soares, Inês Flores-Colen and Maria GLória Gomes. 2014. "Performance of industrial thermal insulation renders". Paper presented at 9th International Masonry Conference 2014, in Guimarães. 7, 8 and 9 July 2014.

Vasconcelos, Graça, Andreia Martins, Sandra Cunha, Aires Camões and Paulo Lourenco. 2013. *Mechanical Behavior of Gypsum and Cork Based Composite Material*. Vol. 361-366.

Veiga, Maria do Rosário. 2010. "Thermal insulation coatings for façades based on mortars: behaviour and quality evaluation". Paper presented at Contribution of Mortars and ETICS to the Energy Efficiency of Buildings, in Lisbon. (*in Portuguese*)

Veiga, Maria do Rosário. 2011. "ETICS and Thermal mortars: Compliance requirements". Paper presented at Seminar: Energy Efficient Façades: ETICS, Thermal Mortats and Windows. What should be required?, in Lisboa. 15 November 2011.

Vejmelková, E., M. Keppert, Z. Keršner, P. Rovnaníková and R. Černý. 2012. "Mechanical, fracture-mechanical, hydric, thermal, and durability properties of lime-metakaolin plasters for renovation of historical buildings". *Construction and Building Materials* no. 31:22-28. https://www.sciencedirect.com/science/article/pii/S0950061811007744.

Velosa, A. and R. Veiga. 2008. "Lime-metakaolin mortars - properties and applications". Paper presented at SB07 Lisbon - Sustainable Construction, Materials and Practices: Challenge of the Industry for the New Millenium, in Rotterdam (Netherlands). 2008. http://www.irbnet.de/daten/iconda/CIB11755.pdf. (*English*)

Wang, Ru and Christian Meyer. 2012. "Performance of cement mortar made with recycled high impact polystyrene". *Cement and Concrete Composites* no. 34 (9):975-981. http://www.sciencedirect.com/science/article/pii/S0958946512001412.

WBCSD. 2000. *Eco-Efficiency: Creating more value with less impact*. Edited by World Business Council for Sustainable Development. Geneva, Switzerland: WBCSD.

Westgate, P., K. Paine and R. J. Ball. 2018. "Physical and mechanical properties of plasters incorporating aerogel granules and polypropylene monofilament fibres". *Construction and Building Materials* no. 158:472-480. https://www.sciencedirect.com/science/article/pii/S095006181732010X.

Worch, Anatol. 2004. *The Behaviour of Vapour Transfer on Building Material Surfaces: The Vapour Transfer Resistance*. Vol. 28.

Xu, Shuqiang, Julin Wang, Qinglin Ma, Xin Zhao and Tao Zhang. 2014. "Study on the lightweight hydraulic mortars designed by the use of diatomite as partial replacement of natural hydraulic lime and masonry waste as aggregate". *Construction and Building Materials* no. 73:33-40. http://www.sciencedirect.com/science/article/pii/S0950061814010782.

Zeng, Qiang, Kefei Li, Teddy Fen-Chong and Patrick Dangla. 2012. "Effect of porosity on thermal expansion coefficient of cement pastes and mortars". *Construction and Building Materials* no. 28 (1):468-475. http://www.sciencedirect.com/science/article/pii/S0950061811005320.

Zhang, Dajiang, Jihui Zhao, Dongmin Wang, Chenyang Xu, Mengyi Zhai and Xiangdong Ma. 2018. "Comparative study on the properties of three hydraulic lime mortar systems: Natural hydraulic lime mortar, cement-aerial lime-based mortar and slag-aerial lime-based mortar". *Construction and Building Materials* no. 186:42-52. http://www.sciencedirect.com/science/article/pii/S0950061818317252.

Zhao, Jun-Jie, Yuan-Yuan Duan, Xiao-Dong Wang and Bu-Xuan Wang. 2012. "Effects of solid–gas coupling and pore and particle microstructures on the effective gaseous thermal conductivity in aerogels". *Journal of Nanoparticle Research* no. 14 (8):1024. https://doi.org/10.1007/s11051-012-1024-0.

Zhao, Shu-yuan, Bo-ming Zhang and Xiao-dong He. 2009. "Temperature and pressure dependent effective thermal conductivity of fibrous insulation". *International Journal of Thermal Sciences* no. 48 (2):440-448. http://www.sciencedirect.com/science/article/pii/S1290072908001191.

Zheng, R., A. Janssens, J. Carmeliet, W. Bogaerts and H. Hens. 2004. "An evaluation of highly insulated cold zinc roofs in a moderate humid region—part I: hygrothermal performance". *Construction and Building Materials* no. 18 (1):49-59. http://www.sciencedirect.com/science/article/pii/S0950061803000254.

Zhou, Ao, Kwun-Wah Wong and Denvid Lau. 2014. "Thermal Insulating Concrete Wall Panel Design for Sustainable Built Environment". *The Scientific World Journal* no. 2014:12. http://dx.doi.org/10.1155/2014/279592.

Zillig, W., K. Lenz and M. Krus. 2003. *Condensation on façades-influence of construction type and orientation*.

ANNEXES

ANNEX 1 – WUFI PRO DATABASE MATERIALS

Table 124 – Physical and hygrothermal properties of aerated concrete, exterior render and gypsum plaster used in the hygrothermal simulations (IBP 2016).

Classification	Property	Aerated concrete block	Exterior render	Gypsum plaster
Basic properties	ρ (bulk) (kg/m³)	600	1310	850
	P (%)	72.0	36.0	65.0
	c (J/kg.ºC)[a]	850	850	850
	λ (dry) (W/mºC)	0.1400	0.8700	0.2000
	μ (dry-cup)	8.3	8.0	8.3
Complementary properties	w_{80} (kg/m³)	10.70	15.0	6.30
	$W_{free\ sat.}$ (kg/m³)	470.00	192.00	400.00
	A_w (kg/m².s$^{0.5}$)	—	—	—
	λ (w-dependent) (W/mºC)	Generated[c]	Generated[c]	Generated[c]
	D_{ws} (m²/s)	Fig. 209-a)	Fig. 209-b)	Fig. 210-a)

[a]WUFI Pro Database (IBP 2016)Generated curve by WUFI Pro calculation (IBP 2016)

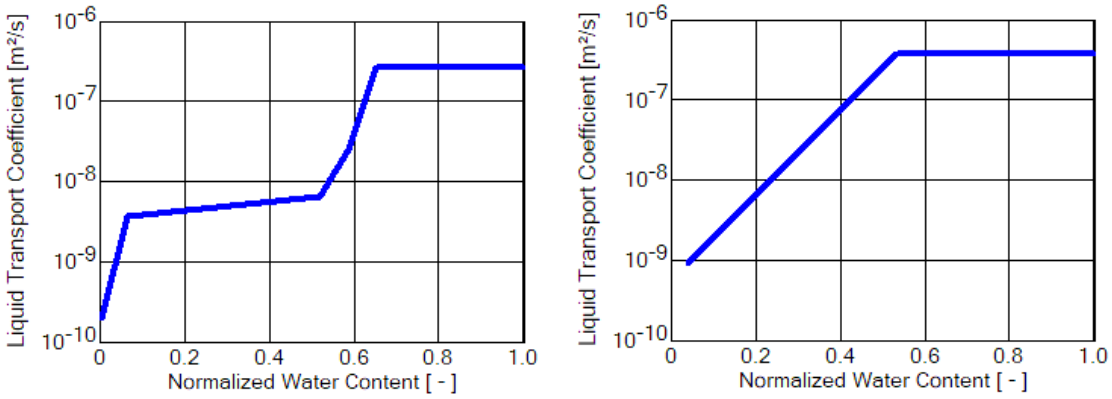

Fig. 209 – Liquid transport coefficient for suction of: a) Aerated concrete block and b) Exterior render (IBP 2016).

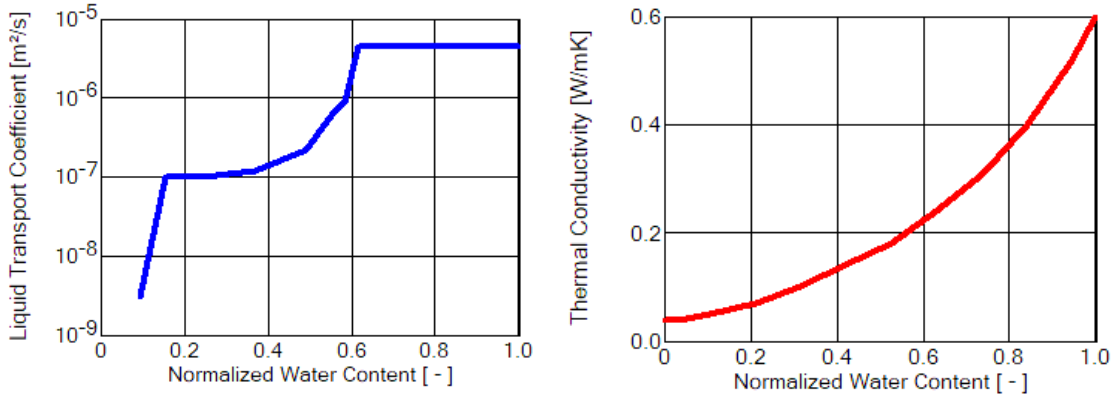

Fig. 210 – a) Liquid transport coefficient for suction of gypsum plaster and b) Thermal conductivity, moisture-dependent: EPS (IBP 2016).

ANNEX 2 – SIMULATION SCENARIOS

Table 125 – Simulation scenarios for exterior application – Porto climate.

Scenario	System	Climate	Solar absorption coefficient	Wall orientation
S1P0.27N	S1	Porto	0.27	North
S1P0.27S				South
S1P0.27E				East
S1P0.27W				West
S1P0.80N			0.80	North
S1P0.80S				South
S1P0.80E				East
S1P0.80W				West
S2P0.27N	S2	Porto	0.27	North
S2P0.27S				South
S2P0.27E				East
S2P0.27W				West
S2P0.80N			0.80	North
S2P0.80S				South
S2P0.80E				East
S2P0.80W				West
ETICSP0.27N	ETICS	Porto	0.27	North
ETICSP0.27S				South
ETICSP0.27E				East
ETICSP0.27W				West
ETICSP0.80N			0.80	North
ETICSP0.80S				South
ETICSP0.80E				East
ETICSP0.80W				West

Table 126 – Simulation scenarios for exterior application – Nancy climate.

Scenario	System	Climate	Solar absorption coefficient	Wall orientation
S1N0.27N	S1	Nancy	0.27	North
S1N0.27S				South
S1N0.27E				East
S1N0.27W				West
S1N0.80N			0.80	North
S1N0.80S				South
S1N0.80E				East
S1N0.80W				West
S2N0.27N	S2	Nancy	0.27	North
S2N0.27S				South
S2N0.27E				East
S2N0.27W				West
S2N0.80N			0.80	North
S2N0.80S				South
S2N0.80E				East
S2N0.80W				West
ETICSN0.27N	ETICS	Nancy	0.27	North
ETICSN0.27S				South
ETICSN0.27E				East
ETICSN0.27W				West
ETICSN0.80N			0.80	North
ETICSN0.80S				South
ETICSN0.80E				East
ETICSN0.80W				West

Table 127 – Simulation scenarios for exterior application – Oslo climate.

Scenario	System	Climate	Solar absorption coefficient	Wall orientation
S1O0.27N	S1	Oslo	0.27	North
S1O0.27S				South
S1O0.27E				East
S1O0.27W				West
S1O0.80N			0.80	North
S1O0.80S				South
S1O0.80E				East
S1O0.80W				West
S2O0.27N	S2	Oslo	0.27	North
S2O0.27S				South
S2O0.27E				East
S2O0.27W				West
S2O0.80N			0.80	North
S2O0.80S				South
S2O0.80E				East
S2O0.80W				West
ETICSO0.27N	ETICS	Oslo	0.27	North
ETICSO0.27S				South
ETICSO0.27E				East
ETICSO0.27W				West
ETICSO0.80N			0.80	North
ETICSO0.80S				South
ETICSO0.80E				East
ETICSO0.80W				West

Table 128 – Simulation scenarios for thermal plastering system S3 – interior application.

Scenario	Climate	Solar absorption coefficient	Wall orientation
S3P0.27N	Porto	0.27	North
S3P0.27S			South
S3P0.27E			East
S3P0.27W			West
S3P0.80N		0.80	North
S3P0.80S			South
S3P0.80E			East
S3P0.80W			West
S3N0.27N	Nancy	0.27	North
S3N0.27S			South
S3N0.27E			East
S3N0.27W			West
S3N0.80N		0.80	North
S3N0.80S			South
S3N0.80E			East
S3N0.80W			West
S3O0.27N	Oslo	0.27	North
S3O0.27S			South
S3O0.27E			East
S3O0.27W			West
S3O0.80N		0.80	North
S3O0.80S			South
S3O0.80E			East
S3O0.80W			West

ANNEX 3 – TEMPERATURE INDEXES

Table 129 – Temperature indicators obtained in system S1, for the north and east orientations.

Climate	Porto				Nancy				Oslo			
Orientation	N		E		N		E		N		E	
α	0.27	0.8	0.27	0.8	0.27	0.8	0.27	0.8	0.27	0.8	0.27	0.8
Tse (ºC)	35.8	40.3	35.9	42.9	31.5	35.4	31.8	44.1	28.6	32.5	28.7	38.7
ΔTse (ºC)	35.0	39.3	35.0	41.9	45.8	49.6	46.2	58.3	44.5	48.5	44.6	54.6
$\Delta T_{interface}$ (ºC)	34.6	38.8	34.6	41.4	45.5	49.2	45.8	57.7	44.2	48.0	44.3	54.1
ΔT_{TR} (ºC)	9.2	11.7	9.0	15.4	15.2	15.2	15.2	17.6	20.4	20.4	20.4	20.4

Table 130 – Temperature indicators obtained in system S2, for the north and east orientations.

Climate	Porto				Nancy				Oslo			
Orientation	N		E		N		E		N		E	
α	0.27	0.8	0.27	0.8	0.27	0.8	0.27	0.8	0.27	0.8	0.27	0.8
Tse (ºC)	35.6	40.0	35.6	42.6	31.2	35.1	31.5	43.6	28.4	32.3	28.6	38.4
ΔTse (ºC)	34.6	38.9	34.6	41.4	45.4	49.2	45.8	57.7	44.2	48.1	44.4	54.2
$\Delta T_{interface}$ (ºC)	34.4	38.6	34.3	41.0	45.2	48.9	45.4	57.2	44.0	47.9	44.2	53.9
ΔT_{TR} (ºC)	8.2	10.6	8.1	15.0	14.3	14.3	14.3	17.5	19.2	19.2	19.2	19.2

Table 131 – Temperature indicators obtained in ETICS, for the north and east orientations.

Climate	Porto				Nancy				Oslo			
Orientation	N		E		N		E		N		E	
α	0.27	0.8	0.27	0.8	0.27	0.8	0.27	0.8	0.27	0.8	0.27	0.8
Tse (ºC)	36.0	40.4	36.0	43.1	31.6	35.6	32.0	44.3	28.6	32.7	28.8	38.8
ΔTse (ºC)	35.2	39.5	35.2	42.1	46.0	49.9	46.4	58.6	44.7	48.7	44.8	54.8
$\Delta T_{interface}$ (ºC)	34.9	39.1	34.9	41.8	45.7	49.5	46.1	58.1	44.4	48.3	44.5	54.4
ΔT_{TR} (ºC)	10.7	11.5	10.8	14.8	17.7	17.9	17.8	18.0	20.4	20.4	20.4	20.4

Table 132 – Temperature indicators obtained in S3, for the north and east orientations.

Climate	Porto				Nancy				Oslo			
Orientation	N		E		N		E		N		E	
α	0.27	0.8	0.27	0.8	0.27	0.8	0.27	0.8	0.27	0.8	0.27	0.8
Tse (ºC)	35.3	39.6	35.3	41.9	31.0	34.6	31.2	42.8	28.3	32.1	28.5	38.1
ΔTse (ºC)	34.2	38.4	34.4	40.7	45.2	48.6	45.4	56.8	44.0	47.8	44.2	53.8
$\Delta T_{interface}$ (ºC)	7.8	8.0	8.0	8.3	10.7	11.0	10.9	11.5	10.6	11.0	10.7	11.5
ΔT_{TR} (ºC)	2.2	2.2	2.4	2.2	4.6	4.5	4.6	4.4	4.4	4.4	4.4	4.4

ANNEX 4 – WATER CONTENT INDICATORS

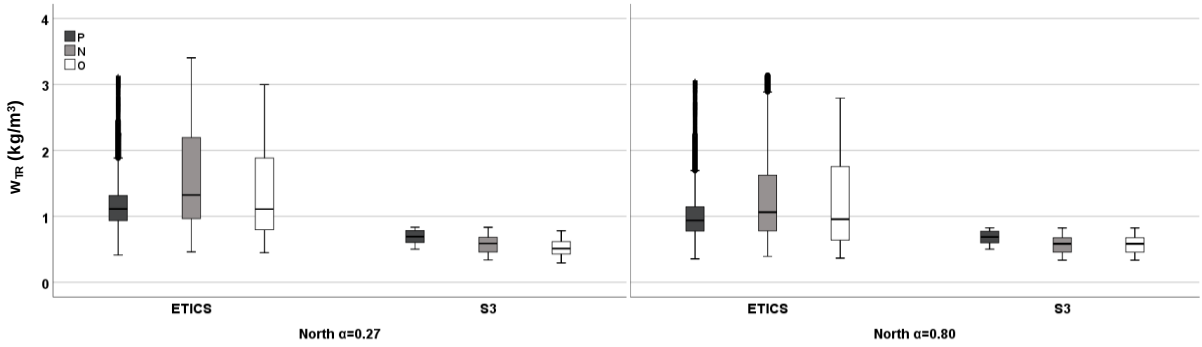

Fig. 211 – Box-plot of the water content in the insulation layer of ETICS and S3 with solar absorption of 0.27 and 0.80, in the north façade.

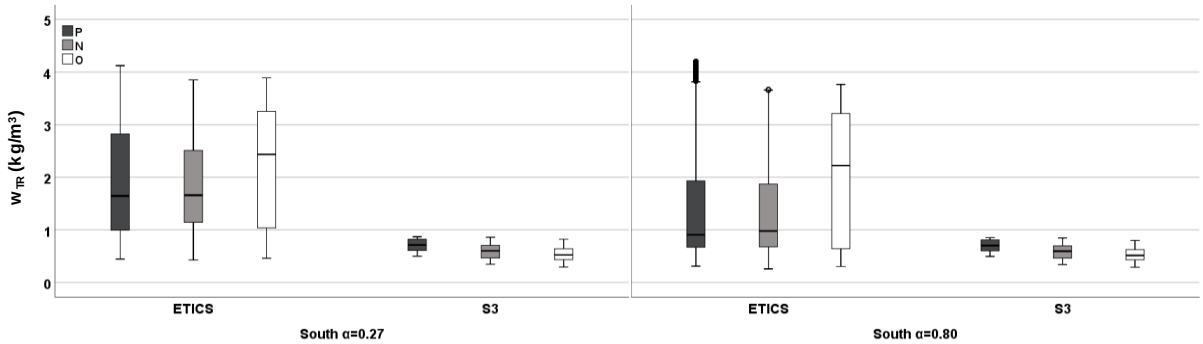

Fig. 212 – Box-plot of the water content in the insulation layer of ETICS and S3 with solar absorption of 0.27 and 0.80, in the south façade.

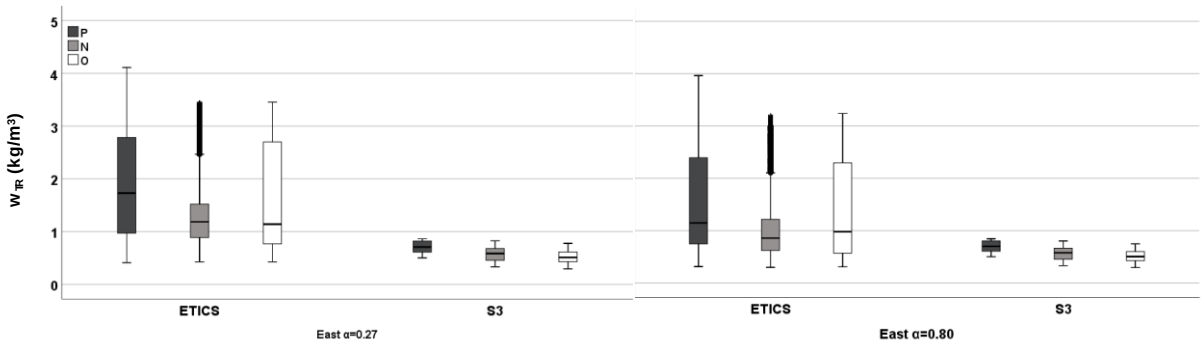

Fig. 213 – Box-plot of the water content in the insulation layer of ETICS and S3 with solar absorption of 0.27 and 0.80, in the east façade.

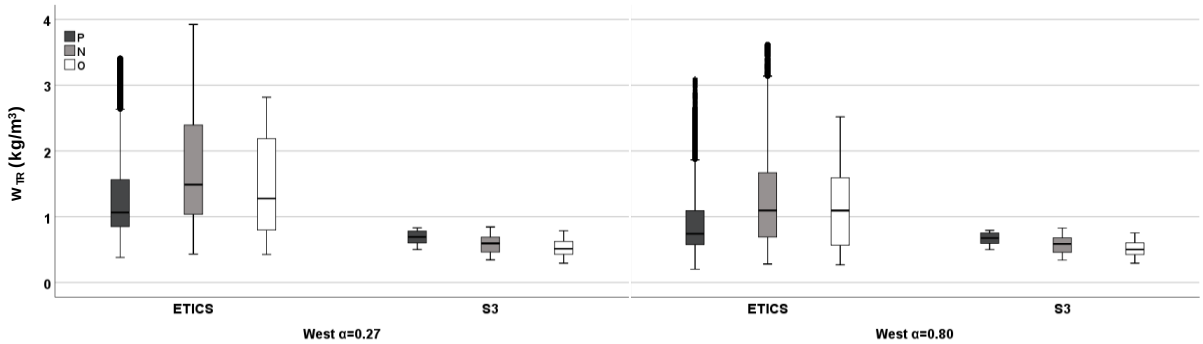

Fig. 214 – Box-plot of the water content in the insulation layer of ETICS and S3 with solar absorption of 0.27 and 0.80, in the west façade.

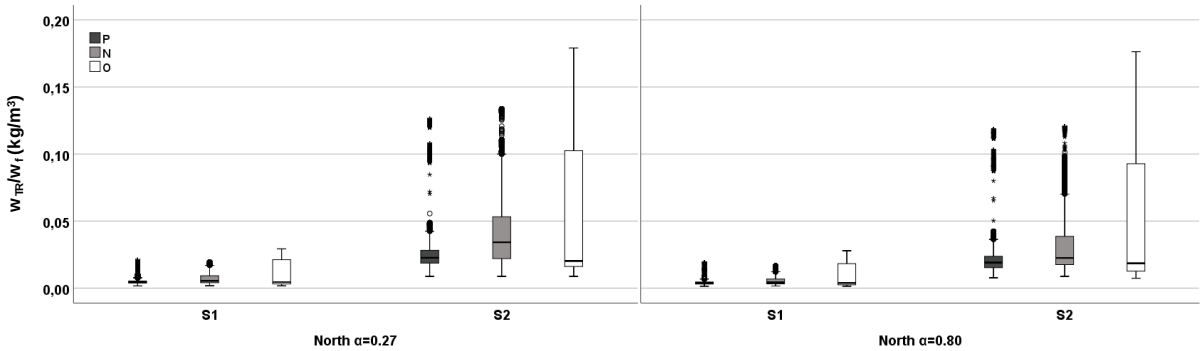

Fig. 215 – Box-plot of the ratio between the water content and the free water saturation in the TR of S1 and S2 with solar absorption of 0.27 and 0.80, in the north façade.

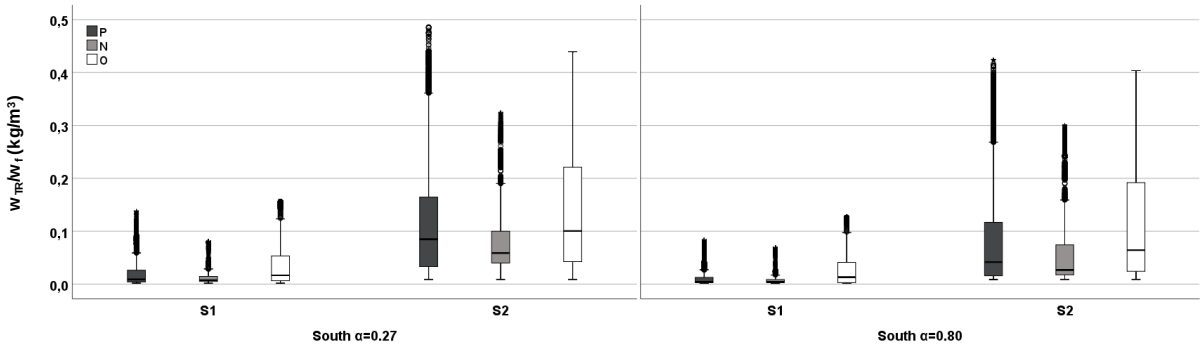

Fig. 216 – Box-plot of the ratio between the water content and the free water saturation in the TR of S1 and S2 with solar absorption of 0.27 and 0.80, in the south façade.

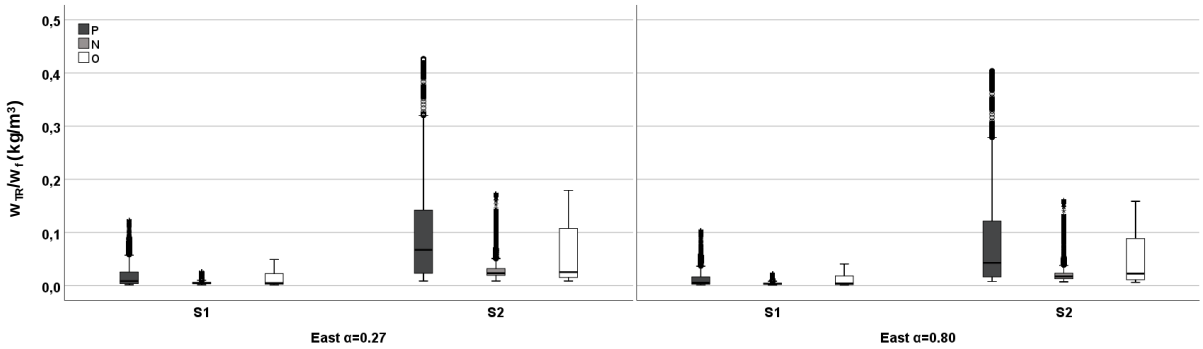

Fig. 217 – Box-plot of the ratio between the water content and the free water saturation in the TR of S1 and S2 with solar absorption of 0.27 and 0.80, in the east façade.

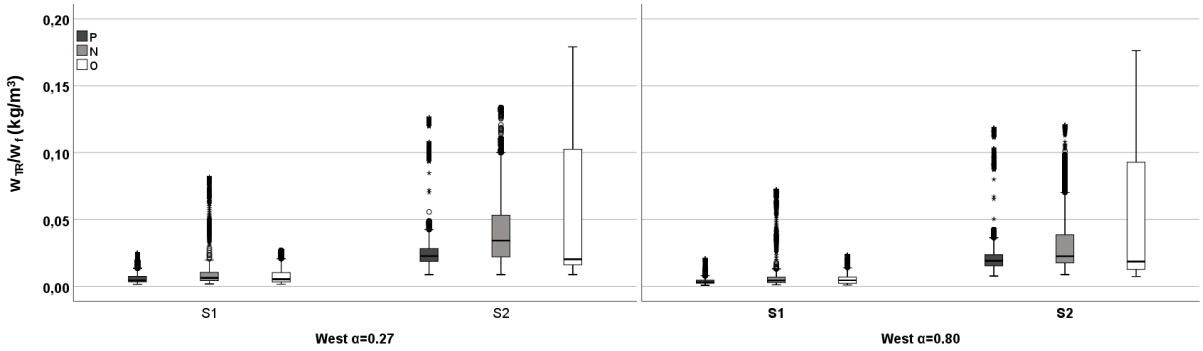

Fig. 218 – Box-plot of the ratio between the water content and the free water saturation in the TR of S1 and S2 with solar absorption of 0.27 and 0.80, in the west façade.